The prediction of thermal stresses and strain in quenched plates of certain low alloy steels.

PRICE, R. F.

Available from the Sheffield Hallam University Research Archive (SHURA) at:

http://shura.shu.ac.uk/20248/

A Sheffield Hallam University thesis

This thesis is protected by copyright which belongs to the author.

The content must not be changed in any way or sold commercially in any format or medium without the formal permission of the author.

When referring to this work, full bibliographic details including the author, title, awarding institution and date of the thesis must be given.

Please visit http://shura.shu.ac.uk/20248/ and http://shura.shu.ac.uk/information.html for further details about copyright and re-use permissions.

SHEFFIELD CITY
POLYTECHNIC LIBRARY
POND STREET
SHEFFIELD S1 1WB

6883

7904531011

19.1.95
19.23.

~~due~~
~~26/1~~ – ~~20.59~~pm.

27.1.95
16.59

29.1.95
20.00.

5/3/95
7.45pm.

12/6/95
20.00

13/6-20:59

14/6/95
17.24

15/6/95
17.12

ProQuest Number: 10700893

All rights reserved

INFORMATION TO ALL USERS
The quality of this reproduction is dependent upon the quality of the copy submitted.

In the unlikely event that the author did not send a complete manuscript
and there are missing pages, these will be noted. Also, if material had to be removed,
a note will indicate the deletion.

ProQuest 10700893

Published by ProQuest LLC (2017). Copyright of the Dissertation is held by the Author.

All rights reserved.
This work is protected against unauthorized copying under Title 17, United States Code
Microform Edition © ProQuest LLC.

ProQuest LLC.
789 East Eisenhower Parkway
P.O. Box 1346
Ann Arbor, MI 48106 – 1346

THE PREDICTION OF THERMAL STRESSES AND STRAIN IN QUENCHED PLATES OF CERTAIN LOW ALLOY STEELS

BY

R.F. PRICE

A THESIS SUBMITTED TO THE COUNCIL FOR NATIONAL ACADEMIC AWARDS IN PARTIAL FULFILMENT FOR THE DEGREE OF

DOCTOR OF PHILOSOPHY
IN INDUSTRIAL METALLURGY

COLLABORATING ESTABLISHMENT:-

Sheffield Laboratories,
Swinden House,
British Steel Corporation.

SPONSORING ESTABLISHMENT:-

Department of Metallurgy,
Sheffield City Polytechnic,
May 1980.

SHEFFIELD CITY POLYTECHNIC LIBRARY
Th
669.94
PR
POND STREET

7904531-01

PREFACE

All the work reported in this thesis was carried out during the period for which the candidate was registered for a higher degree.

In accordance with the regulations for PhD in Industrial Metallurgy, a full course in Metallurgical Process and Management was successfully completed. The details of the course are given below:-

MODULE - 1

Process Metallurgy

Mechanical Metallurgy

Advanced Thermodynamics

MODULE - 2

Accountancy

Micro-Economics and Financial Control

Computational Methods and Operational Research

MODULE - 3

Powder Metallurgy

Metals and Competitive Materials

High Strength Steels

Heat Treatment and Transformations

Quality Control

Solidification of Metals

MODULE - 4

Industrial Case Studies

One of the case studies, which is related to the current research work, is attached with the thesis, as Appendix 3.

The Candidate's performance during the above mentioned courses was assessed by means of written examinations and continuous assessment of specific assignments.

Acknowledgements

The author is heavily indebted to Dr. A.J. Fletcher and Mr. W.T. Cook for their continuous support, encouragement and advice throughout the duration of the work.

Grateful appreciation is also expressed to the Technical Staff of the Department of Metallurgy whose services were invaluable. Special thanks are due to Mr. R. Day and Mr. G. Gregory. Thanks are also due to the Department of Mechanical Engineering for the use of metrology facilities.

The provision of previously unpublished physical and mechanical property data relating to certain low alloy steels, by the Sheffield Laboratories of the British Steel Corporation is especially acknowledged.

The author would also like to express his sincere gratitude to Dr. A.W.D. Hills, Head of Department of Metallurgy, for his initial encouragement to undertake the work and the provision of facilities for the work. Grateful thanks must also be expressed to the Science Research Council for their financial support by way of a Research Studentship.

Thanks are due to friends and colleagues at TI Research Laboratories, Cambridge, for their encouragement and assistance during the preparation of the thesis and especially to Miss C.J. Savill who carried out the typing.

Finally, the support, encouragement and sheer endurance of my Wife and Family deserve greater acknowledgement than words can express.

THE PREDICTION OF THERMAL STRESSES AND STRAIN IN QUENCHED PLATES OF CERTAIN LOW ALLOY STEELS

R.F. Price

Abstract

A mathematical model was used to calculate the internal stresses and strain produced when plates of a high hardenability steel (835M30) were quenched in water, polymer and oil. A prerequisite for the calculations was the experimental determination of relevant physical and mechanical property data not available from other sources; this included the surface heat transfer coefficient during quenching and the mechanical properties of 835M30 steel in the metastable austenitic condition. The results of the thermal stress calculations showed that the production of residual strain was markedly dependent on both the surface heat transfer coefficient and the flow strength of the steel during the early stages of the quench. It was predicted that the low stability of the vapour blanket, found during the early stages of a water quench, gave large variations in distortion. The more consistent values of the surface heat transfer coefficient, obtained during oil quenching, were associated with more reproducible levels of distortion. The predicted residual stress distributions were less sensitive to variations in either the surface heat transfer coefficient or the flow strength of the steel during the early stages of the quench. However, the residual stress distributions were strongly dependent on the flow strength of the material during the martensite transformation. A correlation of the results of the calculations with experimental behaviour showed that agreement was good in the cases of both the residual stresses and strains obtained after a water quench. However, in the case of oil quenched plates, a similar correlation was only obtained with residual strains. A possible explanation for the lack of good correlation in the case of oil quenched plates may be found by consideration of the effect of strain rate on the mechanical properties of the material, particularly during the martensitic transformation.

NOMENCLATURE

Unless stated otherwise in the text, the nomenclature used in the thesis is as shown below. Note that, owing to the common use of the Greek symbol 'α' for both thermal diffusivity and the coefficient of linear thermal expansion, its use has been retained but the two meanings are indicated by the subscripts 'td' and 'ex' respectively.

A = Area, m^2
B_i = Biot number $\left(\frac{hL}{\lambda}\right)$
C_p = Specific heat, $J/kg^{\circ}C$
E = Young's modulus, N/mm^2
F_o = Fourier number $\left(\frac{\alpha_{td} t}{L^2}\right)$
G = Shear modulus, N/mm^2
L = Length, m
M = Mass, kg
M_s = Temperature at the start of the martensite transformation, $^{\circ}C$
M_f = Temperature at the finish of the martensite transformation, $^{\circ}C$
Q = Heat generation term in equation 2.10
V = Volume, m^3
V_Q = Volume after quenching, m^3
V_S = Volume in the softened condition, m^3
$V_{\alpha'}$ = Volume fraction of martensite
V_{γ} = Volume fraction of austenite
W = Strain hardening coefficient $\left(\frac{d\sigma_f}{d\varepsilon_p}\right)$, N/mm^2
Y = Width of plate, m
Z = Thickness of plate, m

a, b } Constants relating linear variation of E and ν with temperature, according to $\frac{E}{1-\nu} = a - b\theta$
exp = Superscript indicating experimentally determined value
h = Surface heat transfer coefficient, $W/m^2\,^{\circ}C$

i = Node positional subscript

j = Number of elements in half-thickness of plate

ℓ = Number of sets of experimental time/temperature values obtained from cooling curves

m = Number of iterations in plasticity calculation

n = Node time superscript

r = Radial distance, m

r_e = External radius, m

r_i = Internal radius, m

t = Time, s

$\left.\begin{matrix} x \\ y \\ z \end{matrix}\right\}$ Cartesian co-ordinates

$\left.\begin{matrix} \Delta_x \\ \Delta_z \end{matrix}\right\}$ Thicknesses of elements in plate

$(\ )_{min}$ = Minimum value

$(\ )_{max}$ = Maximum value

$(\ )_s$ = Stored value

$(\ )_{sum}$ = Sum of values

ε = Strain

ε_{e-p} = Strain due to elastic-plastic behaviour

ε_p = Strain associated with plastic flow

$\varepsilon_{thermal}$ = Strain due to thermal expansion alone

θ = Temperature, °C

θ_{Av} = Average temperature, °C

θ_f = Bulk temperature of quenchant, °C

θ_o = Initial temperature, °C

θ_s = Temperature at surface, °C

θ_{stop} = Temperature at which calculation stopped, °C

θ_t = Temperature at time t, $^{\circ}C$

θ_{TC} = Temperature at thermocouple location, $^{\circ}C$

λ = Thermal conductivity $W/m^{\circ}C$

ν = Poisson's ratio

ρ = Density, kg/m^3

σ = Stress, N/mm^2

$$\left.\begin{array}{ll} \sigma_x & = \text{Stress in x direction} \\ \sigma_y & = \text{Stress in y direction} \\ \sigma_z & = \text{Stress in z direction} \end{array}\right\} \text{Cartesian co-ordinates}$$

$$\left.\begin{array}{ll} \sigma_z & = \text{Axial stress} \\ \sigma_r & = \text{Radial stress} \\ \sigma_\theta & = \text{Tangential stress} \end{array}\right\} \text{Cylindrical co-ordinates}$$

σ_f = Flow stress with uniaxial stress system , N/mm^2

$\sigma_1, \sigma_2, \sigma_3$ = Principal stresses

$(\sigma)_r$ = Stress when edges of plate restrained, N/mm^2

$\bar{\sigma}$ = Mean level of stress in half-thickness of plate, N/mm^2

α_{ex} = Coefficient of linear thermal expansion, $^{\circ}C^{-1}$

α_{td} = Thermal diffusivity, m^2/s

Y_S = Distance between reference points on edges of plate in softened condition

Y_Q = Distance between reference points on edges of plate in quenched condition

Contents

Page

1. INTRODUCTION 13

2. PREVIOUS WORK 16

2.1 Introduction 16

2.2 Experimental Investigations 19

2.2.1 Quench cracking 19

2.2.2 Residual stress measurements 23

2.2.3 Distortion measurements 31

2.3 Prediction of Thermal Stresses During Quenching 39

2.3.1 The calculation of temperature distributions in the body 41

2.3.2 Heat transfer at the surface during quenching 45

2.3.3 The relationship between temperature and position during quenching 55

2.3.4 Calculation of thermal stress during quenching 59

2.4 Conclusions from the Survey of Previous Work 70

3. TEMPERATURE DISTRIBUTIONS IN QUENCHED PLATES 72

3.1 Determination of the Surface Heat Transfer Coefficient During Quenching 72

3.1.1 Experimental procedure for the determination of cooling curves 73

3.1.2 Calculation of the surface heat transfer coefficient 76

3.1.3 Experimental results 81

3.2 Temperature Distributions in Low-Alloy Steel Plates During Quenching 85

3.2.1 Experimental determination of temperature distributions 86

3.2.2 Calculation of temperature distributions in plates of 835M30 steel during quenching 86
3.2.3 Comparison of calculated and experimental temperature distributions 88

4. PREDICTION OF THERMAL STRESS AND STRAIN 90
4.1 Calculation Technique 90
4.1.1 Procedure assuming plastic deformation without strain-hardening 91
4.1.2 Procedure assuming strain-hardening 98
4.2 Data Used in Thermal Stress Calculations 101
4.2.1 Determination of the change in free length of a specimen of 835M30 steel during cooling from 850°C 102
4.2.2 Mechanical properties of 835M30 steel during quenching 103
4.2.3 Stress relaxation 108
4.2.4 Overall volume change accompanying the hardening of 835M30 109
4.3 Stability of the Thermal Stress Calculations 110
4.3.1 Calculation of thermal stress with an infinite flow stress at all temperatures 111
4.3.2 Influence of element size on the calculation of residual stress and strain 111
4.3.3 Influence of the maximum permitted unbalanced force in the plate on the residual stress and strain 112
4.3.4 Influence of the number of time increments on the residual stress and strain distribution 112
4.4 Results of Thermal Stress and Strain Calculations 113
4.4.1 Water quenching 113
4.4.2 Oil quenching 116
4.4.3 Polymer quenching 118

5. EXPERIMENTAL DETERMINATION OF RESIDUAL STRESS AND STRAIN IN QUENCHED PLATES 119

5.1 Experimental Procedures 119

5.1.1 Specimens 119

5.1.2 Heat treatment procedure 119

5.1.3 Measurement of distortion 120

5.1.4 Measurement of residual stress 123

5.2 Results of the Measurements of the Residual Stresses and Strains Present in Quenched Plates 125

5.2.1 Water quenched plates 125

5.2.2 Oil quenched plates 127

5.2.3 Polymer quenched plates 128

6. DISCUSSION 129

6.1 Surface Heat Transfer Coefficients Obtained During Quenching 129

6.1.1 Water quenching 129

6.1.2 Oil quenching 131

6.1.3 Polymer quenching 132

6.2 The Calculation of Temperature Distribution During Quenching 134

6.2.1 Comparison between temperature distributions determined by experiment and by calculation 134

6.2.2 Influence of specimen size on the surface heat transfer coefficient 135

6.3 Mechanical Properties of 835M30 Steel During Quenching 137

6.4 Prediction of Thermal Stress and Strain Developed During Quenching 139

6.4.1 Characteristic stages in the stress-strain cycle 139

6.4.2 Water quenched plates 141

6.4.3 Oil quenched plates 146

6.4.4 Polymer quenched plates 151

6.5 General Discussion 152

7. CONCLUSIONS 156

8. RECOMMENDATIONS FOR FURTHER WORK 159

REFERENCES 161

TABLES 172

FIGURES 191

APPENDICES 295

1. INTRODUCTION

The development of thermal stress in steel components during quenching is a complex phenomenon that has been subjected to a great deal of both experimental and theoretical calculation. It is a problem of considerable importance in the heat treatment of engineering components, since residual stresses produced during the quenching operation may have a detrimental effect on the component in service. Sometimes the stress levels are sufficiently high to cause cracking during, or shortly after, quenching. Furthermore, distortion can necessitate expensive re-grinding operations after heat treatment or may result in components being completely scrapped.

In many cases distortion itself need not be a problem provided its extent is known beforehand and the precise level of distortion can be reproduced consistently. Component dimensions before heat treatment can be adjusted so that the final dimensions after heat treatment are correct. This practice is adopted in the automobile industries for the production of gears in large quantities. Sample gears made from each batch of steel are hardened and the dimensional changes determined. The initial dimensions of that batch of gears are then compensated accordingly so that no correction will be required after hardening. The production of these sample batches is costly and time consuming. Furthermore, even with these precautions, the distortions in the remainder of the batch are not always consistent.

The experimental investigation of residual stresses and distortion after quenching is a laborious and difficult task. The experimental variables that require consideration have proved to be large in number and are often difficult to control. Although the literature contains the results of investigations involving different steels, the lack of standardisation of experimental variables makes the task of correlating the results of different investigations very difficult.

Consequently attempts have been made to calculate the stresses developed during quenching by means of mathematical models. Dubious assumptions, however, have often been made in order to express the problem in a mathematically soluble form and the results obtained have not been adequately tested. Recently, experience has rapidly increased in the application of high speed digital computers to the solution of thermal stress problems, which had previously been intractable. Today the major limitation in the performance of such calculations is probably the availability of accurate mechanical and physical property data. This is especially so in the case of the problem involved in the quenching of steel components. Virtually all of the data required for these calculations is temperature dependent and certain properties change during the quench in a complex manner. In the case of temperatures at which the steel exists in the form of metastable austenite, data is very scarce.

This thesis describes the work carried out during an investigation into the prediction of thermal stresses* and strain during the quenching of plates of a low-alloy steel of high hardenability. The form of a plate was used because this greatly simplifies the stress system involved. The main investigation has been based on a 4¼% Ni Cr Mo steel (835M30). This steel has a sufficiently high hardenability to ensure that the only transformation product formed during the quench from the high temperature, at which austenite was stable, was martensite. Thus this combination of a plate specimen with 835M30 steel represents the simplest situation which exists for the analysis of quenching stresses in a steel that transforms during quenching.

---

*In the context of this thesis, the term 'thermal stress' is assumed to include all stresses which are induced as the result of thermal contraction strain and transformation strain.

An infinite plate made from a steel which is completely martensitic after being quenched is an idealistic situation, and rarely occurs in the production of engineering components. Component shapes are usually much more complex and a homogeneous martensitic structure may not be desired. Surface treatments such as carburising add further complications. But it is still essential that this simple combination be studied and understood thoroughly before further complexities are considered.

The benefits to be expected from such an investigation accrue from a better understanding of the development of thermal stresses and strain during quenching and of the mechanisms that control their formation. Such knowledge will form a basis for the analysis of more complex problems and will also identify the major factors that control the process. Improved knowledge of these factors will lead to a greater degree of control over both residual stress and distortion.

2. PREVIOUS WORK

2.1 Introduction

Stresses which exist in solids that are free from externally applied loads and are at a uniform temperature are called internal stresses or residual stresses. These internal stresses fall into three categories[1,2].

(i) First order internal stresses. These operate over appreciable distances and are balanced throughout the body. They are also commonly known as Macro-Stresses or Body-Stresses, and are the stresses considered in this investigation.

(ii) Second order internal stresses. These operate over much shorter distances than first order internal stresses. The stresses around precipitates or the stresses around inclusions after deformation are examples of their occurrence.

(iii) Third order internal stresses. These only extend over a few interatomic distances, e.g. the lattice stresses induced by solute atoms of different sizes and lattic defects.

Second and third order internal stresses are frequently lumped together as Micro-Stresses or Tesselated Stresses[3].

Scott[4] was one of the earliest workers to recognise that the stresses developed during the hardening of steels arose from the interactions of four factors:

(a) The generation of temperature gradients within the steel.

(b) The thermal contraction of the steel.

(c) The expansions accompanying the transformation of austenite to other phases during quenching.

(d) The modification of stresses by plastic flow.

Qualitative descriptions of the method by which different residual stress distributions may be generated by various combinations of these factors have now been made by numerous authors[4,5,6,7,8]. The mechanism for the development of residual compressive stresses at the surface of non-transformable materials is well understood,[9,10,11] and has been described by Andrews[2]. He initially considered the cooling curves at the surface and centre of a quenched bar (see Figure 1(a)): because the material at the surface cools and contracts initially more rapidly than that at the centre, a tensile stress developed at the surface. This was balanced by compressive stresses in the central portions of the bar. The broken line in Figure 1(b) schematically illustrates the way in which this tensile stress varied as the temperature difference between the surface and centre varied. If there has been no plastic flow the surface stress would be reduced to zero at the point at which the bar has returned to a uniform temperature. However, when plastic flow occurred at either the surface or the centre of the bar, residual stresses would be generated, as shown by the continuous line in Figure 1(b), because the surface and centre of the bar had undergone different degrees of strain.

When a steel transforms to martensite during quenching from a temperature at which the austenite structure is stable, the martensite transformation is accompanied by a significant increase in volume which greatly complicates the development of thermal stresses.[12] Figure 2 shows a typical length/temperature curve (dilatometer curve) produced during the heating and rapid cooling of a plain carbon steel specimen, which transformed from austenite during quenching from the high initial temperature. When a bar of such a steel is quenched, the martensite transformation is initiated at the surface of the bar and the expansions accompanying it are considered to bring about a stress reversal[4], which generates compressional surface stresses balanced by tension stresses within the bar. As the transformation proceeds inwards another stress reversal occurs, and the stresses at the centre of the bar become compressive whilst those at the surface become tensile. Any residual stresses are still a consequence of plastic flow, but their prediction is far more complex.

If the cooling rate and hardenability of the steel are such that bainite or pearlite are formed then the problem becomes still more complex[6]. The formation of these phases occurs over a range of temperatures and is accompanied by different expansions. Even in the absence of any plastic deformation during heat treatment, a hardened steel component will have experienced a change in its overall dimensions because of the different specific volumes of the structures present before and after heat treatment[13,14]. If there is a difference in the specific volumes of the structures present in different parts of a section after quenching e.g. martensitic surface region and bainite core, this misfit will cause residual stresses, even if no plastic deformation had occurred during the quench[15].

Normally it is only possible to measure the changes that have occurred at the end of the quench, when the stresses generated during quenching may manifest themselves in the following ways:-

(i) Quench cracking

(ii) Residual stress

(iii) Distortion of the component

Quench cracking is well known in commercial heat treatment, but its occurrence has been found to be very erratic, and highly dependent on component geometry . The measurement of residual stress is slow, difficult and requires great care if it is to be successful[2,16]. The accurate measurement of distortion is similarly a slow and laborious process, and is strongly dependent on the geometry of the component[6]. The number of significant published investigations of these phenomena have been few; yet their importance is very great. Very few workers have considered more than one of these thermal stress effects at any one time. It has, therefore, been possible to classify these experimental investigations into three categories.

2.2 Experimental Investigations

2.2.1 Quench cracking

Quench cracking is the least satisfactory method by which the development of thermal stresses during quenching may be studied. The occurrence of cracking demonstrates only that at some, often unknown, stage during the quenching process cracking was produced. The levels of stress required for this to occur are generally unknown. Surface cracking appears to indicate that large tensile stresses have been developed at the surface of the material, after the martensite transformation has been completed[17]; although there have been suggestions that the maximum sensitivity to cracking occurs during the transformation process[18].

Scott[4] conducted one of the earliest investigations that involved quench cracking. The work was carried out using tool steels, and it was found that in the case of simple shapes cracking was only prevalent when the whole section transformed into martensite. His results obtained from a series of cylinders with diameters between 6 mm and 50 mm showed that cracking was unlikely under both the most severe and least severe quenching conditions; but was frequent with intermediate quenching severities. Scott supplemented his investigation of cracking with an estimate of the residual axial stresses, obtained from the changes in length of cylindrical specimens when successive layers were ground from their diameters. It was found that a 25 mm diameter cylinder quenched in oil developed similar stresses to those present in a 12 mm diameter cylinder quenched in water. He considered this was due to the presence of similar temperature gradients within both the cylinders. Unfortunately most of the cracks found were longitudinal, and therefore the result of tangential rather than axial stresses. Nevertheless, Scott concluded that as the section size, or the quenching power of the bath, was increased the surface stresses became increasingly tensile until a maximum was reached. Further increases in either of these properties reduced the magnitude of these tensile stresses, which eventually became compressive.

The influence of alloying elements on the susceptibility of steels to quench cracking has been discussed by Jaffe and Hollomon[19] in relation to the selection of alloying elements for hardenability purposes. They found that although an increase in the carbon content and alloy content of a steel affected the specific volumes of austenite and martensite, both structures were almost equally affected. They concluded that the volume change that accompanied the austenite/martensite transformation was nearly independent of composition provided the M_s temperature remained unaltered. However this same volume change was strongly dependent on the transformation temperature; the lower the M_s temperature the greater was the expansion accompanying the transformation. They considered that quench cracking would be least probable if the volume increase accompanying the martensite transformation were minimised. They also suggested that martensite was harder and less ductile when formed at lower temperatures, so that there was less possibility of stress relief during the quench. Jaffe and Hollomon therefore proposed a design philosophy for the selection of alloy additions, which proposed that the requisite hardenability should be achieved with the minimum depression of the M_s temperature, since this involved the least likelihood of quench cracking. However, Wells[20] was unable to find any correlation between quench cracking and the M_s temperature. Chapman and Jominy[21] suggested this lack of correlation was due to the lack of a sufficiently sensitive test specimen and developed one which they considered more reliable (shown in Figure 3). This type of specimen was then used to investigate the influence of carbon content and hence M_s temperature upon quench cracking. They used a range of commercial plain carbon and low-alloy steels for the investigation and concluded that the lower the M_s temperature, the greater was the likelihood for quench cracking. Chapman and Jominy also suggested that the likelihood of quench cracking increased as the hardenability increased.

Kobasko[22], who studied the frequency of the formation of quench cracks in 6 mm diameter cylinders of medium carbon and low-alloy steels, reported similar results to those obtained by Scott[4]. A wide range of cooling rates were achieved by the use of water at various temperatures, aqueous 12% NaOH at 20°C and aqueous saturated NaCl at 20°C. The cooling rate at 350°C was determined for each quenchant from the cooling curves at the centres of other cylinders. These cooling rates, which always produced a fully martensitic structure, were then correlated with the incidence of quench crack formation in a large number of tests (shown in Figure 4). As the cooling rate was increased, the probability of cracking first increased to a maximum and then decreased.

Further evidence of the existence of a critical range of quench severity, within which quench cracking was most likely to occur, has been reported by Bodson et alia[23], who used an acoustic method to study the effects of different media on the quench cracking of 8 to 24 mm diameter cylinders. Two casts of a 0.56%C, 0.75%Mn steel were used: one cast had high residual Cr, Ni and Cu contents (0.35%, 0.25% and 0.24% respectively), whilst the other contained much lower quantities of these elements (0.09%, 0.07% and 0.105% respectively). They found that for a particular quenchant there was a critical diameter at which cracking was most probable. This diameter was larger in the case of the steel with high impurity levels, which was attributed to the greater hardenability of this steel. Of special interest was the existence of a critical specimen diameter at which the incidence of quench cracking was greatest. Bodson et alia also found that an increase in the water temperature reduced the severity of the quench by an extension of the vapour blanket stage *to lower temperatures and also by a reduction in the severity of the nucleate boiling stage.*

Beck[24] has argued that cracking might be the result of a thermal shock associated with the breakdown of the vapour blanket stage. However, Bodson et alia[23] estimated that when specimens were quenched into water at 70°C, the breakdown of the vapour blanket occurred at a time when the core temperature was still around 550°C - 600°C; at these temperatures the core was still austenitic and able to withstand such a thermal shock. They proposed that the occurrence of a critical diameter, at which quench cracking was most pronounced, was due to a complex interaction between thermal and transformation strains which they were unable to interpret.

---

*an explanation of these terms is given later in section 2.3.2

2.2.2 Residual stress measurements

A number of workers have proposed qualitative theories to explain the mechanism by which quenching stresses are developed; these proposals have been supported by experimentally determined residual stress distributions. However, the amount of published work in this field is still relatively small, which is probably due to the absence of a really simple method by which the residual stresses may be measured.

The different methods available for the measurement of residual stresses have been reviewed extensively[2,5,25,26,30]. The majority of the techniques fall into one of two categories; (viz mechanical and x-ray methods), both of which rely on the application of elasticity theory to determine the stresses present from the measured strains. Chemical etching[27], ultrasonic[2] and hardness testing[2] methods have been proposed, but they all suffer from considerable limitations.

The mechanical methods rely on measurements of the relaxation of the sample after a section of it has been removed. The measurement of the deflection may be carried out by measurement of the change in the dimensions of the specimen or by measurements of the changes in the crystal lattice spacings using x-rays[28]. Care is required during the removal of the material, otherwise additional stresses are liable to be introduced. The most widely used mechanical method is the Sachs boring method[29] which has recently been described by Andrews[2]. The technique is applicable to cylinders and assumes complete axial symmetry. In the case of a solid cylinder, an axial hole is drilled and the changes in axial and tangential strain at the circumference are measured as the bore is progressively enlarged. The principal stresses at any point in the cylinder are assumed to be the axial, tangential and radial stresses and their values are given by:

$$\sigma_z = \frac{E}{(1-\nu^2)} \left[(A_o - A) \frac{\partial \Lambda}{\partial A} - \Lambda \right] \qquad 2.1$$

$$\sigma_\theta = \frac{E}{(1-\nu)^2} \left[(A_o - A) \frac{\partial \Phi}{\partial A} - \frac{(A_o + A)}{2A} \Phi \right] \qquad 2.2$$

$$\sigma_r = \frac{E}{(1-\nu)^2} \left[\frac{(r_o^2 - r^2)}{2r^2} \Phi \right] \qquad 2.3$$

where:

$$\Lambda = (\varepsilon_z^o + \nu\varepsilon_\theta^o) \qquad 2.4$$

$$\Phi = (\varepsilon_\theta^o + \nu e_z^o) \qquad 2.5$$

In practice the quantities Λ and Φ are plotted versus A and their derivatives with respect to A found from the slopes of the respective curves. Figure 5(a) shows an example of the plots of Λ and Φ versus A and Figure 5(b) shows the ensuing stress distribution.

The stresses measured by any of the mechanical methods are always macro-stresses.

The x-ray methods involve the determination, by a back deflection technique, of lattice parameters; which are then used to calculate strain. If the sum of the principal stresses is all that is required, a single exposure method may be used where the x-ray beam is normal to the surface[2]. However, if the magnitudes of the individual principal stresses are required, the "$\sin^2\Psi$" or double-exposure method must be used[31]. In this method a first exposure is made with the x-ray beam normal to the surface, and a second exposure made with the beam at an oblique angle to the surface along one of the principal stress directions.

The main limitation to the accuracy of these methods is the precise measurement of the diffraction ring diameters. Jones[32] has suggested that the accuracy of measurement is ±30 MN/m^2, which is independent of the stress magnitude. X-ray methods also suffer from the major disadvantage that the stresses measured are only surface stresses. Andrews[2] has pointed out that the penetration into the steel by the x-ray beam is normally less than 0.02 mm.

One of the earliest investigations of residual stresses was that carried out by Buhler and Buckholtz[33], who quenched plain carbon steel cylinders of various diameters and carbon contents, after which the Sachs boring method was used to determine the residual stress distributions. The residual stress was found to vary in a complex manner with the radial depth. Consequently an attempt was made to correlate only the maximum values (regardless of whether tensile or compressive) from each cylinder with other experimental variables. The results obtained from water quenched cylinders are shown in Figure 6. The replacement of a water quench by an air cool produced a reduction in the maximum residual stresses (see Figure 7).

Buhler and Buckholtz[34] have also measured the residual stress distributions in hollow cylinders of a 0.3%C steel, which were quenched with coolant at either the inner or outer surfaces, or both. The results, shown in Figure 8, showed that the quenched surface always had a compressive residual stress, even when cooling occurred both from the bore and outside surfaces.

Liss et alia[35] have studied the surface residual stresses induced during the quenching of 50 mm diameter cylinders of plain carbon and low-alloy steels. Since the fatigue test was to be used at a later stage of the work, an x-ray technique was used to measure the surface stresses only. Adjusting the pressure of the cold water spray that was used to quench the specimens allowed the production of variations in the rate of cooling. Residual surface stresses were compressive in all the spray quenched specimens, but an increase in the cooling rate always caused the magnitude of this surface stress to increase, as shown in Figure 9. At the highest cooling rates, residual compressive surface stresses of up to 1500 N/mm^2 were obtained from steels which were not hardened completely through the section. However, for these steels they estimated that the "microstructural misfit" between the case and the core (arising from the different specific volumes of the transformation products) could, at the most, account for surface compressional stresses of 690 N/mm^2 only. Therefore they concluded that the increased compressional stresses at the surface must have been due to "thermal plastic straining". This was substantiated by the dependence of the residual stresses on the severity of the quench. The development of high residual compressive surface stresses was ascribed to tensile plastic flow of the surface layers in the early stages of the quench. This plastic flow was "locked in" as the surface temperature was lowered and was considered to enhance the transformation stresses at lower temperatures. Liss et alia found that steels that possessed high hardenability tended to produce lower compressive surface stresses than steels of low hardenability. Nevertheless, the compressive surface stresses in the high hardenability steels could still be enhanced by an increase in the quench severity.

In their investigations of fatigue properties, Liss et alia also used some oil quenched low-alloy steel cylinders of S.A.E. 8645 and S.A.E. 8660 which had been tempered at 315^{O}C and 425^{O}C respectively. These specimens had tensile residual surface stresses of 33 N/mm^2 and 39 N/mm^2 respectively. A result is also given for a water quenched cylinder of S.A.E. 8645 (tempered at 315^{O}C), which had a compressive surface stress of 288 N/mm^2. No suggestions were made about the mechanism by which "thermal plastic straining", which produced compressive stresses at the surface of water quenched specimens, could produce tensile residual stresses at the surface of oil quenched specimens.

Vannes et alia[36] have also used the Sachs method to study the residual stress distribution in quenched hollow cylinders which were substantially smaller than those of Buhler and Buckholtz[34] (8.22 mm outside diameter and 2 mm internal diameter). Since only a limited number of experiments were performed under any given set of experimental conditions, only very general conclusions can be drawn from their work. Like Buhler and Buckholtz[34], they found that the sealed tubes possessed a different residual stress distribution to the open tubes. Thus Figures 10(a) and 10(b) show the residual stress distributions when 0.46%C specimens were water quenched from 840°C with the bores closed and open respectively. Since the relationship between stress and radial distance was complex they used the parameters θ and Z to assess the overall distribution, where:

$$\theta = \int_{r_i}^{r_e} |\sigma_\theta| \, dr \qquad 2.6$$

$$Z = \int_{r_i}^{r_e} |\sigma_z| \, dr \qquad 2.7$$

The magnitudes of the parameters θ and Z obtained in water quenched specimens were greater than the corresponding values obtained in oil quenched material. The stress distributions were strongly dependent on the carbon content of the material which was considered to be due to the influence of carbon on hardenability. In completely martensitic materials the residual stresses were considered to be the result of the plastic strains produced during quenching. In steels which were not completely martensitic after quenching, the residual stresses were considered to be a combination of the plastic strains produced during quenching, and the stresses created by the different specific volumes of the martensite and ferrite - carbide aggregates; as proposed by Liss [35].

The only published work available on the examination of residual stresses in quenched plates is that of Nakagawa and Tamura[37], who used an x-ray technique to measure the residual stresses in the surface of 50 x 50 x 20 mm plates. The materials used in the investigation were steels, containing between 0.08% and 1%C, which were quenched from temperatures between 800°C and 1000°C. They also quenched plates of two low-alloy steels, SNC2 (0.3%C, 0.44%Mn, 2.75%Ni, 0.79%Cr) and SCM3 (0.40%C, 0.72%Mn, 0.03%Ni, 1.05%Cr, 0.22%Mo). Compressive stresses were found at the surfaces of all the plain carbon steel specimens that had been water quenched, with the maximum level of such stresses produced in material with a carbon content of 0.5%. When the carbon content was less than 0.5%, increased residual compressive stresses at the surface were associated with an increase in the austenitisation temperature, but in material containing more than 0.5%C the reverse behaviour occurred. Both of the low-alloy steel plates had residual tensile surface stresses of between 540 and 570 N/mm^2, irrespective of whether the quenchant was water or oil.

The most extensive experimental investigation of quenching stresses was that of Buhler and Rose[38]. They used the Sachs boring method to measure the residual stresses in steel cylinders of different diameters and compositions that had been quenched in water or oil. For a 0.5%C steel the residual stresses became increasingly more compressive as either the diameter of the specimen or the quenching severity was increased (see Figure 11). The 10 mm diameter cylinder of this material was only fully martensitic when water quenched. Figure 12 shows their results for a low-alloy steel (0.13%C, 0.95%Cr, 0.07%Ni, 0.8%Mo, 0.19%V) of much higher hardenability. In this case an increase in the specimen diameter or quench severity altered the surface stress from tensile to compressive (see Figure 12). Buhler and Rose also found that when a 30 mm diameter cylinder of a 0.26%C, 2.27%Cr, 0.28%Mo steel was water quenched, there was a compressive surface stress of 220 N/mm^2 as shown in Figure 13.

From an analysis of their results, Buhler and Rose[38] proposed five different types of behaviour (shown in Figure 14):-

Group 1	Transformation strains have very little influence on the results in this group. During cooling there are tensile stresses at the surface and compressive stresses at the centre. Once the cylinder has cooled to room temperature these stresses are reversed.
Group 2	Transformation strains reduce the stresses at the centre; but the surface is still left substantially in compression.
Group 3	The stresses due to the thermal contractions are almost completely balanced by transformation strains.
Group 4	At the centre of the cylinders the stresses due to thermal contraction are overridden by transformation stresses and the residual stress distribution is almost completely the reverse of that found in Group 1 behaviour.
Group 5	The Group 1 type of behaviour, in which stresses, due to thermal contractions predominate, has been completely reversed by large transformation stresses.

Murry, however, has argued that Buhler and Rose did not adequately take into account the different linear expansions that accompany the transformation of austenite, which according to Lement[13] are at room temperature:-

1.55 - 0.18 x (%C) if austenite → martensite
1.55 - 0.48 x (%C) if austenite → lower bainite
1.55 - 0.74 x (%C) if austenite → upper bainite

Murry has also pointed out that the thermal contractions are strongly dependent on whether the structure is still austenitic (linear contraction of 1.4% for a 500°C temperature drop) or has transformed to ferrite/pearlite/bainite/martensite (linear contraction of about 0.8% for a 500°C temperature drop). Buhler and Rose's explanations of thermal contraction and transformation stresses were therefore considered an oversimplification of the problem. Murry concluded that these differences could be explained on a qualitative basis, provided that the material was considered to be completely plastic when austenitic, but elastic after transformation had occurred. Thus transformation of the surface produced an elastic skin around the cylinder. When, however, the analysis was attempted for a lower hardenability steel, the required residual surface stresses could be explained only when the surface behaved as an elastic/plastic shell, after it had transformed to a mixture of ferrite and pearlite.

Surface hardening processes which alter the specific volume at the surface, but which do not alter the specific volume at the core of a component, will give rise to residual stresses, even in the absence of any significant thermal gradients. Compressive stresses as high as 1060 N/mm^2 have been measured in the surface of specimens which have been nitrided by glow-discharging at 525°C[40]. Carburising similarly leads to compressive surface stresses, but these stresses may be modified by additional thermal and transformation stresses, when the component is quenched[41]. Any retained austenite in the case will reduce the compressive surface stresses[42]. Induction hardening of a steel surface also increases the specific volume of this part of the component after it has been cooled to room temperature; but this situation will again be modified by thermal and transformation stresses during quenching. Compressive surface stresses of around 1000 N/mm^2 have been found in induction hardened surfaces[43,44].

2.2.3 Distortion measurements

The distortions which occur as a result of heat treatment have been classified into 3 types by K. Sachs:[45]

(i) Changes in volume
(ii) Symmetrical changes in shape
(iii) Warping

Thus the transformation of a structure consisting of a ferrite/carbide mixture to a martensitic or bainitic structure via austenite resulted in a small volume increase. But the situation was more complex when the structure produced was not completely martensitic or bainitic, since the final volume then also depended on the quantities of each phase present after transformation. Symmetrical changes in shape were attributed to internal stresses which were symmetrically distributed in the component. Warpage was the result of any of the causes of distortion that did not act symmetrically on the body.

Lement[13] has reviewed the distortion of tool steels; but has distinguished two types of distortion only. He classified the overall volume change as "size distortion"; but did not distinguish between shape change distortion and warpage, but included both these categories in his description of "shape changes". Lement has given equations that may be used for the calculation of the volume changes of carbon tool steels during hardening: different initial and final structures could be accommodated in the calculation. The volume change for the net "reaction" of a ferrite and cementite aggregate that has been transformed to a martensitic structure can be obtained by adding the appropriate "reactions":-

	Volume Change%
Aggregate of Ferrite and Cementite → Austenite	-4.64 + 2.21 (%C)
Austenite → Martensite	4.64 - 0.53 (%C)
Aggregate of Ferrite and Cementite → Martensite	+ 1.68 (%C)

Llewellyn et alia[46] have measured the density change, $\Delta\rho$, that accompanies the overall change from a ferrite/pearlite structure, using a range of carburising steels. Provided there was no retained austenite in the steels, the density change was found to depend on the carbon content only:-

$$\Delta\rho = 84.13 \times (\%C) \qquad \pm 10\ \text{kg/m}^3 \tag{2.8}$$

This is equivalent to a volume change determined by:-

$$\%\ \text{Volume Change} = 1.09 \times (\%C) \qquad \pm 0.13 \tag{2.9}$$

Several general papers have been published that discuss the causes and control of distortion[6,47,48,49,50]. BISRA[47] have summarised the variables that were thought to influence the distortion of steel components during heat treatment, viz:-

(i) Coefficient of thermal expansion.

(ii) Elastic moduli of the steel.

(iii) Stress-strain characteristics of the steel which determine the stress at which plastic yielding will occur.

(iv) Rate of heat abstraction from the part.

(v) Thermal diffusivity of the steel.

(vi) Volume changes due to transformations.

(vii) Hardenability.

(viii) Size and variation of section size and shape.

(ix) Non-uniformity of chemical composition.

(x) Internal stresses derived from previous operations.

(xi) Externally applied forces.

(xii) Anisotropy of properties.

Details were given of the numerical values of the coefficient of thermal expansion, the elastic modulus, the elastic limit and the thermal diffusivity for the range of steels commonly hardened by quenching and tempering.
It was concluded that though each of these parameters was relevant to the development of distortion, they did not vary greatly from one steel to another, although their variation with temperature was recognised. They suggested the most important variables were:

(i) Hardenability.

(ii) Changes in section size.

(iii) Non-uniformity of chemical composition, particularly carburised cases.

K. Sachs[45], who was primarily concerned with tool steels, found that the distortion of these materials was dependent on the orientation of the direction of working.

He attributed this anisotropic behaviour to the difference between the thermal expansion coefficients of the undissolved carbide stringers and the matrix. Fresher[51] has postulated that a slow heating rate, followed by a rapid cooling rate could cause distortion parallel to carbide stringers by a ratcheting mechanism, but not normal to them. Scott and Gray[52] have similarly found the distortion of high chromium tool steels to be strongly dependent on the alignment of carbide stringers. Plate specimens which had been upset forged to produce a more globular carbide distribution did not show this phenomenon.

The geometry of components has a marked influence on distortion. Thelning[6] has reported examples of the dimensional changes that result from hardening of plain carbon, low-alloy and high speed steels. The examples covered a wide range of engineering components and showed the marked way in which different shapes may produce wide variations in distortion behaviour. The proportion of martensite in the cross section had a significant effect on distortion, as also did the presence of residual austenite.

The influence of geometry has also been investigated by Novik et alia[53], who measured the distortion of rings of different shapes and sizes of a low-alloy steel (0.42%C, 0.71%Mn, 0.9%Cr) that had been quenched from 850°C into oil. The initial outside diameter, internal diameter and thickness of the rings all affected the distortion significantly. Child and Plumb[54] have surveyed the factors influencing the distortion of tool steels during the complete heat treatment process, and have demonstrated that the results from one test piece can not be related to those of another.

Dumont et alia[55] have discussed the way in which the selection of a quenching oil may influence distortion. They have suggested that the high temperature stages of cooling above the M_s temperature are frequently neglected when the choice of oils is made. The main criteria in their selection required that nucleate boiling should have ceased before the M_s temperature had been reached[56]. Dumont et alia argued that although the thermal stresses are weak during the early stages of quenching, they may still cause significant distortion on account of the low elastic limit of the material at the high temperatures during the early stages of quenching. They therefore considered the vapour blanket stage of the quench to have a significant effect on distortion, and suggested that a gradual transition from the vapour blanket to nucleate boiling stages would reduce distortion.

The complex influence of geometry on distortion, has led some investigators to use specimens that required only a single measurement to quantify distortion. An example of one such specimen[13] (the 'Navy C') is shown in Figure 15. Others have based their work on simplified forms of engineering components.

Lacoude and Tricot[57], and later Champin, Seraphin and Tricot[58], have used slit-disc specimens (shown in Figure 16), which were inspired by the 'Navy C' type specimen. The results of work on 42CD4, 25CD4 and 16NC6 steels led to the conclusion that the oil bath temperature markedly affected the amount of distortion; furthermore, an optimum oil bath temperature existed which produced minimum distortion. However, this oil bath temperature was found to be dependent on the specimen material, the austenitisation temperature prior to quenching, and the initial grain size of the specimens.

Variations in the dimensions of carburised gears is a common problem in the automobile industry, consequently an appreciable portion of the work carried out on distortion has been done with carburised specimens. Tricot et alia[57,58], who used slit-disc specimens to study the influence of carburisation on distortion, concluded that the distortion of specimens quenched in cold oil varied directly with the steel hardenability. As was the case with non-carburised specimens, an optimum oil temperature was found at which distortion was a minimum. The depth of the carburised case was found to influence distortion, and for case depths of between 0.9 mm and 1.2 mm the distortion was found to increase in proportion to the case depth.

Hopkins and Holland[59] have used 'Navy C' specimens to examine the distortion of a carburised 2%NiMo steel. Two casts of the steel were used, the compositions of which were: A - 0.22%C, 0.24%Si, 0.57%Mn, 0.33%Cr, 1.75%Ni, 0.28%Mo and B - 0.20%C, 0.29%Si, 0.53%Mn, 0.33%Cr, 1.7%Ni, 0.26%Mo. However, although the compositions of the casts were similar, the mean distortion of oil quenched specimens of cast A was found to be twice that of cast B. This inherent difference between the characteristics of the two casts had a greater influence on the distortion than any of the other variables investigated. Unlike Tricot et alia[57,58], Hopkins and Holland found that variations in the case depth of between 0.5 mm and 1 mm had no significant effect on distortion. Likewise, variations in the quenching temperature between the limits of 800°C and 850°C did not affect the amount of distortion.

Practical examples of the distortion of carburised gears have been given by Mocarski[15], who pointed out that an increase in the carbon content of the case altered the characteristics of the martensite transformation (see Figure 17). Thus during quenching, the core transformed before the case, which was still austenitic owing to its lower M_s temperature. Mocarski suggested that under these conditions the soft case distorted in order to accommodate the transformation strains produced in the core.

Llewellyn and Cook[14] have carried out an extensive investigation into the distortion of carburising steels using washer-like specimens. During a previous investigation at the same laboratories[60] using 'Navy C' specimens, gap openings of up to 1.2 mm had been found, which were considerably larger distortions than are normally found with carburised gears. A washer-like specimen was therefore developed (see Figure 18) which represented a simple, toothless gear, although the greater section size made this specimen more susceptible to changes in the steel hardenability. Various low-alloy and Mn-B steels were used in the investigation in both the carburised and non-carburised conditions. Compositions used included chromium contents of up to 3% and nickel contents of up to 4¼%.

Four major factors were found to have a significant influence on distortion:

(i) Cooling rate

(ii) Carburising

(iii) Hardenability

(iv) Composition

Of these variables, cooling rate was by far the most important. Like Mocarski[15], Llewellyn and Cook[14] considered the influence of carburising on distortion to be associated with the different temperatures at which the case and core transformed during quenching. Furthermore, the distortion of steels with low hardenability was affected by carburising to a greater extent than steels with higher hardenabilities. The cores of specimens with low hardenability transformed at relatively high temperatures, and thus the distortion of these specimens was considered more susceptible to a reduction in the M_S temperature of the case as a result of carburising.

The influence of hardenability was investigated by the use of steels of various nickel and chromium contents. Llewellyn and Cook argued that, although hardenability and chemical composition are related, the influence of hardenability on distortion will cease when the hardenability becomes great enough to produce martensite throughout the section. Further alloy additions only depress the M_s and M_f temperatures. Therefore a factor was used to describe the hardenability of the steels, which became unity when the structures became completely martensitic. The distortions of all the non-carburised specimens (with the exception of the boron steels) were then compared with this hardenability factor, provided the value of this factor was less than unity; at higher hardenabilities, the distortions were compared with the M_s temperatures (see Figure 19). A good correlation was obtained with the distortion of a wide range of low-alloy steels, although boron steels exhibited a considerable difference in behaviour from other materials of similar hardenability. The distortion of these steels was generally large, and no satisfactory explanation for their unique behaviour could be given; although it was tentatively suggested that the different behaviour of these steels was the result of marked depression in the M_s - M_f temperature range, on account of the presence of interstitial boron atoms.

Llewellyn et alia[61] have also reported on the distortion of ferritic (0.04%C, 20.64%Cr) and austenitic (0.03%C, 18.6%Cr, 9.47%Ni) stainless steel specimens which had been quenched from 840°C at different rates (see Figure 20). Since neither of these steels transformed during quenching, the distortions were the result of thermal contractions alone. The different behaviours were qualitatively explained by the differences in the thermal conductivities of the materials. Over the temperature range involved, the ferritic steel possessed a 50% higher thermal conductivity than the austenitic steel. It was suggested that the surface regions of the austenitic steel specimen would be cooled more quickly, which would provide early in the quenching process a skin around the outside of the specimen strong enough to withstand the contractional stresses of the core. In the ferritic material, although there would be smaller contractional stresses, the core would be more liable to plastic flow, on account of the lower high temperature strength compared with the austenitic material. Consequently there would be, in this latter case, a reduction of the specimen dimensions.

It has been widely proposed that interrupted quenching can reduce distortion[59,62,63]. K. Sachs[45], however, has reported the effects of martempering on the distortion of a 13%Cr, 2.25%C die steel, where martempering did not produce greatly different distortions from normal oil quenching and, in the case of certain geometries, resulted in increased distortion. This behaviour was attributed to the severity of the molten salt quench to the intermediate temperature in combination with a holding time, which allowed the austenite to relieve the quenching stresses by distortion. Priestner and Hasan[64] found that interrupted quenching increased the bending distortion of their carburised specimens, but reduced it in non-carburised specimens. The explanation of this effect was similar to that of Sachs.[45]

2.3 Prediction of Thermal Stresses During Quenching

Analytical solutions to thermal stress problems are available for simple shapes with simple temperature distributions[65,66,67] provided plastic flow does not occur. When plastic flow occurs, the mathematics of the problem become increasingly more intractable and solutions are available only for special cases[67,63,69], none of which are relevant to the problem involved in the quenching of steel components. Denton[5,16] and Andrews[2] have both described the essential steps required for the calculation of quenching stresses. The first step involves the calculation of the temperature distribution within the body at different times during the quench. Secondly, the elastic stress distribution that results from the change in temperature distribution during each time increment must be found, assuming that external loads and moments are applied to constrain each element within the body. The third step, is the removal of the applied forces and moments, which causes the different elements in the body to deform (either elastic and/or plastic strain), in such a way that not only is complete compatability retained between the elements, but also the internal stresses produce both force and moment equilibrium throughout the body. The complete analysis of the stress and strain behaviour during the whole of the quench is obtained by repeating this process after each time increment during the quench.

It is the possibility of plastic flow during the third step of this procedure that creates the greatest difficulty. In 1947 Russell[70] published the results of calculations of stresses in quenched steel cylinders, in which he assumed the material behaviour was always elastic; this assumption was necessary because, at that time, it was not possible to solve the problem when plastic flow occurred. Only in recent years has the increased use of digital computers enabled attempts to be made at complete solutions to the problem of stress generated in quenched specimens of simple shape. Nevertheless, Russell[70] proposed that before quenching stresses could be calculated, there were five subsidiary problems to be considered:-

(i) The calculation of the temperature distribution throughout the body, allowing for the heat generated during the decomposition of the austenite.

(ii) The progress of the decomposition of the austenite phase at different positions in the body.

(iii) The determination of the elastic constants over the temperature range involved.

(iv) The determination of the flow stresses and plastic behaviour over the temperature range involved.

(v) The influence of pressures set up during partial transformation on the remainder of the transformation.

2.3.1 The calculation of temperature distributions in the body

The effect of time on the temperature distribution within a quenched steel component is described by the differential heat conduction equation[71]

$$\frac{\partial}{\partial x}\left(\frac{\lambda\partial\theta}{\partial x}\right)+\frac{\partial}{\partial y}\left(\frac{\lambda\partial\theta}{\partial y}\right)+\frac{\partial}{\partial z}\left(\frac{\lambda\partial\theta}{\partial z}\right)+Q=\rho Cp\frac{\partial\theta}{\partial t} \qquad 2.10$$

The solution of this equation is difficult and simplifying assumptions are invariably necessary. Three different techniques are available for its solution :

(i) Analytical solutions involving classical calculus techniques.

(ii) Numerical solutions (finite difference and finite element methods).

(iii) Analogue solutions.

Examples of analytical solutions are available in most of the standard heat transfer texts[71,72], but the range of solutions is severely limited by the restrictions required to the initial and boundary value conditions. It is essential that the initial and boundary conditions are invariable, or else vary as some simple function of the variable concerned. It will be seen later that during quenching, all of the thermal properties described in equation 2.10 are temperature dependent. In particular, the boundary condition represented at the surface by the heat transfer coefficient varies markedly with temperature in an irregular fashion. Analytical solutions are not available under these circumstances.

Various numerical methods for the solution of the transient heat conduction problem have been proposed. Finite difference solutions have been given by Dusinberre[73] and Adams and Rogers[74]. Two categories of finite difference solutions exist which are either explicit or implicit. For the one-dimensional problem the explicit formulation is given by:[74]

$$\frac{\theta_i^{n+1} - \theta_i^n}{\Delta t} = \alpha_{td}\left[\frac{\theta_{i+1}^n - 2\theta_i^n + \theta_{i-1}^n}{(\Delta x)^2}\right] \qquad 2.11$$

when

$$\frac{\alpha_{td}\Delta t}{(\Delta x)^2} = \tfrac{1}{2} \qquad 2.12$$

this reduces to the well known Schmidt formulation:-[73]

$$\theta_i^{n+1} = \frac{\left(\theta_{i+1}^n + \theta_{i-1}^n\right)}{2} \qquad 2.13$$

The implicit formulation is given by

$$\frac{\theta_i^{n+1} - \theta_i^n}{\Delta t} = \alpha_{td}\left[\frac{\theta_{i+1}^{n+1} - 2\theta_i^{n+1} + \theta_{i-1}^{n+1}}{(\Delta x)^2}\right] \qquad 2.14$$

Attempts have been made to compromise between the implicit and explicit formulations; the Crank-Nicolson method[75] falls into this category:-

$$\frac{\theta_i^{n+1} - \theta_i^n}{\Delta t} = \frac{\alpha_{td}}{2(\Delta x)^2}\left[\left(\theta_{i+1}^{n+1} + \theta_{i+1}^{n}\right) - 2\left(\theta_i^{n+1} + \theta_i^n\right) + \left(\theta_{i-1}^{n+1} + \theta_{i-1}^{n}\right)\right] \qquad 2.15$$

when

$$\frac{\alpha_{td}\Delta t}{(\Delta x)^2} = 1 \qquad 2.16$$

this reduces to the simpler form[75]:-

$$\theta_i^{n+1} = \tfrac{1}{4}\left(\theta_{i+1}^{n+1} + \theta_{i+1}^{n} + \theta_{i-1}^{n+1} + \theta_{i-1}^{n}\right) \qquad 2.17$$

Rigorous derivations of these finite difference formulations can be obtained from expansions of the Taylor Series[76]. The representation of the differentials by finite differences gives an error resulting from the truncation of the Taylor Series and is of the order of $(\Delta x)^2$.[74] Truncation errors can be tested for by comparing solutions obtained with different values of Δx.[77] Inaccuracies may also arise as a result of the growth of errors during the course of the solution. In the case of explicit solutions, errors will not grow provided[74]

$$\frac{\alpha_{td}\Delta t}{(\Delta x)^2} \leq \tfrac{1}{2} \qquad 2.18$$

Implicit formulations do not suffer from this drawback and are stable for all values of the left hand side of the equation 2.18[78].

The finite difference methods of solution are particularly suitable for use with digital computers, are not dependent on fixed boundary conditions, and can be modified to allow for temperature dependent thermal properties and latent heat evolutions[79]. The methods of formulation can also be modified to analyse two and three dimensional heat flow[74].

Finite element methods for the solution of the differential heat conduction equation have also been developed for use with digital computers.[80,81,82] The relevant equations for the interior nodes of an infinite plate subjected to one-dimensional heat flow have been given by Lemmon and Heaton[83] as:

$$\left(\tfrac{1}{6} - \phi M\right)\theta_{i-1}^{n+1} + 2\left(\tfrac{1}{3} - \phi M\right)\theta_{i}^{n+1} + \left(\tfrac{1}{6} - \phi M\right)\theta_{i+1}^{n+1}$$

$$= \left[\tfrac{1}{6} + (1 - \phi)M\right]\theta_{i-1}^{n} + 2\left[\tfrac{1}{3} - (1 - \phi)M\right]\theta_{i}^{n}$$

$$+ \left[\tfrac{1}{6} + (1 - \phi)M\right]\theta_{i+1}^{n} \qquad 2.19$$

where:-

$$M = \frac{\alpha_{td}\Delta t}{(\Delta x)^2} \qquad 2.20$$

The equation reduces to a backward-difference form for $\phi = 1$, a forward-difference form for $\phi = 0$, and mid-difference form for $\phi = \frac{1}{2}$. The physical difference between this finite element formulation and the finite difference formulations is that the finite element method uses a weighted average of three discrete temperatures for the thermal storage term, whilst the finite difference methods use a central temperature only. Lemmon and Heaton have shown this leads to only a slight improvement in accuracy whilst the stability limitations are much more restrictive. Furthermore, the finite element methods require substantially more computer time.

Several workers have developed analogue methods of solution to transient heat conduction problems. Liebermann[84] has described an electrical analogue, and hydraulic analogues have been described by Juhasz[85] and Coyle[86]. The accuracy of these methods is limited by the control of experimental variables and it is difficult to use results from them directly for subsequent digital computations.

2.3.2 Heat transfer at the surface during quenching

The heat transferred from the surface of a body represents one of the boundary conditions for equation 2.10 and must therefore be established if the thermal stress problem is to be solved.

(a) General characteristics of surface heat transfer during quenching

The relationship between time and temperature during quenching of a steel component in a liquid is now well understood. Figure 21 shows typical cooling curves at the surface and centre of a hot solid when quenched into a cold liquid; the simplest classification involves the following stages[87]:-

Stage A′ is extremely brief and is sometimes called the "initial liquid contact stage". It is usually considered unimportant, and its detection requires a very sensitive measuring system; even then it may be undetectable in some quenchants. Stage A, the "vapour blanket stage" is characterised by the formation of a vapour blanket around the specimen. It occurs when the heat flux from the specimen is greater than that required to form a continuous film of vapour around the specimen surface. The vapour blanket acts as an insulator so that the cooling rate is low. Heat transfer occurs mainly by radiation through the vapour blanket to the surrounding liquid.

Stage B, the "vapour transport cooling stage" or "nucleate boiling stage" is characterised by the highest cooling rate. The temperature difference between the specimen surface and quenchant is too small to maintain an unbroken vapour blanket, and the liquid in contact with the hot surface generates nucleate boiling. Heat transfer involves the removal of latent heat of vaporization of the liquid.

Stage C, the "liquid cooling stage" or "convection stage" commences when the specimen surface is too cool to nucleate vapour bubbles, and boiling ceases. Heat transfer is by natural or forced convection, depending on whether or not the quenchant is agitated.

A number of highly empirical tests have been used commercially[88,89] to assess quenchants, under circumstances where the primary concern has been the time taken for a specimen to cool to a specific temperature, regardless of the heat transfer mechanisms involved. The characterisation of the quenchant behaviour from cooling curves obtained by temperature measurements within the specimen are of limited value, although this technique has been widely used to analyse and compare the behaviours of different quenchants.[23,90,91,92] Quench data presented in the form of cooling curves cannot be used directly in the solution to the differential heat conduction equation. Furthermore, even though the heat transfer mechanisms operating during the quench are dependent on the temperature at the specimen surface, the vast majority of published cooling curves refer to temperatures measured at the centre of specimens.[90,91,92] Knowledge of the variation of the surface heat transfer coefficient with surface temperature is required for the correct analysis of quenchant behaviour, since this information can be used directly in the calculation of time-temperature distribution in quenched components.[93]

(b) The measurement of surface heat transfer coefficients during quenching

The surface heat transfer coefficient, h, is defined by:-[98]

$$\lambda \left(\frac{d\theta}{dx} \right)_{\text{surface}} = h \left(\theta_{\text{surface}} - \theta_{\text{environment}} \right) \qquad 2.21$$

During quenching, when the heat flow at the surface and the rate of change of surface temperature are both very high, the direct measurement of these entities is very difficult.[96,97] Therefore, in practice, it is necessary to measure the temperatures at interior points, and to extrapolate the results in order to determine the temperature and temperature gradient at the surface.[98]

The easiest solution to the problem was the "lumped parameter" approach,[99,100] when it was assumed that there was negligible temperature gradients within the specimen. In this case the heat flux from the specimen was given by:

$$Q'' = -\left(\frac{V}{A} \right) \rho \; Cp \; \frac{d\theta}{dt} \qquad 2.22$$

where Q" is the heat flow rate per unit area.

This approach was considered accurate provided that the Biot number was less than 0.2.[101,102] Bergles and Thompson[99] used it with water quenched copper specimens and suggested that with a maximum Biot number of 0.24 their results were accurate to within ±3°C. The "lumped parameter" approach was also used by Simon and Bigot[96] to calculate the heat fluxes produced during the quenching of thermocouple junctions.

Lambert and Economopoulos,[98] who developed cylindrical and plate probes to measure h, found that perturbations in the surface heat flux became progressively more attenuated as the distance of the point of temperature measurement from the surface was increased. Figure 22 shows the variation of the mean error "t" in h values as a function of the depth beneath the surface of a 20 mm diameter probe. Unfortunately, Lambert and Economopoulos have not given details of the absolute magnitude of h on which these calculations were based. Because of the practical problems of drilling small deep holes accurately, thermocouples were located at 1 mm depth, and an implicit finite difference solution of the heat conduction equation was used to obtain h from the experimental cooling curve data.

Paschkis and Stolz[95] have also pointed out that the thermocouple should be located as close to the surface as possible. During investigations with 25 mm and 50 mm diameter spheres, it was found that temperature gradients could be ignored when the values of h were low (e.g. in vapour blanket and convection stages). At higher values of h, when significant temperature gradients occurred within the specimens (e.g. in nucleate boiling stages), they developed two methods of solution[95] based on an electrical analogue and a numerical step-wise solution to the inverse heat conduction problem. With very high heat transfer rates, both methods of solution were liable to become unstable.

Beck and Chevrier[103] have used cooling curves measured at the centres of cylinders of 10 to 30 mm diameter to determine surface heat fluxes. Radial heat flow only was considered, despite a diameter to height ratio of merely 1:3. The use of an explicit finite difference method to analyse the cooling curve data required small time intervals in order to meet the relevant stability criteria: thus a typical experiment lasted 60 seconds and involved about 60 experimental readings, whereas 1,000 readings were needed for the numerical analysis of the results. The problem was overcome by fitting polynomials to the experimental data and interpolating to obtain temperatures at the required small time increments.

Mitsutsucka and Fukuda[104] have also used an explicit finite difference method to evaluate h from cooling curves measured at the centres of quenched plates of 28 mm thickness. For each value of experimental time and temperature they made an initial estimation of h, which was used to obtain a calculated time and temperature at the end of the step. The estimate of h was then successively adjusted until, at the end of each step, adequate agreement was reached between the calculated and experimental time/temperature data.

(c) Comparison between surface heat transfer during quenching and that obtained during steady state conditions

Nukiyama[105] and Farber and Scorah[106] were some of the earliest workers to investigate steady state boiling phenomena by heating wires submerged in water. These results were expressed as the "boiling curve", shown in Figure 23. Although a large amount of research has been carried out on heat transfer by nucleate boiling under steady state conditions,[107,108,109,110] it has been found that the correlations between heat transfer and the other experimental variables concerned are prone to large errors.

This has been attributed to the complexity of the velocity and temperature profiles that occur in the multiphase environments which are present.[74] In particular, the most difficult problem has been considered to be the estimation of the point at which a transition from nucleate boiling to film boiling has occurred.

Mitsutsuka and Fukuda[111] found that all the characteristic stages in the boiling curve were present in cooling curves measured near the surface of quenched specimens. Bergles and Thompson[99] directly compared the surface heat transfer fluxes in the steady state with those obtained during quenching, and concluded that there were significant differences between them. Some of the differences, however, were subsequently attributed to erroneous variations between the surface conditions of the specimens used.

Lambert and Economopoulos[98] have pointed out that, for the purposes of subsequent heat transfer calculations, a knowledge is not required of the complex heat transfer mechanisms that occur during quenching. Surface heat transfer coefficients evaluated during the course of a quench were considered applicable provided that the surface conditions of the specimens used to evaluate h were comparable with those which occurred in practice.

(d) Influence of experimental variables on the surface heat transfer coefficient

(i) Type of Quenchant

This has the largest influence on h. Numerous surveys have been carried out on the influence of different quenchants during quenching[55,87,91,112], although much of the data is presented only in the form of cooling curves. Most quenchants are either aqueous solutions or oil: aqueous quenchants usually give higher cooling rates. However, solutions of NaCl and NaOH give faster cooling rates than water alone. Mixtures of water with polymers or oils are reported to be capable of cooling rates intermediate between those of water and oil alone.[95,113] Quenching oils are usually categorised as fast, intermediate and slow, although the only significant differences between such oils has been shown to be the temperature at which the vapour blanket breaks down.[94] Recently, substantial industrial interest has been shown in certain polymer quenchants[92,114] which become less soluble in water as the temperature of the solution is increased and are said to exhibit "inverse solubility". This class of polymers are soluble in water at low temperatures only (e.g. below ~80°C).[113] When a component is quenched, the water solution around it is warmed and a layer of the polymer is deposited on the component, which reduces the surface heat transfer coefficient.[113]

(ii) Component Size and Shape

Component shape is known to have an influence on h. Nucleate boiling commences at edges and corners[87,99,104] and vapours may be trapped in any recesses. The direction in which a component is quenched also has an influence. Mitsutsuka and Fukuda[115] found that the value of h obtained on the underneath surface of a plate, quenched in a horizontal position, was substantially different from that obtained at the upper surface. This was due to the entrappment of vapour underneath the plate.

Originally it was believed that h was largely independent of the object size, provided the size of the object being quenched was sufficiently small in relation to the volume of quenchant used.[95] However, Kobasko and Federov[116] have proposed a "self-regulating" thermal process that can occur at the surface of water quenched components: the mechanism of this process is dependent on specimen size, though the mechanism has been strongly criticised by Troyanov.[117] Also, from thermocouples located at the centres of water quenched plates, Mitsutsuka and Fukunda[115] found that h decreased as the plate thickness was increased, (e.g. for a 28 mm thick plate, the maximum value of h was 7,790 W/m^2°C at 250°C, whereas for a 110 mm thick plate it was 5,230 W/m^2°C at 190°C).

Beck and Chevrier[103] reported a dependence of h on specimen size during experiments that involved the quenching of nickel cylinders in boiling water. Figure 24 reports their results, which showed the variation of surface heat flux with surface temperature (calculated from thermocouple measurements made at the centres of the cylinders). It was observed that nucleate boiling started at the bottom of the cylinders and moved upwards as a front (shown schematically in Figure 25). The dependence of h on the diameter of the cylinders was attributed to an anomoly caused by the narrow width of the nucleate boiling front. Thus the sharp increase in cooling rate experienced at the centre of the cylinder as the nucleate boiling front moved up past it, was reduced by the vapour blanket and convection stages above and below it respectively. They proposed that this effect was accentuated as the cylinder diameter was increased, so that h appeared to be influenced by the specimen diameters.

Paschkis and Stolz[95] quenched both 25 mm and 50 mm diameter spheres during the course of their work but have not reported any dependence of h on specimen size.

(iii) Material

The surface heat transfer coefficient was originally considered to be independent of the specimen material[93]. Differences between the surface heat transfer coefficients of specimens made from different materials were attributed to the different nature of the oxide films present[95]. Thus Lambert and Economopoulos[98] compared h values from a water quench using nickel and mild steel specimens. Provided the steel specimens were oxide free they found that there was little difference in behaviour (see Figure 26). However, Beck and Chevrier[103] found that the heat flux at the surface of 30 mm diameter cylinders when quenched in water was different in the cases of nickel and aluminium cylinders (see Figure 27). Initially these differences were attributed to the narrow width of the nucleate boiling front as already described above. Thus differences in the thermal properties of the specimens were considered to produce a similar effect to a change in specimen size. However, in a more recent paper with Flament and Moreaux[118] they have reported the surface heat fluxes measured from 16 mm diameter Al, Ni and Ag cylinders when quenched in boiling water (see Figure 28). Owing to the small diameter of these specimens the different values of h obtained with the different materials were not attributed to the relatively narrow width of the nucleate boiling front as before. They concluded that the temperature at which the vapour blanket broke down and the maximum nucleate boiling heat flux were apparently dependent on the specimen material. Thus making it impossible to completely characterise a quenchant by a heat flux relationship dependent on the surface temperature alone.

(iv) Surface Condition

Steady state experiments have shown that surface condition is a major variable.[108,109] Surface roughness affects radiation heat transfer[119] and hence the generation of a stable vapour blanket. Surface roughness also has a considerable effect during the nucleate boiling stage, since it has a marked influence on the nucleation and release of vapour bubbles, and increased roughness extends the range of temperatures over which nucleate boiling occurs.[108]

Surface oxides and other deposits have been found to have a complex effect on the surface heat transfer coefficient during quenching. Lambert and Economopoulos have found that the magnitude of the surface heat transfer coefficients obtained during the quenching of mild steel specimens were generally reduced by an increase in the amount of surface oxidation (see Figure 29). For steady state nucleate boiling, Labunstov[109] has suggested that the "wettability" of the surface can significantly affect surface heat transfer. Furthermore, he obtained evidence that small quantities of scale or oxide may, in some cases, enhance surface heat transfer by aiding nucleation. Paschkis and Stolz[95] considered that carbonaceous deposits, which had formed on the surface of specimens during oil quenching, had aided surface wetting and hence produced an 80°C rise in the temperature at which the vapour blanket stage ended and transition boiling commenced. An essential part of this hypothesis proposed that liquid/solid contact occurred during transition boiling. At the time, this proposal was controversial[120,121,122] but Kesselring et alia[123], and Canon and Park,[124] have more recently demonstrated that such solid/liquid contact can occur.

Beck and Chevrier[125,126] found that a thin layer of a material of low thermal conductivity can actually accelerate cooling. This phenomenon was attributed to the layer restricting heat transfer initially and de-stabilising the vapour blanket. Figure 30 shows the influence of a 0.5 mm layer of $CaSO_4$ on the cooling curve of a plain carbon steel specimen.

(v) Initial Specimen Temperature

Paschkis and Stolz [95] measured the surface heat transfer coefficients of silver spheres when quenched from temperatures between 430°C and 870°C into cold still water. The results obtained showed that as the initial specimen temperature was lowered, the vapour blanket took longer to become established, but the values of the surface heat transfer coefficient were the same for the remainder of the quench.

(vi) Quenchant Temperature

The initial temperature of a quenchant controls the amount of heat that must be transferred to the quenchant before boiling occurs; hence the initial temperature of a quenchant has a pronounced effect on the surface heat transfer during quenching.[127] The stability of the vapour blanket stage is increased as the initial temperature of the quenchant is increased and the vapour blanket persists to lower temperatures.[23,95,103,111]

(vii) Quenchant Agitation

The general effect of increased agitation is to accelerate the overall cooling rate, and the control of agitation is a long established principle in quenching operations.[87] Mansion[91] has investigated the influence of agitation on the cooling mechanism of oils and found that agitation did not greatly affect the temperature ranges over which the different heat transfer mechanisms operated. The cooling rate in the nucleate boiling stage was slightly increased, but the greatest effect occurred in the vapour blanket and convection stages. Paschkis and Stolz[95] and Lambert and Economopoulos[98] found the greatest effect of agitation occurred in the vapour blanket stage, where it reduced the stability of the vapour blanket. In extreme cases, e.g. spray quenching, the vapour blanket may become completely broken up.[128] These findings are in agreement with those of Labunstov[109], who concluded that under steady state conditions, the heat transfer in the nucleate boiling stage was insensitive to circulation, though circulation affected the minimum and maximum surface temperatures at which nucleate boiling occurs.

2.3.3 The relationship between temperature and position during quenching

The relationship between temperature and position in a quenched specimen may be determined either experimentally or else by the solution of the relevant heat conduction equations. The first method involves the determination of the relationship between time and temperature by the use of thermocouples placed at various depths in the specimen.[126,129] Temperatures at intermediate locations must be found by interpolation. This technique is the most reliable, but it is extremely laborious and the results are normally applicable only to one specific set of experimental conditions. The alternative involves the solution of the differential heat conduction equation, using the relevant boundary conditions and material properties. This method is very versatile since it may readily be adapted to any experimental situation. However, it is in practice limited by the lack of accurate physical property data required in the calculation.

A development of the experimental technique was employed by Tokihiro and Tamura[130], who determined cooling curves at the centre of a quenched specimen. From this "master cooling curve" predictions were made at the centres of specimens of various sizes by the use of empirical relationships.

Archambault and Chevrier[131] have used an implicit finite difference method to calculate the temperature gradients produced in nickel cylinders that had been quenched in boiling water. This utilised a bi-dimensional solution to the heat conduction problem, with heat extracted radially from the cylindrical surface as well as axially through the bottom of the cylinder. The thermal properties of nickel were considered to be independent of temperature so that the surface heat transfer coefficient was the only temperature dependent variable. The effect of temperature on the surface heat transfer coefficient was represented by two linear functions, which approximated to results obtained in the vapour blanket and nucleate boiling stages. The calculated temperatures at the centre of the cylinder agreed well with those measured experimentally.

Unlike nickel, the thermal conductivity and specific heat of steel vary considerably with temperature[132], and should be taken into account if accurate solutions to the differential heat conduction equation are required. Fitzgerald and Sheridan[133] have analysed the re-heating of slabs by the use of an explicit formulation of the differential heat conduction equation for one-dimensional heat flow:

$$\theta_i^{n+1} = \theta_i^n \left(\alpha_{td}\right)_{\theta_i^n} \left(\frac{\Delta t}{(\Delta x)^2}\right)\left(\theta_{i-1}^n - 2\theta_i^n + \theta_{i+1}^n\right) \qquad 2.23$$

Since this investigation involved the heating of a low-carbon steel, the relationship between temperature and both thermal conductivity and specific heat were well known.[134] The effect of temperature on density was not included in their evaluations of thermal diffusivity since the mass of the elements remained constant during heating. The value of thermal diffusivity used at each step in the solution, $\left(\alpha_{td}\right)_{\theta_i^n}$, was based on the temperature of the element at the end of the previous time interval.

Davis[135] has investigated the effect of the introduction of variable thermal properties into calculations of the temperature distributions within quenched steel plates. For elements within the plate, the same finite difference formulation as Fitzgerald and Sheridan was used (equation 2.23), but an iterative method was applied to the surface element. Thus the thermal properties at the old time were used to obtain a first estimate of the surface element temperature at the new time. The temperature at the old and new time were averaged and the thermal properties of the surface element at the average temperature were then used to obtain a second estimate for the surface temperature at the new time. The process was repeated until adequate agreement was achieved. Figure 31 shows the comparison made by Davis between calculated and actual temperatures in a 100 mm mild steel plate that had been water quenched from 900°C. It is evident that there was good agreement at most positions in the plate, but less agreement close to the quenched edge. The surface heat transfer coefficient used in the calculations was given a value of 4.2×10^4 W/m^2°C, but Davis made no reference to the quenching conditions used during the experiment.

Hengerer et alia[136] have used an implicit finite difference method to calculate the temperature distributions in 50 - 1600 mm plates and 100 - 2000 mm diameter cylinders of various low-alloy steels. These calculations used physical property data that varied with temperature[137] (see Figure 32). The surface heat transfer coefficient was obtained from the relationship between temperature and time at a point 0.5 mm below the surface of a cylindrical specimen of the appropriate material: this calculation assumed that no temperature gradient existed in the cylinder during the quench, which must be considered very improbable in view of the high rates of cooling involved. The calculated temperature distributions were compared with published experimental data but reasonable agreement was only found in a limited number of cases.

A major limitation to the accurate calculation of temperature distributions during the quenching of steel plates has been the lack of accurate data relating to the surface heat transfer coefficient and thermal properties of the material during quenching. Unfortunately, most of the data available on the variation of the thermal properties of steels with temperature has been obtained during the heating cycle,[134] when hardenable steels are ferritic or martensitic for most of the temperature range. Atkins et alia,[138] however, have provided data for the variation of λ and Cp of a 3½%Ni, 1.55%Cr, 0.45%Mo, 0.3%C, 0.1%V steel for both the heating stage and the subsequent quenching operation from the temperature at which austenite had become stable (see Figures 33 and 34). This data clearly shows that the values of λ and Cp vary significantly between heating in the ferritic condition and cooling from the high temperature austenitic condition.

2.3.4 Calculation of thermal stress during quenching

(a) Solutions using classical calculus methods

Several general texts are now available on the subject of thermal stresses. Johns[66] has dealt with thermo-elastic stresses associated with steady-state and some transient temperature distributions. Benham and Hoyle[69] have given solutions to steady-state and transient thermoelastic problems, and have also indicated a method of solution to similar problems when plastic flow is present in some parts of the material. The most authoritative texts on the subject are those due to Boley and Weimer[67] and Manson[139] which deal with situations where regions of both elastic and plastic deformation are produced. Boley and Weiner[67] have defined the complete problem to be solved when a thermal gradient generates elastic stresses provided that no thermo-mechanical coupling occurs and the temperature distribution is known; thus the problem involves:-

6 stress components: σ_{xx}, σ_{yy}, σ_{zz}, σ_{xy}, σ_{yz}, σ_{zx}

6 strain components: ε_{xx}, ε_{yy}, ε_{zz}, ε_{xy}, ε_{yz}, ε_{zx}

3 displacement components: u, v, w

The values of these functions must be such that the boundary conditions and the following 15 equations are met throughout the body:

3 equilibrium equations:

$$\frac{\partial \sigma_{xx}}{\partial x} + \frac{\partial \sigma_{xy}}{\partial y} + \frac{\partial \sigma_{xz}}{\partial z} + X = 0 \qquad 2.24$$

$$\frac{\partial \sigma_{xy}}{\partial x} + \frac{\partial \sigma_{yy}}{\partial y} + \frac{\partial \sigma_{yz}}{\partial z} + Y = 0 \qquad 2.25$$

$$\frac{\partial \sigma_{xz}}{\partial x} + \frac{\partial \sigma_{yz}}{\partial y} + \frac{\partial \sigma_{zz}}{\partial z} + Z = 0 \qquad 2.26$$

6 stress-strain relations:

$$\varepsilon_{xx} = \frac{1}{E}\left[\sigma_{xx} - \nu(\sigma_{yy} + \sigma_{zz})\right] + \alpha_{ex}\theta \qquad 2.27$$

$$\varepsilon_{yy} = \frac{1}{E}\left[\sigma_{yy} - \nu(\sigma_{zz} + \sigma_{xx})\right] + \alpha_{ex}\theta \qquad 2.28$$

$$\varepsilon_{zz} = \frac{1}{E}\left[\sigma_{zz} - \nu(\sigma_{xx} + \sigma_{yy})\right] + \alpha_{ex}\theta \qquad 2.29$$

$$\varepsilon_{xy} = \frac{1}{2G}\sigma_{xy}; \quad \varepsilon_{yz} = \frac{1}{2G}\sigma_{yz}; \quad \varepsilon_{zx} = \frac{1}{2G}\sigma_{zx} \qquad 2.30$$

And 6 strain-displacement relations:

$$\varepsilon_{xy} = \frac{1}{2} \nu_{xy} = \frac{1}{2}\left(\frac{\partial u}{\partial y} + \frac{\partial v}{\partial x}\right) \qquad 2.31$$

$$\varepsilon_{yz} = \frac{1}{2} \nu_{yz} = \frac{1}{2}\left(\frac{\partial v}{\partial z} + \frac{\partial w}{\partial y}\right) \qquad 2.32$$

$$\varepsilon_{zx} = \frac{1}{2} \nu_{zx} = \frac{1}{2}\left(\frac{\partial w}{\partial x} + \frac{\partial u}{\partial z}\right) \qquad 2.33$$

$$\varepsilon_{xx} = \frac{\partial u}{\partial x}\,; \quad \varepsilon_{yy} = \frac{\partial y}{\partial y}\,; \quad \varepsilon_{zz} = \frac{\partial w}{\partial z} \qquad 2.34$$

Solutions to these equations can only be obtained by classical calculus techniques in a small number of cases, where assumptions can be made that allow the simplification of the above equations. Where plastic flow is an additional complication, solutions have only been obtained to special, simple problems. Weiner[68] has described an elasto-plastic transient thermal stress analysis of a plate free from edge restraint that was heated on one surface only. The solution method was based on the Prandtl-Reuss stress-strain relations and the Von Mises yield criteria for plane stress conditions. The material was assumed to exhibit no strain hardening. In order to obtain a solution, Weiner assumed constant thermal and mechanical properties and simplified the temperature distribution, but the method of solution did not incorporate the effect of strain due to transformations. When this technique was taken a stage further by Boley[140], who assumed both a temperature dependent flow stress and the possibility of time dependent stress-strain behaviour, a complete analytical solution was no longer possible and numerical methods were employed to achieve an approximate solution. The solution still did not include the effects of strains due to phase changes, which are essential in the case of the quenching of steels.[70] Weiner and Huddleston[141] were able to obtain an elasto-plastic solution for the progression of a phase transformation in a cylinder, but only when there was a constant temperature distribution within the specimen.

(b) Alternative methods of solution

Chevrier[10] has calculated the stresses developed during the quenching of aluminium alloy cylinders. This material exhibited no transformation during quenching and the variations of both Young's modulus and the uniaxial flow stress with temperature were easily measured. The temperature distributions used by Chevrier in the stress calculation were obtained directly from thermocouples located in a quenched cylinder. A constant strain hardening rate was assumed, together with constant values of the thermal expansion coefficient and Poisson's ratio. The equations used by Chevrier to calculate the stress under elastic conditions were:-

$$\sigma_r = \frac{-\alpha_{ex}E}{(1-\nu)} \cdot \frac{1}{r^2} \int_{r_1}^{r_2} \theta . r . dr + \frac{E}{(1-\nu)(1-2\nu)} \cdot C_1$$

$$- \frac{E}{(1-\nu)} \cdot \frac{1}{r^2} \cdot C_2 \qquad 2.35$$

$$\sigma_\theta = \frac{\alpha_{ex}E}{(1-\nu)} \cdot \frac{1}{r^2} \int_{r_1}^{r_2} \theta . r . dr - \frac{\alpha_{ex}E\theta}{(1-\nu)}$$

$$+ \frac{E}{(1-\nu)(1-2\nu)} \cdot C_1 + \frac{E}{(1+\nu)} \cdot \frac{1}{r^2} C_2 \qquad 2.36$$

$$\sigma_z = \sigma_r + \sigma_\theta \qquad 2.37$$

Chevrier divided the cylinder into elements and, by the application of the relevant boundary conditions, evaluated the integration constants C_1 and C_2 in equations 2.35 and 2.36. The elastic stresses present in the cylinder were then determined at the end of each of a series of small time increments into which the quenching period had been divided. At each stage the calculation of elastic stresses was followed by the application of the Von Mises plasticity criterion:-

$$T_1 = (\sigma_r{}^2 - \sigma_\theta{}^2 - \sigma_r\sigma_\theta) - \sigma_f \qquad 2.38$$

In cases where plastic flow occurred, the original estimate of stress was replaced by the appropriate value of the flow stress. However, Chevrier made no adjustment to the stresses in that part of the specimen subject to elastic stress, which must inevitably follow an adjustment to the stresses in the parts subject to plastic deformation. Archambault[142] modified Chevrier's method of calculation by the addition of an extra stage after the application of the plasticity criterion; during this stage the internal stresses were rebalanced. Since this change in the stresses also required a modification to the stresses in the plastic zone, Archambault employed an iteration technique[139] to obtain a state of equilibrium after the application of the yield criterion; The calculations of Chevrier and Archambault both demonstrated that, in the absence of transformation strains, tensile plastic flow at the surface resulted in a compressive residual surface stress at the end of the cooling process.

Spektor and Stepanova[143] have published the results of the calculation of the stresses developed during the quenching of plates of a 1%C, 1.3%Cr steel. However, no details were given of the method of calculation and no references are cited. The results showed that the surface stresses in 10 mm and 20 mm plates became initially tensile, then compressive during the transformation of the surface region to martensite, and finally tensile after the transformation of the centre of the plates. Although the surface strain could reach a value close to 10^{-2} during the course of quenching, the final strain was often less than 10^{-3}. No supporting experimental residual stress or strain measurements were presented.

Toshioka et alia[129] devised an approximate method that may be used to calculate the stresses induced during the quenching of 0.45%C steel cylinders. It was suggested that the time taken for the steel to cool had no bearing on the generation of stress, which depended only on the strains induced in the different parts of the specimen by the changes in the temperature distribution. Temperature distributions within the cylinders were expressed as:

$$\theta_r = \left[1 - A\left(\frac{r}{R}\right)^2\right]\theta_o \qquad 2.39$$

The temperature distribution within a cylinder during the quench was thus defined in terms of the temperature at the centre of the cylinder, and different quenching severities were simulated by alterations to A. The flow stress was considered to be zero whilst the material was in the austenitic condition, but during the transformation to martensite the flow stress increased by an amount that was in proportion to the volume fraction of martensite present. The boundary between the elastic and plastic regions was assumed to exist in that part of the cylinder which was in the process of transformation from austenite to martensite. During cooling the precise position of this boundary was found by a balance between the forces exerted inside of the central zone, as a result of the formation of martensite, with those occurring in the outer region. The effect of temperature on the thermal expansion coefficient, Young's modulus and Poisson's ratio were ignored, together with the effect of strain hardening. The results obtained showed that during the initial stages of transformation the surface stresses were compressive; but later, high tensile values were obtained in this part of the specimen when A was less than 0.65 (equivalent to quenching in slow and intermediate oils). However, when A was greater than 0.65, the final surface stresses were compressive. Toshioka et alia used the technique to estimate the conditions under which specimens of low hardenability steels could be completely transformed to martensite without cracking.

Fletcher[144] has recently proposed a numerical method for the determination of the stresses and strains in plates of low-alloy steel which transformed completely to martensite during quenching: this technique has been used as a basis for the current work. The method considered heat transfer only through the thickness of the plates, so that stresses were developed only in the plane of the plate. The temperature distributions within the plate were determined by the use of an explicit finite difference method, with the relevant thermal properties taken from various published sources. Young's modulus and the flow stress of the material, whilst in the austenitic condition, were both approximated to linear functions of temperature, and the martensite transformation strain was calculated from lattice parameter values. The quantity of martensite produced at temperatures between the M_s and M_f temperatures was assumed to be proportional to the difference between the actual temperature and the M_s temperature. After each time increment the thermal stresses associated with the change in temperature distribution were initially considered to be elastic, and distributed in such a way that there was no net force on the plate. The Von Mises yield criterion was then applied, assuming no strain hardening, which caused the forces within the plate to become unbalanced. By an iteration process the required prior elastic stress distribution, which would give no net force on the plate after yielding, was determined. By this method it was possible to follow the development of stresses and strains during the quenching process and the method predicted the final shape distortion as well as the residual stress distribution. No experimental evidence was presented in support of the results of the calculations.

Atkins et alia[138] have been the only workers to deal with the effect of stress relaxation on the generation of thermal stress during quenching. Stress relaxation processes were considered important because they were dealing with large rotor forgings, which were cooled relatively slowly. Initially the elastic stress distribution was calculated at the end of each time increment in the cooling process. Stress relaxation was assumed to occur only to the outer layer of the rotor during the course of the time increment but, like Chevrier,[10] no attempt was made to redistribute the elastic stresses over the unrelaxed portions of the cylinder, which was necessary if force and moment equilibrium were to be maintained within the rotor.

Several workers have used the finite element method to analyse the generation of stress in quenched steel specimens.[145,146,147] The finite element method is now well documented and is essentially a process through which the structure is approximated to an assemblage of elements. The elements are considered interconnected at a discrete number of nodal points at their boundaries. The state of displacement in each element is defined by functions in terms of the nodal displacements. The state of stress throughout each element is defined in terms of these strains (including any initial strains), and the elastic properties of the material. Matrices of the relevant equation are set up for all the elements in the structure and solved. Zienkiewiez[145] has pointed out that the finite element method is equivalent to an approximate minimisation with respect to nodal displacements, and represents a minimisation of the potential energy of the system.

Although the finite element method is now well established as a powerful technique of stress analysis, the great complexity of the data required in the calculation of the thermal stress generated during quenching has led to the representation of this data by the use of various approximations. The accuracy of the calculations has been adversely affected by many of these approximations.

Inoue et alia[148] have used a finite element technique to analyse the stresses developed during the water quenching of 12%Cr steel cylinders. The specimen considered was completely transformed to martensite during quenching, and therefore the transformation strains used in the calculations were a function of temperature alone. A finite element method was first used to determine the temperature distribution; although no descriptions were given of the thermal property data used, apart from a heat generation term relating to the martensite transformation. The dubious nature of this data is shown by the shape of the cooling curves which suggested that the formation of martensite produced very large increases in temperature before the cooling process re-commenced. Strain hardening was taken into account but the details of the method by which this was done were not given. Furthermore, no description was given of the way in which the martensite transformation affected the flow stress of the material during the martensite transformation. The results of these calculations were compared only with measurements of the stresses at the surface of a quenched cylinder, although good agreement was found at this point (see Figure 35).

Toshioka[149] has likewise used the finite element technique to calculate the distortions produced in quenched steel bars. A finite element method was used to calculate the effect of time on the temperature distribution using the data shown in Table 1, which was obtained from previously published work. The materials considered were a 0.37%C steel (S38C) and a 0.39%C, 1.7%Ni, 0.8%Cr, 0.17%Mo steel (SNCM8), and the effects of the pearlitic, bainitic and martensitic transformations were taken into account in the calculations. The mechanical property data, thermal expansion coefficients and transformation strains used by Toshioka are given in Table 2. Toshioka compared only the calculated values of residual strain with experimentally measured data, Figure 36 shows this comparison in the case of 200 mm diameter, 400 mm length cylinders of SNCM8 after water quenching, which were the only results that could be directly compared. Reasonable agreement was found in the case of the change in diameter but the length changes did not show good agreement.

Fujio et alia[150] have calculated the stresses developed in 50 mm diameter cylinders of 0.45%C steel when quenched in water. A classical method was employed to determine the time-temperature distribution within the cylinders during the quench, which required that the surface heat transfer coefficient, the thermal conductivity, and the specific heat of the steel were all assumed to be constant during the course of the quench. Since transformation products other than martensite were likely to be produced in the cylinders during a water quench, the volume fractions of martensite present at different radial depths were determined from hardness measurements on an experimentally quenched cylinder; the form of the dilatometer curve used at different radial depths in the cylinder in the calculation depended on the fraction of martensite present at that depth (see Figure 37). The yield stress data was obtained from interpolations involving the yield stress of the material at room temperature in either the martensitic or annealed conditions (points M and P respectively in Figure 38), and a single high temperature value of the yield stress at 900°C, given in published work on the steel concerned. Strain hardening was not discussed in their paper. The Sachs boring method was used to measure the residual stress distributions in an experimentally quenched cylinder, which were compared with the computed values, as shown in Figure 39.

The results obtained indicated that the calculated residual stresses were dominated by the specific volumes associated with the different structures present.

(c) Influence of stress on the decomposition of austenite

None of the thermal stress calculations described so far include any reference to the possible influence of stresses, developed during the early stages of the quench, on the decomposition of the austenite; even though their possible importance was pointed out by Russell as early as 1947.[70]

The effect of pressure on the decomposition of austenite during quenching has been studied by Schmidtman and May,[151] and Nilan,[152] who found that high pressures stabilised the austenite and depressed the temperatures at which bainite and martensite began to form. It is well known that plastic deformation just above the M_s temperature can produce martensite and that an upper M_d temperature exists, above which martensite cannot be formed by plastic deformation.[12] Furthermore, prior plastic deformation in the austenitic condition may raise the temperature at which bainite and martensite begin to form.[153] Thus it is possible that the M_s temperature may be altered when an external force is applied to the material. For example, Mirzayev et alia[154] have reported an abnormal drop in the flow stress of 18%Cr, 12%Ni steels at temperatures just above the M_s temperature, which they attributed to the formation of martensite under the influence of elastic stresses. An increase in the deformation rate was found to reduce the magnitude of the anomalous effect.

Although a number of "stress dilatometers", in which the dilations of stressed specimens can be measured whilst they are being quenched, have been built,[155,156] the results of investigations into the influence of stress on the transformation strains associated with the formation of martensite in quenched specimens have yet to be published.

2.4 Conclusions from the Survey of Previous Work

The major variables, which affect the production of residual stresses and distortion during the quenching of steel parts, have been found by experimentation to be hardenability, section size and shape, quenchant and the M_s temperature. The interaction of these factors is not clearly understood and a theoretical analysis of the stress generation process is needed. Some attempts have been made to calculate the thermal stresses produced during the quenching of steel components, but there remains a shortage of the accurate property data required in these calculations, and dubious assumptions have often been made. Few of the results of these calculations have been correlated with experimental results, and even where this has been carried out, it has not been over a range of conditions. For example, only Toshioka[149] has attempted to correlate theoretical and experimental distortions, and he neglected to compare theoretical and experimental residual stresses. In other cases, the comparison of stresses has only been made at the surface of the component. Although the accurate determination of the temperature distribution in quenched specimens is fundamental to the correct calculation of thermal stress, this aspect of the problem has often been neglected. Again, lack of physical property data makes the accurate calculation of temperature distributions difficult and the sensitivity of the surface heat transfer coefficient to small variations in the experimental conditions reduces the reliability of results obtained by either calculation or experiment.

It is concluded that the further collection of data, both thermal and mechanical, is required if the thermal stress generated during quenching is to be predicted successfully. In particular, the quenching conditions need to be expressed quantitatively with reference to the relevant property data. There is also a great need for more correlation between the experimental measurement of temperature distributions, residual stresses and distortions and the predictions of these quantities made by the use of mathematical models.

3. TEMPERATURE DISTRIBUTIONS IN QUENCHED PLATES

The determination of the temperature distributions produced during quenching is a fundamental prerequisite to the prediction of thermal stress. The method used in the present work has been to calculate the temperature distributions produced during quenching by the solution of Fick's Law of heat conduction using appropriate boundary conditions. Since this required the use of physical property data, which were generally not available, the first stage of the work involved the determination of the data required. This was followed by the calculation of the temperature distributions generated during the quench. The final stage of this section involved the correlation of the predicted temperature distributions with those determined experimentally.

Thermo-mechanical coupling was assumed to be negligible as proposed by Boley and Weiner[67]. It was therefore possible to determine the temperature distributions before proceeding to consideration of the determination of thermal stress.

3.1 Determination of the Surface Heat Transfer Coefficient During Quenching

One of the boundary conditions used in the solution of the differential thermal conduction equation, 2.10, is obtained from the surface heat transfer coefficient. However, previous workers have shown the surface heat transfer coefficient to be highly dependent on experimental conditions. It was therefore necessary to measure the surface heat transfer under the same experimental conditions as were to be used in the later stages of the work, when the generation of thermal stresses was to be considered.

3.1.1 Experimental procedure for the determination of cooling curves

The quenching of all specimens was carried out in tanks, the dimensions of which are shown in Figure 40. A fixture (also shown in Figure 40), which incorporated two variable speed stirrers and a pair of channel guides, was used to ensure that specimens were always quenched in the same manner. This fixture was interchangeable between all the quenching tanks used.

Two types of specimen were eventually used for the measurement of the surface heat transfer coefficient. Specimen Type A, shown in Figure 41, consisted of a 3.3 mm thick plate of A.I.S.I. 304 austenitic stainless steel (composition given in Table 3) in which a single chromel-alumel thermocouple was located at a point on a plane mid-way between the two large surfaces. A.I.S.I. 304 material was chosen on account of the absence of any phase transformations during the course of quenching from 850°C: hence its thermal properties were accurately known[157]. Because the specimens were thin it was assumed that no temperature gradients were present in them at any time: this allowed the use of the "lumped parameter" approach[99], in which the internal thermal resistance of the plate is considered negligible in comparison with that at its boundary.

The cooling curves obtained with the 3.3 mm thick stainless steel specimen indicated that under some conditions a temperature gradient was produced during quenching. Therefore, the use of the "lumped parameter" approach was considered questionable as it might give rise to inaccuracies. Furthermore, the specimen was so thin that the whole cooling process merely took a few seconds. This also was another possible source of error.

Since the values of the surface heat transfer coefficient reported in previous works were generally rather higher than those obtained in the present investigation, it was decided to use another technique, which was more accurate; but very much more complex.

Type B specimens (shown in Figure 42, composition given in Table 3) were substantially thicker (15 mm) than the Type A specimens (3.3 mm), and the assumption of negligible internal thermal resistance was no longer reasonable. Hence the calculation of the surface heat transfer coefficient with these specimens took into account the existence of temperature gradients within the specimen during quenching. Three thermocouples were located in the specimen, one at its centre and one just beneath each surface. The latter will be referred to subsequently as the sub-surface thermocouples. Data from the thermocouple at the centre of the plate was used only to check the accuracy of the thermal gradients, calculated from the temperature measurements at the sub-surface positions, during quenching. The latter data alone was used to calculate the surface heat transfer coefficient.

The accuracy of measurement of the surface heat transfer coefficient during quenching depends upon the accuracy of measurement of the surface temperature and the heat flux passing through the surface[98]. When large temperature gradients exist in the specimen during quenching the error in the calculation of the surface heat transfer coefficient is minimised by the measurement of temperatures as close as possible to the surface. However, the nearer the position of temperature measurement to the surface of the specimen, the more rapid is the change in temperature; in which case, the response time of the temperature measuring and recording system may introduce errors[98]. The sub-surface location of the thermocouples was therefore a compromise, which minimised the overall error in the results.

Holes for the sub-surface thermocouples were initially drilled parallel to, but 2 mm beneath, the quenched surfaces. The initial thickness of the specimen was 16.5 mm, but after the insertion of the thermocouples it was lightly rolled at 900°C, to ensure close contact between the thermocouples and the specimen. The eventual thickness of the specimen, after a final grinding operation, was 15 mm. The method used to determine the surface heat transfer coefficient required the position of the sub-surface thermocouples to be known very accurately. Therefore, after the completion of the quenching experiments, the specimen was sectioned through the plane containing all of the thermocouple hot junctions, which allowed the precise position of the thermocouples to be determined. Both the sub-surface thermocouple hot junctions were found to be 1.8 mm beneath their respective surfaces.

Before each experiment the surfaces of both the Type A and Type B specimens were cleaned with 400 grade silicon carbide paper, unless indicated otherwise*. The specimens were heated in a muffle furnace at 850°C, prior to quenching, until the thermocouples in the specimens reached the furnace temperature. The specimens were then transferred manually from the furnace to the quench tank. Care was taken to ensure that the immersion of the specimen caused the minimum disturbance to the quenchant. A Rikadenki B461 chart recorder (maximum frequency response 1.75 Hz) was used to record the temperatures indicated by the thermocouples in specimen Types A and B during the course of quenching.

---

*Provided the specimen surfaces were cleaned before each experiment the surfaces acquired only a slight tarnish during the normal heating cycle. The thickness of oxide produced was sufficiently thin to allow the passage of light and the reflectivity of the surface remained high. This surface condition is referred to as unoxidised. Subsequent heat treatments, without re-cleaning the surface, resulted in the growth of the oxide layer so that it became opaque. This surface condition is referred to as oxidised.

Quenching was carried out into three different quenchants: water, oil and a polymer quenchant. In all cases the temperature of the quenchant was 20°C at the start of each quench and, owing to the large volume of quenchant used, the temperature of the quenchant never rose by more than 1°C during the quench. Water quenching was carried out in still tap water; but oil quenching using R.D.N. 175 oil (properties given in Table 4), was carried out with both stirrers in the quench tank operating at 50 rpm. Cooling rates intermediate between those of water and oil were required for use in the subsequent thermal stress work. For this purpose various concentrations of Aquaquench 1250 polymer quenchant[112] (a polyalkalene glycol which exhibits the property of "inverse solubility" in water) were also tested. During the quenches that involved the use of the polymer quenchant both stirrers in the quench tank were operated at 50 rpm to ensure a fresh supply of liquid at the specimen surfaces, which is essential for the effective operation of these quenchants[158].

3.1.2 Calculation of the surface heat transfer coefficient

The surface heat transfer coefficient was derived from the cooling curves obtained with the thin Type A specimens (3.3 mm) by using the "lumped parameter" approach[99]. In which case the surface heat transfer coefficient may be obtained at any time during the quench from:-

$$h = \frac{MCp}{At} \ln \left\{ \frac{\theta_f - \theta_t}{\theta_f - \theta_o} \right\} \qquad 3.1$$

However, the specific heat of A.I.S.I. 304 is temperature dependent[157] (see Figure 43); though the variation is nearly linear and, by the method of least squares, the specific heat was approximated to vary according to:-

$$Cp = 500.05 + 0.1948\theta \ J/kg^{o}C \qquad 3.2$$

The values of specific heat employed in the solution of equation 3.1 were evaluated from equation 3.2 using the average temperature of the specimen over the time interval involved.

Owing to the increased likelihood of temperature gradients within the thicker Type B specimens (15 mm) the application of equation 3.1 was no longer considered to be justified and it was necessary to treat the heat transfer within the plate more rigorously than in the case of the thin specimens. However, since both the surface boundary conditions and the physical properties of the material involved were temperature dependent, it was not possible to use any of the known analytical solutions to the differential equation that represents the variation of temperature with time and position within the specimens. viz,

$$\frac{\partial\theta}{\partial t} = \alpha \frac{\partial^2\theta}{\partial z^2} \qquad 3.3$$

Hence a finite difference solution was employed to determine the temperature distribution within the specimens, in which the temperature was calculated only at specific values of distance and time. For this purpose the plate was divided into a series of elements, with nodal points at the centres of the elements. Temperatures were calculated at specific time intervals at these nodal points. The temperature of an element i at the end of n + 1 time intervals was given by [74]:-

$$\theta_i^{n+1} = \theta_i^n + \frac{\alpha t d \Delta t}{(\Delta z)^2} \left[\theta_{i+1}^n - 2\theta_i^n + \theta_{i-1}^n \right] \qquad 3.4$$

The boundary condition at the plate surface was given by [74]:-

$$\theta_1^n = \theta_3^n - 2\,\frac{h\Delta z}{\lambda}\left[\theta_2^n - \theta_f\right] \qquad 3.5$$

Figure 44 shows the location of the nodes near the surface of the plate.

Another boundary condition existed at the opposite face of the plate. However, provided the surface heat transfer coefficient was the same at both surfaces, the temperature variation through the plate thickness was symmetrical about the centre of the plate. A central boundary condition then existed, where the temperature gradient was always zero.

Thus $$\theta_{j-1}^n = \theta_{j+1}^n \qquad 3.6$$

where the total number of elements in the plate is 2j. The accuracy of the surface heat transfer coefficients determined using equations 3.4 and 3.5 was clearly very dependent upon the accuracy of α_{td} and λ, both of which were temperature dependent over the temperature ranges involved [157] (see Figure 43). Thus the variations of these quantities with temperature were approximated to two linear functions, using the method of least squares, and the values of α_t and λ were evaluated for each element at each time interval from:-

$$\alpha_{td} = 0.4062 \times 10^{-5} + 0.1625 \times 10^{-8}\,\theta_i^n \ \text{m}^2/\text{s} \qquad 3.7$$

$$\lambda = 15.46 + 0.01384\,\theta_i^n \quad \text{W/m}^\circ\text{C} \qquad 3.8$$

Equations 3.4 and 3.5, in conjunction with the condition that all nodes were initially at θ^o may be used to calculate the temperature distributions in the plate at any time. Conversely, provided the relationship between time and temperature were known at a single node from t=0, these same equations may be used to determine the relevant values of the unknown surface heat transfer coefficient. Equation 3.4, however, was subject to the stability criterion[74]:-

$$\frac{\alpha_{td}\Delta t}{(\Delta z)^2} \leq \tfrac{1}{2} \qquad 2.20$$

The boundary condition represented by equation 3.5 was also subject to a stability criterion[74]:-

$$\left(\frac{1}{2 + \frac{h\Delta z}{\lambda}}\right) \geq \frac{\Delta t\,\alpha_{td}}{(\Delta z)^2} \qquad 3.9$$

The minimum time interval at which data could be obtained from the experimental cooling curves was 0.3s; but the maximum possible time interval allowable in the finite difference equations, as a result of the stability criteria given in equations 2.20 and 3.9, was much smaller than 0.3s. This difficulty was overcome by employing an initial estimate of h to calculate the temperature distributions over several of these smaller time intervals (using equations 3.4 and 3.5) until the total time was equal to the interval within which experimental measurements of temperatures could be made (>0.3s). Comparison between these calculated and experimental temperatures indicated whether or not the estimate of h used in the calculation of temperature was correct.

If the agreement between the calculated and experimental temperature at the position of the sub-surface thermocouple was within 1^oC, the initial estimate of the surface heat transfer coefficient was considered correct over that time interval, and the next time interval was considered. If the necessary agreement was not achieved, the initial estimate of the surface heat transfer coefficient for that time interval was corrected and the process repeated until adequate agreement was achieved. The use of a conventional marching technique to correct the initial estimate of h would have required the use of an excessive amount of computer time. Therefore, to allow more rapid convergence between the predicted and experimental temperatures, it was initially assumed that no temperature gradients existed within the material. This allowed the use of equation 3.1 and the experimental cooling curve to make an initial estimate of the surface heat transfer coefficient.

viz

$$(h_\ell)_{\text{initial}} = \frac{MCp}{A(t_0^{\text{exp}} - t_1^{\text{exp}})} \ln \left\{ \frac{(\theta_{TC}^{1})^{\text{exp}} - \theta_f}{\theta_{TC}^{o} - \theta_f} \right\} \qquad 3.10$$

Using this initial estimate of h, equations 3.4 and 3.5 were used to calculate the temperature at the thermocouple hot junction at time t_1^{exp}, when the first experimentally determined temperature was available. When the agreement between calculated and experimental temperatures was inadequate, the h value currently applied was corrected using:-

$$(h_\ell)_{\text{corrected}} = (h_\ell)_{\text{initial}} + (\Delta h)_\ell \qquad 3.11$$

where there are ℓ sets of experimental time & temperature data.

A good estimate of the change in surface heat transfer coefficient $(\Delta h)_\ell$ was obtained by the use of equation 3.1 together with a comparison of the predicted and experimental temperatures at the sub-surface position.

viz

$$(\Delta h)_\ell = \frac{MCp}{A(t_\ell^{\text{exp}} - t_{\ell-1}^{\text{exp}})} \ln \left\{ \frac{(\theta_{TC}^{\ell})^{\text{exp}} - \theta_f}{\theta_{TC}^{\ell} - \theta_f} \right\} \qquad 3.12$$

Since the location of the thermocouple did not coincide exactly with any of the nodes, it was necessary to obtain the calculated temperature at the position of the thermocouple by interpolation between nodal temperatures. Temperature profiles near the surface were non-linear, particularly during the early stages of the quench, and Bessel's interpolating polynomial[159] was therefore employed for the interpolation process.

The calculation of the surface heat transfer coefficient was made using a computer program written in Fortran IV language. Figure 45 shows the flow chart on which the program was based.

3.1.3 Experimental results

(a) Water quenching

The relationships obtained between temperature and time during the quenching of the Type A specimens (3.3 mm) is shown in Figure 46. Figure 47 shows the effect of specimen surface temperature on the surface heat transfer coefficient, that was calculated from the information in Figure 46, by the method described in section 3.1.2. The results obtained showed that the cooling rate during the early part of the quench was low and corresponded to the formation of the vapour blanket. However, the duration of this was short and erratic. The maximum values of h obtained, which were associated with the nucleate boiling stage, were between 9,000 and 12,000 $W/m^2 {}^\circ C$ and occurred at around $350^\circ C$.

At this point the more accurate Type B specimens (15 mm) were developed and used under the same conditions to evaluate h during water quenching. Figure 48 shows the relationship between temperature and time during the first quench carried out with the Type B specimen. The vapour blanket stage (characterised by a low cooling rate at the start of the quench) was almost absent at one surface, although clear evidence of this stage was obtained at the opposite face. This produced the surprising result that during the initial stages, the thermocouple at the centre cooled more rapidly than the thermocouple immediately beneath the surface on which a vapour blanket was formed. Hence, after 6 seconds the temperature registered at the centre of the plate was 735°C whilst that beneath the surface, where the stable vapour blanket had formed, was 752°C. When the plate was reheated, without any cleaning of the specimen surface, and requenched; stable vapour blankets were formed at both surfaces (see the cooling curves shown in Figure 49).

When the specimen was requenched with unoxidised surfaces, the same behaviour occurred (Figure 50) as had been found during the initial quench (Figure 48). The stable vapour blankets shown in Figures 48 and 50 occurred at the same surface of the specimen. A close examination of this surface revealed that some surface imperfections, introduced when the specimen had been lightly rolled, had not been fully removed. Both faces of the plate were therefore ground back to remove all surface flaws and re-finished with 400 grade silicon carbide paper. (The depth of the sub-surface thermocouples referred to earlier in section 3.1.1 applies after this grinding operation.)

When the specimen was now quenched in the oxide-free condition, the vapour blanket stage was almost completely absent from both surfaces (Figure 51). However, when the specimen was requenched in the oxidised condition (i.e. surfaces not cleaned after the previous experiment), stable vapour blankets developed at both faces of the plate (see Figure 52). The specimen was again quenched in the unoxidised condition, and similar results to those shown in Figure 51 were obtained.

The relationships between temperature and time obtained during the quenching of unoxidised Type B specimens were used to determine the effect of surface temperature on the surface heat transfer coefficient. Figure 53 shows the coefficients obtained using five such cooling curves. Although these results showed two sharp discontinuities, the use of linear relationships between these points was a convenient method by which the surface heat transfer coefficient data might be introduced into the subsequent calculations of temperature distribution and thermal stress. Figure 54 shows the relationships used for this purpose derived from the results shown in Figure 53 by the method of least squares. A more complex curve fitting procedure was not considered to be justified, on account of the degree of uncertainty in the values of the surface heat transfer coefficient. This uncertainty is clearly shown by the magnitude of the standard deviations of the results, also shown in Figure 54.

The cooling curve measured at the centre of the Type B specimen provided a check on the accuracy of the calculations used in the determination of h. During these calculations (described in section 3.1.1) the temperature distribution across the thickness of the plate was determined. Thus calculated temperatures at the centre of the plate were available for comparison with experimental values. Figure 55 shows both the calculated and experimentally determined relationships between time and temperature at the centre of the specimen: these results indicate that h was correctly calculated and that the correct thermal property data had been used in the calculations.

(b) Oil quenching

The relationships between temperature and time produced when Type A specimens were quenched were used to determine the effect of temperature on the surface heat transfer coefficient, using equation 3.1 (see Figure 56). The corresponding data obtained with Type B specimens were used to determine the effect of surface temperature on the surface heat transfer coefficient using equations 3.4 and 3.5 and the technique described in section 3.1.2 (see Figure 57).

The variations in h obtained were found to be much more consistent than those obtained during water quenching, and there were no significant differences between the behaviour of the two faces of the Type B specimen. No significant changes were found in the cooling curves and the behaviour of the surface heat transfer coefficient when Type B specimens were quenched without re-cleaning: thus a small amount of oxidation had no significant effect on the magnitude of the surface heat transfer coefficient.

The results obtained from both Type A and Type B specimens were very similar (cf. Figures 56 and 57); the only significant difference was a shift in the temperature at which the maximum value of h occurred from 380°C in the case of Type A, to 355°C in the case of Type B. The average values of h obtained at each temperature were used to derive a relationship between this property and surface temperature (see Figure 58). As was the case with a water quench, this relationship could be represented by a set of linear equations, each of which covered a specific range of temperatures. This information was subsequently used in the thermal stress calculations.

(c) Polymer quenching

Type B specimens alone were used to investigate the relationship between surface temperature and h when quenching into a polymer quenchant. At a polymer concentration of 10% by volume, there was little difference between the cooling curves obtained (Figure 59) and those obtained by the use of water alone (Figure 51). It was found necessary to increase the polymer concentration to 25% by volume, if cooling rates sufficiently lower than those obtained by the use of water alone were to be produced (Figure 60). With this concentration of polymer a well defined stage occurred at the start of the quench when the cooling rate was low and relatively constant. The specimen was observed during this stage of the quench to be surrounded by a vapour blanket. Quenching the specimen in the oxidised condition produced similar cooling curves to those obtained with unoxidised specimens.

The effect of surface temperature on the values of h, obtained during quenching in the solution that contained 25% by volume of the polymer, are shown in Figure 61. Similarly to the cases of water and oil quenching, a series of linear relationships were obtained to represent the variation of the surface heat transfer coefficient with surface temperature (Figure 62).

Table 5 summarises the variations of h with surface temperature established from the experimental work using the different quenchants. These values were used in all the subsequent calculations of temperature distributions.

3.2 Temperature Distributions in Low-Alloy Steel Plates During Quenching

In this stage of the work the values of the surface heat transfer coefficient, which had been determined experimentally, were used to calculate the temperature distributions produced in the steel plates during quenching that were to be used subsequently in thermal stress calculations. The calculated temperature distributions were then correlated with experimentally measured temperature distributions in order to test the accuracy of the data used in the former.

3.2.1 Experimental determination of temperature distributions

A plate of 835M30 (composition given in Table 3) was fitted with thermocouples, as shown in Figure 63. This plate was the same size as the largest plate considered in the subsequent thermal stress calculations. The plate was electroplated with a 0.05 mm layer of Ni over its surfaces to prevent oxidation and finished using 400 grade silicon carbide paper. To ensure uni-dimensional heat flow through the thickness of the plate, its edges were insulated with a 6 mm thick layer of Kaol Wool, held in position by a nickel band. The outputs from the thermocouples were recorded using a Credshire 200 data logger. This plate was then quenched in the unoxidised condition from 850°C into still water at 20°C and agitated R.D.N 175 oil, in an identical manner to that used for the surface heat transfer coefficient described in section 3.1.1.

3.2.2 Calculation of temperature distributions in plates of 835M30 steel during quenching

The temperature distributions within a 40 mm thick plate were calculated by the use of equation 3.4 in the case of the inner elements and by equation 3.5 in the case of the surface element. Since the plate was cooled from both faces, it was only necessary to compute temperatures for half of the plate thickness and equation 3.6 was used to represent the second boundary condition at the central plane. The appropriate relationship between h and surface temperature, given in Table 5, was used to obtain the value of h appropriate to a specific temperature. This value of h was then used to calculate θ_2^{n+1}. The variations of thermal conductivity and thermal diffusivity for the alloy 830A31 were modelled using a series of linear relationships (least squares method), shown in Figures 64 and 65, given in Table 6. The thermal diffusivity values were obtained from apparent specific heat values for the cooling of the material, and therefore for calculation purposes they effectively incorporated the free energy change accompanying the austenite to martensite transformation[160]. There are small variations between the compositions of 835M30 and 830A31 (see Table 3), but 830A31 was the nearest composition to 835M30 for which relevant property data was available. The values of λ and α_{td} used to evaluate any new nodal temperature, θ_i^{n+1}, were those based on the temperature of the node at the time θ_i^n.

The chosen time interval, Δt, used in equation 3.4 and 3.5 was such that the stability criteria specified in equations 2.20 and 3.9 were met. Truncation errors are more probable if Δz is large (see section 2.3.1). Thus Figure 66 shows the effect of a variation in the number of elements in the half-plate (and hence Δz) on the temperatures calculated at the surface and centre of a plate cooled with a Biot number $\left\{\frac{hL}{2\lambda}\right\}$ of 4. The greatest effect was obtained at the surface, but even then the discrepancy produced by a reduction in the number of elements from 160 to 20 was less than 2%. In all subsequent calculations 40 elements were used in the half-plate, unless specified otherwise. This number of elements was chosen as a reasonable compromise between accuracy and computer time, since the use of more than 40 elements gave only a small improvement in accuracy.

Figure 67 shows a flow chart on which a computer program (written in the Fortran IV language) was based to carry out the calculation of the temperature distributions. These calculations were carried out using both constant and variable values of thermal conductivity and thermal diffusivity. The constant values used were the average values between 850°C and 100°C, viz 25.2 $W/m^2\,^{o}C$ and 0.5279×10^{-5} m^2/s for λ and α_{td} respectively, and were obtained from the data shown in Figures 64 and 65.

3.2.3 Comparison of calculated and experimental temperature distributions

As the calculated temperature distributions in the quenched plates were important as the starting point for the subsequent thermal stress calculations, it was considered necessary at this stage to consider the accuracy of these results. This was achieved by a comparison of the calculated and experimental temperature distributions.

(a) Water quenching

Figure 68 shows a comparison of the predicted and experimentally determined cooling curves, which were obtained at the centre of the 40 mm thick plate during a water quench: the calculated curves employed both constant and variable values of h, λ and α_{td}. Although none of the available data allowed a very high correlation between the experimental and predicted curves, a reasonable fit may be obtained by the use of constant values of λ and α_{td}. Since in subsequent thermal stress calculations the temperature distributions in the plate are of the greatest importance, these are compared in Figure 69. Thus this figure compares the experimental temperature distributions at various stages in the quenching process with those predicted by the use of constant values of λ and α_{td} at the same stage in the quenching process. (In this case the comparison is not at equal times, but at equal centre temperatures.) In the early stages the calculation predicts slightly more severe temperature gradients to those measured experimentally, but in the later stages the calculated temperature gradients were smaller than those determined experimentally.

The comparison of the predicted temperature profiles obtained by the use of constant values of λ and α_{td}, with those calculated by the use of variable values of λ and α_{td}, confirms that there is little justification for the use of the latter (see Figure 70).

(b) Oil quenching

Figure 71 shows a comparison of the calculated and experimentally determined cooling curves obtained at the centre of the 40 mm 835M30 plate during oil quenching; the calculated curves were obtained by the use of both variable and constant values of λ and α_{td}. Some improvement in agreement was obtained during the first 200 seconds of the quench by using the variable thermal properties. However, in the later stages of the quench there was little advantage to be gained by the use of variable properties, and by the end of the quench the constant thermal properties provided an equally accurate result.

The comparison of measured and computed temperature distributions was especially important when oil quenching was considered, because the temperature differences within the plate were so much smaller than in the case of the water quenched plates. Figure 72 shows the comparison of experimental and computed (using constant λ and α_{td} values) temperature distributions, which demonstrated reasonable agreement. Again the temperature distributions were compared with equal temperatures at the plate centre.

4. PREDICTION OF THERMAL STRESS AND STRAIN

4.1 Calculation Technique

The technique used to calculate the thermal stresses generated during quenching was based on the approach described by Fletcher[144]. Thermo-mechanical coupling was neglected[67], so that the equations governing transient heat conduction (described in section 3) provided data that could be used directly in the calculation of thermal stress and strain. The whole quenching period was divided up into a series of small time intervals, and at the end of each interval the stress problem was solved using the following process.

(a) Calculation of the new temperature distribution (Section 3).

(b) Determination of the change in stress in each part of the plate due to thermal contraction and transformation strains, assuming complete restraint at the edges of the plate and fully elastic conditions.

(c) The edge restraint was removed and the new stress found in each part of the plate, still assuming fully elastic conditions.

(d) The modifications in stress were calculated at each point in the plate resulting from plastic flow in those parts of the plate where the flow stress of the material had been exceeded. When this occurred it was also necessary to re-distribute the elastic stresses within the plate.

During stages (b), (c) and (d) the stress distribution within the plate was maintained so that all forces and moments were in equilibrium. By carrying out this process for successive temperature distributions during quenching, it was possible to predict the stress and strain for the whole plate throughout the quench.

4.1.1 Procedure assuming plastic deformation without strain-hardening

(i) Temperature distribution

The temperature distribution within the plate was determined using the finite difference procedure described in section 3.2.2. The results obtained, already given in section 3, had shown that no significant improvements in accuracy were obtained when temperature dependent functions for λ and α_{td} were used. Hence constant, average values of λ and α_{td} were used in all subsequent thermal stress computations. This enabled considerable savings to be made in computer time, since it was then possible to reduce equation 3.5 to the well known Schmidt formulation[73]:

$$\theta_i^{n+1} = \frac{\theta_{i+1}^n + \theta_{i-1}^n}{2} \qquad 3.5$$

where

$$\frac{\alpha_{td}\, \Delta_t}{(\Delta z)^2} = \tfrac{1}{2} \qquad 4.1$$

The boundary conditions employed were the same as those given already in section 3 (i.e. equations 3.5 and 3.6), and the values of the surface heat transfer coefficient were those given in Table 5.

The calculation of the temperature distributions required the use of small values of the time increment, owing to the effect of the magnitude of this variable on the stability and accuracy of the calculations (described in section 3.2.2). However, it was not found necessary to carry out the stress calculation at the end of each of these small time intervals. Instead the size of the time interval used between each stress calculation was normally such that the temperature of the surface of the specimen fell by 1°C during this interval. Similarly it was not found necessary to divide the plate between centre and surface into 40 elements, as was the case in the calculation of temperature distributions. Consequently only ten elements were required in the stress calculation, and the temperature of these larger elements was calculated from the average temperature obtained in the smaller 'temperature elements' contained within them.

(ii) Stress calculation assuming completely elastic conditions.

The plate was considered to be sub-divided into elements, as shown in Figure 73. It was assumed that uni-dimensional heat flow occurred through the thickness of the plate only, thus away from the edges of the plate the stress acting through the thickness of the plate was approximated to zero[67] (i.e. $\sigma_z \approx 0$). Furthermore, the stresses acting in the plane of the plate were equal (i.e. $\sigma_x = \sigma_y = \sigma$); σ_x and σ_y being principal stresses. The change in stress experienced by each element, when the plate was completely restrained at its edges, and when fully elastic conditions apply, has been given by Fletcher[144]:

$$\left(\Delta\sigma_i^{n+1}\right)_r = \frac{E\alpha_{ex}}{(1-\nu)} \left[\theta_i^n - \theta_i^{n+1}\right] \qquad 4.2$$

The subscript r signifies complete edge restraint. Young's modulus and Poisson's ratio are both dependent on temperature in the case of most steels[157], and errors may be introduced if these variables vary significantly in the temperature range between θ_i^n and θ_i^{n+1}. However, it was evident from Figure 74 that the variation of the ratio E to $(1 - \nu)$ could conveniently expressed as a linear relationship in the case of 830A31 steel, which was the nearest composition to 835M30 for which relevant data was available.

Thus

$$\frac{E}{(1 - \nu)} = a - b\theta \qquad 4.3$$

The following relationship (derivation given in Appendix 1) for the change in stress, took account of the variation of E and ν between θ_i^n and θ_i^{n+1}:

$$\left(\Delta\sigma_i^{n+1}\right)_r = \alpha_{ex} \left\{ a\left[\theta_i^n - \theta_i^{n+1}\right] - \frac{b}{2}\left[\left(\theta_i^n\right)^2 - \left(\theta_i^{n+1}\right)^2\right]\right\} \qquad 4.4$$

The values of α_{ex} were obtained from the dilatometer curves of 835M30 specimens during cooling from 850°C and are described in detail in section 4.2.1. Within the range of cooling conditions considered, the hardenability of 835M30 was sufficient to ensure that at the end of the quench a fully martensitic structure was always formed throughout a 40 mm thick plate.

The total stress in each element at the new time was given by:

$$\left(\sigma_i^{n+1}\right)_r = \sigma_i^n + \left(\Delta\sigma_i^{n+1}\right)_r \qquad 4.5$$

When the restraint was removed from the edges and the plate became free, the stress σ_i^{n+1}, $i = 1,j$, became zero at all positions at the surface that forms the edges of the plate. At distances greater than approximately one plate thickness in from the edge, this can be approximated to:

$$\sum_{i=1}^{i=j} \sigma_i^{n+1} \simeq 0 \qquad 4.6$$

This was achieved in the computation by an evaluation of the average stress present in the half-plate, which was subtracted from the stress in each element:

$$\left(\overline{\sigma^{n+1}}\right)_r = \frac{\sum_{i=1}^{i=j} \left(\sigma_i^{n+1}\right)_r}{j} \qquad 4.7$$

$$\sigma_i^{n+1} = \left(\sigma_i^{n+1}\right)_r - \left(\overline{\sigma^{n+1}}\right)_r, \; i = 1, j \qquad 4.8$$

This process was equivalent to the removal of restraint from the edges of the plate and ensured that condition 4.6 was met.

Moment equilibrium was automatically satisfied by the symmetry of the stress distribution about the centre of the plate. Because the plate was always considered to be cooled from both surfaces, the moments generated by elements in either half of the plate were always in equilibrium.

viz

$$\sum_{i=1}^{i=2j} \sigma_i^{n+1} . z_i = 0 \qquad 4.9$$

Where z_i is the distance from the centre of each element to the plane about which moments are taken.

(iii) Application of yield criterion.

The von Mises maximum shear strain energy criterion was used to test whether yielding occurred during each time interval. This criterion states that deformation occurs when:[161]

$$(\sigma_1 - \sigma_2)^2 + (\sigma_2 - \sigma_3)^2 + (\sigma_3 - \sigma_1)^2 = 6G \times \text{constant} \qquad 4.10$$

Under plane stress conditions (i.e. $\sigma_z = 0$, $\sigma_{xz} = 0$ and $\sigma_{yz} = 0$) and with all stresses in the plane of the plate equal (i.e. $\sigma_x = \sigma_y = \sigma$) the von Mises criterion reduces to:

$$2\sigma^2 = 6G \times \text{constant} \qquad 4.11$$

This is the same criterion as the one used in the case of a uniaxial stress system (i.e. $\sigma_2 = \sigma_3 = 0$), so that flow occurred in any element when the stress exceeded the flow stress determined by means of uniaxial tensile tests of the same material in the same condition. The effect of temperature on the uniaxial flow stress of 835M30 in the metastable austenitic condition was not available at the start of the investigation; consequently this data was determined during the present work (see section 4.2.2). This data was used to obtain values of the uniaxial flow stress at the temperature produced in each element during each time interval. These values of the uniaxial flow stress, $\sigma_{f_i}^{n+1}$, were then compared with the previously calculated values of the elastic stress in each element, σ_i^{n+1}:

$$\left.\begin{array}{ll} \text{if } |\sigma_i^{n+1}| > |\sigma_{f_i}^{n+1}|, & \sigma_i^{n+1} = \sigma_{f_i}^{n+1} \\ \text{if } |\sigma_i^{n+1}| \leq |\sigma_{f_n}^{n+1}|, & \sigma_i^{n+1} = \sigma_i^{n+1} \end{array}\right\} \qquad 4.12$$

Initially, strain-hardening was assumed to be zero, as had been the case in the work of Fletcher[144]. If plastic flow occurred in any element, the replacement of the elastic stress by the flow stress caused the forces in the plate to become unbalanced, and condition 4.6 was no longer met. It was therefore necessary to establish a stress distribution, which produced zero net force in the plate after the yield criterion had been applied. This was achieved by an efficient iteration process which involved the following stages:

(a) The elastic stresses in each element at time $n+1$ were determined assuming fully elastic conditions;

(b) The elastic stress in each element was compared with the appropriate value of σ_f, using 4.12: when σ_f was exceeded, the original was replaced by σ_f, otherwise no change in stress level occurred;

(c) The new average stress present in the plate, $\bar{\sigma}^{n+1}$ was found;

(d) If $\bar{\sigma}^{n+1}$ was less than a specified level (usually 0.1 N/mm^2) the stress determination was considered complete and the next stage of the calculation was begun. However, when $\bar{\sigma}^{n+1}$ exceeded the required amount, $\bar{\sigma}^{n+1}$ was subtracted from the elastic stresses previously obtained in each element at stage (a);

(e) Stages (b), (c) and (d) were repeated using the new values of the elastic stress until $\bar{\sigma}^{n+1}$ fell below the required level.

At the end of this process the stress distribution produced after the application of the yield criterion for the last time resulted in a negligible unbalanced force being present within the plate: this stress distribution was used in the next step in the computation. This procedure for the determination of the plastic region in the plate has proved stable and efficient, but between 4 and 20 iterations were usually necessary to reduce the average stress in the plate to below 0.1 N/mm^2.

Figure 75 shows, schematically, the changes in the stress distribution that result from the application of the yield criterion. In reality the stress at each point in the quenched plate would change monotonically from that shown by the broken line in (a) of Figure 75, which existed at time t, to that shown in (d) of Figure 75 at time t+Δt. Only small amounts of plastic flow occurred as a result of thermal stresses during quenching. Consequently changes in the cross sectional area of the elements were considered to have a negligible effect on the stress computations.

(iv) Determination of strain.

The initial estimate of the strain increment produced during any time interval was related to the temperature change generated during this time (equation 4.4). This strain was used to produce the first estimate of elastic stress, prior to the application of the yield criterion. During the iterative procedure used to determine the effect of plastic flow, the initial estimate of the elastic strain was changed, until the subsequent application of the yield criterion produced zero net force in the plate. When a change in the elastic stress had occurred during this iterative procedure, a corresponding change in the elastic strain was required.

Thus $$\left(\Delta\varepsilon_i^{n+1}\right) = \frac{\sigma_i^n}{(a - b\theta_i^n)} - \frac{\sigma_i^{n+1'}}{(a - b\theta_i^{n+1})} \qquad 4.13$$

where a and b are the constants previously defined in equation 4.3 and $\sigma_i^{n+1'}$ is the estimate of the elastic stress immediately before the final application of the yield criterion.

The total strain generated in an element was considered to consist of two parts: the first, $(\varepsilon_i^n)_{thermal}$, arises from the free change in dimensions produced by the change in temperature of the element; whilst the second arises from movements generated by constraints that are associated with non-uniform changes of temperature within the plate. It is solely the latter that gives rise to thermal stress. It was only necessary to consider the total strain achieved at the end of the quench when comparisons were to be made between predicted and experimentally determined distortions.

4.1.2 Procedure assuming strain-hardening

The uniaxial tensile tests of 835M30 in the metastable austenitic condition (described later in section 4.2.2) showed that some strain-hardening was possible at the strain rates associated with the quenching process. Consequently the procedure used to calculate thermal stress was modified to incorporate strain-hardening behaviour. To achieve this it was necessary to determine the increased flow stress that resulted from plastic deformation in previous time steps. These modified values were incorporated into the application of the von Mises criterion, as described above (section 4.1.1 (iii)).

The strain-hardening coefficients obtained from tensile tests on 835M30 in the metastable austenitic condition (section 4.2.2) were dependent upon temperature. Since the maximum strains involved in the work considered were less than 1%, strain-hardening rates of the steel were represented by two linear coefficients.

$$\left(\frac{d\sigma_f}{d\varepsilon_p}\right)_{\varepsilon_p\ 0\rightarrow 0.5\%} = W_1 \qquad 4.14$$

$$\left(\frac{d\sigma_f}{d\varepsilon_p}\right)_{\varepsilon_p\ 0.5\rightarrow 1.0\%} = W_2 \qquad 4.15$$

Where W_1 and W_2 are both temperature dependent, ε_p is the plastic strain obtained from the uniaxial tensile tests, shown schematically in Figure 76.

It was assumed that the increases in flow stress produced during each time interval during cooling could be added together, in order to obtain the total increase in this property. This enabled flow stress data, obtained at constant temperatures, to be used to determine the degree of strain-hardening generated during continuous cooling. However, this technique relies on the assumption that no recovery occurs during the cooling process.

Between the M_s and M_f temperatures it was assumed that plastic deformation would occur in the much softer austentite phase alone. Thus strain-hardening data obtained from austenitic material was also relevant at these lower temperatures.

At the end of each time increment, Δt, it was necessary to calculate the increase in flow stress which had occurred in each element as the result of strain-hardening alone, in order to calculate the effect of strain-hardening on the current value of flow stress. The flow stress used at the start of the stress calculation at time $t+\Delta t$ was obtained from the equation:

$$\left[\sigma_{fi}^{n+1}\right]_1 = \left[\sigma_{fi}^{n+1}\right]_{\varepsilon_p = 0} + \left\{\left[\sigma_{fi}^{n}\right]_{final} - \left[\sigma_{fi}^{n}\right]_{\varepsilon_p = 0}\right\} \qquad 4.16$$

Where $\left[\sigma_{fi}^{n+1}\right]_1$ is the flow stress used at the start of the stress calculation at time n+1. $\left[\sigma_{fi}^{n+1}\right]_{\varepsilon_p = 0}$ is the flow stress of the element at the relevant temperature in the absence of any prior plastic deformation. $\left[\sigma_{fi}^{n}\right]_{final}$ and $\left[\sigma_{fi}^{n}\right]_{\varepsilon_p = 0}$ are the final and initial flow stresses during the previous time increment. The bracketted difference on the right hand side of equation 4.16 is equal to the increase in yield stress due to all the previous strain-hardening experienced by the element during the quench. No data was available for the magnitude of the Bauschinger effect for steels in the metastable austenitic condition: this effect has not been taken into account in the present calculations.

In order to apply the yield criterion in the presence of strain-hardening, a similar procedure was used to that described in section 4.1.1 (iii). Thus the first application of the yield criterion at each time step was made using $\left[\sigma_{fi}^{n+1}\right]_1$. However, when the next iteration was made, and the stress in each element was compared with the flow stress; a new value of the flow stress, $\left[\sigma_{fi}^{n+1}\right]_2$, was used which was calculated from the latest estimate of the plastic strain using:

$$\left[\sigma_{fi}^{n+1}\right]_2 = \left[\sigma_{fi}^{n+1}\right]_1 + W_1 \text{ or }_2 \times \left[\varepsilon_{pi}^{n+1}\right]_1 \qquad 4.17$$

where $\left[\varepsilon_{pi}^{n+1}\right]_1$ is the estimate of plastic strain from the first iteration.

Here $W_{1 \text{ or } 2}$ is the strain-hardening coefficient, defined in equations 4.14 and 4.15. Otherwise the application of the yield criterion is as described in section 4.1.1 (iii).

The incorporation of the strain-hardening into the plasticity calculation increased the number of iterations required to determine the equilibrium stress distributions; but no instabilities were developed.

Figure 77 shows the flow chart on which was based the computer program (written in Fortran IV), used for the complete thermal stress calculation.

4.2 Data Used in Thermal Stress Calculations

The data used for the determination of the time-temperature distribution has already been described in section 3. In order to carry out the remaining part of the thermal stress calculations the following additional data was necessary:-

(i) The relationship between temperature and length of a dilatometer specimen of 835M30 not subject to any restraint during cooling from 850°C.

(ii) Young's modulus, Poisson's ratio, and the stress-strain behaviour of 835M30 in uniaxial tension at all temperatures during cooling from 850°C, when austenite is stable.

To enable the comparison to be made between experimentally determined distortions and those predicted by calculation, it was also necessary to know the overall increase in volume accompanying the hardening of 835M30.

4.2.1 Determination of the change in free length of a specimen of 835M30 steel during cooling from 850°C

A suitable dilatometer curve for 835M30 was not available at the time this work was begun and it was therefore necessary to determine this data during the early stages of the programme. A Linseis horizontal dilatometer was used for this part of the work, with cylindrical specimens, 5 mm diameter and 30 mm length. These were protected from oxidation by an inert gas atmosphere, contained within a silica glass tube. The specimens were heated to 850°C by a tube furnace, positioned outside of the silica glass tube which contained the atmosphere (Figure 78). When the specimens were to be quenched, the tube furnace was slid horizontally away and a stream of inert gas was passed over them. Additional cooling was applied to the outside of the silica glass tube, by means of a cold air blast.

Adjustment of the gas flow allowed the production of cooling rates between 1°C/s and 5°C/s at 400°C. It was evident from the isothermal transformation diagram for 835M30 (see Figure 79) that martensite was the only transformation product obtained by the use of this range of cooling conditions. Thus all of the relationships between specimen length and temperature obtained during quenching from 850°C were very similar. However, Table 7 shows the expansion coefficients of the austenitic phase obtained in each case, together with the M_s temperatures, and the total length changes that accompanied the transformation. The independence of all these values from the cooling rate showed, not only that no thermal stresses had been generated during the cooling of the dilatometer specimens, but also that the austenite→martensite transformation was the sole structural change involved. Result (e) in Table 7 represented the average behaviour, and the dilatometer curve for this result is shown in Figure 80. The following relationships, based on this result, were used to model the relationship between temperature and the length of the dilatometer specimen:

$$\left.\begin{array}{lll} \theta > 300^{\circ}C & \varepsilon_{thermal} & = 2.1407 \times 10^{-5}\theta - 0.01066 \\ 288^{\circ}C < \theta < 300^{\circ}C & \varepsilon_{thermal} & = -0.00422 \\ 90^{\circ}C < \theta < 288^{\circ}C & \varepsilon_{thermal} & = \dfrac{(y' - 1.4435)}{581.23} \\ \theta < 90^{\circ}C & \varepsilon_{thermal} & = 0.6133 \times 10^{-5}\theta - 0.0015 \\ \text{where} & & \\ & y' = 1.0102 + 0.1804\,(x') - 0.35024\,(x')^{2} & \\ & \quad - 1.0244\,(x')^{3} - 0.82481\,(x')^{4} & \\ & x' = 0.0080193\theta - 1.3079 & \end{array}\right\} 4.18$$

The value of the thermal expansion coefficient, α_{ex}, used in equation 4.4 to calculate the elastic stress produced in each element under conditions of full restraint, when the element was cooled from θ_i^n to θ_i^{n+1}, was therefore obtained from:-

$$\left[\alpha_{ex}\right]_{\theta_i^n \to \theta_i^{n+1}} = \frac{\left[\varepsilon_{thermal}\right]_{\theta_i^n} - \left[\varepsilon_{thermal}\right]_{\theta_i^{n+1}}}{\theta_i^n - \theta_i^{n+1}} \qquad 4.19$$

The values used for the thermal expansion coefficient of each element were thus obtained directly from the relevant part of the dilatometer curve, and at the appropriate temperature incorporated the transformation strains accompanying the formation of martensite.

4.2.2 Mechanical properties of 835M30 steel during quenching

Uniaxial tensile tests were carried out on specimens of 835M30 which contained metastable austenite. Thus the specimens, which had been austenitised at 850°C, were quickly cooled to the appropriate testing temperature and tested whilst still in the austenitic condition. For temperatures below 700°C, a horizontal testing arrangement was used, as shown in Figure 81. The specimens were held in grips which were electrically insulated from the rest of the testing machine, by means of the layer of Syndanio (A). The application of an electric current across the terminals (B) produced resistance heating of the specimen, which could also be heated by means of a cylindrical furnace which surrounded it (C). The furnace was maintained at the desired test temperature but the application of the resistance heating allowed the austenitisation temperature to be attained in the specimen only. The removal of this resistance heating caused the specimen temperature to fall very rapidly to that of the furnace, within which it was contained. At this point a uniaxial load was applied along the axis of the specimen and the stress-strain relationship of the material under examination was measured by means of a Hounsfield tensometer. For this purpose, the grips of the tensometer were attached at D and E, and the stress-strain relationships determined by the use of standard procedures.

A series of jets of argon were used to aid the rapid cooling of the specimen to the test temperature, and also to prevent oxidation of the specimen. The specimen temperature was continuously monitored by a chromel-alumel thermocouple, spot welded at the centre of the specimen gauge length. The stress-strain relationships of 835M30 were determined at temperatures between 275°C and 700°C using this apparatus. All specimens were initially austenised for 10 minutes at 850°C before being cooled to the test temperatures. The maximum time taken to cool to the lower temperature was 90 seconds, although an additional period was added to allow the specimen temperature to stabilise.

The test procedure described above was satisfactory provided the specimen was in the austenite condition at the test temperature. When test temperatures below the M_s temperature were used (viz < 300°C), there was a tendency for the specimen to fracture in the shoulders at the end of the gauge length. This occurred because the material in the specimen shoulders had not reached the austenitisation temperature during the previous heat treatment which was only effective along the specimen gauge length. Thus, when the temperature fell below the M_s temperature; the gauge length, which was partially martensitic, was able to withstand a greater load than the softer shoulders, despite the greater cross-sectional area of the shoulders. This tendency became more pronounced at lower temperatures, as the amount of martensite present in the specimen gauge length increased.

This equipment was unsuitable at test temperatures above 700°C, since the mass of the insulated specimen grips caused the specimens to sag during testing. Testing above 700°C was therefore performed with the axis of the specimens in the vertical position, using lighter specimen grips in an Instron tensile testing machine. Austenitisation of the specimens by the use of resistance heating was no longer possible, and the specimen temperature was therefore maintained solely by the use of a tube furnace around the specimen. With this arrangement the specimen could be cooled within the furnace from 850°C to 700°C in 40 minutes. Although this rate of cooling was very slow, the isothermal transformation diagram of 835M30 (see Figure 79) showed there would be no decomposition of the austenite in this time interval. Again an austenitisation treatment of 10 minutes at 850°C was employed before the specimens were cooled to the testing temperature.

In order to assess the strain rates likely to occur in the quenched plates, an initial calculation was made of the thermal stresses produced during the quenching of a plate using a Biot number $\left(\frac{}{2\lambda}\right)$ of 5.03, together with the dilatometer data previously described in section 4.2.1. The mechanical property data used in the calculation was the same as that used by Fletcher[144]. Figure 82 shows the predicted variation in strain with time at the surface and centre of the plate, together with the strain rates at various stages of the quench. From a consideration of these strain rates, and the capabilities of the tensile testing equipment, it was concluded that tensile properties should be determined at 3 strain rates:-

(a) $\dot{\varepsilon} = 0.33 \times 10^{-3}\ s^{-1}$

(b) $\dot{\varepsilon} = 0.65 \times 10^{-3}\ s^{-1}$

(c) $\dot{\varepsilon} = 5.8 \times 10^{-3}\ s^{-1}$

The tensile properties of particular relevance to the present investigation were the flow stress, σ_f, and the strain hardening coefficients W_1 and W_2 (see Figure 76). No suitable extensometers were available to measure the elongation of the specimen gauge length directly during testing. Therefore the crosshead movements of the tensile testing machine were used to determine strain. Figure 83 shows the variation of flow stress with temperature at different strain rates. At the lower strain rates the duration of the tensile test was sometimes greater than 5 minutes, and at temperatures below 350°C a test of this duration might be associated with the formation of some bainite (see Figure 79). Therefore only the highest strain rate ($5.8 \times 10^{-5}\ s^{-1}$) was used at the lower temperatures.

From the results shown in Figure 83 it was evident that the estimated variations in the strain rate did have a significant effect upon the flow stress. It was also apparent from Figure 82 that the strain rate varied in a complex manner during the course of the quench. But it was not possible to incorporate flow stress data as a function of both temperature and strain rate in the calculations of thermal stress. Use was therefore made of temperature dependent flow stress data at a constant strain rate. An accommodation was made for the influence of the two known extremes of the strain rate on the flow stress by using upper and lower range approximations for the variation of the metastable austenite flow stress during the quench (also shown in Figure 83). All calculations of thermal stresses were repeated using both the upper and lower approximations for the flow stress.

The flow stresses used in the thermal stress calculations at temperatures lower than the M_s temperature were a function of the volume fractions of martensite and austenite, and their respective flow stresses[129,144].

viz

$$\sigma_f = V_{\alpha'} \left(\sigma_f\right)_{\alpha'} + V_\gamma \left(\sigma_f\right)_\gamma \qquad 4.20$$

The volume fractions of austenite and martensite present at different temperatures were calculated from the relationship between temperature and length of the dilatometer specimen, using the method shown in Figure 84. A value of 1600 N/mm^2 was used for the flow stress of material that possessed a 100% martensite structure[157].

The effect of temperature on the strain-hardening coefficients W_1 and W_2 are shown in Figure 85(a) and (b). These results exhibited a very marked dependence on strain rate, especially at temperatures below 400°C. However, the introduction of a strain-hardening coefficient which was dependent on strain rate into the calculations presented considerable difficulties; furthermore it was not clear that such additional complications could be expected to produce a significant improvement in the accuracy of the thermal stress calculation (the increases in the flow stresses due to strain-hardening were unlikely to be great, owing to the relatively small amounts of plastic strain produced). Therefore two simple approximations for the variations of W_1 and W_2 with temperature were made for use in the thermal stress calculations (also shown in Figure 85(a) and (b)).

The most relevant data available for the variation of Young's modulus and Poisson's ratio during a rapid cool designed to produce a martensitic structure in a low-alloy steel was that given by Atkins et alia[138]. This data had been determined for 830A31, which is very similar in composition to 835M30, as already described in section 3.2.2. Figure 74 shows the variation of $\frac{E}{1-\nu}$ with temperature derived from data given by Atkins et alia, and the linear approximation used in the calculation (as described previously in section 4.1.2).

4.2.3 Stress relaxation

The method used to calculate thermal stresses assumed that negligible stress relaxation occurred. Nevertheless, it was still considered useful to have some knowledge of the stress relaxation properties of 835M30 to enable an assessment of its possible effect to be made.

Using the same treatment cycle as that used for the determination of the flow stresses, previously described in section 4.2.2, specimens of 835M30 were austenitised in the Instron tensile testing apparatus and cooled to the appropriate test temperature. The specimens were then strained at the highest strain rate of 5.8×10^{-5} s^{-1} until 1% plastic strain had been recorded. At this point the crosshead movement of the machine was stopped and the relaxation of the load remaining on the specimen recorded.

Figure 86 shows the results of stress relaxation tests carried out at 830°C, 790°C, 742°C and 700°C. It is evident that at temperatures above 700°C a time interval of only a few seconds produced some reduction in the stress level.

4.2.4 Overall volume change accompanying the hardening of 835M30

The structure of the plate prior to hardening consisted of a mixture of ferrite and carbide, but after the austenitisation and quenching treatment the structure contained only martensite. These structural changes were accompanied by a volume change that was not associated with the changes in dimensions produced by the thermal gradients present during the quench. Thus the change in dimensions, produced by this change in structure, must be added to those predicted by the thermal stress calculations. To this end cylindrical specimens of 835M30, 10 mm diameter and 90 mm long were heat treated for 3 hours at 630°C to ensure that the initial structure consisted only of ferrite and carbide. The volume of the specimen at this stage was determined by the use of an Archimedes technique, which involved the measurement of the masses of the specimen in air and distilled water. The specimen was heated for 1 hour at 830°C and then water quenched, after which the volume was redetermined at room temperature. The percentage net volume change was calculated by the use of the following equation:-

$$\%\Delta V = \left(\frac{V_Q - V_S}{V_S}\right) \times 100 \qquad 4.21$$

All heat treatments were carried out in a muffle furnace, but in order to prevent oxidation of the specimens during heat treatment each specimen was contained within a silica tube filled with argon. The accuracy of the balance used was ±0.2 mg and four separate weighings were carried out to obtain the change in volume of each specimen. Thus the results of the determination of the volume change, produced by the austenitisation and quenching treatment, were subject to an absolute error of ±0.011% due to balance inaccuracies. In the case of the corresponding isotropic length change the absolute error was ±0.0037%.

Table 8 shows the volumes of the specimens in the softened and quenched conditions, together with the net volume changes associated with the hardening of the specimens. The average net volume change was 0.381% which was equivalent to a linear isotropic change of 0.127%.

After the volumes of the specimens had been determined in the quenched condition, the specimens were placed for ½ hour in liquid nitrogen. The volumes of the specimens were again re-determined. It was found that the volumes of the specimens were unaltered which indicated that a negligible amount of retained austenite had been present in the samples at the end of the quench to room temperature.

4.3 Stability of the Thermal Stress Calculations

The stability criteria relevant to the finite difference solution of the differential heat conduction equation have already been described in section 3.2.2. Additional tests were applied in the case of the thermal stress calculations to ensure that the procedures used were stable. During all these checks, the computation procedure and the data used to generate the temperature distributions remained unchanged. Table 9 contains the data used in the stability tests unless specified otherwise in the relevant parts of the text.

4.3.1 Calculation of thermal stress with an infinite flow stress at all temperatures

For the purpose of this test alone, the computer program used to calculate the thermal stresses was modified so that the flow stress was infinite at all temperatures during quenching. Under these conditions no plastic flow occurred and the residual stress and strain at the end of the quench should be zero. Therefore, the presence of residual stress and strain at the end of the calculation would indicate the build up of errors during the operation of the computer program. The computed residual stress and strain results are given in Table 10. These results showed that at the end of the quench there was virtually zero residual stress and strain, which suggested that the procedure used was stable and not subject to a build up of errors, despite the use of 3,100 time steps during the whole quenching period.

4.3.2 Influence of element size on the calculation of residual stress and strain

Figures 87(a) and (b) show the effect of element size on the calculated distribution of residual stress and strain respectively at the end of a quench. With the exception of the number of elements, which varied in the manner shown in Figures 87(a) and (b), the data used in these calculations was that given in Table 9. The results obtained indicate that only very small improvements were obtained by the use of more than 10 elements. Therefore this number of elements was used during all the subsequent calculations of thermal stress and strain.

4.3.3 Influence of the maximum permitted unbalanced force in the plate on the residual stress and strain

An error was introduced in each time interval by the small finite value of the unbalanced force remaining in the plate after the final application of the plasticity criterion. Therefore a determination was made of the effect of variations in the magnitude of this unbalanced force on the residual surface stress and strain at the end of the quench. Figure 88 shows the surface stress and strain produced at the end of the quench when the maximum permissible unbalanced force gave rise to stresses that varied between 10 N/mm^2 and .01 N/mm^2. As the maximum permissible unbalanced stress was reduced from 10 N/mm^2 to 1.0 N/mm^2 there was a significant variation in the residual surface stress and strain, but the effect of a further reduction in the magnitude of this stress to .01 N/mm^2 was relatively small. During all the subsequent calculations of thermal stress and strain, the maximum permissible unbalanced stress was fixed at 0.1 N/mm^2, which was considered a suitable compromise between the accuracy and the computer time required to carry out the calculation.

4.3.4 Influence of the number of time increments on the residual stress and strain distribution

As already described in section 4.1.1 (i), the different temperature distributions during the quench, obtained from the finite difference solution of the differential heat conduction equation, were only employed for the calculation of thermal stresses and strain when the temperature at the surface or centre of the plate had decreased by more than a prescribed amount. A variation in the magnitude of this prescribed temperature drop allowed a change in the number of steps used in the thermal stress and strain calculations. Hence it was possible to establish the effect of the size of the time interval on the stability and accuracy of the stress calculation.

Figure 89 shows the effect of the total number of time steps used in the calculation on the magnitude of residual surface stress and strain at the surface of the plate; these calculations used the data given in Table 9. It is evident that as the number of steps was increased there was initially some irregular variations in the predicted stresses and strains; but between 200 and 2,000 steps the results of the calculations were reasonably stable. Consequently, the number of steps used in the subsequent calculations of thermal stress and strain lay between these two limits.

4.4 Results of Thermal Stress and Strain Calculations

The mathematical model described in section 4.1 was used to calculate the thermal stress and strain generated in the plate when quenched under various conditions, which corresponded with those under which plates were quenched experimentally (see section 5 below). The values of the physical and mechanical properties used are summarised in Tables 11, 12 and 13: Table 11 also refers to the numbers of the figures which contain the results of the computer calculations, and also gives a key to the abbreviations employed to describe the different data used in the calculations.

4.4.1 Water quenching

(i) 40 mm thick plate

Calculations PR1 to PR6 (see Table 11) show the effect of flow stress and surface heat transfer coefficient on the stress and strain generated when a 40 mm thick plate of 835M30 was quenched in water. The surface heat transfer coefficient had already been found to vary significantly from quench to quench when water was used as the quenchant (see section 3.1.2). The different relationships employed for the flow stress of the austenite and the surface heat transfer coefficient were found to influence the predicted stress and strain very significantly (see Figures 92 and 93). However, the generation of stress and strain during the quenching of the plates was found to follow the same general pattern under all the conditions considered. Therefore the effect of time on the distribution of stress and strain during the quench has been presented for one quench only - PR1/W40/hAv/UFS*.

Thus Figure 90 shows the relationship between stress and strain in the surface and central elements of the plate predicted by the calculation PR1/W40/hAv/UFS; and the stress distributions across the plate at various stages during the quench are shown in Figure 91. During the initial stages of the cooling process a tensile stress was developed at the plate surface, but this was balanced by compressive elastic stresses towards the centre of the plate. As the temperature difference between the surface and centre became greater, the surface tensile stress increased until plastic deformation occurred: further increases in stress only occurred when the flow stress of the material increased (such an increase was due to a reduction in temperature and strain-hardening). Similarly, the compressive stress at the centre of the plate increased until it produced plastic deformation, and then increased at a rate dependent on the change in flow stress.

---

*An explanation of these abbreviations is given at the bottom of Table 11.

The maximum tensile stress at the surface occurred when it had cooled to 379°C, which corresponded with the development of the maximum temperature difference between the surface and centre of the plate. As cooling proceeded further, the temperature difference between the surface and centre of the plate was reduced. Consequently, the surface stress became less tensile and, conversely, the stress at the centre became less compressive. When the surface had cooled below 290°C (i.e. $<M_s$ temperature), there was a rapid expansion, which accompanied the martensite transformation and the stress at the surface became highly compressive (see Figure 91(b)). However, plastic flow at the surface was prevented by the equally rapid increase in the flow stress of the material that accompanied the transformation. The generation of a large compressive stress at the surface caused the stress at the centre to become increasingly tensile; but the material at the centre was still at a high temperature (around 700°C, where plastic flow occurred at much lower stress levels than was the case at the surface of the plate at that time): thus considerable tensile plastic flow was produced at the centre of the plate. As the transformation of austenite to martensite approached completion at the surface, those elements nearer to the centre also began to transform: this produced another reversal of the stress distribution within the plate (see Figures 91(c), (d) and (e)).

(ii) 20 mm thick plate

Calculations PR7 to PR12 (see Table 11) simulated the thermal stress and strain generated during the water quenching of a 20 mm thick plate of 835M30. Figure 94 shows the relationship between stress and strain in the surface and central elements obtained by calculation PR7/W20/hAv/UFS. The results obtained were very similar to those calculated in the case of a 40 mm plate (eg. calculation PR1/W40/hAv/UFS, described above), except there was a reduction in the extent of the plastic flow, which led to changes in the residual stress, and there were some small changes in the temperatures at which the various stages of the generation of thermal stress and strain (cf. Figures 90 and 94).

As in the case of the 40 mm plate, the use of the different relationships for the surface heat transfer coefficient and the flow stress of the austenite were found to influence the predicted residual stress and strain very significantly (see Figures 95 and 96). Though again the generation of stress and strain during the quench was found to follow the same general pattern under all the conditions considered.

4.4.2 Oil quenching

The relationships between thermal stress and strain during the oil quenching of 20 mm thick plates of 835M30 were predicted by calculations PR13/OIL20/UFS and PR14/OIL20/LFS. The variation of the surface heat transfer coefficient with temperature during the quench was represented by a single set of values in the case of oil quenching (see Table 5(d)), since it had been found in the earlier experimental work that a consistent variation of the surface heat transfer coefficient with temperature was obtained during several such quenches (see section 3.2.1). Thus two calculations only were required, which examined the influence of variations in the relationship between the flow stress of the austenite and temperature during the quench. Since the results of these calculations differed only slightly from one to another, only results of calculation PR13/OIL20/UFS have been presented in detail. Thus Figure 97 shows the relationship between thermal stress and strain at the surface and central elements of the plate when quenched in oil, and Figure 98 shows the distribution of stress in the plate at various stages during the quench.

The results reported in Figure 97 are basically similar to those obtained by a water quench, thus tensile and compressive stresses were developed initially at the surface and centre respectively and the magnitude of both these stresses increased until plastic flow occurred at both the surface and central regions. However, much less plastic flow occurred than was the case when water quenching was used: this was due to the smaller values of the surface heat transfer coefficient that existed during the stable vapour blanket stage at the start of the quench.

There was an initial peak in the tensile stress at the surface, which occurred at 740°C (see Figures 97 and 98(a)). This coincided with the development of an initial peak in the temperature difference between the surface and centre of the plate when the heat transfer at the surface of the plate was still in the vapour blanket regime. The stress at both the surface and centre was then reduced (see Figure 98(b)) until at 546°C the surface stress had become slightly compressive. However, the onset of nucleate boiling, which involved a sharp increase in the surface heat transfer coefficient, caused the temperature gradient within the plate to increase once more: this was associated with the development of an increasingly tensile stress at the surface (see Figures 97 and 98(c)), which eventually produced further plastic flow in this region of the plate. The flow stress of the material at the centre of the plate was not exceeded at this stage in the cooling process.

As nucleate boiling subsided, and the magnitude of the surface heat transfer coefficient fell, the stress at the surface became less tensile, until just before the start of the martensite transformation (see Figure 98(d)) when it became compressive. At this stage the temperature difference between the surface and centre of the plate was merely 27°C, so that the progressive transformation of the austenite to martensite caused only small modifications to the existing stress distributions (see Figures 98(d),(e) and (f)).

The use of the different relationships that described the variation in the flow stress of the austenite with temperature during the quench had only a small effect on the predicted residual stress and strain (see Figures 99 and 100).

4.4.3 Polymer quenching

The prediction of thermal stress and strain within plates cooled in a polymer quenchant were obtained from calculations PR15/AQUA20/UFS and PR16/AQUA20/LFS (see Table 11). As in the case of oil quenching, a single set of values was employed to model the variation of the surface heat transfer coefficient with temperature. Thus the two calculations carried out investigated the influence of variations in the relationship between the flow stress of the austenite and temperature. Once again, since the results of these calculations differed only slightly, only the results of calculation PR15/AQUA20/UFS have been presented in detail (see Figures 101 and 102).

The predicted variation in thermal stress and strain was similar to that predicted in the case of water quenching (cf. Figures 94 and 101), though less plastic flow was produced at both the surface and centre. The use of the different relationships between the flow stress of the austenite and temperature did affect the calculated residual stress and strain to some extent (see Figures 103 and 104).

5. EXPERIMENTAL DETERMINATION OF RESIDUAL STRESS AND STRAIN IN QUENCHED PLATES

In this stage of the work, plates of 835M30 steel were quenched and the residual stress and strain in the plates was determined experimentally. The thickness of the plates, and quenchants used, were the same as those used for the calculations described in section 4.4.

5.1 Experimental Procedures

5.1.1 Specimens

Specimens of Type C and D, with thicknesses of 40 mm and 20 mm respectively, were used for this stage of the work (see Figure 105). All the specimens were made from 835M30 steel, the composition of which is given in Table 3. Heat treatments were carried out in a muffle furnace purged with argon, but the specimens were first electroplated with 0.05 mm of nickel to prevent the formation of surface oxide during transfer from the furnace to the quenching tank. This thickness of nickel represented a maximum of only 0.5% of the thickness of the plates and was considered to have a negligible effect on the thermal stress distribution. To ensure uni-dimensional heat flow during quenching, the edges of the plates were insulated with a 6 mm thick layer of Kaol Wool ceramic fibre insulation which was lightly held in position by a band of steel. The tension of the steel band was so low that no significant constraining forces were applied to the edges of the plates.

5.1.2 Heat treatment procedure

The first stage of the heat treatment performed on all the 835M30 plate specimens was a softening treatment that involved heat treatment at 630°C for 2 hours, followed by a furnace cool in the muffle furnace. This ensured that the material was in the ferritic condition and that any residual stresses from previous operations were removed. The surfaces of the plates were then lightly cleaned with 400 grade silicon carbide paper, to obtain constant surface conditions before each quench. The dimensions of the plates were measured, using the technique described later in section 5.1.3, and the plates then fitted with the Kaol Wool insulation around their edges.

Austenitisation was carried out at 850°C. In order to ensure adequate soaking time, a thermocouple was held in contact with the specimen inside the furnace. When the temperature of this thermocouple had reached 850°C the specimens were kept in the furnace for a further 1½ hours, after which they were quenched. Quenching was carried out in the same tank that had previously been used for the determination of the surface heat transfer coefficients (described in section 3.1.1), and care was taken to ensure the minimum disturbance of the quenchant when the specimens were transferred from the furnace to the quenching tank. The conditions in the quenching tank were the same as those which had been used earlier in the determination of the surface heat transfer coefficients. Once the specimens had cooled to the temperature of the quenchant, they were removed and their new dimensions and residual stress distributions measured.

5.1.3 Measurement of distortion

Preliminary experiments were carried out using 40 x 125 x 125 mm Type C plates which had been oil quenched. After quenching, the changes in dimensions between the opposite edges of the plate were found to vary between 0.15 mm and 0.05 mm when measured using a micrometer.

However, this method of measurement gave an accuracy of only around ±0.025 mm, which was considered insufficient for the changes involved. Measurements were then made using a Societe Genevoise Universal Measuring Machine that gave a consistent accuracy which was better than ±0.001 mm. This machine was used for all subsequent measurements of the dimensions of the plate specimens.

The positions at which the dimensions of the specimens were determined are shown in Figures 106 and 107. The change in the distance between the reference points A to K on the edges of the plate, were then used to determine the distortions produced during each quench using:-

$$\%\Delta Y = \frac{Y_Q - Y_S}{Y_S} \times 100 \qquad 5.1$$

Re-measurement of the specimen dimensions was made no later than 48 hours after the specimen had been quenched, the first 24 hours of which allowed the specimens to acclimatise to the conditions in the Metrology laboratory where the measurements were made.

Even with insulation around the edges of the plates, which ensured uni-dimensional heat flow almost up to the edges of the plate, measurements made close to the edges of the plate were affected by departure from the "infinite" plate condition. Boley and Weiner[67] demonstrated, by the application of Saint-Venant's principle, that edge effects in plates subjected to thermal stress are negligible at more than one thickness of the plate away from the edge.

Although measurements of the change in plate length and width (i.e. the x and y directions in Figure 73) were affected by the presence of the plate edges, it was possible to obtain some information about the strain generated in these directions at points away from the edges by measurements of the change in thickness of the central portion of the plate. Thus, since no stress existed in a direction perpendicular to the plane of the plate, measurements of the percentage change in the thickness of the plate on a line connecting the mid points of the two large faces could be directly related to the changes in the length and width of the plate. However, since the lines on which these measurements were made traversed all the elements into which the plate had been divided (Figure 73), this change in thickness was associated with the mean change in the length and widths of all these elements. Thus the change in thickness of an individual element was given by:

$$\%(\varepsilon_z)_{e-p} = \left(\frac{T_Q - T_S}{T_S}\right) \times 100 - \frac{\%\Delta V}{3} \qquad 5.2$$

The terms T_Q and T_S are defined in Figure 108.

The term $\frac{\%\Delta V}{3}$ is due to the change in dimensions that arose as a result of the change from the ferrite and carbide structure, present before austenitising, to a martensitic structure, after hardening. As has been stated above this change in volume was independent of the generation of thermal stress.

The strain in the z direction, $\%(\varepsilon_z)$, at the centre of the plate was related to the strain in the x and y directions (i.e. in the plane of the plate) by:

$$\left(\%\bar{\varepsilon}_x\right)_{e-p} = \frac{1}{2}\sum_{n=1}^{n=2j} \%\left((\varepsilon_z)_n\right)_{e-p} \qquad 5.3$$

assuming of course that $\left(\%\bar{\varepsilon}_x\right)_{e-p} = \left(\%\bar{\varepsilon}_y\right)_{e-p}$

The strain $\%\bar{\varepsilon}_x$ was due only to the presence of thermal gradients, so that the total mean strain produced in this direction was given by:

$$\%\ (\bar{\varepsilon}_x)_{total} = \frac{1}{2}\sum_{n=1}^{n=2j} \%\left((\varepsilon_z)_n\right)_{e-p} + \frac{\%\Delta V}{3} \qquad 5.4$$

Although the amount of strain in the x direction varied from element to element, a measurement of the average strain, which was known to be unaffected by edge effects, was of the greatest value.

Figure 109 shows the change in thickness at different positions in a 17 x 119 x 119 mm plate of 835M30 which had been water quenched. The results confirmed the existence of an appreciable region at the centre of the plate where the change in thickness was relatively constant.

5.1.4 Measurement of residual stress

A destructive, mechanical technique was used to measure the residual stress distribution throughout the thickness of the plates. The procedure used was developed by Treuting and Read[162], but modified by Andrews[2]: however, it was found necessary to modify further the calculation of the effect of the removal of a layer of material on the stresses present in the remainder.

The technique consisted of a measurement of the change in strain at one surface of the plate, whilst successive layers of the plate were removed from the opposite surface. The removal of large quantities of very hard material required the use of surface grinding at a very slow rate (1 mm of plate thickness per hour). Even then it was necessary to cool the specimen with large quantities of water if stresses were not to be introduced by the grinding operation. A long period of time was required to complete the stress determination in a complete section, which presented considerable difficulties with respect to the stability of the instruments used to measure the output from the strain gauges. This situation was aggravated by the oscillation of the bed of the surface grinding machine and the presence of large quantities of water in the vicinity of the strain measuring equipment.

The main problem experienced was the penetration of water into the insulation around the strain gauge. Satisfactory readings were eventually obtained with the arrangement shown in Figures 110 and 111. To insure against the introduction of spurious signals not connected with the strain in the plate, a second strain gauge was installed as a standard on the spacing plate used to support the plate on the bed of the surface grinding machine. Both strain gauges were read each time a strain measurement was made and the differences between the readings was used to calculate the residual stresses present in the layer which had just been removed. All of the strain gauges used were rosettes of the Tokyo Sokki Kenkyujo FRA-6-11 type, each of which contained three arms. The rosettes were fixed at the centre of the plate surface, as shown in Figure 110. All the strain measurements were made using a Sangamo Type C52 Direct Reading Transducer Meter. During all the stress determinations the changes in strain were found to be independent of the orientation of the strain gauges i.e. all stresses in the plane of the plate were equal at the surface of the plate, and the mean of the results obtained from the three arms of the rosettes was used in the subsequent calculation of stress.

A Burdett surface grinding machine was used to remove the layers from the plates, utilising the grinding conditions given in Table 14. Strain gauge readings were made after 1 mm thick layers of the plate had been removed. This material was removed by a series of cuts 0.075 mm deep, but the last 0.125 mm of each millimetre layer was removed by smaller cuts, the last being only 0.025 mm deep: this ensured that surface stresses induced as a result of surface grinding were the minimum possible. After each 1 mm layer had been removed, the plate was allowed to stand until the small amount of heat generated by grinding had been dissipated and the strain gauge readings had stabilised. This normally took between 5 and 15 minutes.

The method by which the residual stresses were calculated from the strain gauge results is given in Appendix 2. It was not possible to measure the stresses throughout the whole thickness of the plates as there was a minimum possible thickness to the remaining plate, below which grinding was not possible. However, in each case an estimate of the residual stress in the remaining parts of the plate was obtained by consideration of the following:-

(i) There must be equilibrium of forces acting in the plane of the plate.

(ii) There must be equilibrium of moments within the plate.

(iii) The residual stress distribution should be symmetrical about the centre of the plate.

5.2 Results of the Measurements of the Residual Stresses and Strains Present in Quenched Plates

5.2.1 Water quenched plates

Specimens of types C and D were prepared from 835M30 material, the composition of which is given in Table 3: these were quenched in still water at 20°C, using the procedure described in section 5.1.2.

The distortions produced when a 40 mm plate (Type C specimen) had been quenched, softened and re-quenched under identical conditions are given in Table 15. The mean values of the distortions at positions A to K are also shown graphically in Figure 112, together with the average distortions calculated from the thickness changes at the centre of the specimen, (using equations 5.2 and 5.4) which were free from edge effects: the latter are shown by the horizontal lines. The average strain represented by the latter were very high in comparison to the strain values obtained by direct measurement of the length, which were very significantly affected by the edge effect.

The residual stresses present in the plate after the final quench were determined using the procedure described in section 5.1.4; except that after 22 mm of the thickness had been ground from the plate another strain gauge was attached to the freshly ground surface and grinding resumed on the opposite surface until a further 8 mm had been removed from that surface. Figure 113 shows the results of the residual stress determination. An estimate of the residual stress present in the remaining 10 mm of the plate was made, based on the considerations given in section 5.1.4.

Similarly, the distortions produced when a 20 mm plate (Type D specimen) had been quenched in water are given in Table 16. The mean values of the distortions at positions A to K are also shown graphically in Figure 114, together with the average distortion calculated from the change in thickness at the centre of the plate (shown as a horizontal line). This plate, which had a much greater width to thickness ratio than the Type C specimen, had warped slightly during quenching. This warpage was reflected in the lack of symmetry in the dimensional changes about the centre of the plate (see Figure 114). However, the measurement of the change in thickness at the centre of the plate would not have been affected by this warpage.

In the case of this thinner specimen the discrepancy between the average strain determined from the thickness measurements and the strains obtained directly from length measurements was very much smaller than that observed from the 40 mm specimens.

The results of the residual stress determination on the Type D specimen are shown in Figure 115. 16 mm of the 20 mm thickness were removed by grinding, using the strain gauge technique to measure the changes in strain. Since the plate had been reduced to 4 mm thickness, the stress in the opposite surface to that which the strain gauge had been attached to, was easily determined by grinding 1 mm from the surface and measuring the change in curvature of the plate[163]. Measurements of the plate curvature were made using a Rank Xerox Talylin surface profilometer. The stress in the remaining 3 mm of the plate was estimated from the considerations given in section 5.1.4.

5.2.2 Oil quenched plates

Oil quenching was carried out using R.D.N. 175 oil at 20°C and both agitators in the quenching tank were operated at 50 rpm; otherwise the quenching procedure was the same as that described in section 5.1.2. Table 17 shows the distortions which were generated in a Type D specimen during quenching and Figure 116 shows the mean distortions between the edges of the plate obtained from measurements of the change in length of the plate, and the average result calculated from the change in thickness at the centre of the plate (shown as a horizontal line). A slight warpage of this specimen also occurred during quenching, which introduced errors into the measurement of the distortions between the edges of the plate and accounts for the non-symmetrical appearance of the width changes shown in Figure 116. Nevertheless, the change in thickness at the centre of the plate was considered free from warpage effects.

The results of the residual stress determination for this plate are shown in Figure 117. The general level of these stresses was substantially less than those found in the case of the water quenched specimens (Figures 113 and 115).

5.2.3 Polymer quenched plates

Polymer quenching was carried out using a 25% by volume aqueous solution of "Aquaquench 1250" at 20°C, with both agitators in the quenching tank rotated at 50 rpm. Otherwise the details of the heat treatment procedure were the same as those described in section 5.1.2. Table 18 shows the distortions which were generated in a Type D specimen during quenching and Figure 118 shows the mean distortions between the edges of the plate, obtained from the changes in width of the specimen, and the average result calculated from the change in thickness at the centre of the plate (shown as a horizontal line). This specimen exhibited only a slight warpage and the distortions were nearly symmetrical about the centre of the plate.

The results of the residual stress determination are shown in Figure 119. The general level of stress was closer to that found in the case of the water quenched 20 mm plate (see Figure 115) than the oil quenched 20 mm plate (see Figure 117). Conversely, it is interesting to note that the distortions generated in the polymer quenched plate were closer to those produced in the oil quenched 20 mm plate (compare Figures 116 and 118) than those produced in the water quenched 20 mm plate (see Figure 114).

6. DISCUSSION

6.1 Surface Heat Transfer Coefficients Obtained During Quenching

The determination of the surface heat transfer coefficients reported here involved the measurement of the relationships between time and temperature just below the surface of the specimen. This was necessary because the variation in h during a quench manifested itself in modifications to the rate of change of temperature with time within the specimen, and these modifications were attenuated at points towards the centre of the specimen. The values of h were subsequently used to calculate the temperature distributions during the quenching of specimens of various dimensions. The accuracy with which h is determined is dependent upon the accuracy of the data employed in the calculations. Comparison of the experimentally determined relationships between temperature and time at the centre of the quenched plate, used in the determination of h, with the predicted relationship between the same variables was reasonably good (Figure 55). This indicates that the values of h used in the determination of the latter relationship were accurate and justifies the use of the determined values of h in the subsequent calculations of thermal stress and strain.

6.1.1 Water quenching

Although careful attempts were made to maintain constant experimental conditions, the magnitude of the surface heat transfer coefficients obtained during a series of similar quenches were subject to considerable variation. Thus small variations in the condition of the surface could produce wide variations in the rates of cooling obtained at a point just below the surface of the specimen (Figure 48).

Only when both surfaces were prepared with extreme care to the same high standard of finish (400 grade) were similar curves obtained (Figure 51).

Oxidation of the surface during heat treatment also had a similar effect on the surface heat transfer coefficient. In the absence of any oxidation the stable vapour blanket, normally considered to be a characteristic of water quenching, was almost entirely absent, although the production of even a thin layer of opaque oxide was associated with a well defined vapour blanket stage (Figure 52). The influence of the oxide layer on the characteristics of the quenching process may be associated with either a change in the emissivity of the surface, as the oxide layer becomes opaque, or else with a change in the topography of the surface, as particles of oxide modify the shape of surface imperfections.

This relationship between the layer of oxide and the surface heat transfer coefficient is contrary to the work of Beck and Chevrier[125,126], who deposited much thicker layers of materials with low conductivity onto the surface of the steel. Under these circumstances the flow of heat was impeded by the insulating layer, resulting in insufficient generation of vapour at the surface of the specimen (Figure 30). Thus a stable vapour blanket was suppressed. However, in the present work the oxide layer was very thin (of the order of the wavelength of light) and unlikely to have acted as an insulating layer.

The wide variations between the values of the surface heat transfer coefficients obtained during quenches into water at 20°C (Figures 47 and 53) are thought to be partly due to the low stability of the vapour blanket stage and hence its sensitivity to the influence of minor variations in experimental variables, such as surface condition. Similar results have been reported by Bigot[127] and by

Adams and Rogers[14]. The latter pointed out that it is very difficult to establish the temperature at which one regime takes over from the other, owing to the low stability of the film boiling regime. Bigot[127] has suggested that the thickness of the vapour blanket during quenching is dependent upon the ratio of the heat transferred by convection through the vapour, to that transferred by radiation. Figure 120, which shows the results of Bigot's calculations, suggests that the thickness of the vapour blanket obtained becomes smaller as the initial temperature of the quenchant or the surface temperature, is reduced. Thus the very thin layers associated with a quenchant at 20°C may explain the unstable nature of the vapour layer.

The low stability of the vapour blanket has important practical implications. Following the work of Stolz et alia[95], it has been widely thought that during water quenching the nucleate boiling peak occurs at around 150°C to 200°C. On occasions[55] this has been associated with the formation of quench cracks, since this temperature range lies between the M_s and M_f temperatures of many steels. The present work clearly shows that it is possible for this nucleate boiling peak to occur at much higher temperatures, e.g. in the range 300°C to 450°C. Even more significantly, the present work also suggests that, where the surface is virtually oxide free, the vapour blanket stage may be almost absent. Hence very high rates of heat transfer may occur from the start of the quench (Figure 51).

6.1.2 Oil quenching

A well-established vapour blanket stage, associated with a low value of the surface heat transfer coefficient, persisted at surface temperatures down to 550°C, regardless of whether or not the specimen surface was oxidised.

Nucleate boiling occurred over a much narrower range of temperature than was the case with a water quench and the maximum values of the surface heat transfer coefficient were substantially lower than the maximum values obtained during water quenching (compare Figures 57 and 53).

The most relevant data available for comparison with the present values of surface heat transfer coefficient was obtained by Stolz et alia[95], (Figure 121). However, even here a precise comparison is not possible, on account of the different temperatures and physical properties of the quenchants. Nevertheless, it is apparent from a comparison of Figures 57 and 121 that considerable similarities exist between the results obtained by Stolz et alia with a slow oil, and that found in the present work, which used RDN 175. The differences in the peak values of h can probably be explained by the different physical properties of the two oils.

Very consistent values of the surface heat transfer coefficients were obtained during a series of oil quenches under identical conditions: this contrasts with the results obtained using water quenchants (compare Figures 53 and 57). This has important implications for the industrial quenching of components, since variations in the surface heat transfer coefficient from quench to quench have a significant effect on the distortion present after the completion of the quench (this will be discussed later in section 6.4.2). Thus the very consistent values of the surface heat transfer coefficient during oil quenching may explain the widely held opinion that the distortion produced by an oil quench is much more consistent than that obtained after a water quench.

6.1.3 Polymer quenching

The results obtained do not clearly show the advantages of the polymer quenchant relative to water. The concentration of polymer required to produce a significant effect on the relationship between time and temperature during quenching was high, and even at the highest concentration used (25% by volume) the values of the surface heat transfer coefficient obtained during the nucleate boiling stage were only marginally less than the lowest values obtained during the same stage of the water quench (compare Figures 53 and 61).

It has been proposed that this type of polymer quenchant does not produce a vapour blanket at the start of the quench, although low values of the surface heat transfer coefficient occur during this stage of the cooling process, on account of a film of polymer deposited onto the specimen surface[113]. The results of the present work clearly showed a reduction in heat transfer during the early stages of the quench, which persisted down to around 800°C (Figures 60 and 61). It is tentatively suggested that this reduction was due to the formation of a vapour blanket rather than the deposition of polymer onto the specimen surface. That any polymer could resist degradation whilst in contact with a steel surface above 800°C is unlikely.

When the 'vapour blanket' did break down, there was a rapid increase in the surface heat transfer coefficient at temperatures between 800°C and 600°C, and the values of this property over this temperature range were similar to those obtained by the use of a water quenchant (compare Figures 53 and 61). Below 600°C a small reduction in the surface heat transfer coefficient did occur before this property again rose to a higher level at lower temperatures (Figure 61). This effect was not produced during a water quench and would therefore appear to be associated with the polymer additions. Deposition of a layer of polymer at these temperatures might be responsible for this effect.

6.2 The Calculation of Temperature Distributions During Quenching

6.2.1 Comparison between temperature distributions determined by experiment and by calculation

The accuracy of the results obtained from the solution of the differential heat conduction equation, used to calculate the temperature distributions, clearly depends upon the accuracy of the physical property data employed. Therefore, a comparison between the calculated and experimentally determined temperature distributions, provides an essential check on the accuracy of the predictions made in these calculations.

From Figure 69 it is apparent that, in the case of water, reasonable agreement has been obtained between the calculated and experimentally determined temperature distributions in a 40 mm plate of 835M30 steel. The poorest agreement occurred during the early stages of the quench, which may be explained by discrepancies in the values of the surface heat transfer coefficient employed during the initial part of the quench. It can be seen from Figure 70 that the use of average values for the thermal conductivity and specific heat of the steel, rather than temperature dependent functions, introduced only small errors in the calculation and these errors were significantly less than the discrepancies between the calculated and experimental temperature distributions during the early part of the quench (Figure 69).

It is possible that the nickel plating used to protect the surface of the plate of 835M30 steel may have resulted in a change in the duration of the vapour blanket stage compared to that experienced in the case of the stainless steel specimens employed to determine the surface heat transfer coefficient. As already discussed in section 6.1.1, the duration of the vapour blanket stage during quenching into water at 20°C varies erratically and is susceptible to variations in surface condition. This would explain the discrepancy between the calculated and experimentally determined temperature distributions during the early stages of the quench.

In the later stages of the quench, the calculations predicted slightly less severe temperature gradients within the plate than those measured experimentally. The reason for this is not clear, although a greater value of the surface heat transfer coefficient during the nucleate boiling stage would have resulted in an improved correlation.

Better agreement between the calculated and experimentally determined temperature distributions was obtained in the case of oil quenching (compare Figures 72 and 69). This improved agreement may be explained by the more reproducible values of the surface heat transfer coefficient obtained during oil quenching, (compare Figures 57 and 53). The agreement between the calculated and experimentally determined temperature distributions confirms that the correct values for the thermal properties of 835M30 steel were used in the calculations.

6.2.2 Influence of specimen size on the surface heat transfer coefficient

Earlier in section 2.3.2 it was pointed out that the surface heat transfer coefficient was originally considered to be independent of specimen size[93], but more recently the work of Mitsutsuka and Fukuda[115], and Beck and Chevrier[103] has cast doubts on this suggestion. Of special significance is the assertion by Flament et alia[118] that it is thus impossible to characterise a quenchant by a heat flux relationship dependent on the surface temperature alone. However, the present work has shown that in the case of oil quenching, very similar values of h may be obtained from both the 3.3 mm and 15 mm AISI 304 steel specimens (compare Figures 56 and 57). When these values for the surface heat transfer coefficient were used to calculate the temperature distributions produced in a 40 mm 835M30 steel specimen, good agreement was obtained with experimentally measured temperature distributions (Figures 71 and 72). This indicates that a similar relationship exists between the surface temperature and surface heat transfer coefficient for the 3.3 mm, 15 mm and 40 mm plates during oil quenching.

In the case of water quenching, although some difference was found between the values of h obtained from the 3.3 and 15 mm plates of AISI 304, the results are nevertheless essentially similar (Figures 47 and 53): the maximum value obtained using the 3.3 mm plate (11,800 $W/m^2 {}^\circ C$) is very similar to the lowest peak value obtained from the 15 mm plate (12,300 $W/m^2 {}^\circ C$). When the values of h obtained from the 15 mm plate were used to calculate the temperature distributions produced in the 40 mm plate of 835M30 steel, same measure of agreement was again obtained with experimentally determined temperature distributions (Figures 68 and 69).

The present work therefore shows that a simple relationship exists between the surface temperature and the surface heat transfer coefficient,over a certain range of experimental conditions (certainly 3.3 mm to 40 mm thick plates in the case of oil quenching; 15 mm to 40 mm and possibly also down to 3.3 mm thick plates in the case of water quenching). However, there has been no investigation of such relationships with plate thickness in excess of 40 mm.

6.3 Mechanical Properties of 835M30 Steel During Quenching

The experimentally determined variation of the flow stress of 835M30 with temperature during a rapid cool from 850°C is shown in Figure 83. These results were used to derive the values of flow stress used in the thermal stress calculations; Figure 122 compares this data with the values used by Fujio et alia[150], Fletcher[144] and Toshioka[149]. The data used by Fujio were obtained from a linear interpolation between the tensile strength of a 0.45% C steel in the annealed and quenched conditions at room temperature and a single determination of the high temperature strength at 875°C. The values used by Fletcher were those determined by Harrington[164] over a limited range of temperatures: these latter results were obtained using an earlier version of the apparatus used in the present work. The flow strengths employed by Toshioka were linear interpolations from measurements of the flow strengths of austenitic steels at 0°C, 550°C, 800°C and 1000°C (see Table 2). The comparison shown in Figure 122 indicates that the best agreement is between the values used by Toshioka and those used in the present work. The differences between the present results and those obtained by Harrington are probably the result of modifications to the apparatus which ensured that specimens were rapidly cooled to the lower test temperatures and tested before any bainite was formed, together with an improved method of supporting the specimens at the higher temperatures.

An important feature of the variation of flow strength with temperature (Figure 83) was the marked increase in flow strength at temperatures just below the M_s temperature. This behaviour was in agreement with the model used in the subsequent thermal stress calculations, which assumed that at temperatures between the M_s and M_f the flow strength of the material varied in proportion to the flow strengths and volume fractions of austenite and martensite present (Equation 4.20 and Figure 84). The dilatometer curve, that shows the relationship between length and temperature of specimens of 835M30 cooled from 850°C (Figure 80), clearly indicates that a small reduction in temperature below 290°C produced a large increase in the volume fraction of martensite present in the specimen, and thus the flow strength of the material was calculated to increase sharply at this stage of the quench. This is an important point because, as will be discussed later in sections 6.4 and 6.5, the rate of increase of flow strength during the martensitic transformation has a marked effect on the residual stress distribution predicted at the end of the quench.

The effects of temperature and strain rate on the strain hardening rate of 835M30 in the austenitic condition show two interesting phenomena (Figure 85). A reduction in the strain rate caused a small maximum in the strain hardening coefficients at temperatures between 500°C and 700°C. Furthermore at temperatures below 500°C a decrease in the strain rate caused the strain hardening coefficients to decrease significantly. Although the reasons for these effects are not clear, it is tentatively suggested that a complex interaction between the strain hardening coefficient, temperature and strain rate may lead to some decomposition of the austenite phase at treatment times much shorter than those required in stress free specimens. It is interesting to note that the temperature of the nose of the pearlite transformation in the isothermal transformation diagram of 835M30 (Figure 79) coincides with the temperature at which the strain hardening rate develops a maximum (Figure 85).

The only comparable strain hardening data available for metastable austenite is that used by Toshioka[149]. It is apparent from the comparison shown in Figure 123 that the mean values of strain hardening rate used in the present work are very similar with those used by Toshioka.

6.4 Prediction of the Thermal Stress and Strain Developed During Quenching

6.4.1 Characteristic stages in the stress-strain cycle

The generation of thermal stress and strain during quenching followed a sequence that was very similar in all the cases examined. The identification and understanding of the different stages of this sequence, experienced at the surface and centre of the plate, simplifies the analysis of the results obtained with different quenchants and plate thicknesses, thus enabling the results to be interpreted more clearly and concisely. The stages identified were as follows:-

(i) Initially the surface cooled more rapidly than the centre of the plate and tensile stresses were developed at the surface of the plate (A-B in Figure 124). Even for the lowest quenching severity considered (20 mm plate, oil quenched), the tensile stresses at the surface increased to values in excess of the very low flow stress of the material at the high temperatures in question (B-C in Figure 124). The tensile stresses developed in the surface regions of the plate were accompanied by the development of compressive stresses in the remainder of the plate (A-B' in Figure 124) which produced, in every case considered, some compressive plastic flow in the central regions of the plate (B'-C' in Figure 124). (Note that the onset of plastic flow at the surface and centre of the plate usually occurred at different times.) The tensile stress at the surface of the plate reached a maximum value (C in Figure 124) and then fell; the tensile region at the surface was now no longer cooling more rapidly than the central compressive region.

(ii) When the cooling rate at the centre of the plate exceeded that at the surface of the plate, the stresses at the surface became less tensile (C-D in Figure 124) as the surface regions contracted less quickly than the central regions. Simultaneously the compressive stress at the centre was reduced until it became tensile (C'-D' in Figure 124). When the temperature at the surface of the plate had cooled below the M_s temperature, the material at the surface commenced the expansion associated with the formation of martensite. This expansion caused the stress at the surface to become significantly more compressive, and the stress at the centre correspondingly more tensile. In the case of 835M30 the tensile stresses produced at the centre of the plate by the expansions accompanying the formation of martensite in the surface regions of the plate were sometimes large enough to cause plastic flow towards the centre (D'-E' in Figure 124), on account of the relatively low flow stress of the material in this region of the plate. However, compressive plastic flow was not produced at the surface owing to the rapid increase in flow strength associated with the martensite transformation.

(iii) Once the surface had cooled to near the M_f temperature, and the material in this part of the plate again started to contract, the compressive stress at the surface was reduced and in some cases eventually became tensile (D-E in Figure 124). At the same time the hotter material within the plate was expanding on account of the martensite transformation which was then taking place.

This caused the stress at the centre of the plate to become less tensile and in some cases eventually compressive (E'-F' in Figure 124).

(iv) As the temperature throughout the whole of the plate reached ambient temperature there was a small elastic adjustment in the stresses (E-F and F'-G' in Figure 124).

This summary of the characteristics of each of the stages occurring during a quench has, for simplicity, considered the behaviour only at the surface and centre of the plate. The behaviour of material between the surface and centre was transitional between that at the surface and the centre. However, there was always at least one plane between the surface and the centre of the plate where the stress was zero, though the depth of this plane beneath the surface was not fixed.

The plastic flow that had occurred during the quench lead to the presence of a residual stress and strain, which remained in the plate after the cooling process was completed.

6.4.2 Water quenched plates

(i) Predicted relationships between thermal stress and strain

It is apparent from the results shown in Figures 90 and 94, that the predicted relationships between stress and strain at the surface and centre of the 40 mm plate, were very similar to those predicted in the case of the 20 mm plate. Owing to the large temperature gradients generated within the plates during the initial part of the quench (Figure 69), large amounts of tensile plastic flow were predicted at the surface, coupled with large amounts of compressive plastic flow at the centre. However, the surface experienced no further plastic flow once it had cooled below 386°C and

379°C in the cases of the 20 mm and 40 mm plates respectively (Figures 94 and 90). This was a consequence of the rapid increase in flow strength of the material during subsequent cooling. Thus, although the progress of the martensite transformation was associated with the generation of very high compressive stresses at the surface of the plates (1215 N/mm^2 and 1230 N/mm^2), the flow strength of the material increased even more rapidly at the same time.

During further cooling of the surface the high compressive stresses were unloaded elastically and the final stresses at the surface were relatively low; these were either compressive or tensile, depending upon the data used in the calculations (Figures 92 and 95).

Consideration of Figures 90 and 94 shows that plastic strain was generated in the surface regions of the plate only during the very early stages of the quench. It is very difficult to control the removal of heat during this part of the cooling process, owing to the instability of the vapour blanket. Thus the inconsistencies in the surface heat transfer, referred to in section 6.1.1, are likely to be associated with irregular variations in the amount of plastic strain introduced during apparently identical quenches. The marked dependence of residual distortion on the magnitude of the surface heat transfer coefficient is shown in Figures 93 and 96.

The predicted levels of residual distortion at the end of the quench were also dependent on the values of the austenite flow stress used in the calculations (Figures 93 and 96); though the effect was complex owing largely to the development, in the initial part of the quench, of plastic regions at both the surface and centre of the plate.

The predicted residual stress distributions (Figures 92 and 95) were significantly less susceptible to the use of different values for the austenite flow stress in the calculations than were the levels of residual distortion (Figures 93 and 96). The residual stress distributions were also little affected by the use of different values for the variation of the surface heat transfer coefficient during the water quench (Figures 92 and 95).

(ii) Comparison between predicted and experimental results

From a comparison of Figures 93 and 112 on the one hand and Figures 96 and 114 on the other, it is apparent that the experimentally determined residual distortions for the 40 mm and 20 mm water quenched plates both fell within the range predicted by calculation, provided the experimentally determined distortions were derived from measurements made at the centre of the plate (i.e. at points free from edge effects). The form of the residual stress distribution predicted by calculation in both the 40 mm and 20 mm plates (Figures 92 and 95) is in general agreement with that determined experimentally (Figures 113 and 115), although the levels of the predicted residual stresses were generally greater than the experimental values in both plates.

The maximum residual stress determined experimentally was only 275 N/mm^2, which was significantly lower than the corresponding values obtained by others. Thus Buhler and Rose[38] have reported experimentally determined residual stresses of up to around 500 N/mm^2 in water quenched cylinders made from various steels and with diameters similar to the thickness of the plates used in the present investigation (see Figures 11 and 12). Again, Nakagawa and Tamura[37] measured residual stresses of between 540 N/mm^2 and 570 N/mm^2 at the surface of 20 mm thick plates of low-alloy steel that had been quenched in water and oil.

Two possible explanations for the low levels of the experimental residual stress results are suggested. The first is that some stress relaxation may have occurred between the plates being quenched and the residual stresses being determined. However, this is considered unlikely owing to the short time interval between the plates being quenched and the residual stresses being determined (a maximum of 3 days); and the stress distributions measured within the plates were relatively symmetrical about the centre of the plates, despite a delay of usually about 2 days between the stresses being determined in the opposite sides of the plates. The most likely explanation for the discrepancy between the calculated and experimental residual stresses in the present work,is that the latter are not representative of the stress system considered in the mathematical model on which the calculations are based. Thus the experimental results were carried out on plates of finite dimensions, whilst the calculations assume an infinite plate. The use of this model required that plane stress conditions existed and that all stresses in the plane of the plate were equal (i.e. $\sigma_x = \sigma_y = \sigma$). But at the edges of a free plate this cannot be so, since here $\sigma = 0$. It is clear that even with the provision of insulation around the edges of the plate,to ensure unidimensional heat flow right up to the edges of the plate, some edge effect exists which will affect the value of σ in the vicinity of the edge.

During the measurement of residual stresses, successive layers of material were removed from the plates: this technique assumed that a re-adjustment of the state of stress and strain occurred in the remaining part of the plate,and that the stresses removed and re-adjustments within the plate were uniform across the width of the plate. Thus low values of residual stress close to the plate edges can be expected to reduce the values of stress obtained by such measurements.

The precise stress distribution in the vicinity of the edges is not known, but an estimate may be obtained by the application of Saint-Venants principle. Hence the stress is assumed to be free from edge effects at a distance of one plate thickness from the edge of the plate[67], and it is also assumed that the stress is reduced linearly to zero as it approaches the edge of the plate. Thus the distribution of stress in any slice of the plate before its removal in the residual stress determination procedure is as shown in Figure 125. The measured stress, σ_m, is then related to the actual stress in the element:-

$$\sigma_m \simeq \frac{\sigma_a(Y - 2Z) + 2(\frac{\sigma_a}{2}) \times Z}{Y} \qquad 6.1$$

Thus the actual stress, σ_a, is given by:-

$$\sigma_a \simeq \sigma_m \left(\frac{Y}{Y - Z} \right) \qquad 6.2$$

The correction factor, $\frac{Y}{Y - Z}$, varies according to the initial plate dimensions and is 1.56 for the 40 mm plate, and 1.2 for the 20 mm plate. It is apparent that if the experimental residual stress results shown in Figures 113 and 115 are multiplied by a factor of 1.56 and 1.2 respectively, a much improved agreement with the predicted residual stresses shown in Figures 92 and 95 is obtained, though the experimental residual stresses still remain slightly less than the calculated values.

Although these corrections are based on well accepted theoretical principle, there is some experimental evidence to support it. Thus Figure 109 shows the variation in the thickness of a quenched plate. Since there is, according to the mathematical model, no stress in the thickness direction, the observed variations in thickness are due to the effect of the edge on the stresses present in the plane of the plate.

6.4.3 Oil quenched plates

(i) Predicted behaviour

The predicted relationship between stress and strain at the surface and centre of the 20 mm plate when quenched in oil (Figure 97) exhibited two significant differences from the behaviour predicted in the case of water quenched plates (Figure 94). Much less plastic flow occurred during oil quenching and the sharp increase in surface heat transfer, associated with the nucleate boiling peak, resulted in an additional small amount of tensile plastic flow at the surface of the plate.

During the initial part of the vapour blanket stage, tensile and compressive plastic flow occurred at the surface and centre respectively, as was the case in water quenching. However, during the long vapour blanket stage the surface heat transfer coefficient remained low and even fell slightly as the temperature was reduced (see Figure 58). This caused the stress at the surface to become slightly compressive until the surface had cooled to 546°C (Figure 97). Below this temperature the cooling rate at the surface increased rapidly, owing to the increase in the surface heat transfer coefficient associated with nucleate boiling of the quenchant. Thus the plate surface cooled sufficiently rapidly between 490°C and 435°C to produce a small additional stage of tensile plastic flow.

Below 435°C the surface cooled more slowly than the remainder of the plate and the stress at the surface was consequently reversed. The magnitude of the compressive stress produced at the surface was further increased by the expansion that accompanied the formation of martensite, once the surface temperature had fallen below the M_s. The temperature gradient within the plate at this stage in the process was very much smaller than that in the water quenched plates. For example, in the 20 mm oil quenched plate there was merely a 27°C difference between the temperature at the surface and centre of the plate when the surface had cooled to 290°C, compared with a 442°C difference in temperature at the same stage of the water quench.

The small temperature gradients present within the oil quenched plate while the martensite transformation was taking place, caused much smaller changes in stress than was the case with a water quench. The maximum compressive stress developed at the plate surface was 490 N/mm^2 (compared with 1215 N/mm^2 in the 20 mm water quenched plate), and was insufficient to generate any tensile plastic flow at any point in the plate.

The elastic contribution to the total strain in the oil quenched plate was of a similar order of magnitude to that contributed by plastic strain (see Figure 97). This contrasts with the behaviour predicted in the case of the water quenched plate, where the final strain contained a relatively small elastic component (see Figure 94).

(ii) Comparison between predicted and experimental results

From a comparison of the predicted and experimentally measured distortions remaining in the 20 mm oil quenched plate (Figures 100 and 116), it is apparent that the distortion predicted by calculation was slightly greater than that determined experimentally, although they were both very appreciably smaller than was the case in the 20 mm water quenched plate (compare with Figures 96 and 114).

However, the degree of agreement between the predicted and experimental residual stress distributions was very poor (Figures 99 and 117): the sole common feature being the low level of stresses involved. An increase in the experimentally determined values by a factor of 1.2, to compensate for the reduction in the experimentally determined stress towards the edge (see section 6.4.2), increases the difference between the experimental and predicted residual stress distributions. Thus the calculations predicted a residual compressive stress at the surface and a tensile stress at the centre, while the experimental results showed the reverse stress distribution.

A residual tensile stress at the surface requires that either compressive plastic flow occurs during the formation of martensite in the surface region, or else tensile plastic flow occurs in the soft austenite centre. Consideration of Figure 97 indicates that either possibility is feasible to only a very limited extent. Thus, the generation of a residual tensile stress at the surface would require extensive modification of the physical and mechanical property data used in the calculation. A critical examination of this data, together with the assumptions on which the mathematical model is based, suggests two points where an improvement might lead to a reduction in the discrepancy between prediction and experiment.

Firstly, the assumption that stress relaxation did not occur during the cooling process, while valid in the case of the water quench, is dubious in the case of an oil quench, where the time taken to reach room temperature was much longer. For instance 21 seconds after the start of an oil quench, the calculated temperature at the centre of a 20 mm plate was calculated to be 700°C. From Figure 86 it is apparent that in such a time interval some stress relaxation can be expected.

Although the mathematical model on which the calculations are based does not accommodate stress relaxation, an approximation for this effect may be obtained by a reduction in the values of flow stress employed at each temperature above the M_s temperature. The effect of such a reduction is two-fold: firstly, the compressive stress set up at the centre during the initial stages of the quench is reduced, which leads to a higher tensile stress in this part of the specimen after the stress reversed. Secondly, the lower flow stress at the centre during the later part of the quench increases the likelihood that tensile plastic flow will occur. As has already been suggested this increases the probability that a residual tensile stress can occur at the surface.

However, even when the flow stress of the austenite was reduced at temperatures above 790°C from 30 N/mm^2 to 15 N/mm^2 and at temperatures below 350°C from 145 N/mm^2 to 100 N/mm^2, the residual stress, although reduced in magnitude, was still compressive. These reductions are greater than those justified by a consideration of the stress relaxation data in combination with the relationship between time and temperature during the cooling of the plate. Thus stress relaxation would appear to form only a partial explanation of the lack of agreement between calculation and experiment.

The second possible modification to the flow stress data arises from the uncertainty attached to this property during the martensite transformation. As has been stated in section 6.3 the experimental determination of this information is very difficult, and the method used to obtain the required data relied upon certain assumptions, viz,

(i) that the room temperature flow stress of En 30B (835M30) given by Woolman and Mottram[157] is correct;

(ii) that the flow strength of a mixture of austenite and martensite is given by equation 4.20;

(iii) that the M_s and M_f temperatures are unaffected by the prior deformation of the austenite.

If these assumptions lead to an overestimate of the flow stress of the material below M_s then the residual stress at the surface of an oil quenched plate may become more compressive than the true value. Thus, a reduction in the flow strength of the martensite phase from 1600 N/mm^2 to 600 N/mm^2 allowed a small quantity of compressive plastic flow at the surface, which reduced the level of residual compressive stress in this region of the specimen. However, it was still not possible to generate a residual tensile stress at the surface.

The results of calculations, in which both the austenite flow strength was reduced and the flow strength of the material whilst in the transformation range was reduced, showed it was just possible to produce tensile stresses at the surface of the plate and compressive stresses at the centre of the plate (Figure 126). However, if it is proposed to modify the data used in the prediction of thermal stress during oil quenching, similar changes should be made to the calculation of thermal stress during water quenching. These changes, which improve the degree of agreement between prediction and experiment in the case of the oil quench, reduce the degree of agreement found with the water quench. There is some justification for the application of the stress-relaxation effect to oil quenching, since the cooling time was much greater than was the case with the water quench. However, modifications to the martensite flow strength are obviously unable to produce an overall improvement to the degree of agreement between prediction and experiment in the case of both quenchants.

6.4.4 Polymer quenched plates

(i) Predicted behaviour

The stress-strain behaviour predicted at the surface and centre of a 20 mm plate of 835M30 when quenched in a 25% solution of Aquaquench 1250 polymer quenchant is shown in Figure 101. From a comparison with Figure 94, which shows the relationship between stress and strain during the water quenching of a 20 mm plate, it is apparent that similar behaviour is predicted in both cases. This is due to the similarity in the values of the surface heat transfer coefficient employed in the two calculations (compare Figures 54 and 62), although the surface heat transfer coefficients produced by the polymer quenchant were generally slightly lower. Consequently less plastic flow was generated in the initial stages of the quench into the polymer quenchant than was the case with water.

The large values of the surface heat transfer coefficient that were present when the surface of the plate was at the M_s temperature (e.g. at $\theta_s = 300^{\circ}C$, $h = 5,300\ W/m^2\ {}^{\circ}C$) resulted in large compressive stresses at the plate surface (920 N/mm^2), coupled with a large amount of tensile plastic flow at the centre. Hence the predicted residual stress distribution was similar to that predicted in the case of water quenching (compare Figures 103 and 95), with a small tensile stress at the surface, which increased to a maximum at a point beneath the surface, before reversing to a maximum compressive value at the centre of the plate.

(ii) Comparison between predicted and experimental results

A comparison of Figures 103 and 119 shows that a degree of agreement was obtained between the predicted and experimental residual stresses, particularly when the experimental values are increased by a factor of 1.2, to account for the edge effect as previously discussed in section 6.4.2. However, it is interesting to note that the maximum value of the predicted stress at a point just below the surface (Figure 103) is just absent in the case of the experimentally determined stresses (Figure 119).

From a comparison of Figures 104 and 118 it is apparent that there is a considerable difference between the predicted and experimentally determined distributions of distortion within the plate. It is known that the surface heat transfer coefficients that had been determined during a polymer quench were particularly susceptible to a high level of variability at surface temperatures between 500°C and 800°C (Figure 61). At this stage the vapour blanket was breaking down and a layer of polymer was probably formed on the specimen surface. This variability may be the reason for the poor level of agreement between the predicted and experimental residual strains, since the associated plastic flow was produced at temperatures above 500°C.

On the other hand, the better agreement obtained in the case of the stresses, may be that these were mainly influenced by the high values of surface heat transfer obtained during the later stages of the quench when the surface heat transfer coefficient values were more consistent. However, further work is required to increase our understanding of this type of quenchant.

6.5 General Discussion

The objective of this work was to predict the thermal stress and strain produced in plates of low-alloy steel during quenching. It was apparent from a review of previous work in the same field that empirical experimentation had failed to yield more than a qualitative understanding of the complex behaviour that occurs during the quenching of steel specimens. This may be attributed to the complexity of the problem and the difficulties of controlled experimentation. An alternative approach to the problem has been the direct calculation of thermal stresses during quenching. However, though methods of calculation had been developed it was considered that often insufficient care had been given to the selection of the data used in the calculations and none of the results of the calculations had been adequately correlated with experimental behaviour.

The approach taken in the present work was to consider the simplest situation, viz a simple plate of high hardenability steel that produced 100% martensite on quenching, such that a relatively simple means could be employed to calculate the thermal stress and strain produced during quenching. However, considerable emphasis was placed upon the correct selection of data for use in the calculations and the correlation of the results of the calculations, as fully as possible, with experimentally determined results. Thus it was necessary to determine, by experiment, data that was not available. This, in particular, included the surface heat coefficients of the quenchants used, and the mechanical properties of the steel involved at various temperatures during quenching from the stable high temperature austenitic condition. The results of the thermal stress and strain calculations were correlated with experimentally determined results of the distribution of temperature, residual stress and residual strain, obtained at a range of quenching severities.

During the present investigation it was found that the temperature distribution, that had been calculated prior to the calculation of thermal stress and strain, correlated well with selected temperature measurements in quenched plates. However, the experimental results obtained were particularly susceptible to small changes in the conditions of the experiment, owing to the low stability of the vapour blanket. The best agreement between calculated and experimental values of residual stress and strain were obtained with water quenched plates of both 40 mm and 20 mm thickness; although it was necessary to take careful account of edge effects in the experimental results, in order to enable valid comparisons to be made. However, in the cases of both oil quenched plates and polymer quenched plates, less favourable correlations were obtained.

Though plates quenched in the polymer quenchant exhibited a residual stress distribution which showed some agreement with that obtained by calculation, there was a considerable difference between the level of residual strain determined by calculation and by experiment. A possible explanation for the poor correlation of the residual strains may have been errors in the values employed of the surface heat transfer coefficient at the higher temperatures, which supports the original premise regarding the importance of the correct selection of data for such calculations.
In the case of oil quenched plates agreement was obtained between the calculated and experimentally determined values of residual strain but not residual stress. Stress-relaxation (assumed to be negligible in the calculations) is considered to be a contributory factor in the poor correlation of residual stresses owing to the relatively low cooling rates involved in oil quenching. However, stress-relaxation effects are not considered to be solely responsible for the discrepancies between the experimental and calculated values of residual stress. It is thought that significant modifications to the flow strength of the material during the formation of martensite are necessary to bring about the required changes in the calculated residual stress distribution. Once again this supports the original premise regarding the selection of data for such calculations.

The significance of the correct selection of data is further amplified when a comparison is made between the residual stress distributions in water and oil quenched plates. In order to achieve the correct calculation of residual stresses in the oil quenched plates (i.e. tensile surface stress) it is necessary that sufficiently low values of flow stress be employed at the surface of the plate, to enable some compressive plastic flow to occur in this region during the formation of martensite. A characteristic of the calculated and experimental residual stress distributions in both the 40 mm and 20 mm plates, when water quenched, was a pronounced maximum tensile stress just below the surface. The prediction of this peak was associated with the absence of any compressive plastic flow in the surface regions of the plate at this stage in the quench, despite significantly greater stresses being developed than in the case of oil quenching (compare Figures 94 and 97). Thus it is clear that any reduction of flow stress in the material below the M_s temperature would not produce an overall improvement in the agreement between calculated and experimental residual stress distributions in both oil and water quenched plates.

The effect of different values of the flow stress of the material, during the formation of martensite, on the residual stress distribution at the end of the quench is clearly shown in Figure 127. This figure shows the results of calculations carried out for a plate cooled with a Biot number of 2.0 (approximately equivalent to a 20 mm plate quenched into a 25% solution of the polymer quenchant), but with the flow strength of the martensite phase assigned various values within the range 1600 N/mm^2 to 600 N/mm^2. The results of these calculations show that the residual stress distribution in the surface regions of the plate is strongly dependent on the flow strength of the martensite phase. Therefore, it is apparent that an improved knowledge of the mechanical properties of steels during this stage of the quench is essential to any further work in this field.

7. CONCLUSIONS

1. A mathematical model of heat transfer in an infinite plate has been used to calculate the temperature distributions produced during the quenching of specimens of 835M30 steel in water, oil or polymer quenchants. The results of these calculations are in good agreement with the experimentally determined temperature distributions in finite plates of the same material.

2. The mathematical model has been extended in order to determine the thermal stress and strain associated with temperature gradients in quenched plates of a steel (835M30) that transforms completely to martensite during the quench. The degree of agreement between the calculated and experimentally determined residual stresses and strains at the end of the quench was dependent upon the quenchant, being best in the case of water and worst in the case of oil.

3. The distribution of residual strain predicted by the mathematical model at the end of the quench was predominantly affected by plastic flow during the early stages of the quench, and thus sensitive to variations in the surface heat transfer coefficient and the flow strength of the material at this stage in the cooling process.

4. The distribution of residual stress predicted by the mathematical model was found to be markedly dependent on the flow stress of the material below the M_s temperature, owing to the large strains associated with the formation of martensite.

5. The vapour blanket formed during the initial stages of a quench into water at 20°C was very unstable, which led to marked variations in the surface heat transfer coefficient. This was associated with significant differences in the residual strain at the end of individual quenches, though the residual stress values were consistent. The presence of an opaque film of oxide on the surface of the specimen aided the formation of a stable vapour blanket during the early stages of the quench.

6. The average maximum value of the surface heat transfer coefficient obtained during the nucleate boiling stage of a water quench was 13,500 W/m^2°C with the range of maximum values lying between 12,200 W/m^2°C and 18,500 W/m^2°C.

7. A concentration of 25%"Aquaquench 1250" polymer quenchant was required to produce a significant reduction in the value of the surface heat transfer coefficient,relative to that obtained when quenching into water alone. At this concentration the maximum value of the surface heat transfer coefficient was 7,000 W/m^2°C.

8. The use of an oil quenchant produced very low values of the surface heat transfer coefficient (a maximum of 2,000 W/m^2°C) coupled with a very limited nucleate boiling stage.

9. The use of a simple mathematical model that assumed no temperature gradient in a thin specimen produced values of the surface heat transfer coefficient that

were lower in the case of water, but similar in the case of oil, to those obtained at the same surface temperature using thicker specimens with the more accurate finite difference technique. Thus the accuracy of the simpler method may be sufficient for some applications.

8. RECOMMENDATIONS FOR FURTHER WORK

1. The mechanical properties of relevant low-alloy steels should be determined at various strain rates during the martensitic, bainitic and pearlitic transformations. A tensile testing arrangement, in which the specimen is austenitised in-situ prior to cooling and testing at a lower temperature, is unlikely to be suitable for this type of work, owing to the difficulty of producing a structure in the shoulders of the specimen identical to that in the gauge length. An apparatus will therefore be required in which the specimens are heat treated externally from the tensile testing equipment before being rapidly transferred into the equipment and the mechanical properties determined.

2. The calculation of the thermal stresses produced during the quenching of specimens of lower hardenability steels that are not fully martensitic after quenching should only be undertaken once the behaviour of steels, that transform fully to martensite during quenching, can be predicted for all quenching severities. The production of transformation products other than martensite (i.e. bainite or pearlite) during a quench greatly increases the complexity of any thermal stress calculations since the formation of bainite and pearlite are both time and temperature dependent.

3. Further work should be carried out on the stability of the vapour blanket stage in both water and polymer quenchants. Of special value would be more precise knowledge of the influence of experimental variables on the stability of the vapour blanket. Such variables could include the condition of the specimen surface (roughness and state of oxidation) and the condition

of the quenchant (temperature, agitation, and in the case of polymer quenchants, age and concentration). This work should be carried out using specimens with thermocouples just below the surface, as in the present work.

4. Further predictions of thermal stress and strain during quenching would be better if carried out on cylindrical rather than plate specimens, since end-effects would then be restricted to the ends of the cylinders and could easily be minimised experimentally by the use of long cylinders. Furthermore it is considered more likely that uniform surface heat transfer could be achieved using cylindrical specimens than plate specimens.

REFERENCES

1. Orowan E., Symposium on Internal Stresses in Metals and Alloys, Institute of Metals, 1947, (47).

2. Andrews K.W., "Physical Metallurgy Techniques and Applications", Vol II, George Allen & Unwin Ltd, 1973.

3. László F., J.I.S.I., 1943, 147, (173).

4. Scott H., Scientific Papers Bureau of Standards, 1925, 20, (399).

5. Denton A.A., Met. Rev., 1966, 11, 101, (1)

6. Thelning K., "Steel and its Heat Treatment", London, Butterworths, 1975, (466).

7. Visvanathan S., T.I.S.C.O., 1976, Oct, (199).

8. Schmidt W., V.D.I.Z., 1976, 118, 21, (1023).

9. Kempe L.W. et alia, Trans. A.I.M.E., 1934, 111, (158).

10. Chevrier J.C., Thesis, C.N.R.S., Nancy, 1973, (95).

11. Archambault P. et alia, "Heat Treatment '76", Metals Society, 1976.

12. Reed-Hill R.E., "Physical Metallurgy Principles", Princeton, N.J., Van Nostrand, 1970.

13. Lement B.S., A.S.M. Metals Handbook, 8th Ed., Vol 1, 1961, (654).

14. Llewellyn D.T. & Cook W.T., Metals Technology, 1977, 5, (265).

15. Mocarski S., Industrial Heating, 1974, 5, (58).

16. Denton A.A., Tech. Met. Research, Vol 5, Part 2, Ed. Bunshah R.F., New York, John Wiley & Sons, 1971

17. Kobasko N.I., Met. Sci. Heat Treatment, 1975, 3, (287).

18. Toshioka Y., Fukagawa M. & Saiga Y., J.I.S.I. Japan, 1973, 59, 2, (308).

19. Jaffe L.D. & Hollomon J.H., A.I.M.E., 1946, 167, (617).

20. Wells C., A.I.M.E., 1946, 167, (625).

21. Chapman R.D. & Jominy W.E., Metal Progress, 1953, 8, (67).

22. Kobasko N.I., Met. Sci. Heat Treatment, 1970, 11, (900).

23. Bodson et alia, Trait. Therm. 1976, 104, (83).

24. Beck G., Trait. Therm., 1970, 54, (19).

25. Barrett C.S., Metals and Alloys, 1934, 6.

26. Macherauch E., Materials Science and Engineering, 1977, 30, (1).

27. Benson D.K., Met. Trans., 1972, 3, (2547).

28. Doi O. & Sato Y., Bull. Jap. Soc. Mech. Eng., 1971, 14, 71, (383).

29. Sachs G., Z. Metallkunde, 1927, 19, (352).

30. Buhler H., "Residual Stresses in Metals and Metal Construction," New York, Reinhold, 1954.

31. Kirk D., Strain, 1970, 4, (75).

32. Jones B., S.A.E., 1971, 784.

33. Buhler H. & Buckholtz H., Archiv. fur das Eisen., 1931, 5E, 8, (413).

34. Buhler H. & Buckholtz H., Archiv. fur das Eisen., 1933, 5E, 7, (315).

35. Liss R.B., S.A.E., 1969, 78, (517).

36. Vannes A. et alia, Rev. Mét., 1974, 71, 5, (307).

37. Nakagawa Y & Tamura T., J. Soc. Mat. Sci. Japan, 1972, 21, 231, (1099).

38. Buhler H. & Rose A., Archiv. fur das Eisen., 1969, 40, (411).

39. Murry G., Trait. Therm., 1978, 4, 124, (30).

40. Jones B.K. & Martin J.W., Metals Technology, 1977, 11, (520).

41. Almen J.O. & Black P.H., "Residual Stress and Fatigue in Metals", McGraw-Hill, 1963.

42. Mocarski S., Industrial Heating, 1974, 5, (60).

43. Ishi K & Iwamoto Y., Trans. Soc. Aut. Eng., 1970, 78, (1765).

44. Chamenat A. & Flavenot J.F., Trait. Therm., 1978, 4, 124, (61).

45. Sachs K., Metal Treatment & Drop Forging, 1961, Jan-Aug.

46. Llewellyn D.T. & Cook W.T., BSC Internal Report, 1971.

47. B.I.S.R.A., Distortion of Steels During Heat Treatment, 1958, MG/N/150/58.

48. Hollox G.E. & Von Bergen R.T., Heat Treatment of Metals, 1978, 2, (27).

49. Dorigo O., Trait. Therm., 1977, 112, (27).

50. Mocarski S., Industrial Heating, 1974, 7, (26).

51. Fresher J., Archiv. fur das Eisen., 1953, 24, (483).

52. Scott A. & Gray T.H., A.S.M., 1941, 6, (503).

53. Novik F.S. et alia, Industrial Lab., 1975, 41, 5, (733).

54. Child H & Plumb S., Metalworking Production, 1978, 6, (135).

55. Dumont C., Moreaux F., Simon A., & Beck G., Trait. Therm., 1975, 95, (67).

56. Vorobjev V.G., Trait. Therm., 1974, 90, (57).

57. Lacoude A. & Tricot R., Rev. Mét., 1972, 69, 1, (23).

58. Champin B., Seraphin L. & Tricot R., Trait. Therm., 1974, 87, (79).

59. Hopkins A.D. & Holland N.H., J.I.S.I. 1962, 4, (308).

60. Murray J.D., Auto. Eng., 1965, 55, (186).

61. Llewellyn D.T., Lowden M.A.W. & Marriott J.B., BSC Internal Report, 1975.

62. Houghton P.S., "Heat Treatment of Metals", London, Machinery Publishing, 1960.

63. Cullen O.E., Steel Proc. and Conv. 1957, 43, (700).

64. Preistner R & Hasan J., Trait. Therm., 1974, 88, (51).

65. Timoshenko S.P. & Goodier J.N., "Theory of Elasticity", New York, McGraw-Hill, 3rd Edition, 1970.

66. Johns D.J., "Thermal Stress Analysis", London, Pergamon, 1965.

67. Boley B.A. & Weiner J., "Theory of Thermal Stresses", New York, Wiley, 1960.

68. Weiner J., J. App. Mech., 1956, 23, (395).

69. Benham P.P. & Hoyle R.H., "Thermal Stress", London, Pitman, 1964.

70. Russell J.E., Symposium on Internal Stress, Institute of Metals, 1947, (95).

71. Carslaw H.S. & Jaegar J.C., "Conduction of Heat in Solids", 2nd Edition, London, Oxford, 1959.

72. Aparci V.S., "Conduction Heat Transfer", Reading Mass., Addison-Wesley, 1966.

73. Dusinberre G.H., "Heat Transfer Calculations by Finite Differences", Scranton Pa., International, 1961.

74. Adams J.A. & Rogers D.F., "Computer-Aided Heat Transfer Analysis", New York, McGraw-Hill, 1973.

75. Crank J. & Nicolson P., Proc. Camb. Phil. Soc., 1950, 46, (634).

76. Milne W.E., "Numerical Solution of Differential Equations", New York, John Wiley & Sons, 1953.

77. McAdams W.H., "Heat Transmission", 2nd Edition, McGraw-Hill, 1954.

78. Smith G.D., "Numerical Solution of Partial Differential Equations", London, Oxford, 1965.

79. Price P.H. & Slack M.R., Brit. J. App. Phys., 1954, 5, (285).

80. Richardson P.D. & Shum Y.M., A.S.M.E. paper 69 - WA/HT - 36, 1969.

81. Lewis R.D., & Bass B.R., J. Heat Transfer, 1976, 8, (478).

82. Aguirre-Ramirez G. & Oden J.J., A.S.M.E. paper 69 - WA/HT - 34, 1969.

83. Lemmon E.C. & Heaton H.S., A.S.M.E. paper 69 - WA/HT - 35, 1969.

84. Leibmann G., Trans A.S.M.E., 1956, 78, 3, (655).

85. Juhasz S., A.S.M.E. paper 57 - A - 125, 1957.

86. Coyle M.B., Trans. A.S.M.E., 1951, (265).

87. "Metals Handbook", A.S.M., Vol 2, 8th Edition, 1964, (15).

88. Gilliland H.J., Metal Progress, 1960, 10, (111).

89. Weymuiller C.R., Metal Progress, 1972, 7, (63).

90. Wolfson Heat Treatment Centre, University of Aston, "Laboratory Test for Assessing the Quench Rate of an Oil", May 1976.

91. Mansion J., Trait. Therm., 1976, 104 (59).

92. Lemaire D., Trait. Therm., 1976, 104, (71).

93. Paschkis V. & Stolz G., J.O.M., 1956, 8, (1074).

94. Stolz G., Paschkis V., Bonilla C.F. & Acevado G., J.I.S.I., 1959, 10, (116).

95. Paschkis V. & Stolz G., Final Report, 1955-61, Columbia University.

96. Simon A. & Beck G., Rev. Mét., 1966, 63, (211).

97. Beck G. & Bigot R., Rev. Mét., 1965, 62, (681).

98. Lambert N. & Economopoulos M., "Mathematical Models in Metallurgical Process Development", I.S.I., 1969, (29).

99. Bergles A. & Thompson W.G., Int. J. Heat Mass Transfer, 1970, 13, (55).

100. Stolz G., Trans. A.S.M.E., 1960, 2, (20).

101. Rohsenow W.M. & Choi H.Y., "Heat, Mass and Momentum Transfer", N.J., Prentice-Hall, 1961.

102. Kreith F., "Principles of Heat Transfer", 2nd Edition, Scranton Pa., International Textbooks, 1965.

103. Beck G. & Chevrier J.C., Int. J. Heat Mass Transfer, 1971, 14, (1731).

104. Mitsutsuka M. & Fukuda K., J.I.S.I., Japan, 1977, 5, 636, (1008).

105. Nukiyama S., J. Soc. Mech. Eng., Japan, 1934, 37.

106. Farber E.A. & Scorah R.L., Trans. A.S.M.E., 1948, 5, 70, (369).

107. Nishikawa K. & Fujita Y., Int. J. Heat Mass Transfer, 1977, 20, (233).

108. Westwater J.M., "Theory and Fundamental Research in Heat Transfer", Ed. J.A. Clark, 1960.

109. Labunstov D.A., Thermal Engineering, 1972, 9, (21).

110. Eckert E.R.G., Int. J. Heat Mass Transfer, 1977, 20, (1097).

111. Mitsutsuka M. & Fukuda K., J.I.S.I. Japan, 1976, 16, (47).

112. Terrier A., Trait. Therm., 1976, 104, (89).

113. Edgar Vaughan & Co. Ltd., "Aquaquench 1250", Trade lit.

114. Met. Mat. Tech., 1978, 2, (66).

115. Mitsutsuka M. & Fukuda K., J.I.S.I., Japan, 1978, 6, 4, (70).

116. Kobasko N.I., Met. Sci. Heat Treat., 1975, 3, (287).

117. Trayanov G.G., Met. Sci. Heat Treat., 1977, 1, (601).

118. Flament G., Chevrier J.C. & Moreaux F., C.R.Ac. Sci., 1977, 5, 294B, (339).

119. Birkebak R.C. & Abdulkadir A., Int. J. Heat Mass Transfer, 1976, 19, (1039).

120. Westwater J.W. & Santangello J.G., Ind. Eng. Chem., 1955, 47, (1065).

121. Zuber N., Trans. A.S.M.E., 1958, 60, (711).

122. Berenson P.J., A.I.Ch.E., 4th National Heat Transfer Conference, 1960, 18.

123. Kesselring R.C. et alia, A.I.Ch.E., 1967, 13, (669).

124. Canon R.M. & Park E.L., Int. J. Heat Mass Transfer, 1976, 19, (696).

125. Beck G. & Chevrier J.C., C.R.Ac.Sci., 1970, 270C, (1276).

126. Chevrier J.C., Thesis, C.N.R.S., Nancy, 1973, (55).

127. Bigot R., Thesis, C.N.R.S., Nancy, 1964.

128. Mehta A.J. & Geiger G.H., Proc. 19th Mechanical Working and Steel Processing Conf., A.I.M.E., 1977.

129. Toshioka Y. et alia, Trans. I.S.I. Japan, 1972, 12, (6).

130. Tokihiro Y. & Tamura I., J.I.S.I. Japan, 1974, 60, 2, (671).

131. Archambault P. & Chevrier J.C., Int. J. Heat Mass Transfer, 1977, 20, (1).

132. Smithells C., "Metals Reference Book", London, Butterworths, 4th Edition, 1967, Vol 3, (696).

133. Fitzgerald F. & Sheridan A.T., "Mathematical Models in Metallurgical Process Development", I.S.I., 1969, (18).

134. B.I.S.R.A., "Physical Constants of Some Commercial Steels at Elevated Temperatures", London, Butterworths, 1953.

135. Davis W.B., J.I.S.I., 1972, 6, (437).

136. Hengerer V.H. et alia, Stahl u. Eisen, 1969, 89, 12, (641).

137. Uhlitzsch H., Neue Hutte, 1959, 4, (277).

138. Atkins M., Andrews K.W. & Russell J.E., BSC Internal Report, 1973.

139. Manson S.S., "Thermal Stress and Low-Cycle Fatigue", New York, McGraw-Hill, 1966.

140. Boley B.A. & Weiner J., "Theory of Thermal Stresses", New York, Wiley, 1960, (543).

141. Weiner J. & Huddleston J., J. Appl. Mech., 1959, 26, (31).

142. Archambault P., Thesis, C.N.R.S., Nancy, 1976.

143. Spektor A. & Stepanova N., Met. Sci. Heat Treat., 1975, 3, (282).

144. Fletcher A.J., Metals Technology, 1977, 6, (307).

145. Zeinkiewiez O.C., "The Finite Element Method in Engineering Science", New York, McGraw-Hill, 1971.

146. Desai C.S. & Abel J.F., "Introduction to the Finite Element Method", Princeton, N.J., Van Nostrand Reinhold, 1972.

147. Martin H.C. & Carey G.F., "Introduction to Finite Element Analysis", New York, McGraw-Hill, 1973.

148. Inoue T., Haraguchi K. & Kimura S., Trans. I.S.I.J., 1978, 18, (11).

149. Toshioka Y., J.I.S.I. Japan, 1976, 11, 13, (1756).

150. Fujio H., Aida T. & Masumoto Y., Bull. J.S.M.E., 1977, 20, 146, (1051).

151. Schmidtman V.E. & May W., Archiv. fur das Eisen., 1970, 41, (569).

152. Nilan T.G., "Transformation and Hardenability in Steels Symposium", Climax Molybdenum, Michigan, Feb 1967.

153. Smith Y.E. & Seibert C.A., Met. Trans., 1971, 2, (1711).

154. Mirzayev D.A. et alia, Phys. Metals Metall., 1973, 35, 6, (81).

155. Desalos Y., IRSID, Private Communication.

156. Simon A., C.N.R.S., Nancy, Private Communication.

157. Woolman J. & Mottram R.A., "The Mechanical and Physical Properties of B.S. En Steels", London, Pergamon Press, 1966.

158. Beck A.J.T., Heat Treating, 1977, 5, (55).

159. "Interpolation and Allied Tables", H.M. Nautical Almanac Office.

160. Chalmers B. & Quarrel A.G., "Physical Examination of Metals", London, Edward Arnold, 2nd Edition, 1960, (190).

161. Rowe G.W., "An Introduction to the Principles of Metalworking", London, Edward Arnold, 1965, (45).

162. Treuting R.G. & Read W.T., J. App. Phys., 1951, 22, 2, (130).

163. Leaf W., Proc. Soc. Exp. Stress Analysis, 1952, 9, 2, (133).

164. Harrington M., M.Sc. Project, Sheffield City Polytechnic, 1974.

165. R.D.N. 1975 Data Sheet, Witco Chemical Co. Ltd.

Table 1 Thermal Property Data Used By Toshioka[149]

Heat Transfer coefficient, h (W/m^2 $^\circ$C)	Water	$^\circ$C	0	100	110	300	500	1000
		h	628	837	8793	8793	6280	209
	Oil	$^\circ$C	0	200	750	1000		
		h	209	209	1884	1884		
Thermal Conductivity, λ (W/m^2 $^\circ$C)	Ferrite Bainite Martensite	$^\circ$C	0	200	400	800	1000	
		λ	52.3	50.2	41.87	(27.2)	(14.7)	
	Austenite	$^\circ$C	0	1000				
		λ	14.65	27.2				
Specific Heat, Cp (J/kg$^\circ$C)	Ferrite Bainite Martensite	$^\circ$C	0	420	700	800	1000	
		Cp	460	628	837	1005	1885	
	Austenite	$^\circ$C	0	500	1000			
		Cp	502	628	649			
Latent heat of transformation (J/kg)	Austenite → Ferrite:		75,366					
	Austenite → Bainite:		75,366					
	Austenite → Martensite:		83,740					

Table 2 Physical Data Used By Toshioka[149] For Displacement and Stress Calculation

Young's modulus, E $(N/mm^2) \times 10^5$	°C	0	400	550	700	1000
	E	2.107	1.842	1.646	1.372	0.588
Yield Strength (N/mm^2)	°C	0	550	800	1000	
	Austenite	196	98	49	29.4	
	Ferrite	294	98	29.4		
	Bainite	392	343			
	Martensite	490	392			
Strain hardening coefficient $(d\sigma/d\epsilon)$	Austenite	0.02 x E				
	Ferrite	0.08 x E				
	Bainite	0.5 x E				
	Martensite	0.6 x E				
Linear Thermal Expansion Coeff., α_{ex} $(°C^{-1})$	Austenite, $\alpha_{ex} = 11.9 \times 10^{-6} + 8.14 \times 10^{-9}\theta$ Ferrite, $\alpha_{ex} = 16.5 \times 10^{-6} + 7.06 \times 10^{-9}\theta$					
Linear Transformation Expansion, $\Delta\epsilon$ (mm/mm)	$\Delta\varepsilon = 7.15 \times 10^{-3} - 0.460 \times 10^{-5}\theta_f + 0.540 \times 10^{-4}\theta_f^2$ (θ_f = Temperature of transformation finish)					
Poisson's ratio	0.3					

Table 3 Chemical Composition (wt%) of Materials

Material	C	Mn	Si	Ni	Cr	Mo	Fe
A.I.S.I. 304 (Type A & B 'h' specimens)	0.06	1.7	-	10.8	18.0	0.31	Balance
835M30 (Type C & D plate specimens)	0.30	0.72	0.42	4.83	1.25	0.28	Balance
830A31	0.31	0.44	0.20	3.40	1.26	0.47	Balance

Table 4 Properties of RDN 175 Quenching Oil[165]

Specific Gravity	0.861
Open Flash Point	192°C
Closed Flash Point	186°C
Pour Point	-12°C
Redwood Viscosity @ 21°C	184 s
" " @ 60°C	53 s
" " @ 93°C	38 s
Kinematic Viscosity @ 38°C	21.5 s
" " @ 99°C	4.10 s
V.I.	99

Table 5 Variation of h with Surface Temperature

Quenchant	θ (°C)	h (W/m^2 °C)
(a) Water (Average)	>826.8	$1470.$
	$826.8 \rightarrow 381$	$23800. - 27.008\theta$
	$381 \rightarrow 275$	$3504. + 26.236\theta$
	$275 \rightarrow 93.75$	$51.584\theta - 3466.$
	<93.75	$1370.$
(b) Water (Maximum)	>860	$1742.$
	$860 \rightarrow 392.2$	$26900. - 29.253\theta$
	$392.2 \rightarrow 275.3$	$9450. + 15.24\theta$
	$275.3 \rightarrow 90$	$64.7\theta - 4167.$
	<90	$1656.$
(c) Water (Minimum)	>790	$1174.$
	$790 \rightarrow 402.8$	$20438. - 24.385\theta$
	$402.8 \rightarrow 287.1$	$2487. + 20.176\theta$
	$287.1 \rightarrow 90$	$38.47\theta - 2766.$
	<90	$697.$
(d) Oil (RDN 175)	>800	$842.$
	$800 \rightarrow 542$	$1.191\theta - 111.$
	$542 \rightarrow 470$	$11422. - 20.08\theta$
	$470 \rightarrow 434.4$	$1990.$
	$434.4 \rightarrow 308.3$	$11.34\theta - 2937.$
	<308.3	$221. + 1.097\theta$
(e) 25% Aquaquench 1250	>792	$700.$
	$792 \rightarrow 602$	$27933. - 34.47\theta$
	$602 \rightarrow 476$	$25.782\theta - 8364.$
	$476 \rightarrow 276$	$7688. - 7.946\theta$
	$276 \rightarrow 134$	$31.786\theta - 3282.$
	<134	$258. + 5.4\theta$

Table 6 Variation of λ and α_{td} with Temperature

θ (°C)	Property
>355	$\alpha_{td} = 4.0698 + 1.7802 \times 10^{-3}\theta$ mm^2/s
355→286	$\alpha_{td} = 0.03762\theta - 8.668$ "
286→265	$\alpha_{td} = 2.1$ "
265→154	$\alpha_{td} = 11.769 - 0.03644\theta$ "
154→ 20	$\alpha_{td} = 7.357 - 0.00722\theta$ "
>328	$\lambda = 20.1 + 0.00829\theta$ W/m°C
328→223	$\lambda = 33.152 - 0.03143\theta$ "
223→ 20	$\lambda = 25.521 + 0.002726\theta$ "

N.B. Although this data was used in the present calculations involving 835M30, it relates to a similar material 830A31.

Table 7 Results Obtained From The Relationship Between Length & Temperature During the Cooling of 835M30 Dilatometer Specimens

(0.34%C; 0.49%Mn; 0.20%Si; 0.022%S; 0.008%P; 4.29%Ni; 1.36%Cr; 0.29%Mo)

	M_s temperature °C	%ΔL during martensite transformation	α_{ex} in austenitic phase x 10^{-5} °C	$\left(\frac{d\theta}{dt}\right)_{400°C}$ °C/s
a	300	0.350	2.114	2.50
b	300	0.355	2.136	2.21
c	302	0.351	2.159	1.63
d	301	0.347	2.166	2.15
e	300	0.354	2.141	2.19
f	296	0.358	2.106	2.19
g	297	0.342	2.136	1.00
h	301	0.379	2.166	4.82
Average	299.6	0.354	2.141	

Table 8 Changes in Volume Accompanying the Hardening of 835M30

(0.33%C; 0.485%Mn; 0.20%Si; 0.0155%S; 0.005%P; 4.54%Ni; 1.40%Cr; 0.22%Mo)

Volume in softened condition x 10^3mm^3 (ferrite + carbide)	Volume in hardened condition x 10^3mm^3 (martensite)	% Volume change
6.9204	6.9463	0.374
7.0023	7.0343	0.399
6.9407	6.9307	0.376
7.0062	7.0324	0.374
6.8373	6.8615	0.354
6.9521	6.9807	0.411
		Average 0.381

Table 9 Data Used in The Calculation of Thermal Stress in Quenched Plates in Order to Test the Stability of the Calculation Method

Initial temperature of plate	850°C
Quenchant temperature	20°C
Number of elements in half-plate for purpose of calculating temperature distribution	40
Number of elements in half-plate for purpose of stress calculation	10
Max. average stress in half-plate at end of plasticity calculation	±0.1 N/mm^2
Minimum temperature step used in stress calculation	1°C
835M30 density	7700 kg/m^3
835M30 specific heat	620 J/kg°C
835M30 thermal conductivity	26.8 W/m°C
Surface heat transfer coefficient	6740 W/m^2°C
Plate thickness	40 mm
Biot number	5.03
Martensite flow stress	1200 N/mm^2
Austenite flow stress ($\theta > 760$°C)	15 N/mm^2
Austenite flow stress ($\theta < 760$°C)	$396.56 - 0.5075\theta$ N/mm^2

Table 10 Distribution of Residual Stress and Strain* in a Quenched Plate Assuming an Infinite Stress and a Surface Heat Transfer Coefficient of 6,740 W/m^2°C

Depth beneath surface (mm)	1	3	5	7	9	11	13	15	17	19
Residual stress (N/mm^2)	−0.27	−0.26	−0.29	−0.29	−0.11	0.97	0.21	0.27	0.30	0.30
Residual strain	Maximum 1 x 10^{-4}%									

*excluding the homogeneous volume change that accompanies the hardening of 835M30.

Table 11 Key to Individual Calculations of Thermal Stress and Strain

Table 12 contains data common to all the calculations, otherwise the data used was as indicated.

Program run	Data used in program			Relevant figures for results
	Z	h	Austenite Flow Stress	
PR1/W40/hAv/UFS	40 mm	Table 5 (a)	Table 13 (a)	90, 91
PR2/W40/hAv/LFS	"	"	Table 13 (b)	
PR3/W40/hMax/UFS	"	Table 5 (b)	Table 13 (a)	92, 93
PR4/W40/hMin/UFS	"	Table 5 (c)	"	92, 93
PR5/W40/hMax/LFS	"	Table 5 (b)	Table 13 (b)	92, 93
PR6/W40/hMin/LFS	"	Table 5 (c)	"	92, 93
PR7/W20/hAv/UFS	20 mm	Table 5 (a)	Table 13 (a)	94
PR8/W20/hAv/LFS	"	"	Table 13 (b)	
PR9/W20/hMax/UFS	"	Table 5 (b)	Table 13 (a)	95, 96
PR10/W20/hMin/UFS	"	Table 5 (c)	"	95, 96
PR11/W20/hMax/LFS	"	Table 5 (b)	Table 13 (b)	95, 96
PR12/W20/hMin/LFS	"	Table 5 (c)	"	95, 96
PR13/OIL20/UFS	20 mm	Table 5 (d)	Table 13 (a)	97,98,99,100
PR14/OIL20/LFS	"	"	Table 13 (b)	99, 100
PR15/AQUA20/UFS	20 mm	Table 5 (e)	Table 13 (a)	101,102,103,104
PR16/AQUA20/LFS	"	"	Table 13 (b)	103, 104

(W - Water quench; OIL - Oil quench; AQUA - 25% Aquaquench 1250 quench; UFS - Upper limit of austenite flow stresses; LFS - Lower limit of austenite flow stresses; hMax, hAv and hMin - range of h values applicable to water quenches only.)

Table 12 Data Used in Thermal Stress Predictions of 835M30 which are Common to all Program Runs

Initial plate temperature	850°C
Quenchant temperature	20°C
Number of elements in half-plate for temperature computations	40
Number of elements in half-plate for stress computations	10
Density of plate	7.7 Mg/m^3
Thermal conductivity of plate	25.2 W/m°C
Specific heat of plate	705 J/kg°C
Martensite flow stress	1600 N/mm^2
$\frac{E}{1-\nu}$	$2.935 \times 10^{-5} - 141.77\theta$ N/mm^2
Austenite strain hardening coefficient, W_1	4,300 N/mm^2 ($\theta<600$°C)
" " " " W_1	$8{,}950-7.75\theta$ N/mm^2 ($\theta>600$°C)
" " " " W_2	3,700 N/mm^2 ($\theta<600$°C)
" " " " W_2	$10{,}600-11.5\theta$ N/mm^2 ($\theta>600$°C)
Maximum average unbalanced stress at end of plasticity calculation.	0.1 N/mm^2
Minimum temperature step at surface or centre	1°C
Dilatometer data	see equations 4.18

Table 13 Variation of Flow Stress of Austenite with Temperature.

	θ (^{o}C)	σ_f (N/mm^2)
(a) Upper range of experimental data	>850 400 to 850 <400	40.0 $257.2-0.2556\theta$ 155.0
(b) Lower range of experimental data	>790 350 to 790 <350	30.0 $236.5-0.2614\theta$ 145.0

Table 14 Surface Grinding Conditions Employed During the Experimental Determination of Residual Stress in Quenched Plates

Grinding wheel	Universal White Bauxite, WA 46 KV
Spindle speed	2350 R.P.M.
Table speed	250 mm/s
Width of cut	0.5 mm

Table 15 Experimental Results of the Distortion of Type C (40 mm) Plate of 835M30 when Water Quenched

Measurement location	Change in length produced by 1st quench (ΔY)%	Change in length produced by 2nd quench (ΔY)%
1A	0.467	0.445
2A	0.269	0.279
3A	0.209	0.234
4A	0.272	0.306
5A	0.467	0.498
1B	0.450	0.461
2B	0.259	0.276
3B	0.179	0.202
4B	0.269	0.297
5B	0.467	0.475
1C	0.443	0.468
2C	0.265	0.309
3C	-	-
4C	0.262	0.267
5C	0.450	0.465
1D	0.459	0.452
2D	0.272	0.298
3D	0.196	0.238
4D	0.254	0.278
5D	0.427	0.429
1E	0.490	0.473
2E	0.277	0.295
3E	0.212	0.232
4E	0.248	0.274
5E	0.412	0.458

/cont'd...

Table 15 (continued)

Measurement location	Change in length produced by 1st quench (ΔY)%	Change in length produced by 2nd quench (ΔY)%
1F	0.428	0.467
2F	0.247	0.280
3F	0.190	0.194
4F	0.254	0.248
5F	0.420	0.411
1G	0.435	0.468
2G	0.254	0.286
3G	0.160	0.175
4G	0.247	0.267
5G	0.444	0.423
1H	0.461	0.472
2H	0.275	0.288
3H	0.153	0.154
4H	0.253	0.303
5H	0.448	0.451
1J	0.461	0.479
2J	0.267	0.313
3J	0.180	0.190
4J	0.260	0.296
5J	0.454	0.482
1K	0.481	0.501
2K	0.281	0.330
3K	0.213	0.226
4K	0.279	0.328
5K	0.477	0.494

/cont'd...

Table 15 (continued)

Measurement location	Change in length produced by 1st quench (ΔY)%	Change in length produced by 2nd quench (ΔY)%
Mean value at pos.1	0.458	0.469
" " " " 2	0.267	0.295
" " " " 3	0.188	0.205
" " " " 4	0.260	0.286
" " " " 5	0.447	0.459
Average change in plate width, calculated from change in thickness at centre of plate*	0.590 (calculated from -0.853% change in thickness)	0.704 (calculated from -1.04% change in thickness)

* i.e. free from edge effects

Table 16 Experimental Results of the Distortion of Type D (20 mm) Plate of 835M30 when Water Quenched

Measurement location	Change in length produced by quench (ΔY)%	Measurement location	Change in length produced by quench (ΔY)%
1A	-	1F	-
2A	0.439	2F	0.337
3A	0.347	3F	0.268
4A	0.344	4F	-
5A	0.370	5F	-
1B	0.507	1G	0.374
2B	0.453	2G	0.348
3B	0.367	3G	0.277
4B	0.367	4G	0.345
5B	0.387	5G	0.426
1C	0.508	1H	0.382
2C	-	2H	0.356
3C	-	3H	0.289
4C	-	4H	0.362
5C	0.387	5H	0.419
1D	0.480	1J	0.411
2D	0.435	2J	0.408
3D	0.343	3J	0.319
4D	0.379	4J	0.389
5D	0.415	5J	0.446
1E	0.490	1K	0.418
2E	0.414	2K	0.339
3E	0.338	3K	0.299
4E	0.354	4K	0.348
5E	0.400	5K	0.428

/cont'd...

Table 16 (continued)

Measurement location	Change in length produced by quench (ΔY)%	Measurement location	Change in length produced by quench (ΔY)%
Mean value at pos. 1	0.446	Average change in plate width, calculated from change in thickness at centre of plate*	0.445 (calculated from -0.563% change in thickness)
Mean value at pos. 2	0.392		
Mean value at pos. 3	0.316		
Mean value at pos. 4	0.361		
Mean value at pos. 5	0.409		

* i.e. free from edge effects

Table 17 Experimental Results of the Distortion of Type D (20 mm) Plate of 835M30 when Oil Quenched

Measurement location	Change in length produced by quench (ΔY)%	Measurement location	Change in length produced by quench (ΔY)%
1A	0.092	1F	0.104
2A	0.072	2F	0.085
3A	0.050	3F	0.055
4A	0.026	4F	0.028
5A	0.008	5F	0.004
1B	0.088	1G	0.092
2B	0.068	2G	0.074
3B	0.045	3G	0.048
4B	0.019	4G	0.020
5B	-0.004	5G	-0.005
1C	0.085	1H	0.007
2C	0.047	2H	0.061
3C	-	3H	0.034
4C	-0.005	4H	0.010
5C	-0.006	5H	-0.014
1D	0.082	1J	0.064
2D	0.059	2J	0.044
3D	0.035	3J	0.024
4D	0.008	4J	0.002
5D	-0.008	5J	-0.017
1E	0.075	1K	0.053
2E	0.053	2K	0.035
3E	0.027	3K	0.016
4E	0.004	4K	0.0
5E	-0.013	5K	-0.015

/cont'd...

Table 17 (continued)

Measurement location	Change in length produced by quench (ΔY)%	Measurement location	Change in length produced by quench (ΔY)%
Mean value at pos. 1	0.081	Average change in plate width, calculated from change in thickness at centre of plate*	0.066 (calculated from 0.195% change in thickness)
Mean value at pos. 2	0.060		
Mean value at pos. 3	0.037		
Mean value at pos. 4	0.011		
Mean value at pos. 5	-0.007		

* i.e. free from edge effects

Table 18 Experimental Results of the Distortion of Type D (20 mm) Plate of 835M30 when Quenched into 25% Aquaquench 1250

Measurement location	Change in length produced by quench (ΔY)%	Measurement location	Change in length produced by quench (ΔY)%
1A	0.051	1F	0.051
2A	0.033	2F	0.049
3A	0.030	3F	0.050
4A	0.029	4F	0.060
5A	0.036	5F	0.096
1B	0.053	1G	0.055
2B	0.035	2G	0.050
3B	0.026	3G	0.049
4B	0.028	4G	0.066
5B	0.036	5G	0.092
1C	0.054	1H	0.040
2C	0.026	2H	0.038
3C	-	3H	0.043
4C	-	4H	0.064
5C	0.026	5H	0.086
1D	0.053	1J	0.034
2D	0.032	2J	0.033
3D	0.025	3J	0.034
4D	0.019	4J	0.050
5D	0.024	5J	0.072
1E	0.052	1K	0.033
2E	0.035	2K	0.028
3E	0.028	3K	0.031
4E	0.023	4K	0.044
5E	0.031	5K	0.067

/cont'd...

Table 18 (continued)

Measurement location	Change in length produced by quench (ΔY)%	Measurement location	Change in length produced by quench (ΔY)%
Mean value at pos. 1	0.048	Average change in plate width, calculated from change in thickness at centre of plate*	0.061 (calculated from 0.205% change in thickness)
Mean value at pos. 2	0.036		
Mean value at pos. 3	0.035		
Mean value at pos. 4	0.041		
Mean value at pos. 5	0.057		

* i.e. free from edge effects

FIGURE 1: Schematic production of stress in a quenched bar that exhibits no transformation during quenching.

(a) Cooling curves at surface and centre

(b) Stresses generated with no plastic flow (broken line), and high temperature relaxation of stress (solid line).

(After Andrews[2])

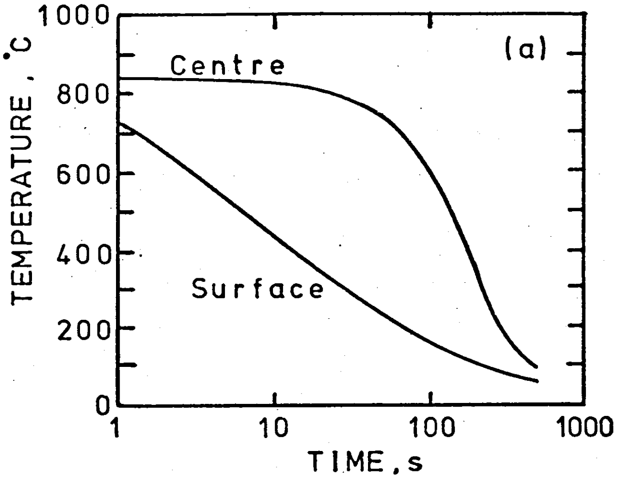
(a)
TEMPERATURE, °C
1000
800
600
400
200
0
1
10
100
1000
TIME, s
Centre
Surface

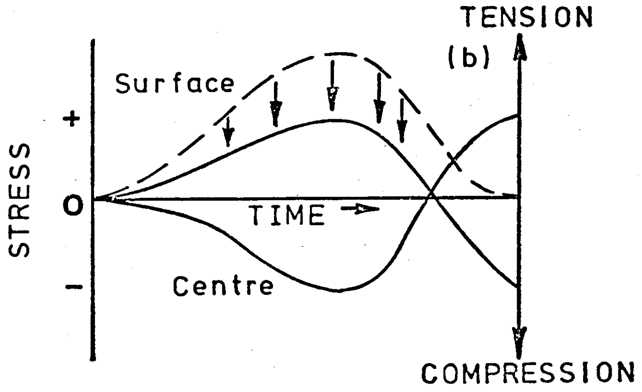
(b)
TENSION
COMPRESSION
STRESS
+
O
−
TIME →
Surface
Centre

FIGURE 2: Typical dilatometer curve obtained from a plain carbon steel specimen[7].

FIGURE 3: Plan view of notched 'crackability test specimen', developed by Chapman and Jominy[21].

FIGURE 4: Variation in probability of cracking with cooling rate of disc specimens. (After Kobasko[22])

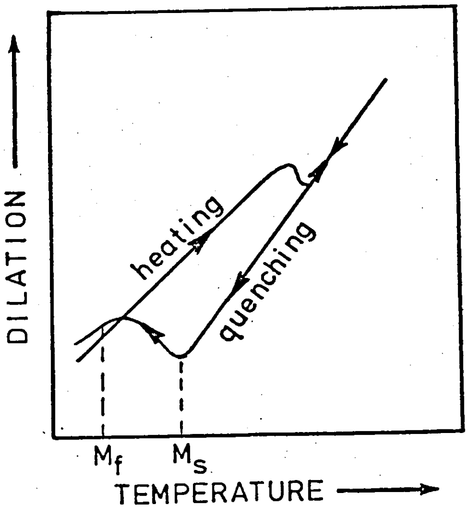
DILATION
heating
quenching
M$_f$
M$_s$
TEMPERATURE

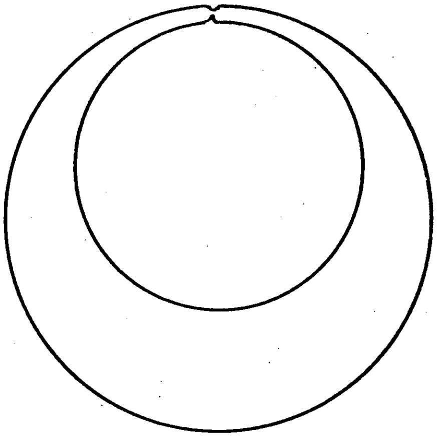

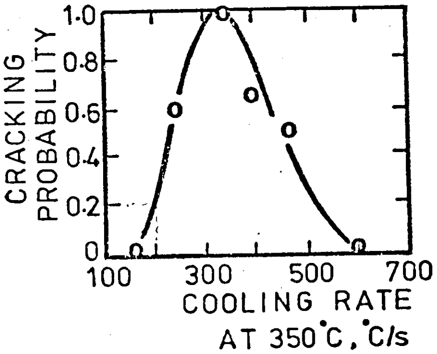
CRACKING PROBABILITY
1.0
0.8
0.6
0.4
0.2
0
100
300
500
700
COOLING RATE AT 350°C, °C/s

FIGURE 5: Schematic illustration of:

(a) the variation in the quantities Λ and Φ during the determination of residual stresses by the Sachs technique and,

(b) the ensuing residual stress distribution.

(After Andrews[2])

FIGURE 6: Influence of specimen diameter and carbon content on the maximum level of residual stress in water quenched steel cylinders.
(After Buhler & Buckholtz[33])

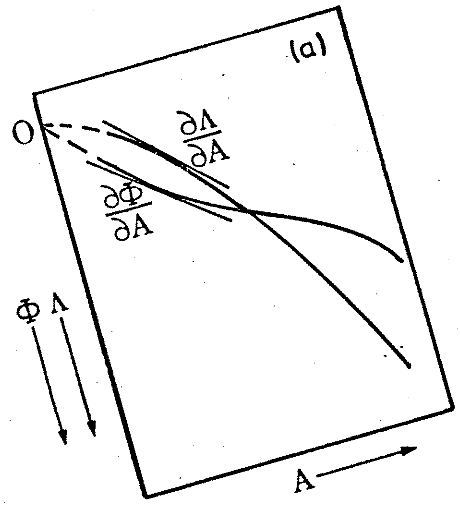
(a)
O
∂Λ/∂A
∂Φ/∂A
Φ Λ
A

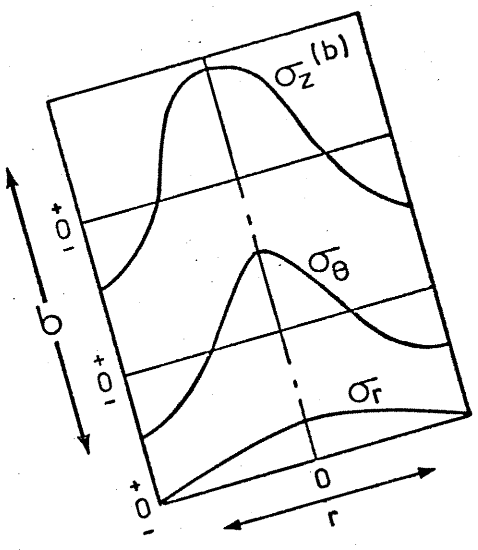
(b)
σz
σθ
σr
+ 0 −
+ 0 −
+ 0 −
σ
0
r

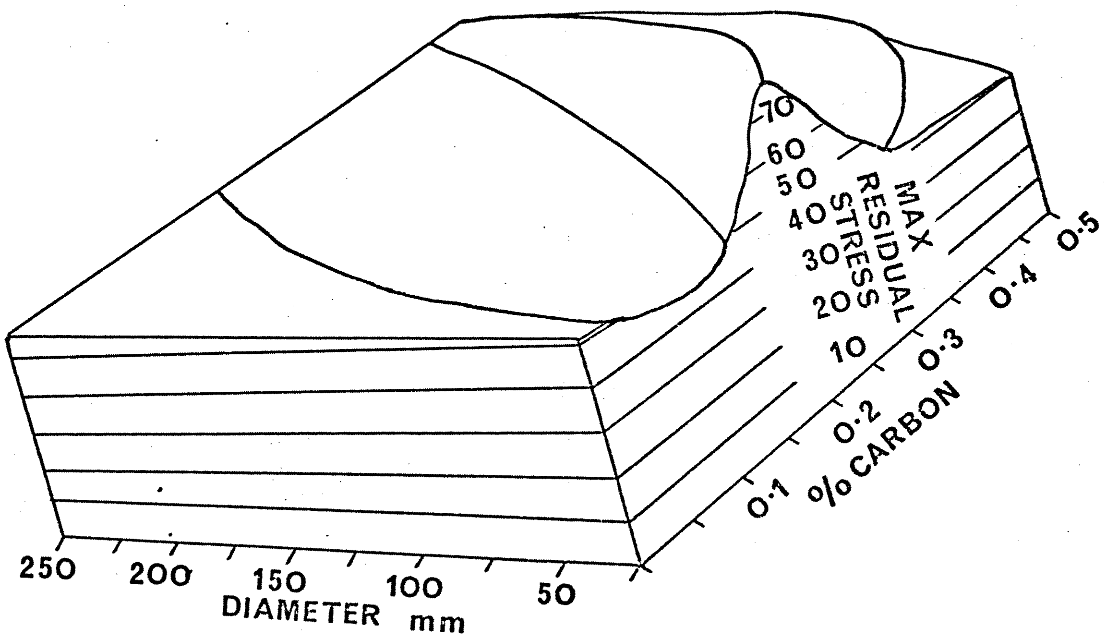
70
60
50
40
30
20
10
MAX RESIDUAL STRESS
0·1
0·2
0·3
0·4
0·5
% CARBON
250
200
150
100
50
DIAMETER mm

FIGURE 7: Influence of carbon content, quenching temperature and quenchant on the maximum level of residual stress in 50mm diameter steel cylinders.
(After Buhler & Buckholtz[33])

FIGURE 8: Distribution of the longitudinal residual stress in a hollow cylinder (55mm O.D., 24mm I.D.) of a 0.3%C steel after quenching in water.
(After Buhler & Buckholtz[34])

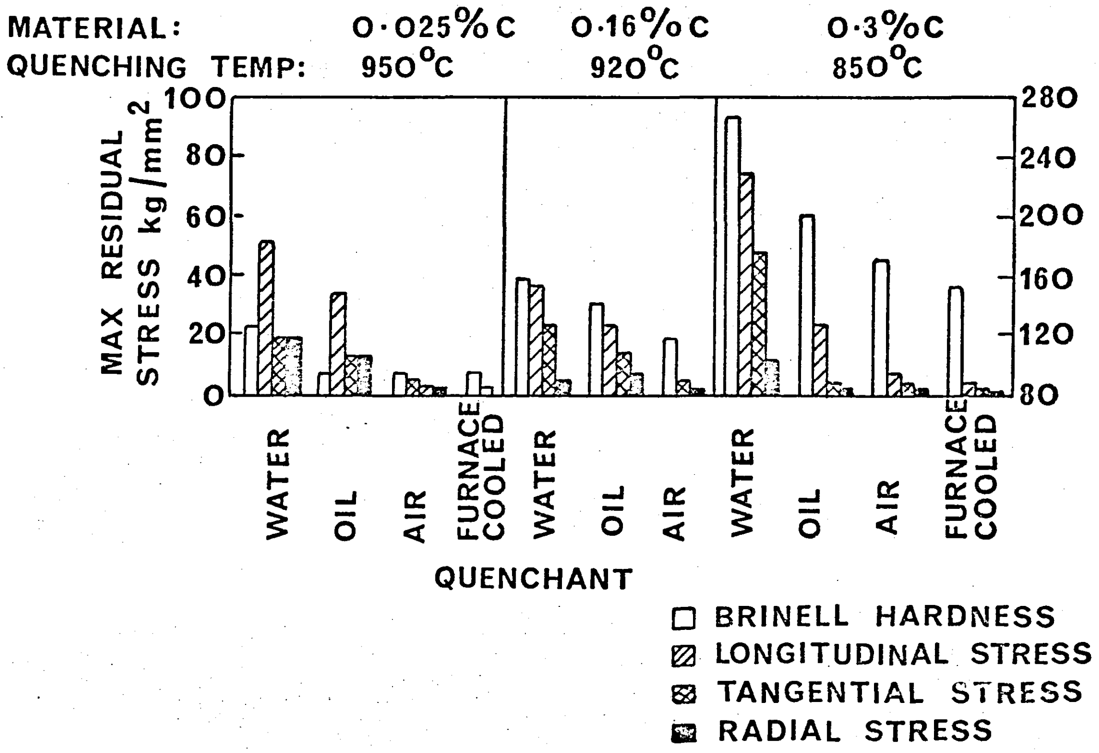
MATERIAL:
QUENCHING TEMP:
0·025%C
950°C
0·16%C
920°C
0·3%C
850°C
MAX RESIDUAL STRESS kg/mm²
100
80
60
40
20
0
280
240
200
160
120
80
WATER
OIL
AIR
FURNACE COOLED
WATER
OIL
AIR
WATER
OIL
AIR
FURNACE COOLED
QUENCHANT
□ BRINELL HARDNESS
▨ LONGITUDINAL STRESS
⊠ TANGENTIAL STRESS
▩ RADIAL STRESS

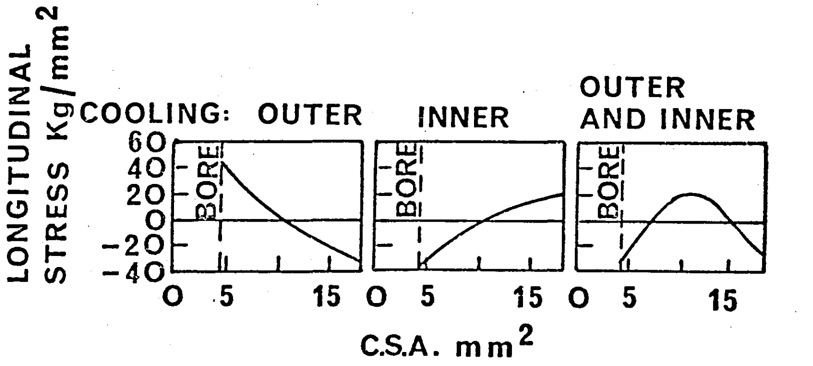
LONGITUDINAL STRESS Kg/mm²
COOLING: OUTER
INNER
OUTER AND INNER
60
40
20
0
-20
-40
BORE
BORE
BORE
0
5
15
0
5
15
0
5
15
C.S.A. mm²

FIGURE 9: Influence of quench severity (due to variation in the pressure of the water spray) on the residual stress in the surface of 50mm diameter cylinders. (After Liss[35]).

FIGURE 10: Distribution of residual in a hollow cylinder(18.22mm O.D., 2mm I.D.) of a 0.46%C steel after quenching in water.

(a) Cooled from outside only.

(b) Cooled from outside and bore.

(After Vannes et alia[36])

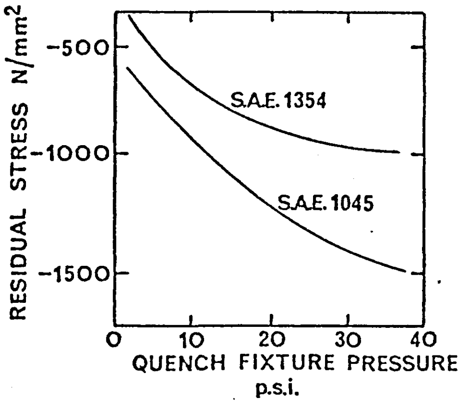
RESIDUAL STRESS N/mm^2
-500
-1000
-1500
S.A.E. 1354
S.A.E. 1045
0
10
20
30
40
QUENCH FIXTURE PRESSURE
p.s.i.

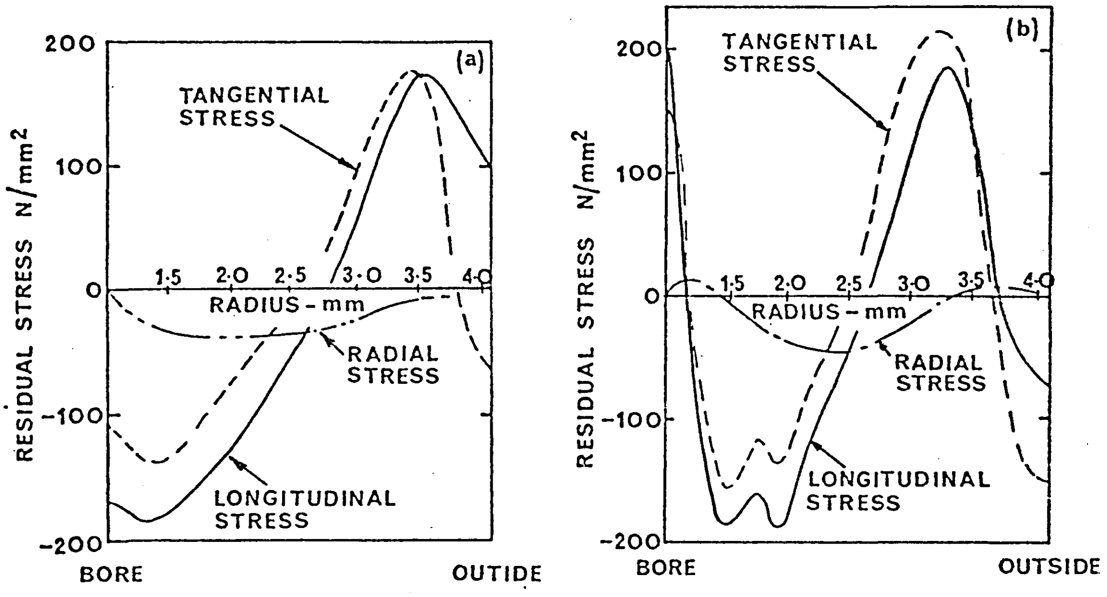
(a)
200
100
0
-100
-200
RESIDUAL STRESS N/mm^2
TANGENTIAL STRESS
RADIAL STRESS
LONGITUDINAL STRESS
1·5
2·0
2·5
3·0
3·5
4·0
RADIUS - mm
BORE
OUTIDE
(b)
200
100
0
-100
-200
RESIDUAL STRESS N/mm^2
TANGENTIAL STRESS
RADIAL STRESS
LONGITUDINAL STRESS
1·5
2·0
2·5
3·0
3·5
4·0
RADIUS - mm
BORE
OUTSIDE

FIGURE 11: Residual stress distribution in 0.5%C steel cylinders after quenching in water (solid line) and oil (broken line).

(a)	100mm	diameter
(b)	50mm	"
(c)	30mm	"
(d)	15mm	"
(e)	10mm	"

(After Buhler & Rose[38])

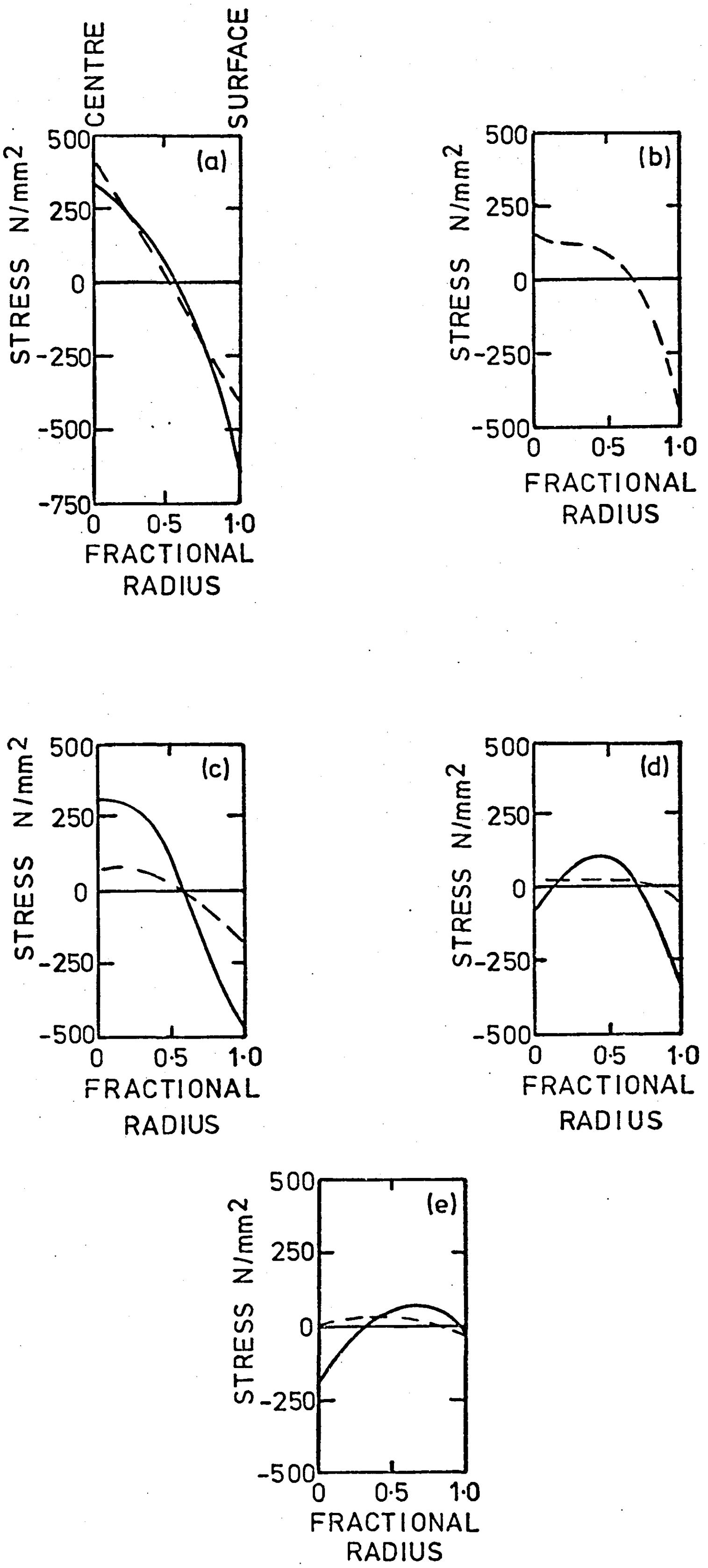
CENTRE
SURFACE
(a)
STRESS N/mm2
500
250
0
-250
-500
-750
0
0·5
1·0
FRACTIONAL RADIUS
(b)
STRESS N/mm2
500
250
0
-250
-500
0
0·5
1·0
FRACTIONAL RADIUS
(c)
STRESS N/mm2
500
250
0
-250
-500
0
0·5
1·0
FRACTIONAL RADIUS
(d)
STRESS N/mm2
500
250
0
-250
-500
0
0·5
1·0
FRACTIONAL RADIUS
(e)
STRESS N/mm2
500
250
0
-250
-500
0
0·5
1·0
FRACTIONAL RADIUS

FIGURE 12: Residual stress distribution in cylinders of 0.13%C, 0.95%Cr, 0.86%Mo steel after quenching in water (solid line) and oil (broken line).

(a) 100mm diameter
(b) 50mm "
(c) 30mm "
(d) 15mm "
(e) 10mm "

(After Buhler & Rose[38])

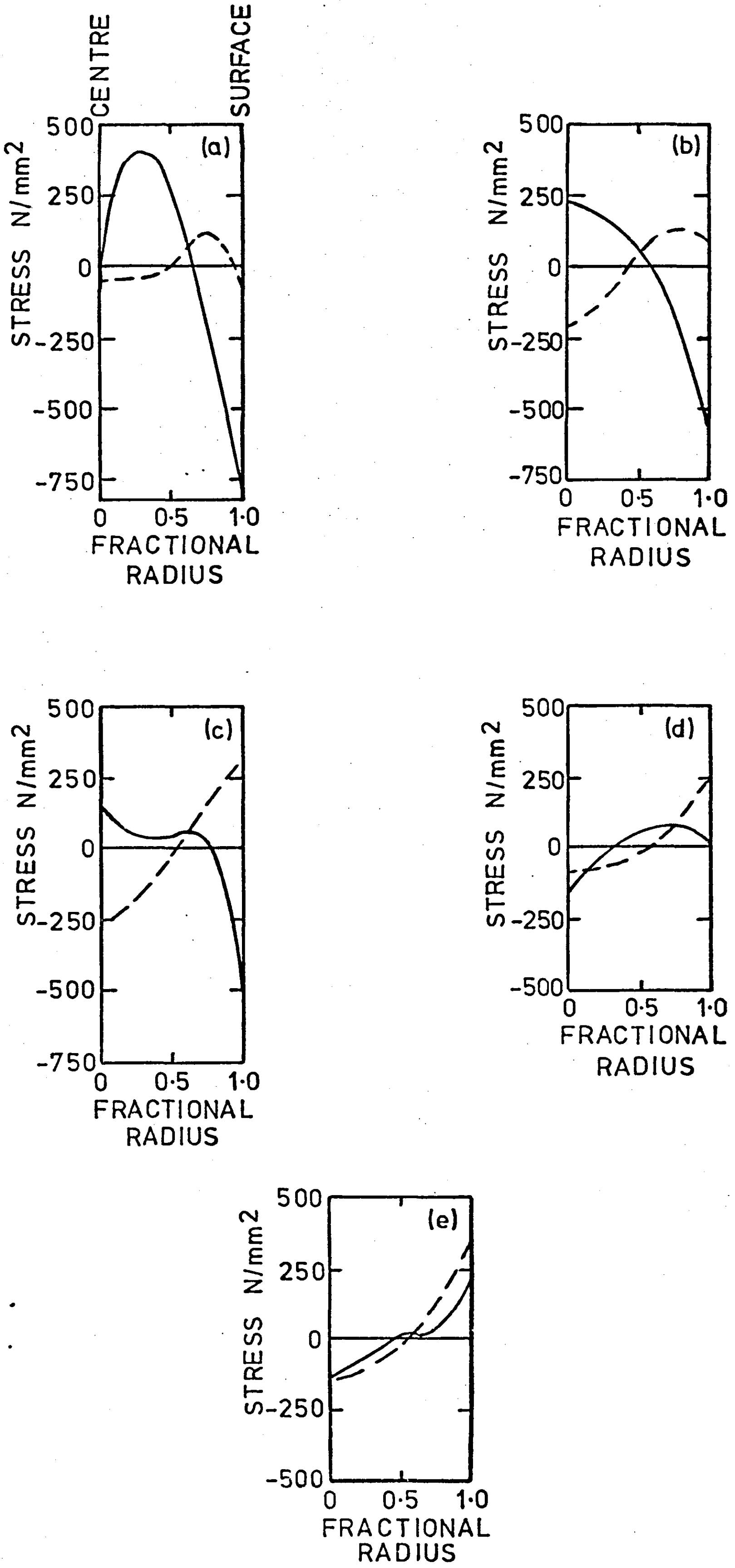
CENTRE
SURFACE
(a)
STRESS N/mm2
500
250
0
-250
-500
-750
0
0·5
1·0
FRACTIONAL RADIUS
(b)
STRESS N/mm2
500
250
0
-250
-500
-750
0
0·5
1·0
FRACTIONAL RADIUS
(c)
STRESS N/mm2
500
250
0
-250
-500
-750
0
0·5
1·0
FRACTIONAL RADIUS
(d)
STRESS N/mm2
500
250
0
-250
-500
0
0·5
1·0
FRACTIONAL RADIUS
(e)
STRESS N/mm2
500
250
0
-250
-500
0
0·5
1·0
FRACTIONAL RADIUS

FIGURE 13: Residual stress distribution in a 30mm diameter cylinder of 0.26%C, 2.27%Cr, 0.28%Mo steel after being quenched into water.

(After Buhler & Rose[38])

FIGURE 14: Classification of residual stress distributions obtained in steel cylinders after quenching.

(After Buhler & Rose[38])

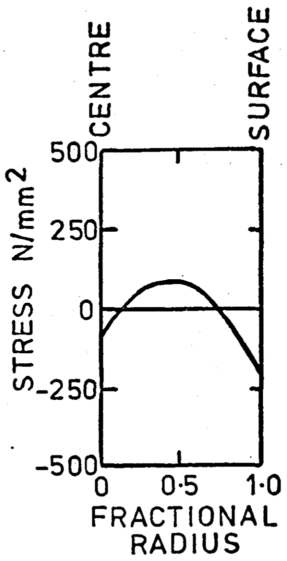
CENTRE
SURFACE
STRESS N/mm2
500
250
0
-250
-500
0
0·5
1·0
FRACTIONAL RADIUS

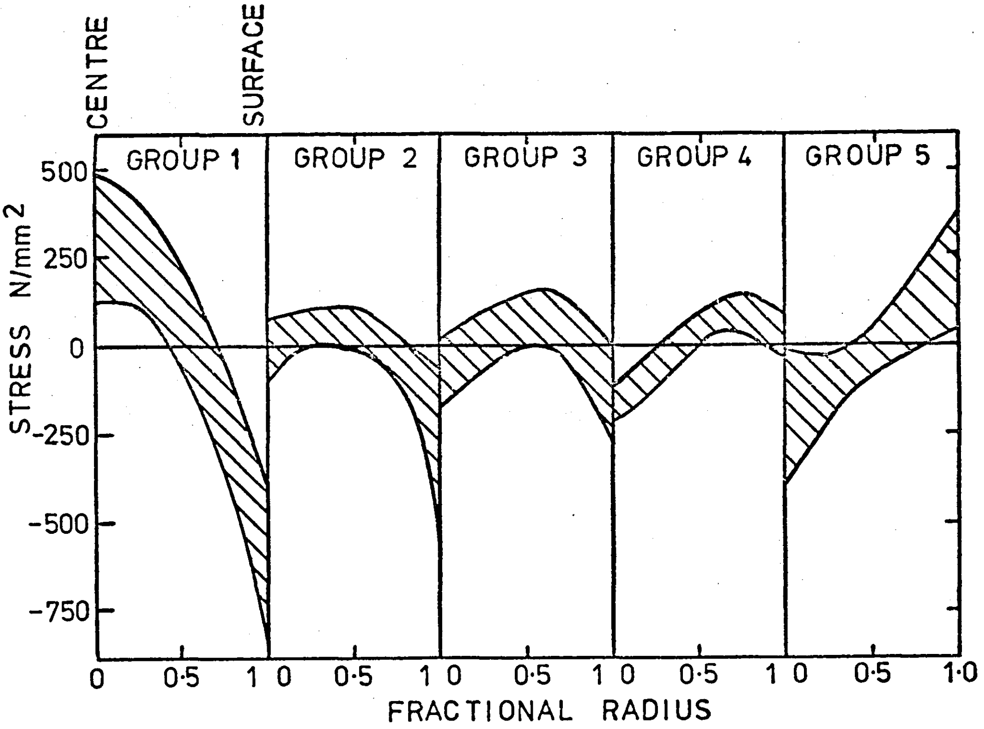
CENTRE
SURFACE
GROUP 1
GROUP 2
GROUP 3
GROUP 4
GROUP 5
STRESS N/mm2
500
250
0
-250
-500
-750
0
0·5
1
0
0·5
1
0
0·5
1
0
0·5
1
0
0·5
1·0
FRACTIONAL RADIUS

FIGURE 15: 'Navy C' specimen for the assessment of distortion characteristics. (Plan view).

FIGURE 16: Slit-disc specimen used by Tricot et alia[57] for the assessment of distortion characteristics.

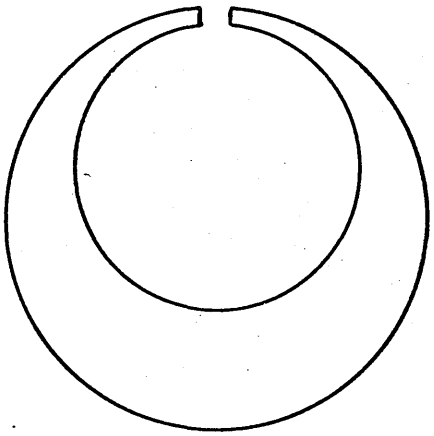

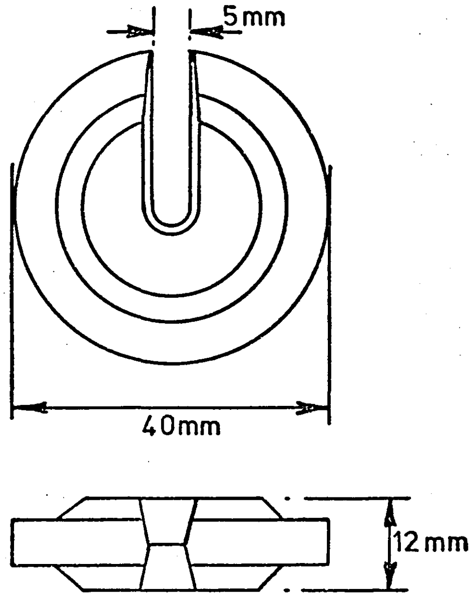
5mm
40mm
12mm

FIGURE 17: Influence of carbon content on the M_s and M_f temperatures in a plain carbon steel, and thus the M_s and M_f temperatures of the case and core in a carburising steel.

(After Mocarski[15]).

FIGURE 18: Washer-like specimen used by Llewellyn & Cook[14] in the investigation of the distortion of carburising steels during quenching.

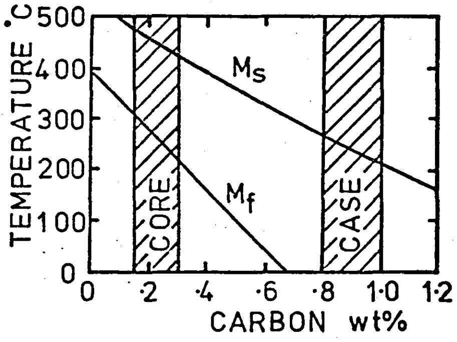
TEMPERATURE °C
500
400
300
200
100
0
0
·2
·4
·6
·8
1·0
1·2
CARBON wt%
Ms
Mf
CORE
CASE

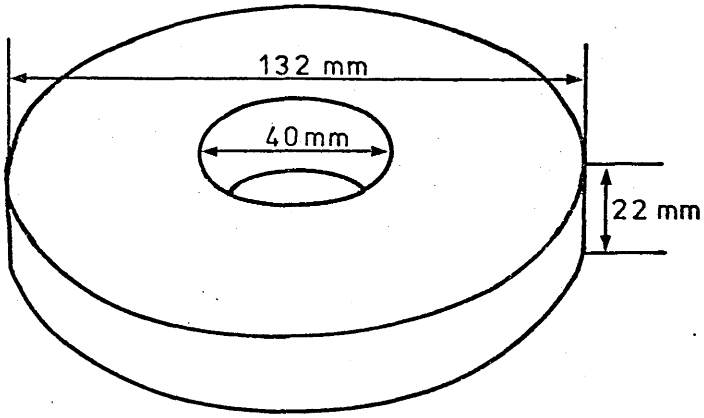
132 mm
40mm
22 mm

FIGURE 19: Relationship obtained by Llewellyn & Cook[14] between the distortion of specimens (shown in Figure 18) and the M_S/Hardenability factor of the steel involved.

(a) Bore diameter

(b) Thickness

(c) Outer diameter

FIGURE 20: Variation in change of outside diameter of washer-like specimens (ΔO.D.) of austenitic and ferritic chromium steels with severity of quench.

A.C. - Air cool

S.O.Q. - Slow oil quench

F.O.Q. - Fast oil quench

W.Q. - Water quench

(After Llewellyn et alia[61])

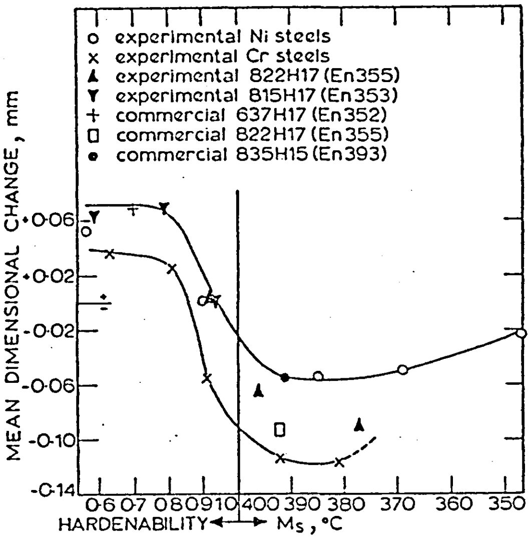
o experimental Ni steels
x experimental Cr steels
▲ experimental 822H17 (En355)
▼ experimental 815H17 (En353)
+ commercial 637H17 (En352)
□ commercial 822H17 (En355)
● commercial 835H15 (En393)
MEAN DIMENSIONAL CHANGE, mm
+0·06
+0·02
-0·02
-0·06
-0·10
-0·14
0·6 0·7 0·8 0·9 1·0 400 390 380 370 360 350
HARDENABILITY ←→ Ms, °C

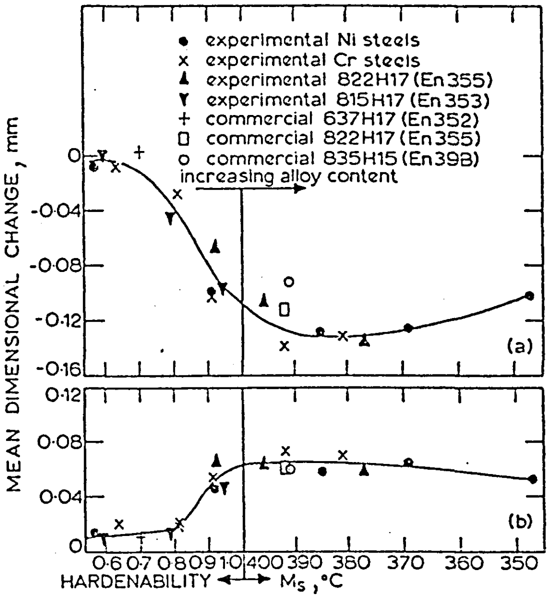
● experimental Ni steels
x experimental Cr steels
▲ experimental 822H17 (En355)
▼ experimental 815H17 (En353)
+ commercial 637H17 (En352)
□ commercial 822H17 (En355)
o commercial 835H15 (En39B)
increasing alloy content
MEAN DIMENSIONAL CHANGE, mm
0
-0·04
-0·08
-0·12
-0·16
(a)
0·12
0·08
0·04
0
(b)
0·6 0·7 0·8 0·9 1·0 400 390 380 370 360 350
HARDENABILITY ←→ Ms, °C

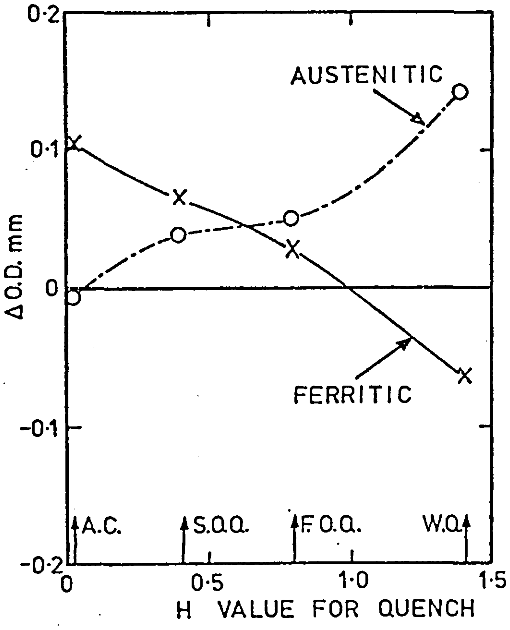
0·2
0·1
0
-0·1
-0·2
Δ O.D. mm
AUSTENITIC
FERRITIC
A.C.
S.O.Q.
F.O.Q.
W.Q.
0
0·5
1·0
1·5
H VALUE FOR QUENCH

FIGURE 21: Typical cooling curves at the surface and centre of a specimen during quenching.

(After A.S.M.[87])

FIGURE 22: Variation of error in surface heat transfer coefficient with depth of measurement beneath surface.

(After Lambert & Economopulos[98])

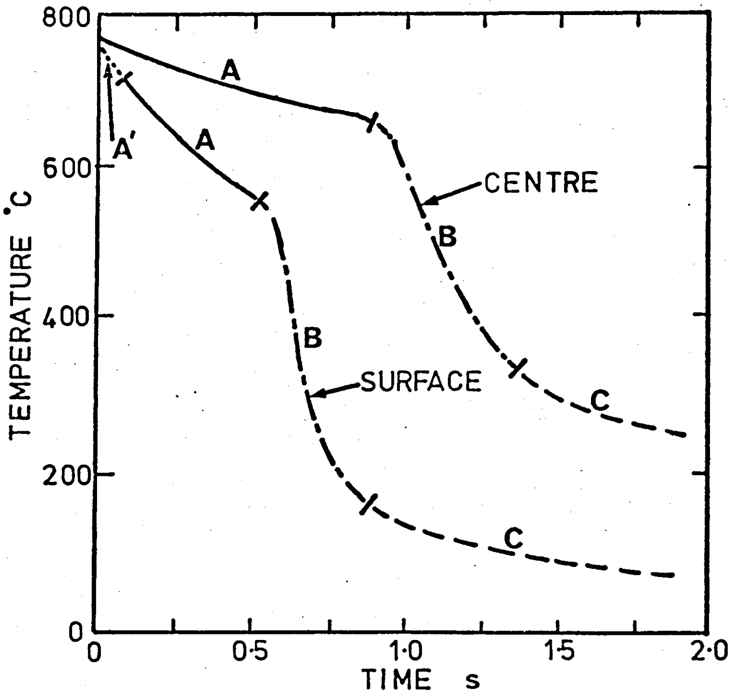
800
600
400
200
0
TEMPERATURE °C
0
0·5
1·0
1·5
2·0
TIME s
A
A'
A
CENTRE
B
B
SURFACE
C
C

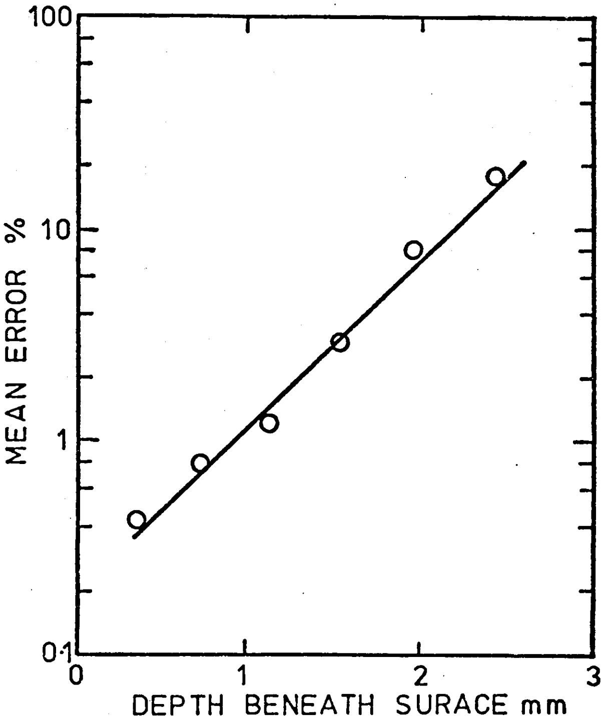
100
10
1
0·1
MEAN ERROR %
0
1
2
3
DEPTH BENEATH SURACE mm

FIGURE 23: Boiling curve of a wire submerged in water showing variation in the surface heat transfer coefficient, h, with the temperature difference, $\Delta\theta$, between the wire and the fluid.

(a) Pure convection heat transfer

(b) Nucleate boiling (bubbles condensing in superheated liquid)

(c) Nucleate boiling (bubbles rising to surface of bath)

(d) Partial nucleate boiling and stable film boiling

(e) Stable film boiling

(f) Heat transfer by radiation taking part

(After Farber & Scorah[106])

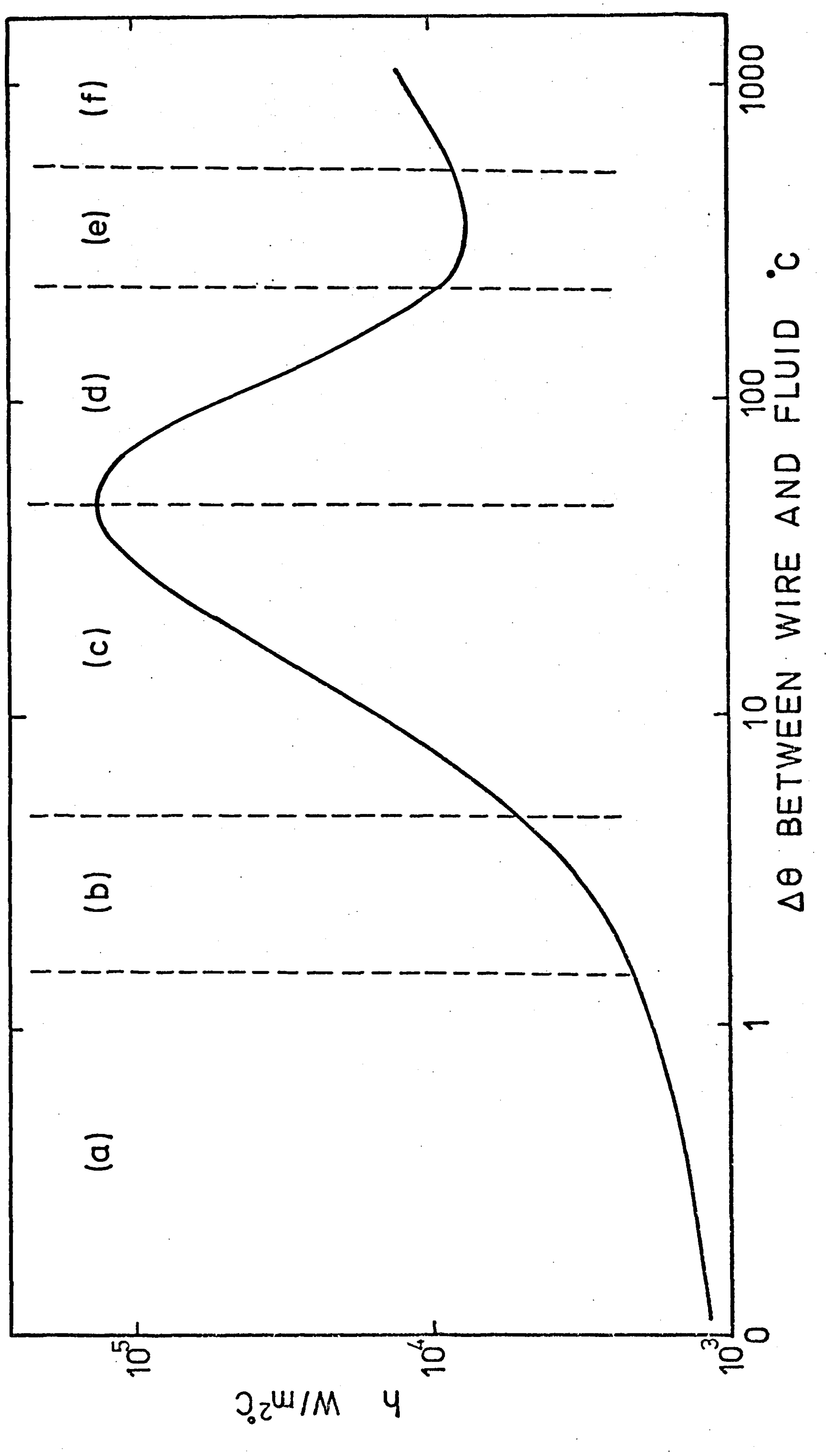
(a)
(b)
(c)
(d)
(e)
(f)
0
1
10
100
1000
ΔΘ BETWEEN WIRE AND FLUID °C
10^5
10^4
10^3
h W/m²°C

FIGURE 24: Variation of surface heat flux with surface temperature obtained from Ni cylinders of various diameters by Beck & Chevrier[103].

(a) 10mm diameter

(b) 15mm diameter

(c) 30mm diameter

FIGURE 25: Schematic representation of the movement of the nucleate boiling front up Ni cylinders when quenched vertically in water.

(After Beck & Chevrier[103])

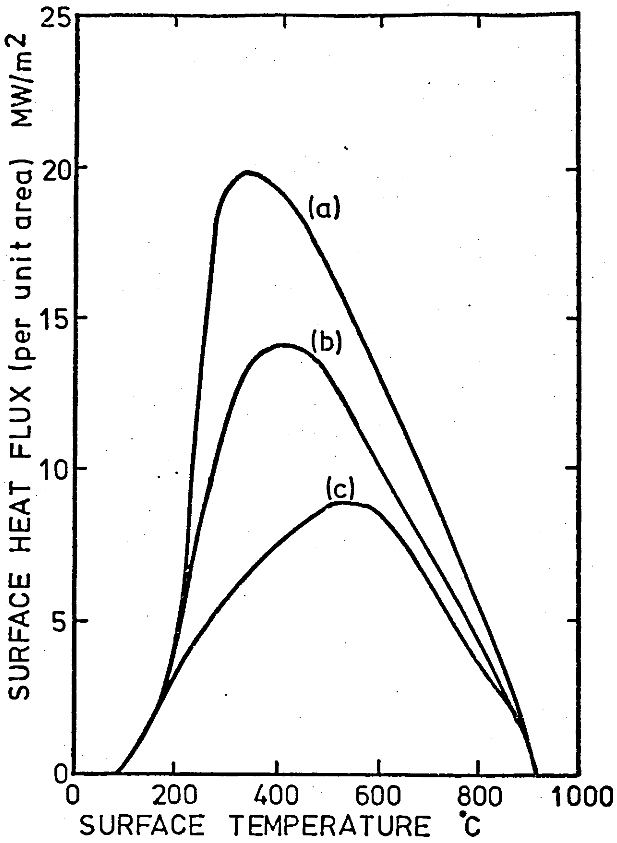

SURFACE HEAT FLUX (per unit area) MW/m2
25
20
15
10
5
0
(a)
(b)
(c)
0
200
400
600
800
1000
SURFACE TEMPERATURE °C

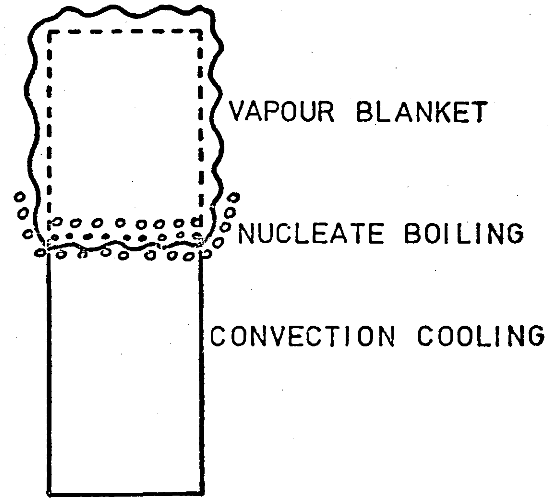

VAPOUR BLANKET
NUCLEATE BOILING
CONVECTION COOLING

FIGURE 26: Influence of specimen material, obtained by Lambert & Economopoulos[98], on the variation in h during quenching into still water.

(a) Nickel probe

(b) Non-oxidised steel probe

FIGURE 27: Influence of specimen material, obtained by Beck & Chevrier[103], on the variation in surface heat flux during the quenching into still water at 60°C of Al and Ni cylinders.

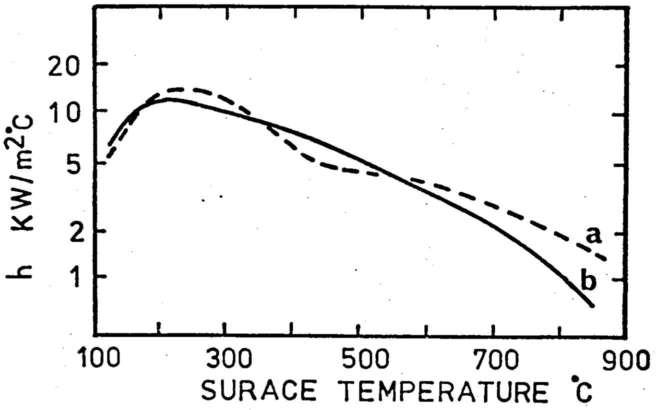

20
10
5
2
1
h KW/m^2°C
100
300
500
700
900
SURACE TEMPERATURE °C
a
b

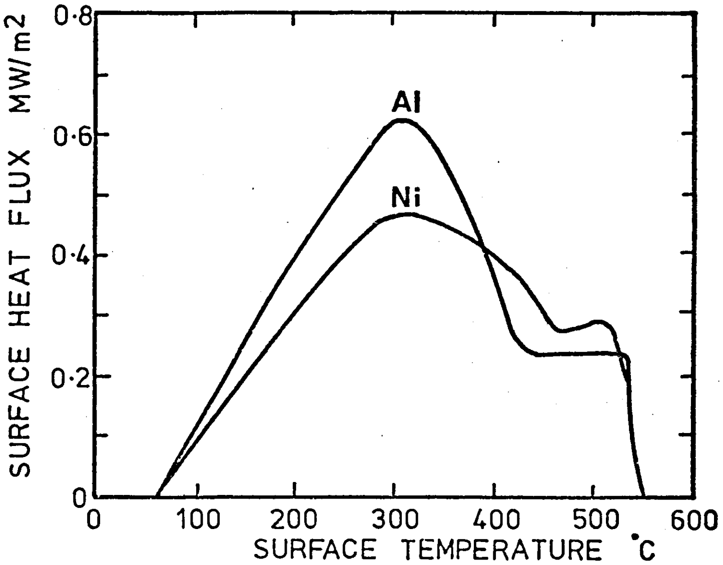

0·8
0·6
0·4
0·2
0
SURFACE HEAT FLUX MW/m2
0
100
200
300
400
500
600
SURFACE TEMPERATURE °C
Al
Ni

FIGURE 28: Influence of specimen material, obtained by Flament et alia[1, 18] on the surface heat flux/surface temperature relationship during quenching into still water at 100°C.

FIGURE 29: Influence of surface condition on the surface heat transfer coefficient during quenching into still water.

(a) Oxidised mild steel probe (heated 2hrs @ 875°C in air

(b) Non-oxidised mild steel probe (heated 10mins @ 875°C in air)

(After Lambert & Economopoulos[98])

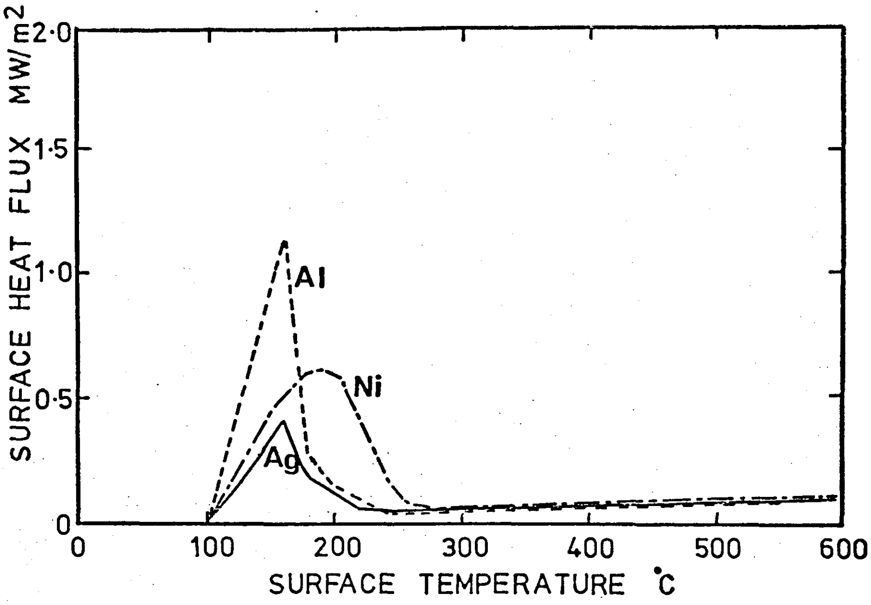
SURFACE HEAT FLUX MW/m²
2·0
1·5
1·0
0·5
0
Al
Ni
Ag
0
100
200
300
400
500
600
SURFACE TEMPERATURE °C

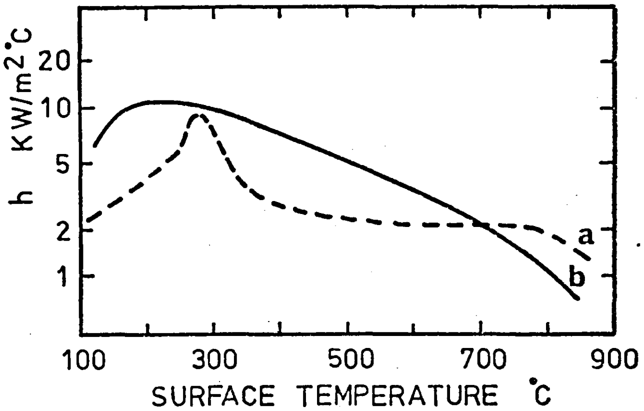
h KW/m² °C
20
10
5
2
1
a
b
100
300
500
700
900
SURFACE TEMPERATURE °C

FIGURE 30: Influence of a surface layer of $CaSO_4$ on the cooling curves obtained from steel cylinders when quenched in water

(a) Surface clean

(b) Surface coated with 0.5mm of $CaSO_4$

(After Chevrier[126])

FIGURE 31: Comparison of calculated and experimental cooling curves in a mild steel slab during water quenching, as determined by Davis[135].

FIGURE 32: Variation in the specific heat of various steels with temperature and final relationship (solid line) used by Hengerer[136].

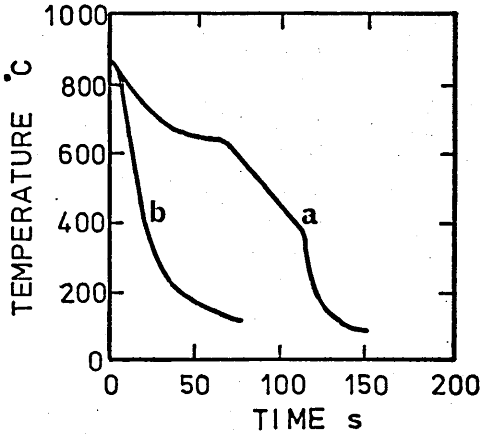

TEMPERATURE °C
1000
800
600
400
200
0
b
a
0
50
100
150
200
TIME s

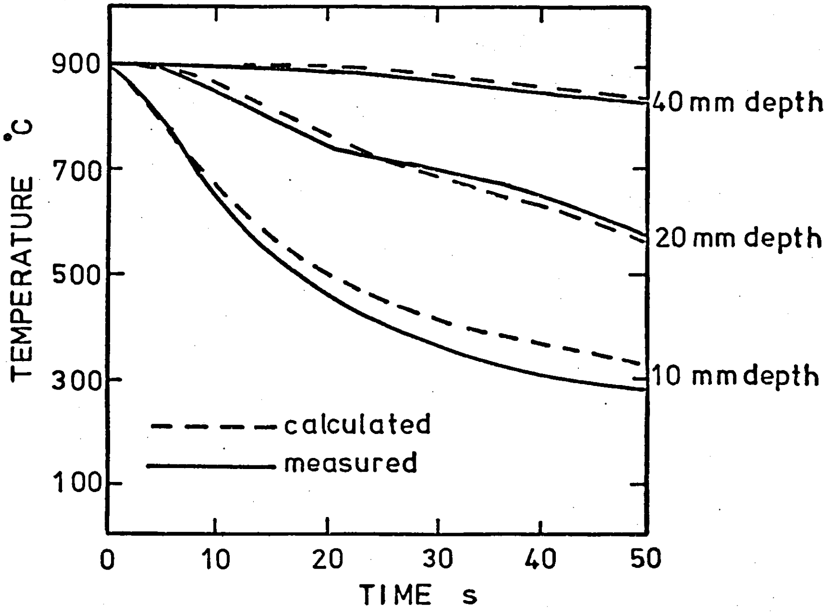

TEMPERATURE °C
900
700
500
300
100
40 mm depth
20 mm depth
10 mm depth
calculated
measured
0
10
20
30
40
50
TIME s

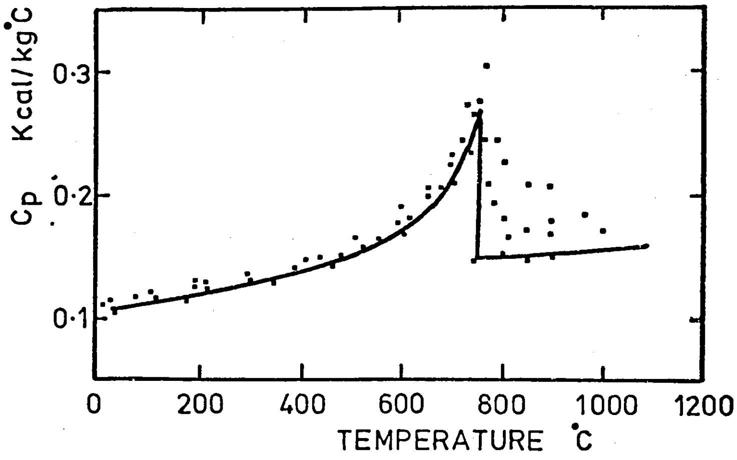

C_p Kcal/kg°C
0·3
0·2
0·1
0
200
400
600
800
1000
1200
TEMPERATURE °C

FIGURE 33: Variation of thermal conductivity with temperature in a 3½% Ni Cr Mo V steel during heating and cooling.

(After Atkins et alia[138])

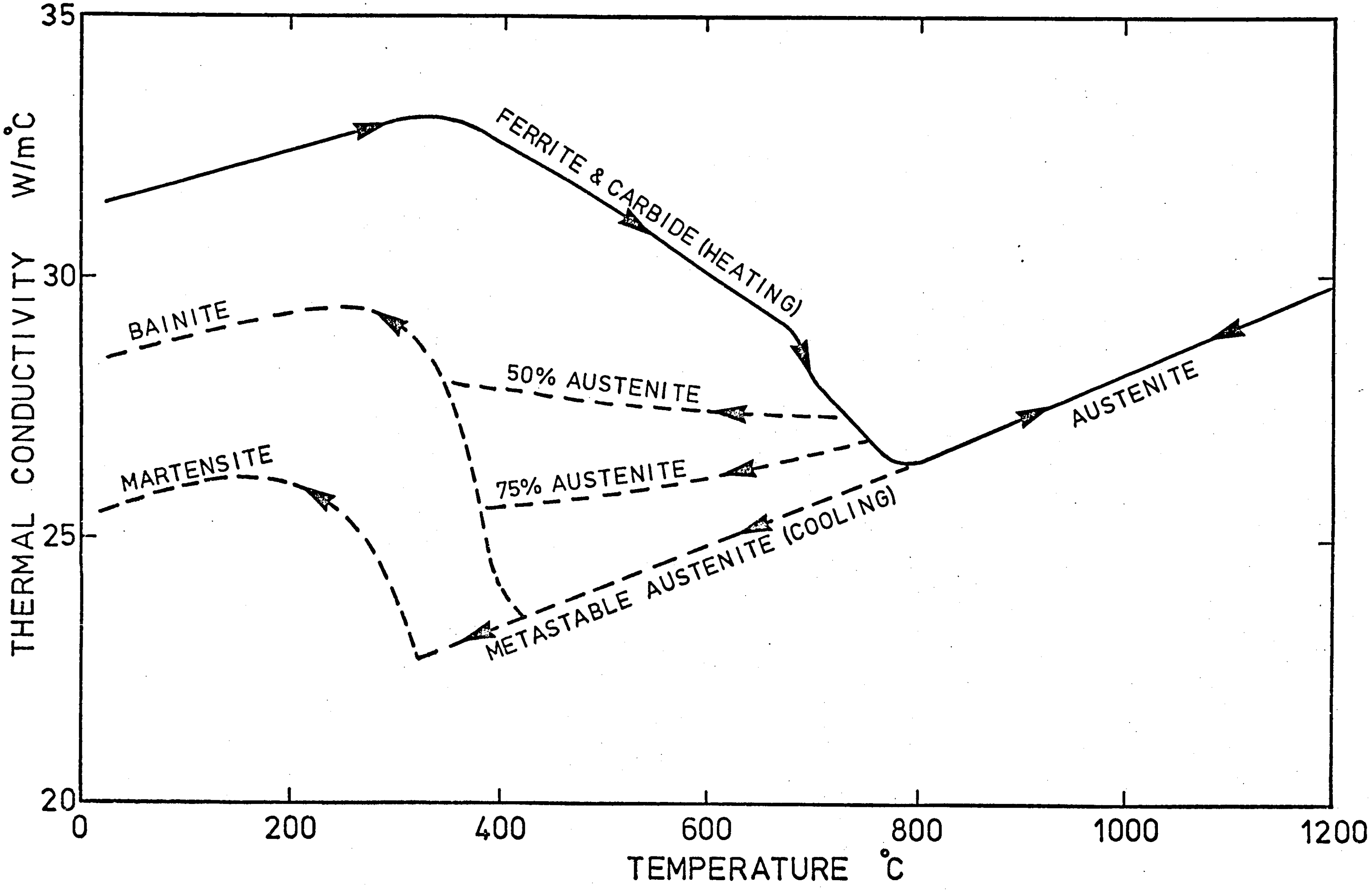
THERMAL CONDUCTIVITY W/m°C
TEMPERATURE °C
35
30
25
20
0
200
400
600
800
1000
1200
FERRITE & CARBIDE (HEATING)
AUSTENITE
BAINITE
50% AUSTENITE
75% AUSTENITE
MARTENSITE
METASTABLE AUSTENITE (COOLING)

FIGURE 34: Variation of specific heat with temperature in a 3½% Ni Cr Mo V steel during heating and cooling.

(After Atkins et alia[138])

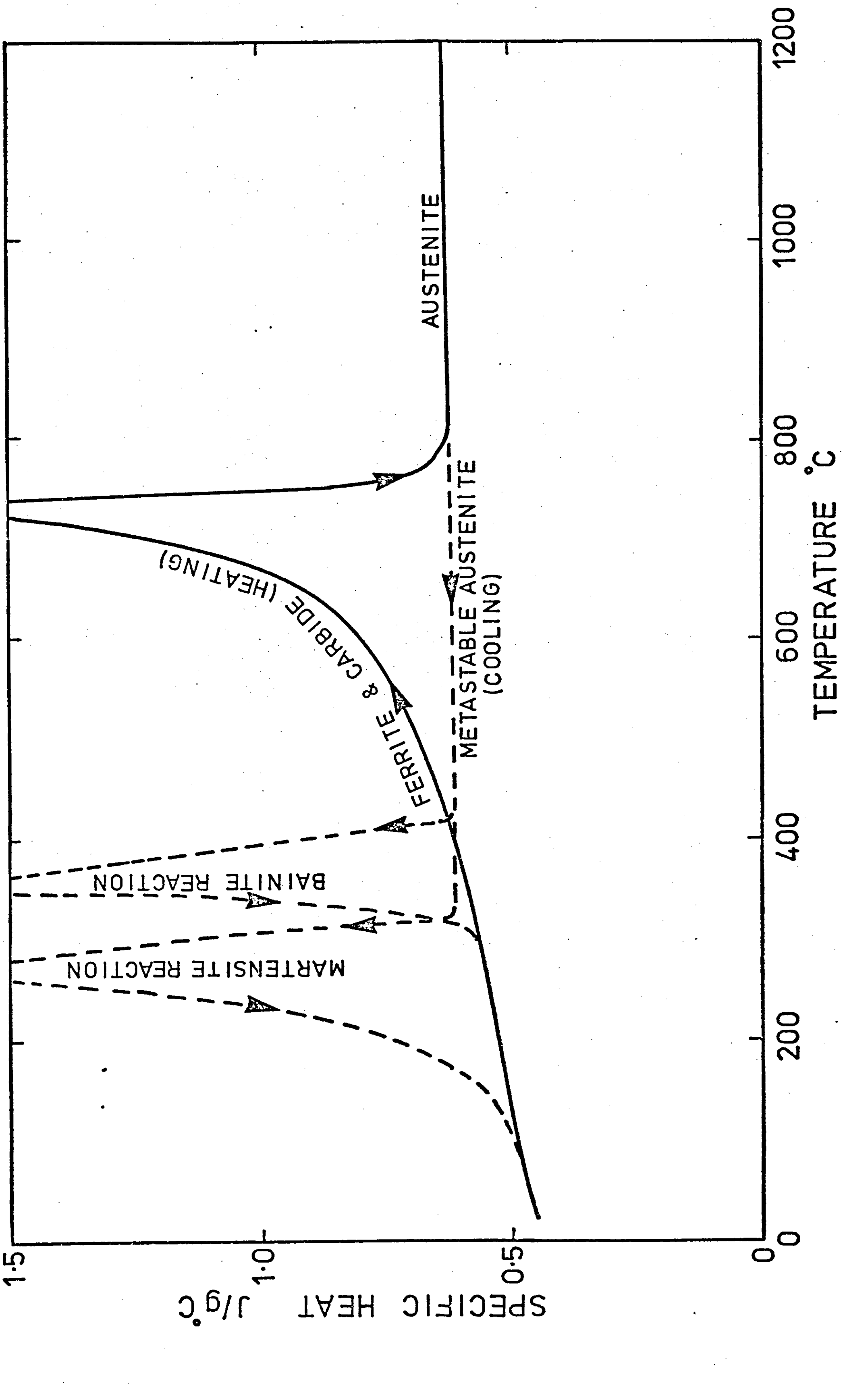
SPECIFIC HEAT J/g°C
0
0·5
1·0
1·5
TEMPERATURE °C
0
200
400
600
800
1000
1200
AUSTENITE
FERRITE & CARBIDE (HEATING)
METASTABLE AUSTENITE (COOLING)
BAINITE REACTION
MARTENSITE REACTION

FIGURE 35: Comparison of calculated residual stress distribution (lines) with experimentally determined residual stress at the surface (circles) of a 12% Cr steel cylinder after being quenched in water.

(After Inoue et alia[148])

FIGURE 36: Comparison of calculated and experimentally determined distortion in a 200mm diameter, 500mm long cylinder of SNCM 8 steel after quenching in water.

(Re-plotted from data given by Toshioka[149])

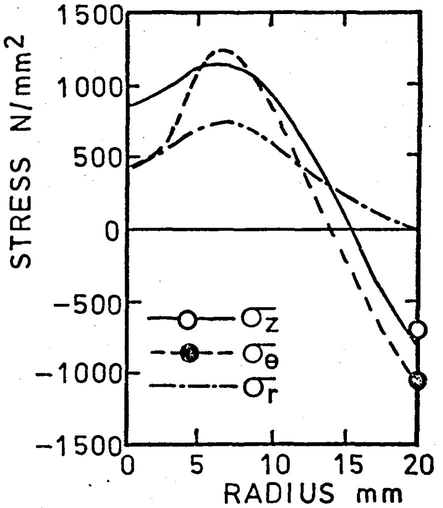
STRESS N/mm²
1500
1000
500
0
−500
−1000
−1500
0
5
10
15
20
RADIUS mm
σ_z
σ_θ
σ_r

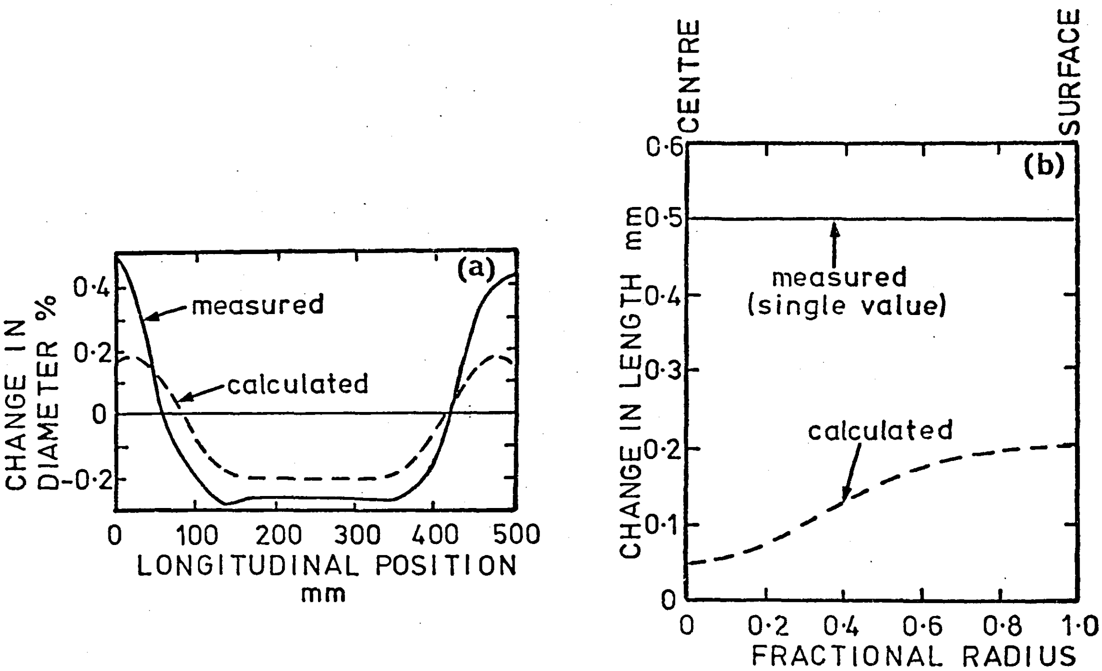
(a)
CHANGE IN DIAMETER %
0·4
0·2
0
−0·2
0
100
200
300
400
500
LONGITUDINAL POSITION mm
measured
calculated
(b)
CENTRE
SURFACE
CHANGE IN LENGTH mm
0·6
0·5
0·4
0·3
0·2
0·1
0
0
0·2
0·4
0·6
0·8
1·0
FRACTIONAL RADIUS
measured (single value)
calculated

FIGURE 37: Variation of free thermal strain with temperature used by Fujio et alia[150].

a - Cooled to produce 0% martensite
b - " " 50% "
c - " " 100% "

FIGURE 38: Variation of flow stress with temperature used by Fujio et alia[150], derived from linear interpolations between values at 875°C and ambient temperature in the pearlitic (P) and martensitic (M) conditions.

a - Cooled to produce 0% martensite
b - " " 50% "
c - " " 100% "

FIGURE 39: Comparison of the calculated and experimental residual stress distributions, obtained by Fujio et alia[150], in a 50mm diameter cylinder of 0.45% C steel after water quenching.

x σ_r)
o σ_θ) Experimental
● σ_z)

———————— Calculated

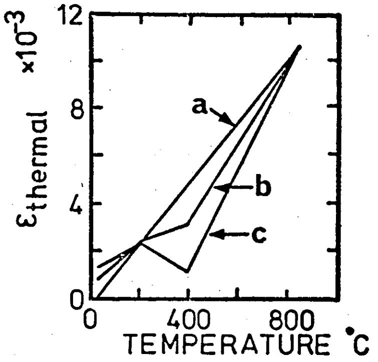

$\varepsilon_{thermal}$ ×10^{-3}
12
8
4
0
0
400
800
TEMPERATURE °C
a
b
c

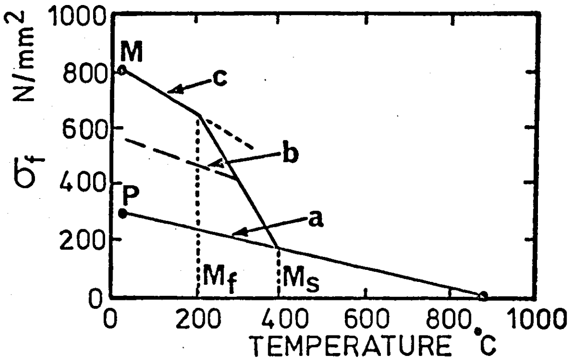

σ_f N/mm^2
1000
800
600
400
200
0
0
200
400
600
800
1000
TEMPERATURE °C
M
P
a
b
c
M_f
M_s

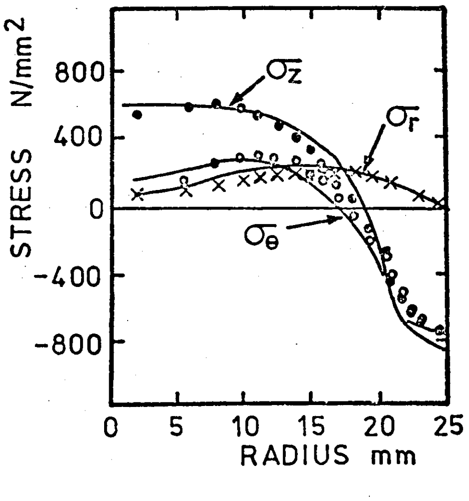

STRESS N/mm^2
800
400
0
-400
-800
0
5
10
15
20
25
RADIUS mm
σ_z
σ_r
σ_θ

FIGURE 40: Quenching tank and fixture used in all experimental quenches.

FIGURE 41: 3.3mm Type A specimen used in the determination of surface heat transfer coefficients during quenching.

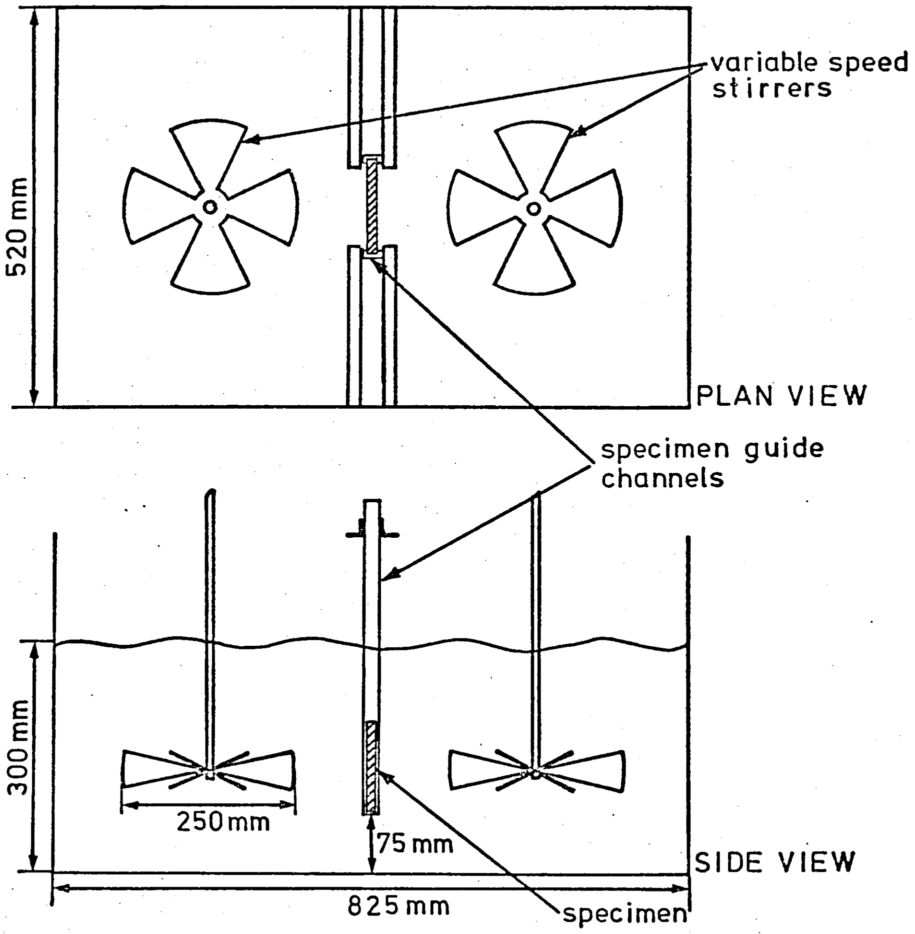
variable speed stirrers
520 mm
PLAN VIEW
specimen guide channels
300 mm
250 mm
75 mm
SIDE VIEW
825 mm
specimen

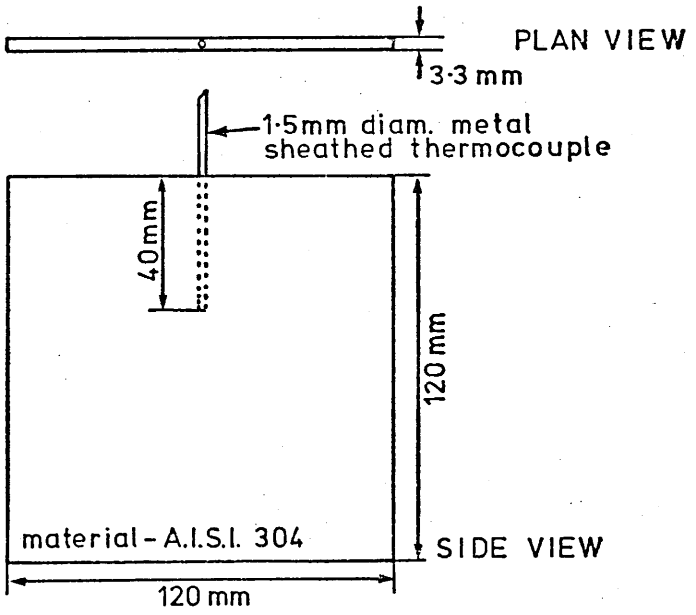
PLAN VIEW
3·3 mm
1·5mm diam. metal sheathed thermocouple
40mm
120 mm
material - A.I.S.I. 304
SIDE VIEW
120 mm

FIGURE 42: 15mm Type B specimen used in the determination of surface heat transfer coefficients during quenching.

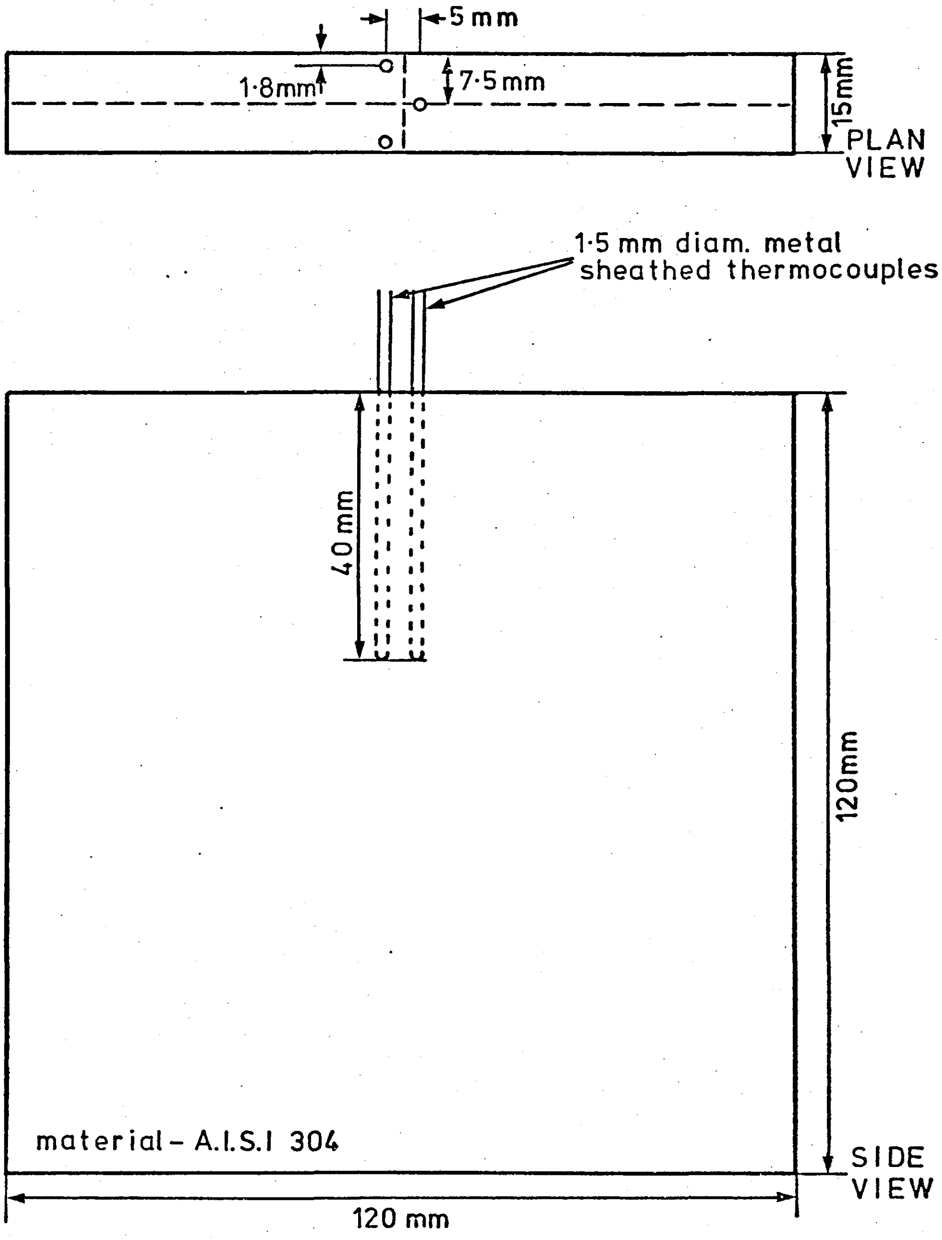
5 mm
1·8mm
7·5 mm
15mm
PLAN VIEW
1·5 mm diam. metal sheathed thermocouples
40 mm
120mm
material – A.I.S.I 304
SIDE VIEW
120 mm

FIGURE 43: Variation in thermal properties with temperature of A.I.S.I. Type 304 stainless steel[157] and relationships used in calculations.

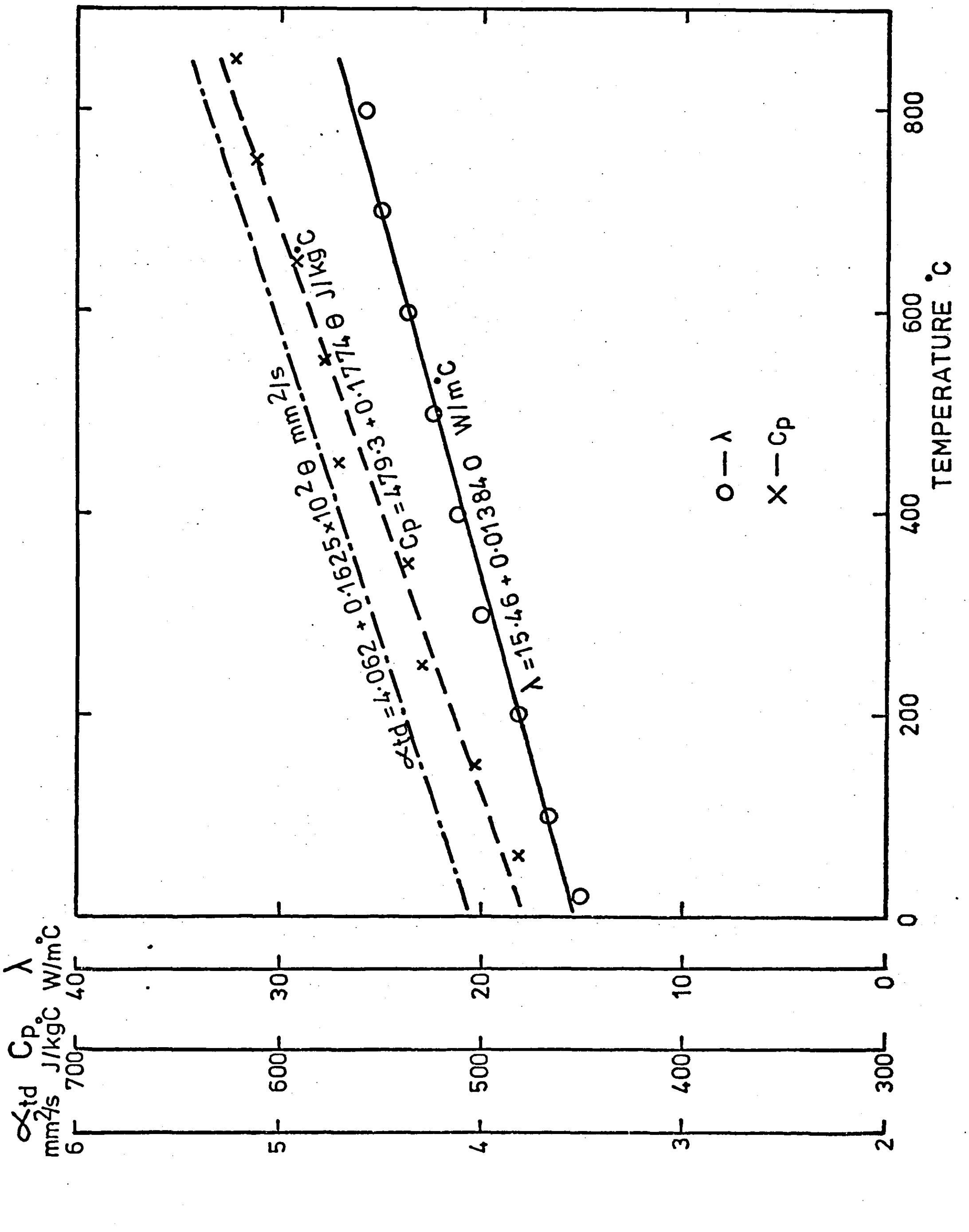
$\alpha_{td} = 4{\cdot}062 + 0{\cdot}1625 \times 10^{2}\,\theta$ mm²/s
$C_p = 479{\cdot}3 + 0{\cdot}1774\,\theta$ J/kg°C
$\lambda = 15{\cdot}46 + 0{\cdot}01384\,\theta$ W/m°C
o — λ
X — C_p
TEMPERATURE °C
0
200
400
600
800
λ W/m°C
0
10
20
30
40
C_p J/kg°C
300
400
500
600
700
α_{td} mm²/s
2
3
4
5
6

FIGURE 44: Location of nodes at surface of plate used in the calculation of temperature.

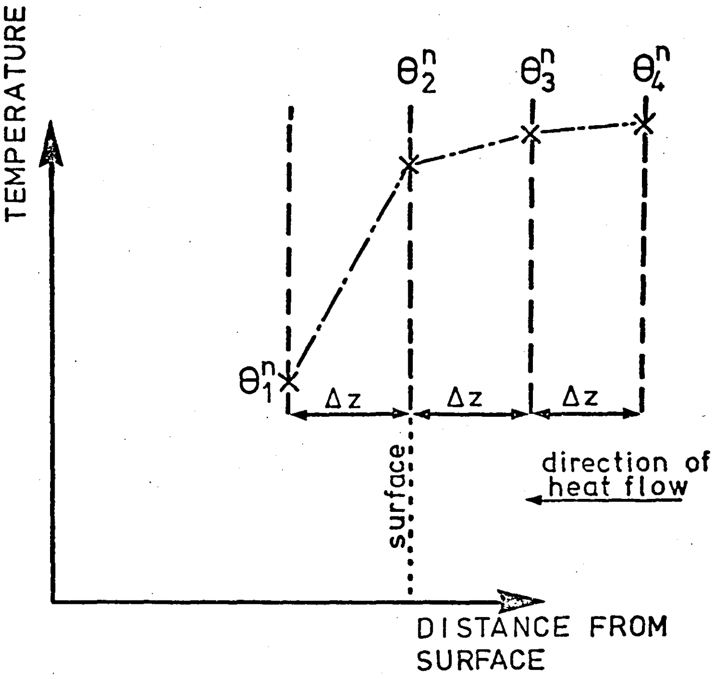
TEMPERATURE
θ_2^n
θ_3^n
θ_4^n
θ_1^n
Δz
Δz
Δz
surface
direction of heat flow
DISTANCE FROM SURFACE

FIGURE 45: Flow chart showing the calculation of h from a cooling curve determined at a sub-surface position in a Type B specimen during quenching.

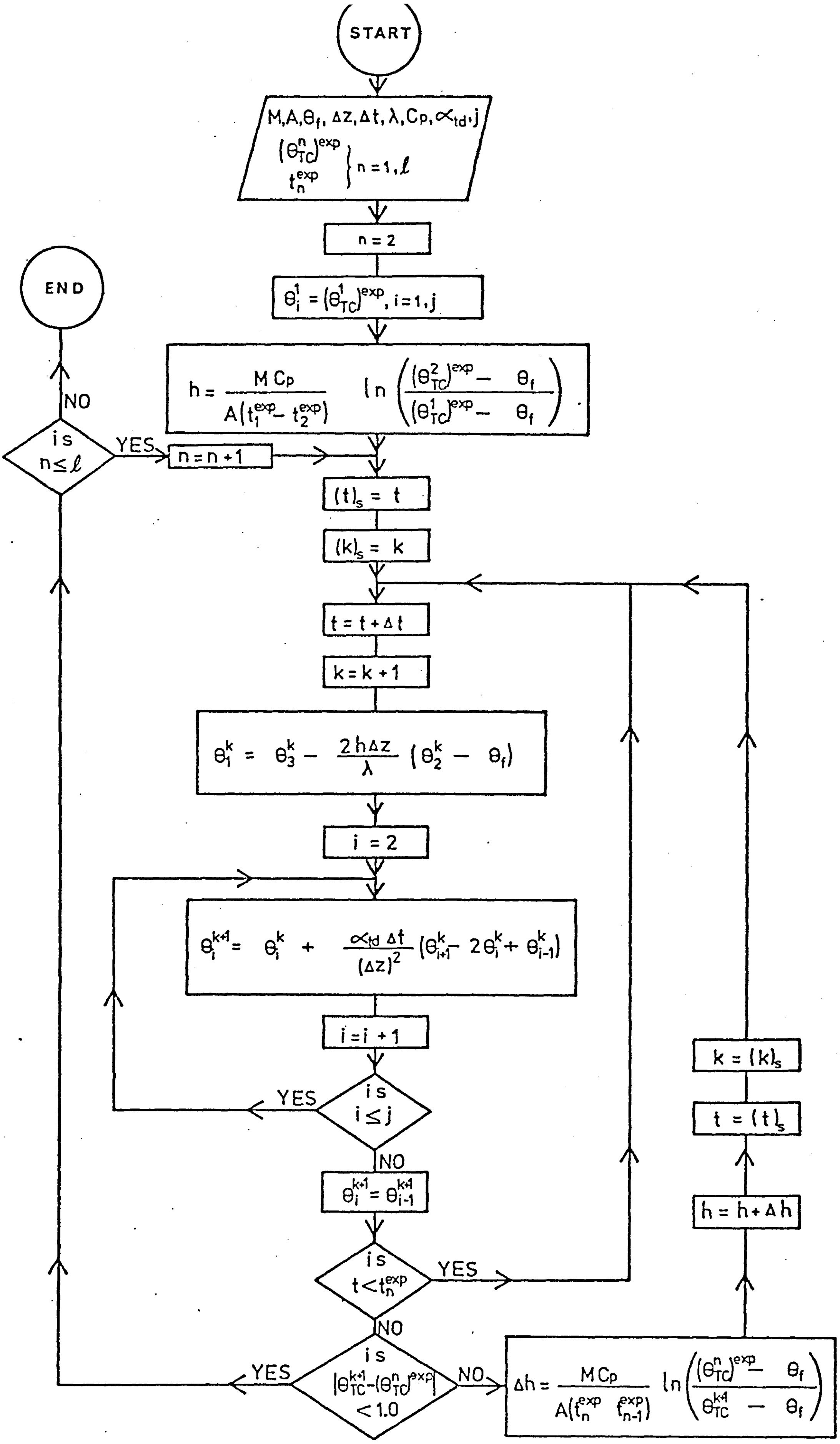
START
$M, A, \theta_f, \Delta z, \Delta t, \lambda, C_p, \alpha_{td}, j$
$(\theta_{TC}^{n})^{exp}$, t_n^{exp} $\}$ $n = 1, \ell$
$n = 2$
$\theta_i^1 = (\theta_{TC}^1)^{exp}, i = 1, j$
$h = \frac{M C_p}{A(t_1^{exp} - t_2^{exp})} \ln\left(\frac{(\theta_{TC}^2)^{exp} - \theta_f}{(\theta_{TC}^1)^{exp} - \theta_f}\right)$
END
NO
is $n \leq \ell$
YES
$n = n + 1$
$(t)_s = t$
$(k)_s = k$
$t = t + \Delta t$
$k = k + 1$
$\theta_1^k = \theta_3^k - \frac{2 h \Delta z}{\lambda}(\theta_2^k - \theta_f)$
$i = 2$
$\theta_i^{k+1} = \theta_i^k + \frac{\alpha_{td}\Delta t}{(\Delta z)^2}(\theta_{i+1}^k - 2\theta_i^k + \theta_{i-1}^k)$
$i = i + 1$
YES
is $i \leq j$
NO
$\theta_i^{k+1} = \theta_{i-1}^{k+1}$
is $t < t_n^{exp}$
YES
NO
YES
is $|\theta_{TC}^{k+1} - (\theta_{TC}^n)^{exp}| < 1.0$
NO
$\Delta h = \frac{M C_p}{A(t_n^{exp} \; t_{n-1}^{exp})} \ln\left(\frac{(\theta_{TC}^n)^{exp} - \theta_f}{\theta_{TC}^{k+1} - \theta_f}\right)$
$h = h + \Delta h$
$t = (t)_s$
$k = (k)_s$

FIGURE 46: Cooling curves obtained from individual quenches of unoxidised Type A specimens into water.

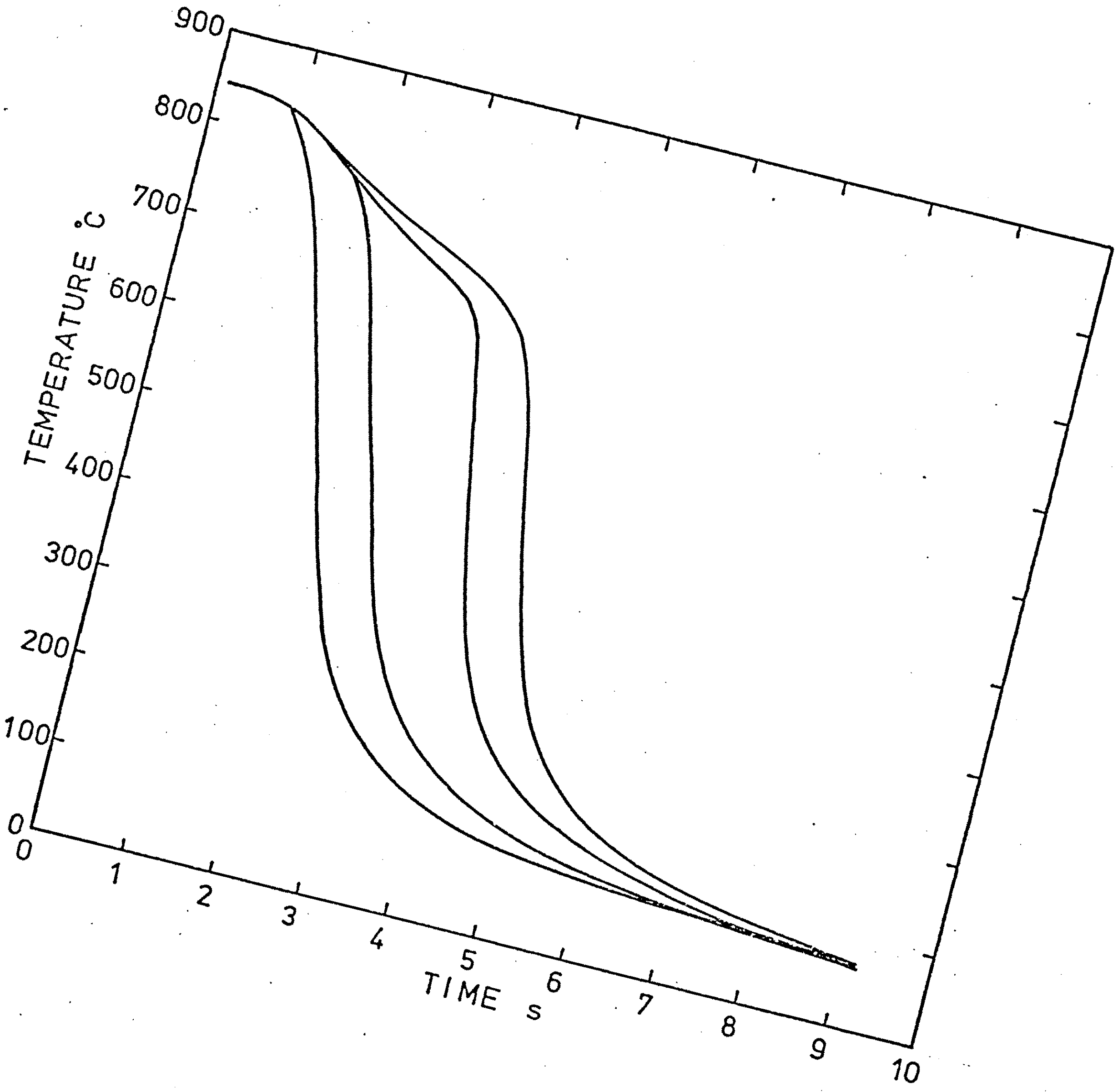
TEMPERATURE °C
900
800
700
600
500
400
300
200
100
0
TIME s
0
1
2
3
4
5
6
7
8
9
10

FIGURE 47: Variation in h with specimen temperature (smoothed) obtained from cooling curves of Type A specimen (see Figure 46) when quenched in water in the unoxidised condition.

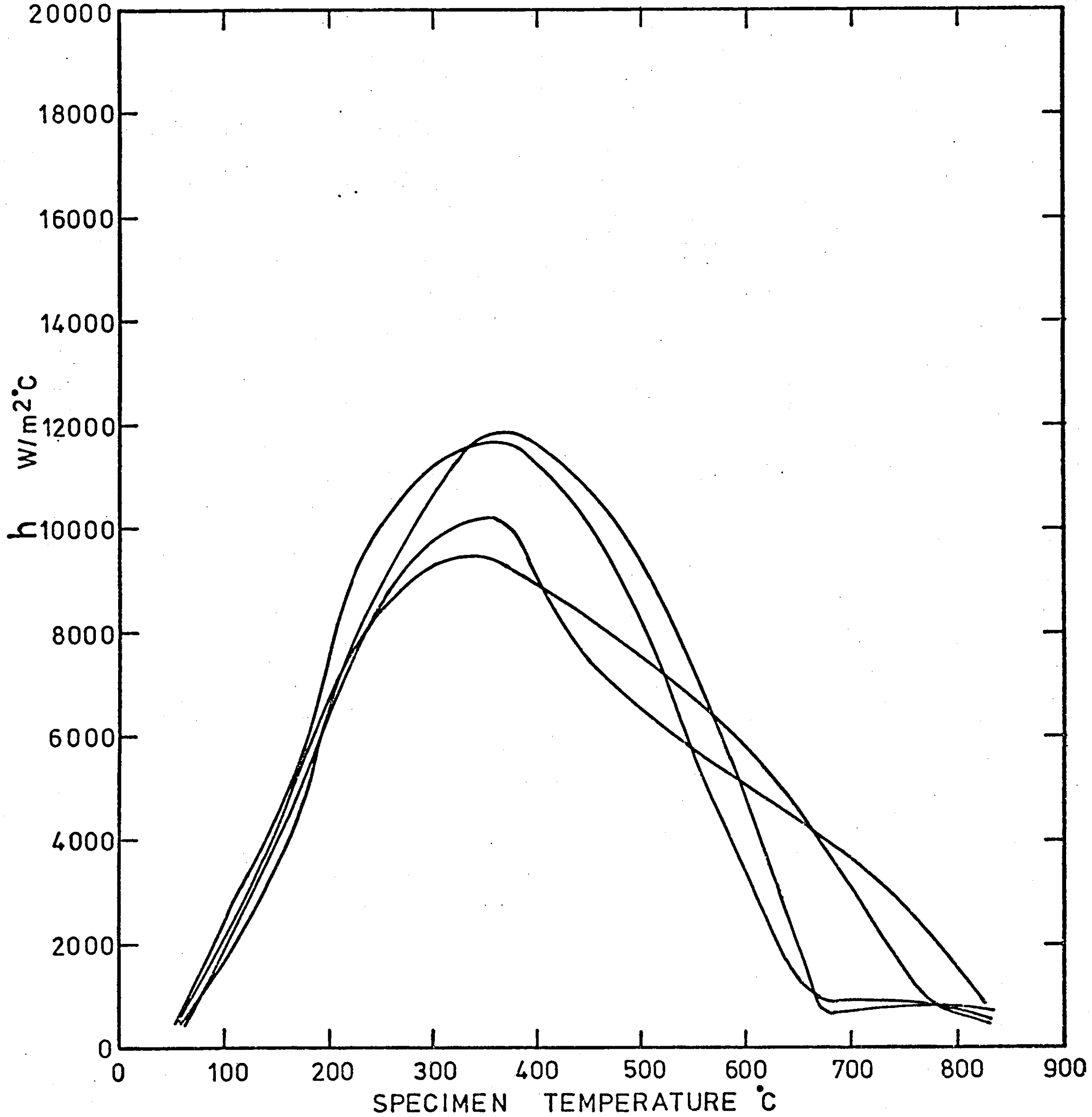
20000
18000
16000
14000
12000
10000
8000
6000
4000
2000
0
h W/m^2°C
0
100
200
300
400
500
600
700
800
900
SPECIMEN TEMPERATURE °C

FIGURE 48: Cooling curves obtained during the initial quench of the Type B specimen in the unoxidised condition in water.

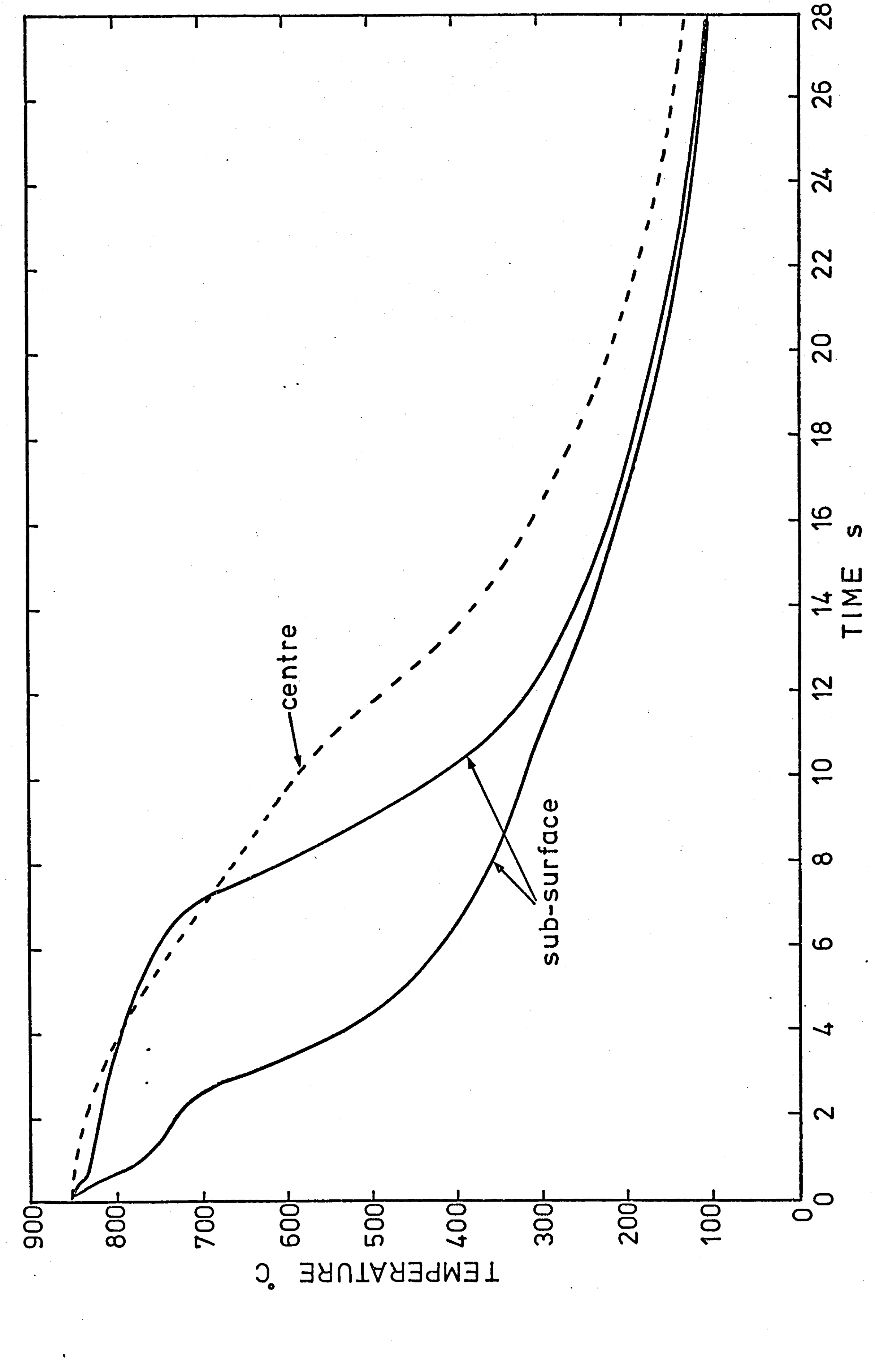

TEMPERATURE °C
900
800
700
600
500
400
300
200
100
0
TIME s
0
2
4
6
8
10
12
14
16
18
20
22
24
26
28
centre
sub-surface

FIGURE 49: Cooling curves obtained during the second quench of the Type B specimen in the oxidised condition in water.

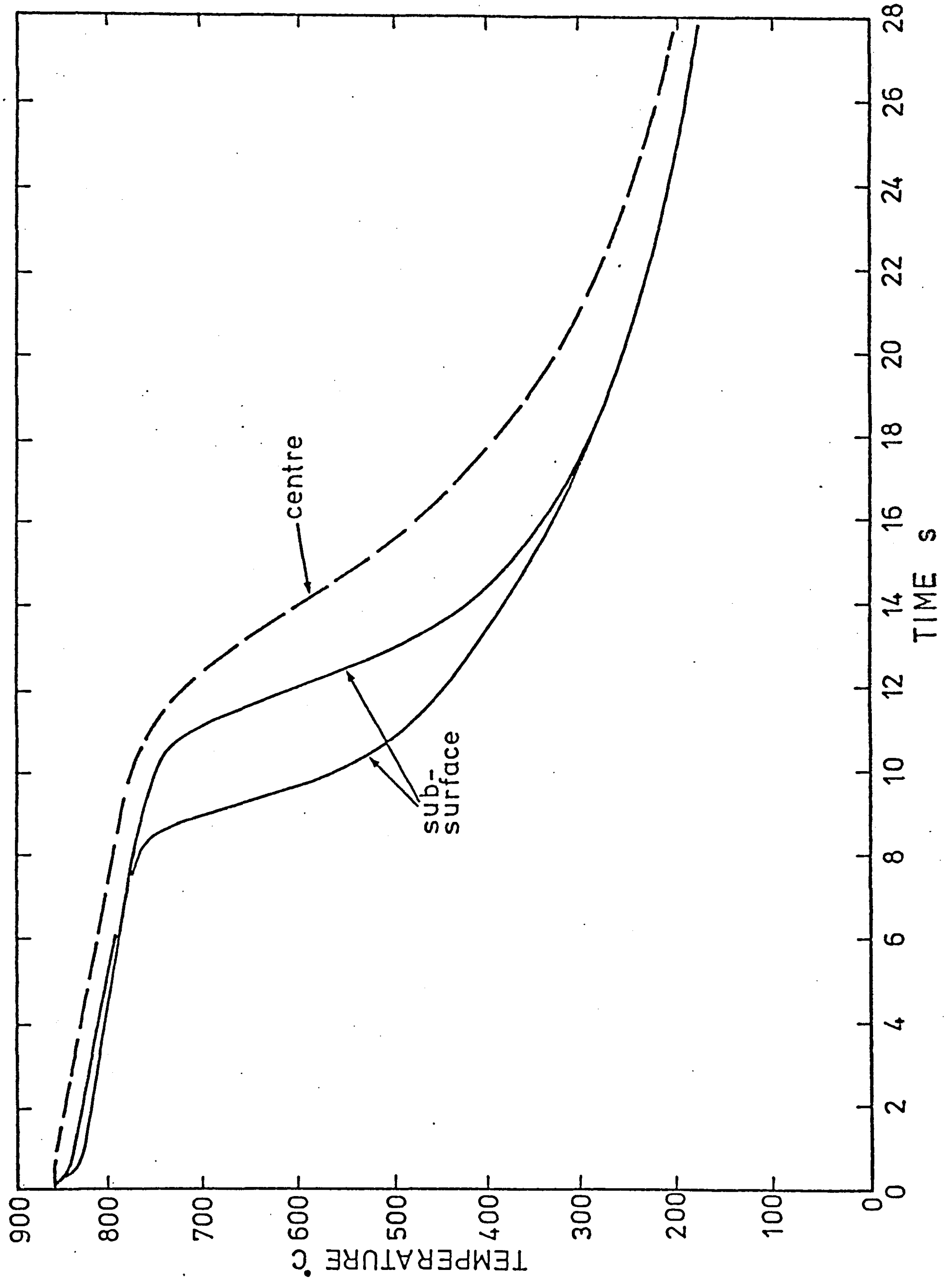
TEMPERATURE °C
900
800
700
600
500
400
300
200
100
0
TIME s
0
2
4
6
8
10
12
14
16
18
20
22
24
26
28
centre
sub-
surface

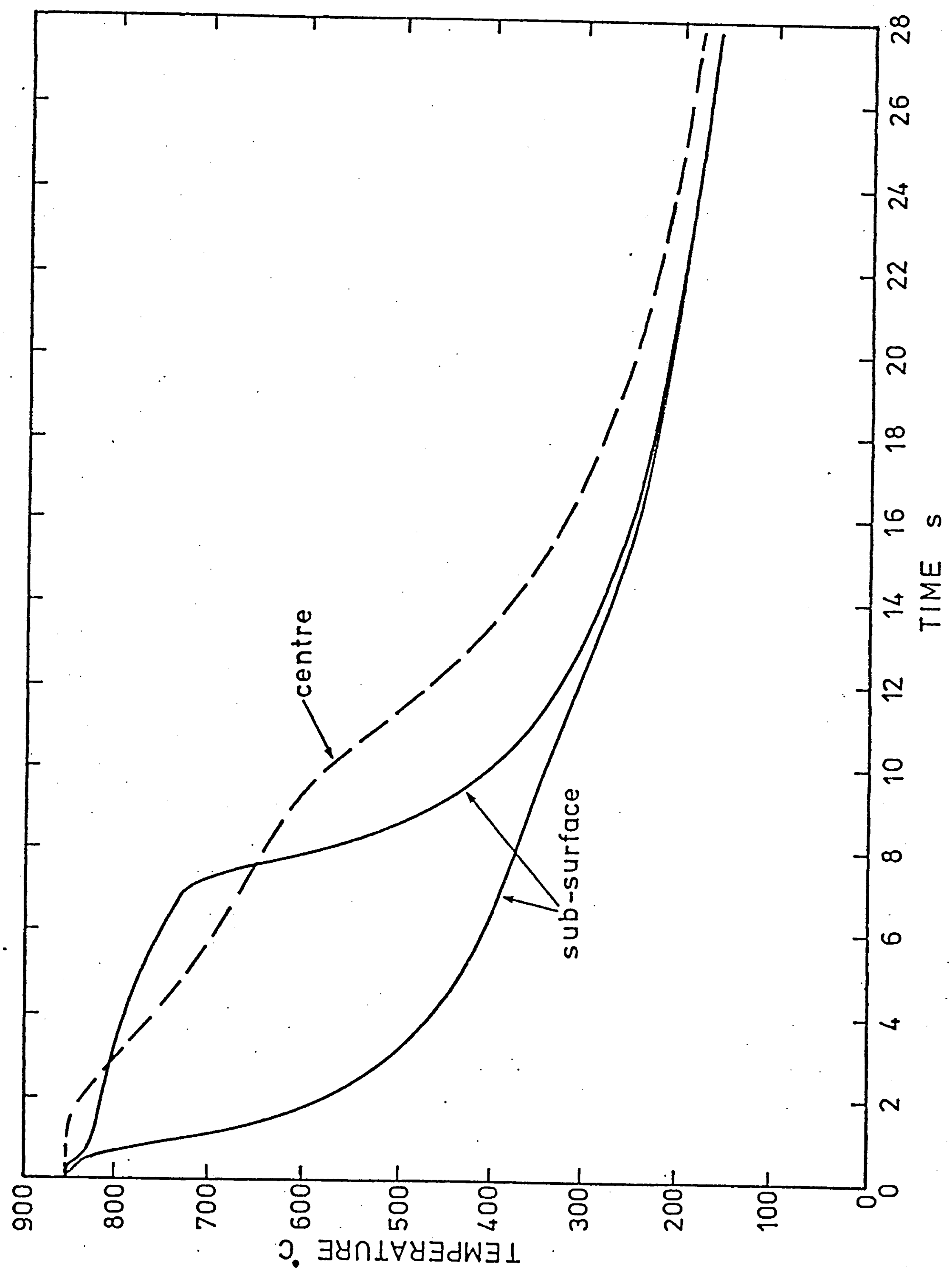
TEMPERATURE °C
900
800
700
600
500
400
300
200
100
0
TIME s
0
2
4
6
8
10
12
14
16
18
20
22
24
26
28
centre
sub-surface

FIGURE 51: Cooling curves obtained during the quenching of the Type B specimen in water after the surfaces had been ground. (Unoxidised).

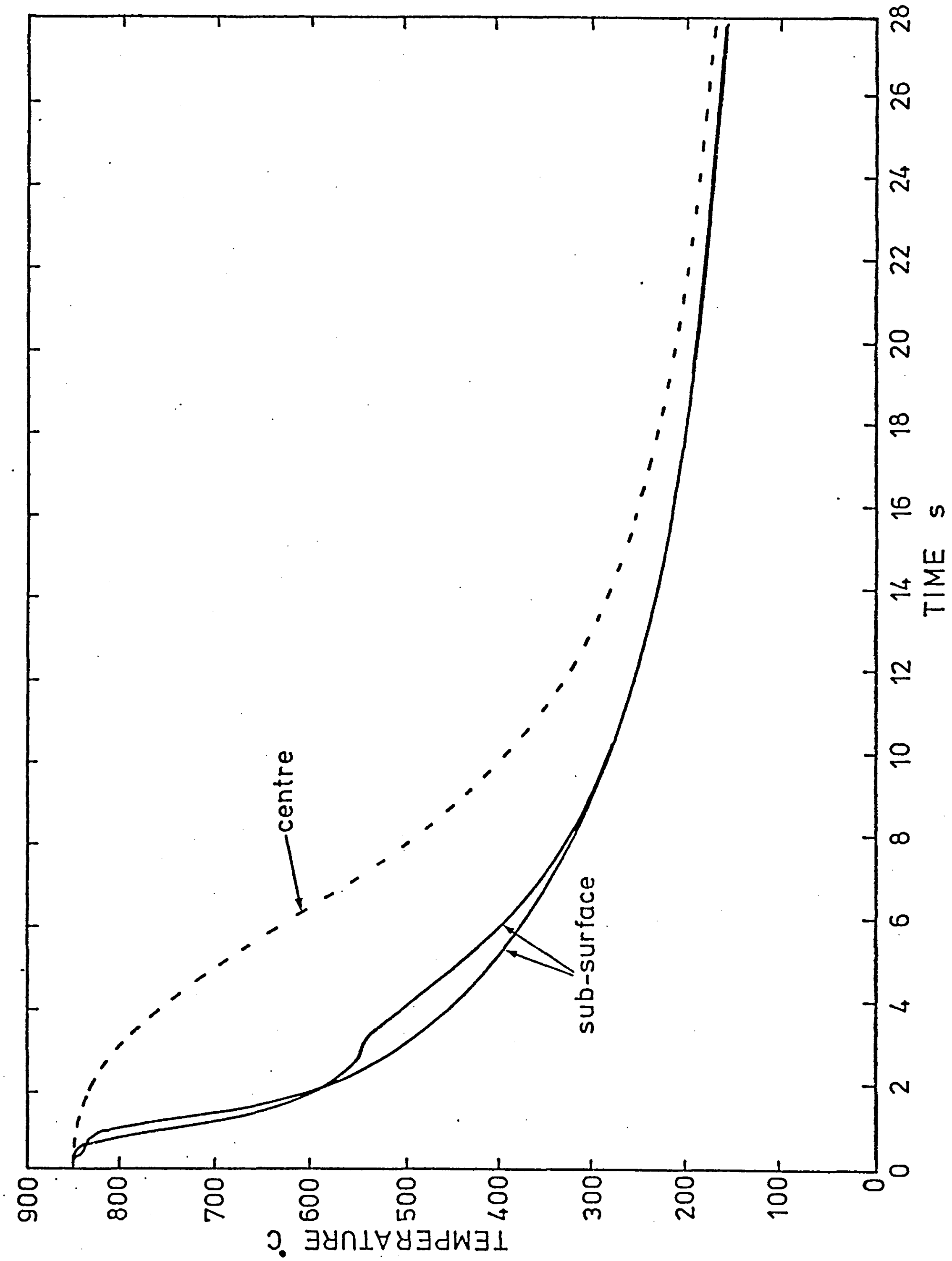
centre
sub-surface
TEMPERATURE °C
900
800
700
600
500
400
300
200
100
0
TIME s
0
2
4
6
8
10
12
14
16
18
20
22
24
26
28

FIGURE 52: Cooling curves obtained during the quenching of the Type B specimen in water after the surfaces had been ground and re-oxidised.

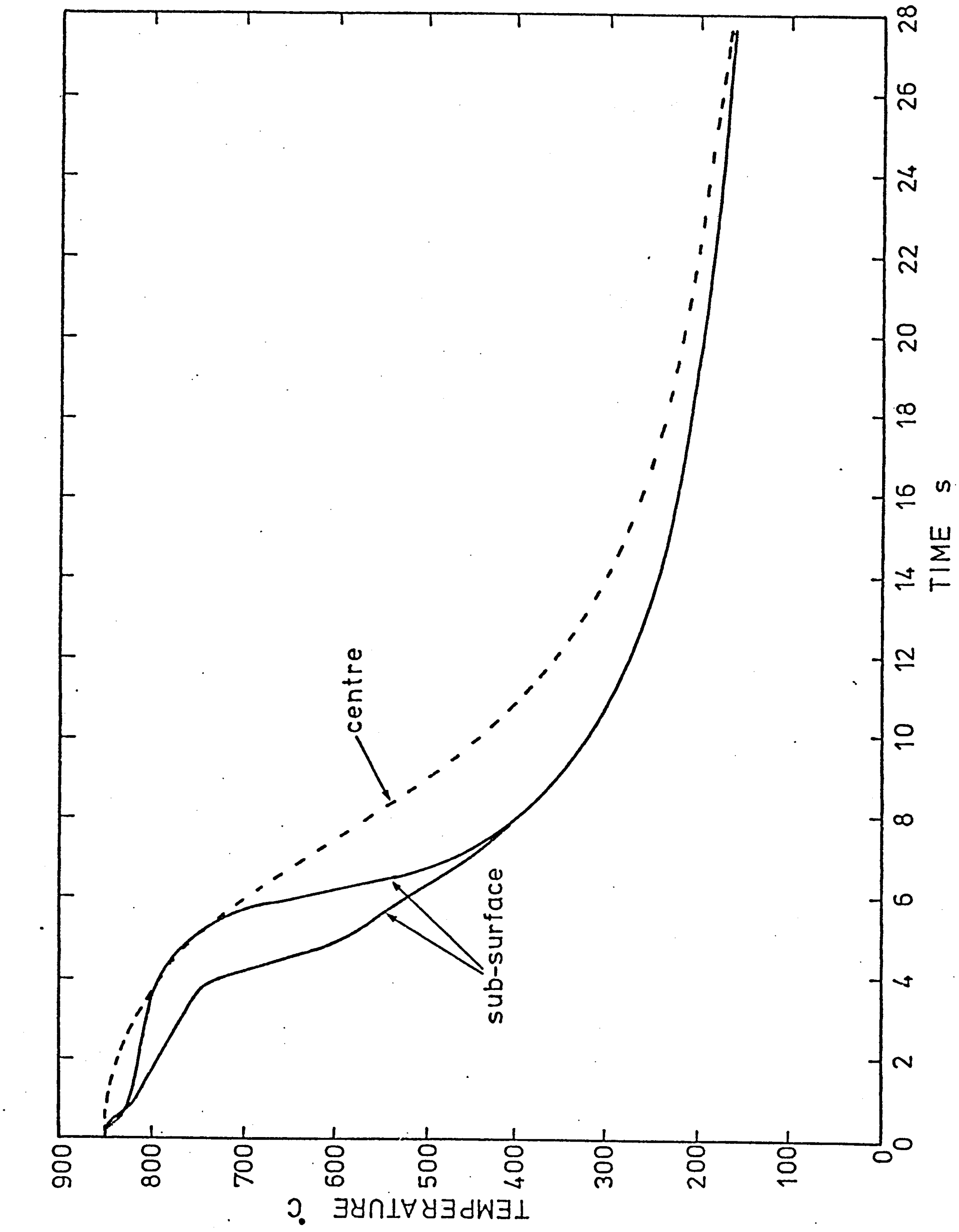
TEMPERATURE °C
900
800
700
600
500
400
300
200
100
0
TIME s
0
2
4
6
8
10
12
14
16
18
20
22
24
26
28
centre
sub-surface

FIGURE 53: Variation in h with surface temperature (smoothed) obtained from individual quenches of the Type B specimen in water in the unoxidised condition.

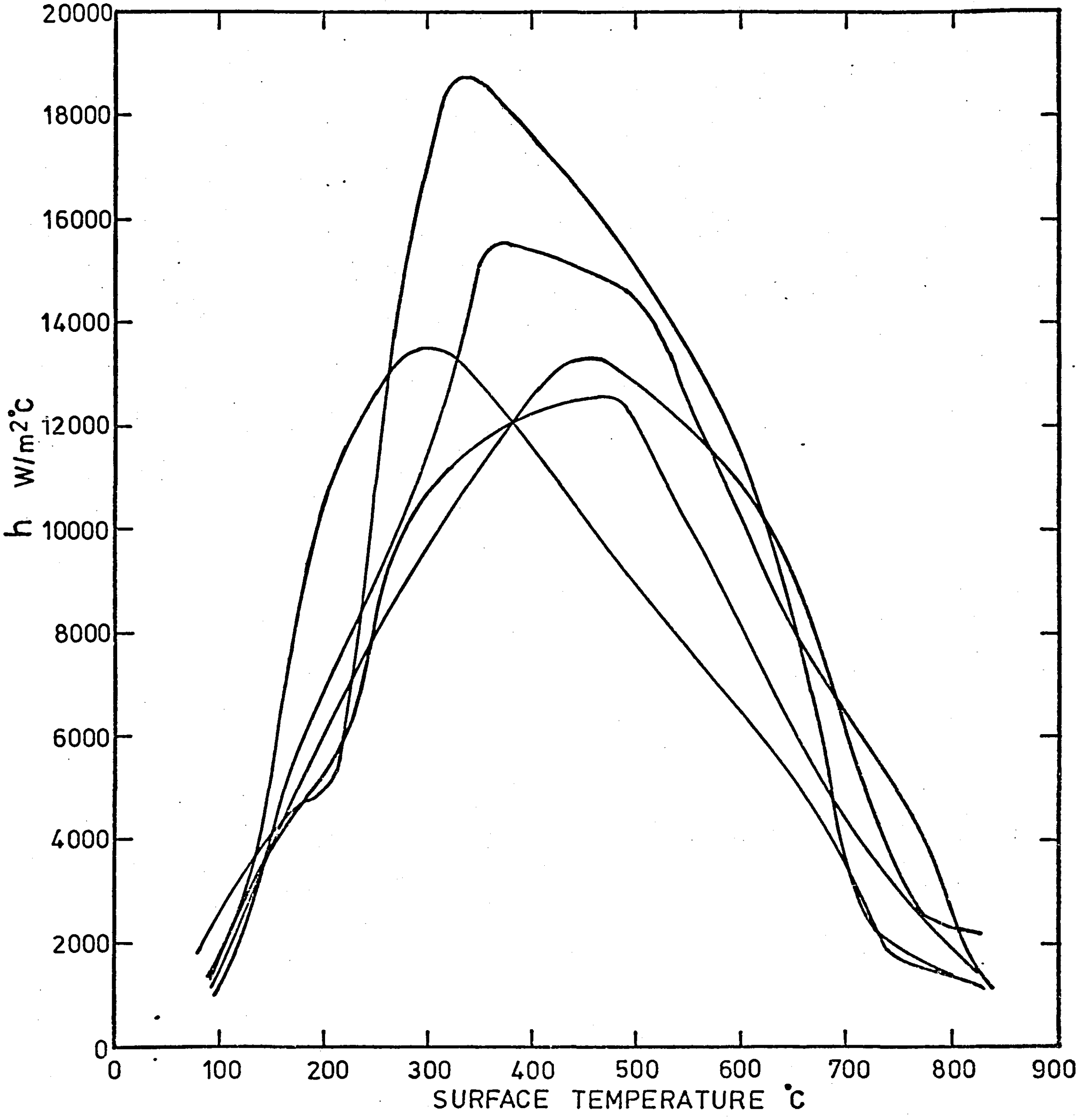
20000
18000
16000
14000
12000
10000
8000
6000
4000
2000
0
h W/m2°C
0
100
200
300
400
500
600
700
800
900
SURFACE TEMPERATURE °C

FIGURE 54: Relationship between h and surface temperature used in subsequent calculations of temperature in unoxidised water quenched plates. (Obtained from a consideration of the average value, ± 1 standard deviation, of the results shown in Figure 53).

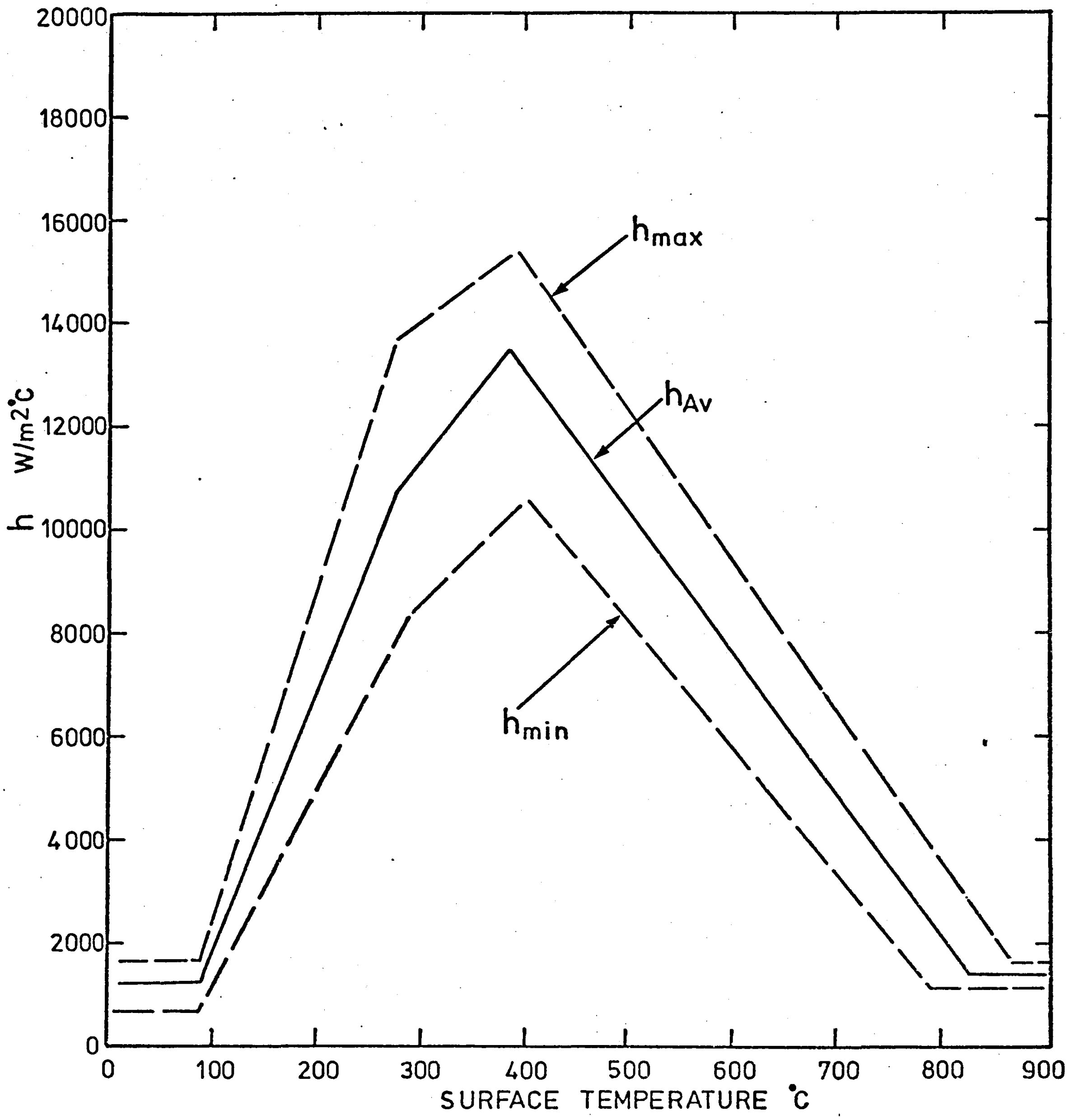
h W/m²°C
20000
18000
16000
14000
12000
10000
8000
6000
4000
2000
0
0
100
200
300
400
500
600
700
800
900
SURFACE TEMPERATURE °C
hmax
hAv
hmin

FIGURE 55: Comparison of calculated and measured cooling curves at the centre of Type B specimen when quenched in water (unoxidised).

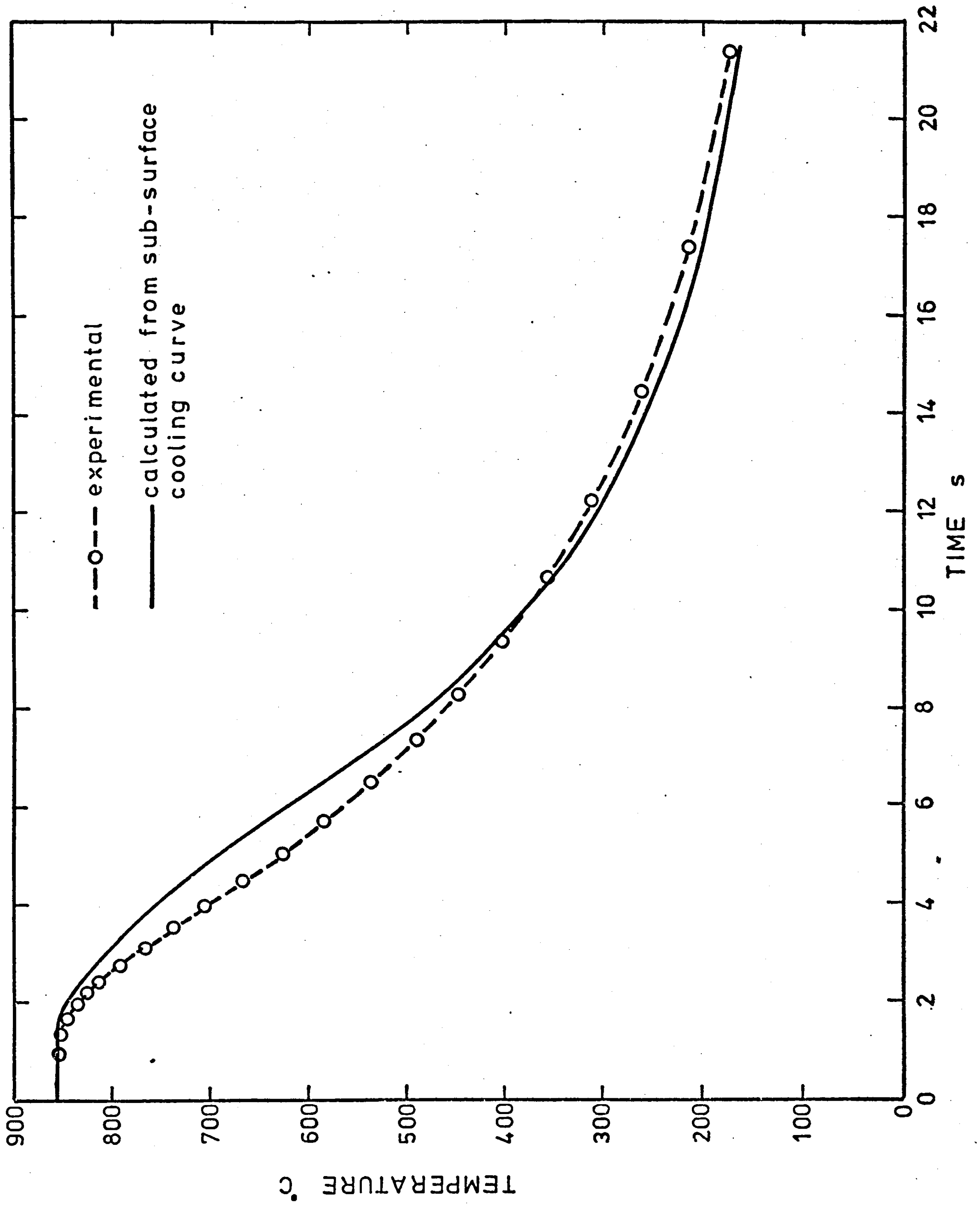

experimental
calculated from sub-surface cooling curve
TEMPERATURE °C
TIME s
0
100
200
300
400
500
600
700
800
900
0
2
4
6
8
10
12
14
16
18
20
22

FIGURE 56: Variation in h with specimen temperature obtained from individual quenches of unoxidised Type A specimens in R.D.N. 175 oil.

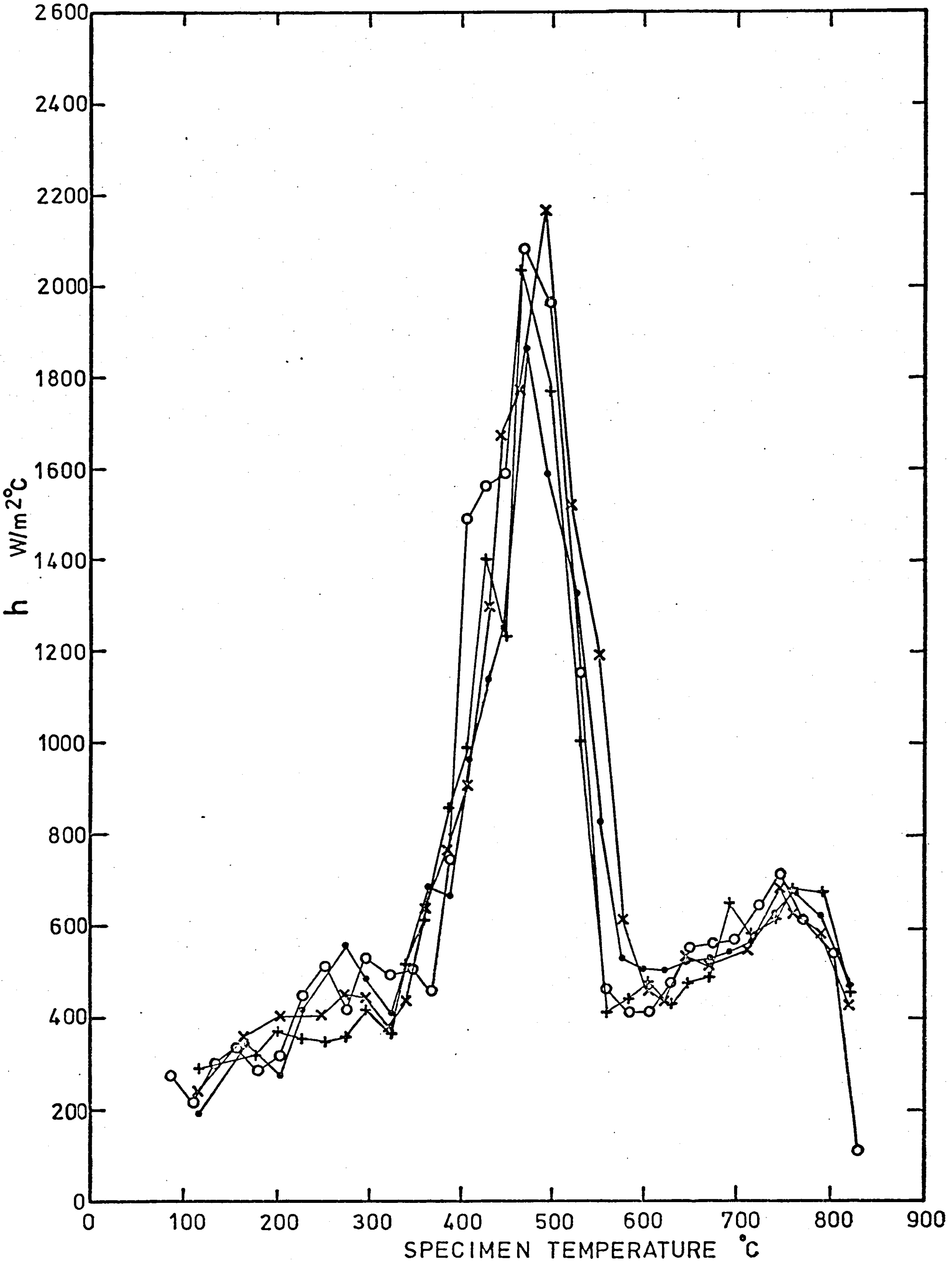

h W/m2°C
0
200
400
600
800
1000
1200
1400
1600
1800
2000
2200
2400
2600
0
100
200
300
400
500
600
700
800
900
SPECIMEN TEMPERATURE °C

FIGURE 57: Variation in h with surface temperature obtained from individual quenches of Type B specimen in R.D.N. 175 oil.

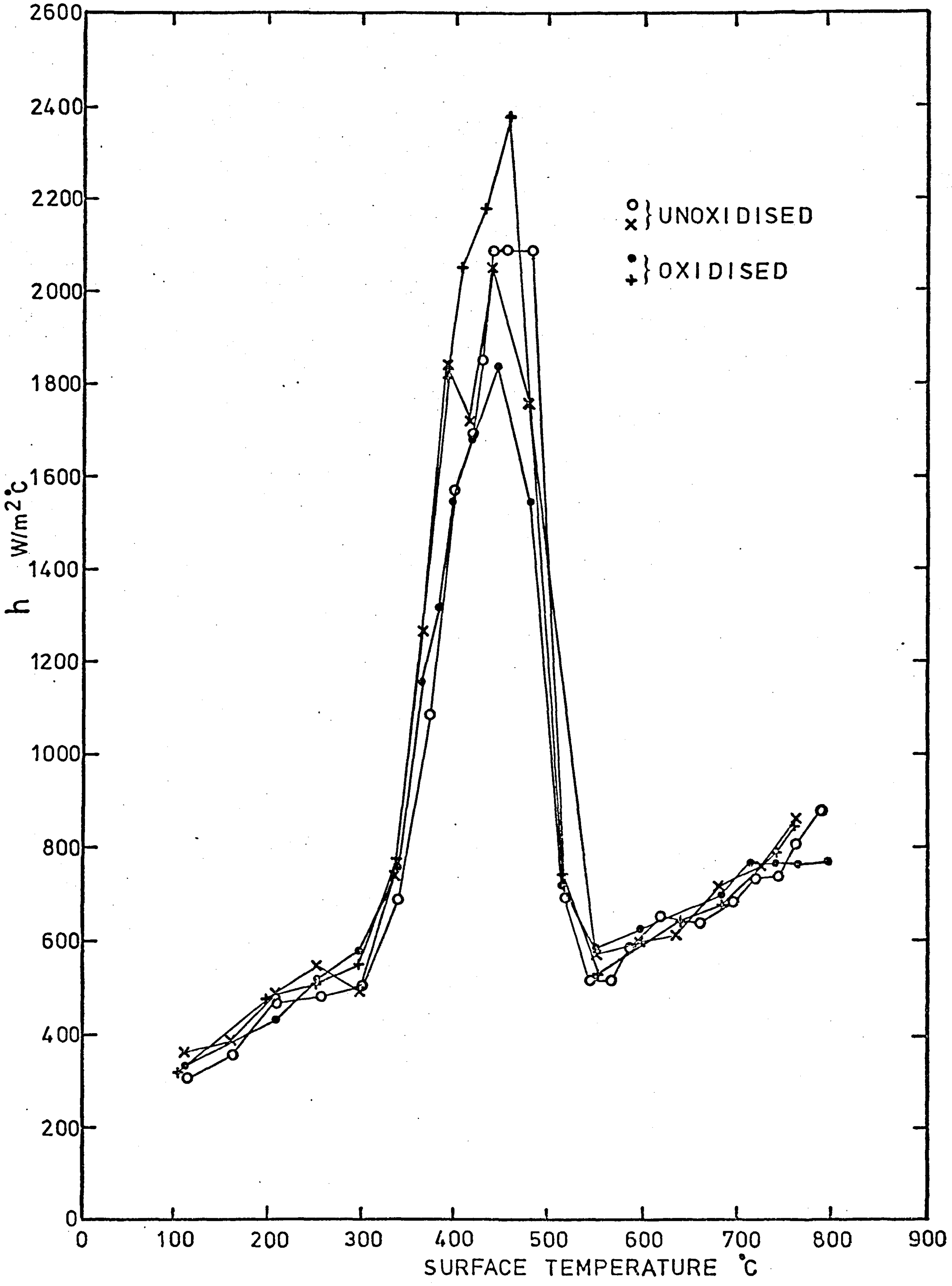

h W/m²°C
2600
2400
2200
2000
1800
1600
1400
1200
1000
800
600
400
200
0
0
100
200
300
400
500
600
700
800
900
SURFACE TEMPERATURE °C
○
× } UNOXIDISED
●
+ } OXIDISED

FIGURE 58: Relationship between h and surface temperature during oil quenching (derived from data shown in Figure 57) used in subsequent calculations of temperature in plates during oil quenching.

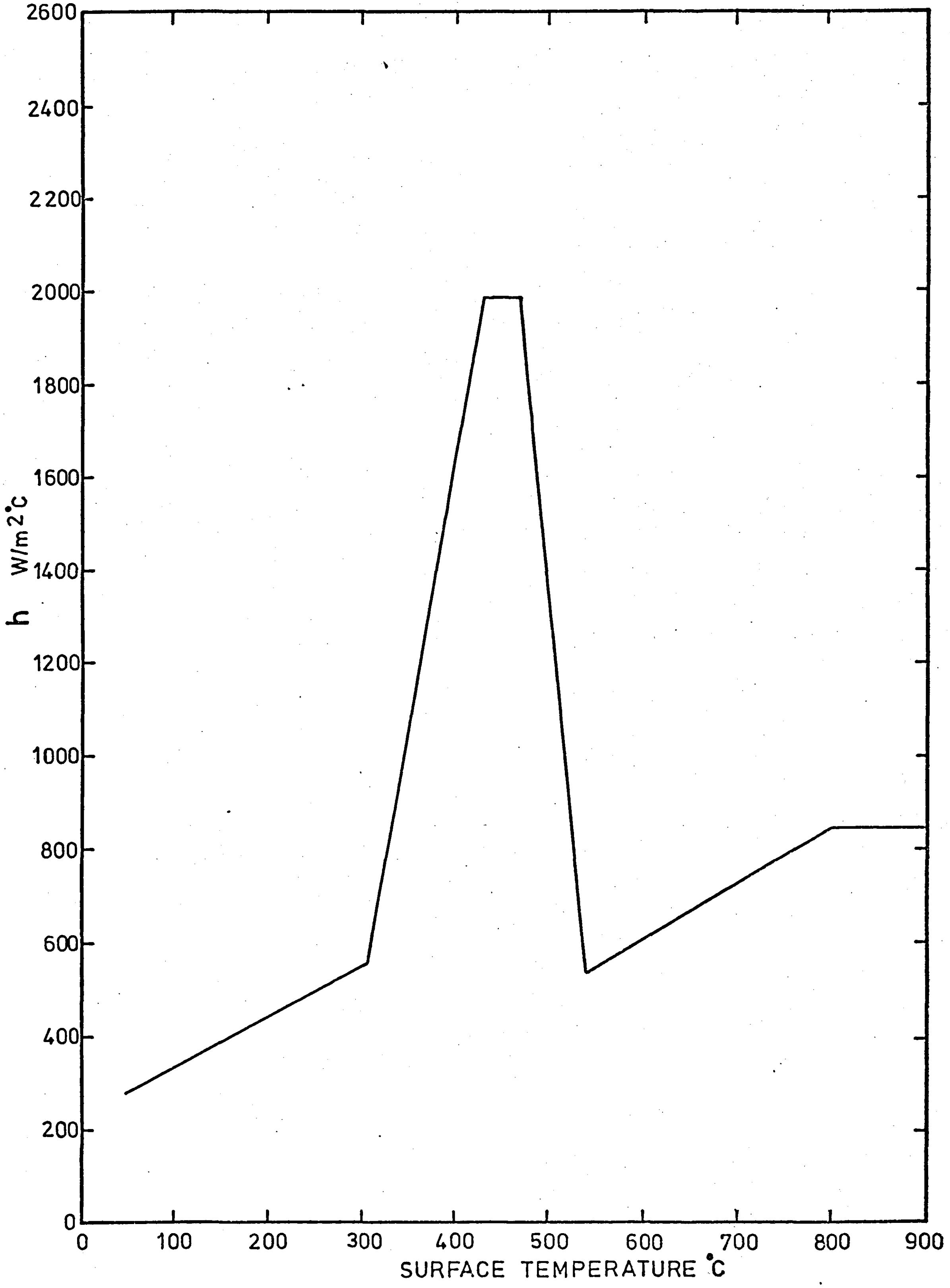

h W/m2°C
2600
2400
2200
2000
1800
1600
1400
1200
1000
800
600
400
200
0
0
100
200
300
400
500
600
700
800
900
SURFACE TEMPERATURE °C

FIGURE 59: Cooling curves obtained during the quenching of unoxidised Type B specimen in a 10% aqueous solution of 'Aquaquench 1250' polymer quenchant.

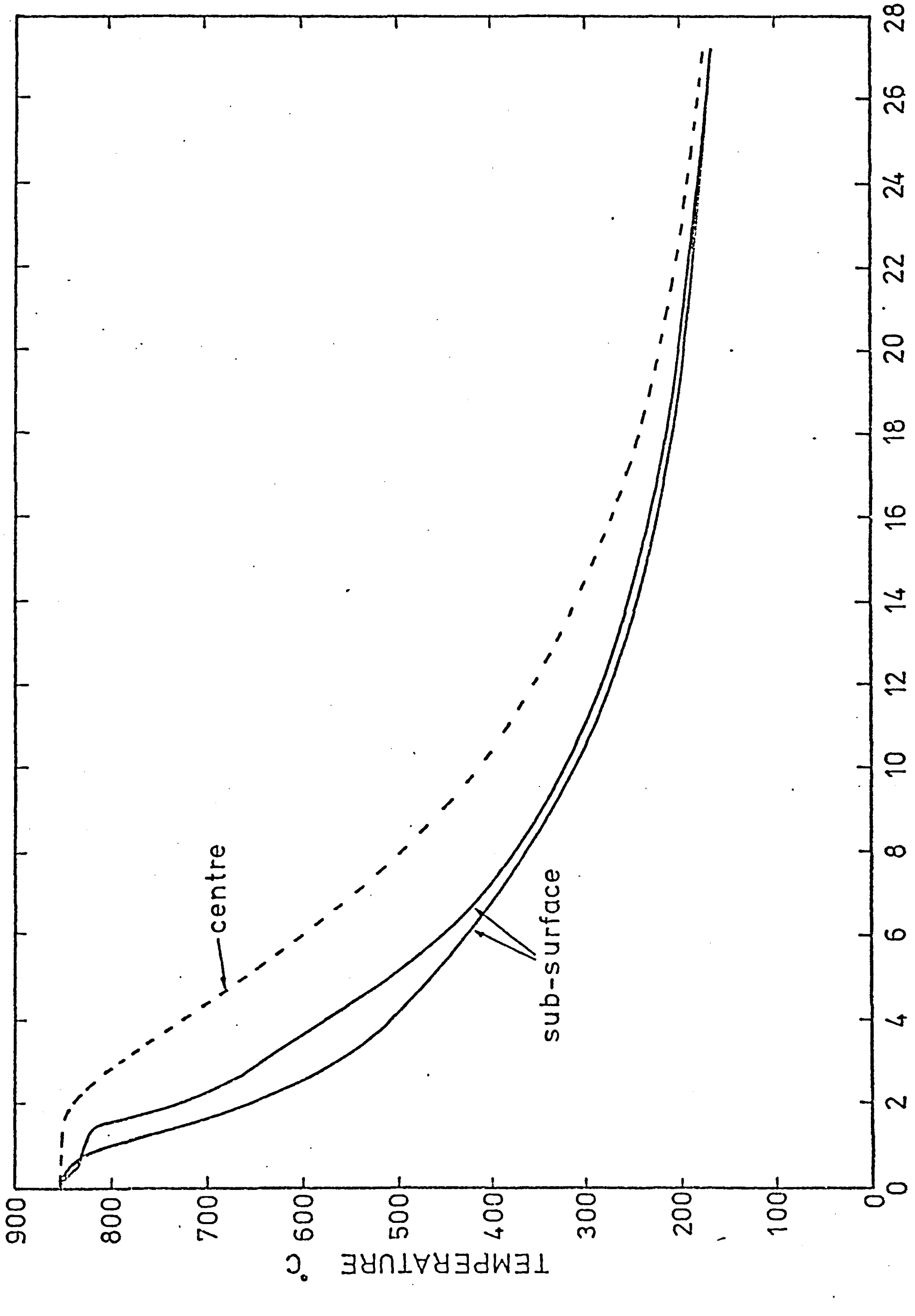
TEMPERATURE °C
900
800
700
600
500
400
300
200
100
0
TIME s
0
2
4
6
8
10
12
14
16
18
20
22
24
26
28
centre
sub-surface

FIGURE 60: Cooling curves obtained during the quenching of unoxidised Type B specimen in a 25% aqueous solution of 'Aquaquench 1250' polymer quenchant.

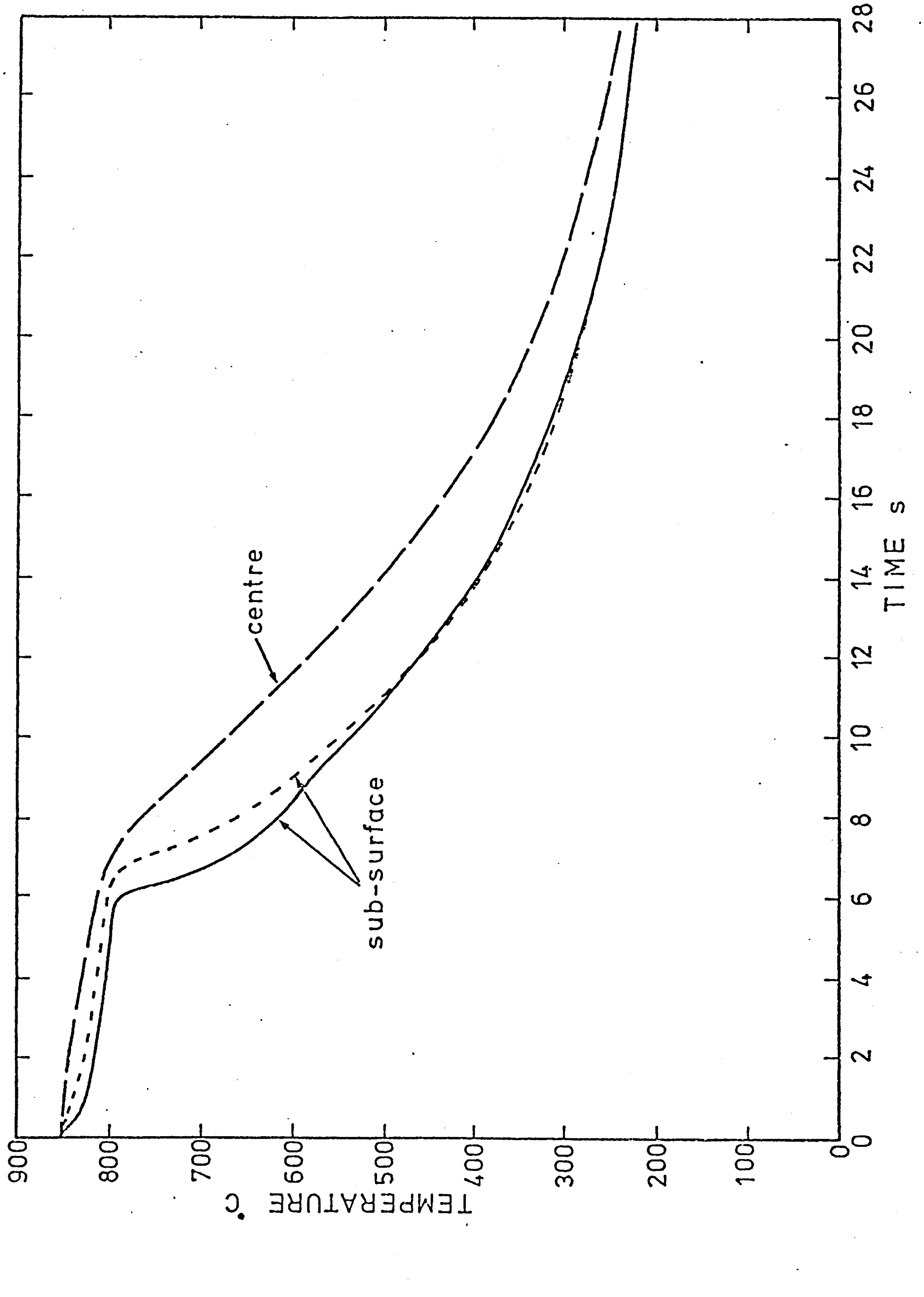

TEMPERATURE °C
900
800
700
600
500
400
300
200
100
0
TIME s
0
2
4
6
8
10
12
14
16
18
20
22
24
26
28
centre
sub-surface

FIGURE 61: Variation in h with surface temperature obtained from individual quenches of the Type B specimen (unoxidised) in 25% 'Aquaquench 1250' polymer quenchant.

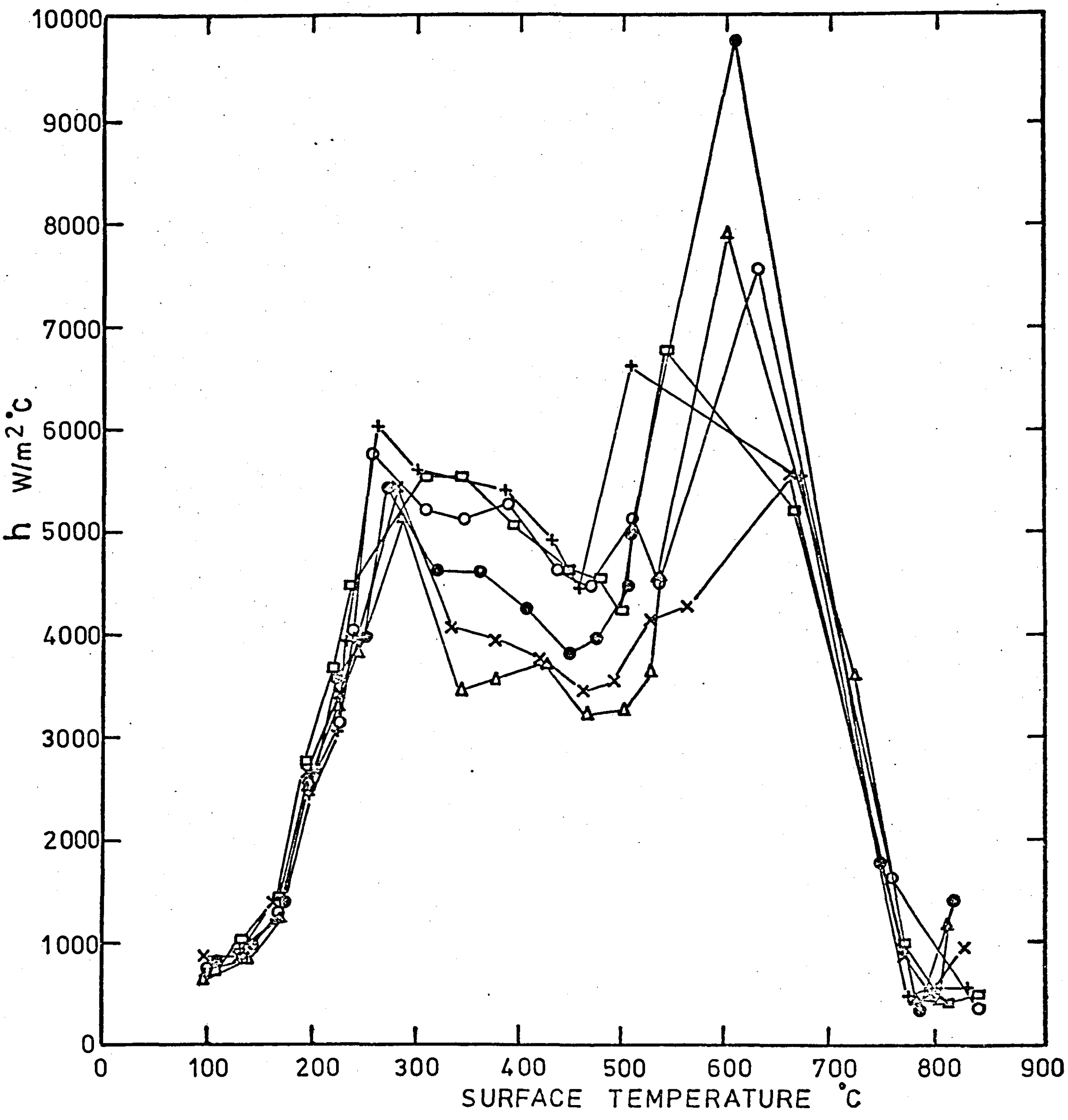

10000
9000
8000
7000
6000
5000
4000
3000
2000
1000
0
h W/m^2°C
0
100
200
300
400
500
600
700
800
900
SURFACE TEMPERATURE °C

FIGURE 62: Relationship between h and surface temperature during quenching into 25% 'Aquaquench 1250' (derived from data shown in Figure 61) used in subsequent calculations of temperature in plates during polymer quenching.

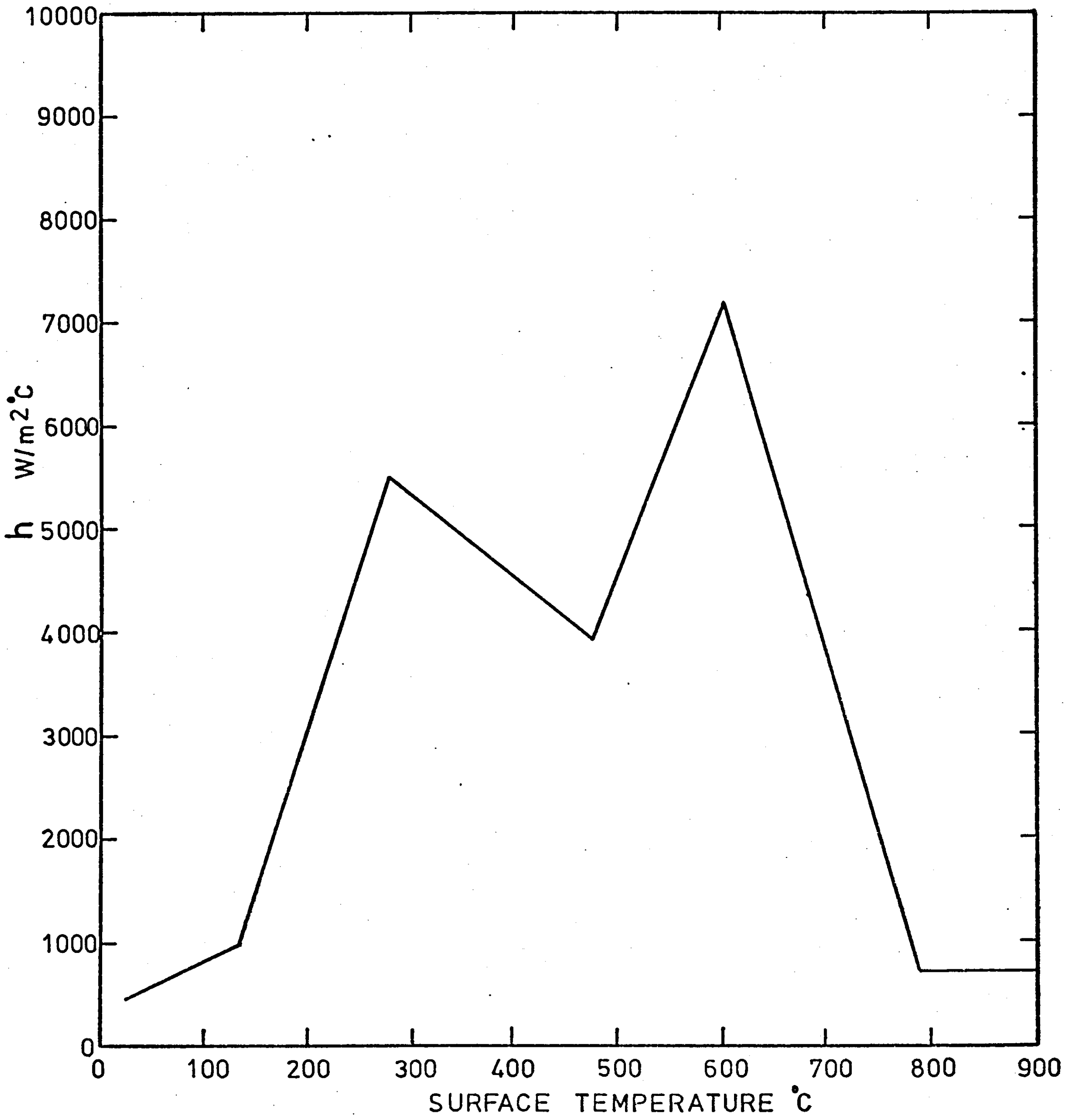
10000
9000
8000
7000
6000
5000
4000
3000
2000
1000
0
h W/m^2°C
0
100
200
300
400
500
600
700
800
900
SURFACE TEMPERATURE °C

FIGURE 63: 40mm plate of 835M30 steel used to determine experimental temperature distributions during quenching, showing location of thermocouples.

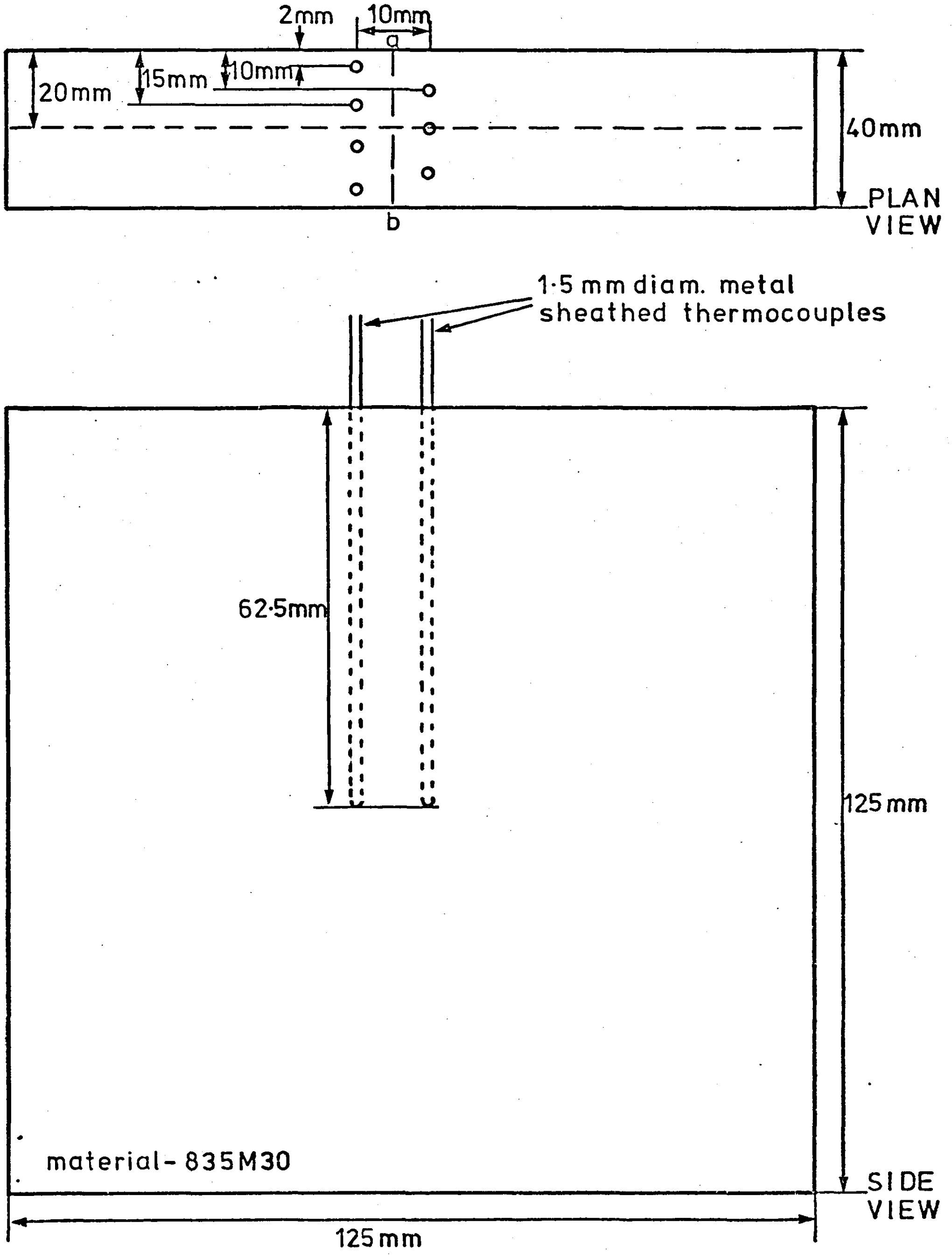
2mm
10mm
a
20mm
15mm
10mm
40mm
b
PLAN VIEW
1·5 mm diam. metal sheathed thermocouples
62·5mm
125mm
material - 835M30
SIDE VIEW
125mm

FIGURE 64: Variation in thermal conductivity with temperature used in the calculation of temperature distributions in 835M30 steel during quenching.
(Derived from data given by Atkins et alia[138] for 830A31 steel).

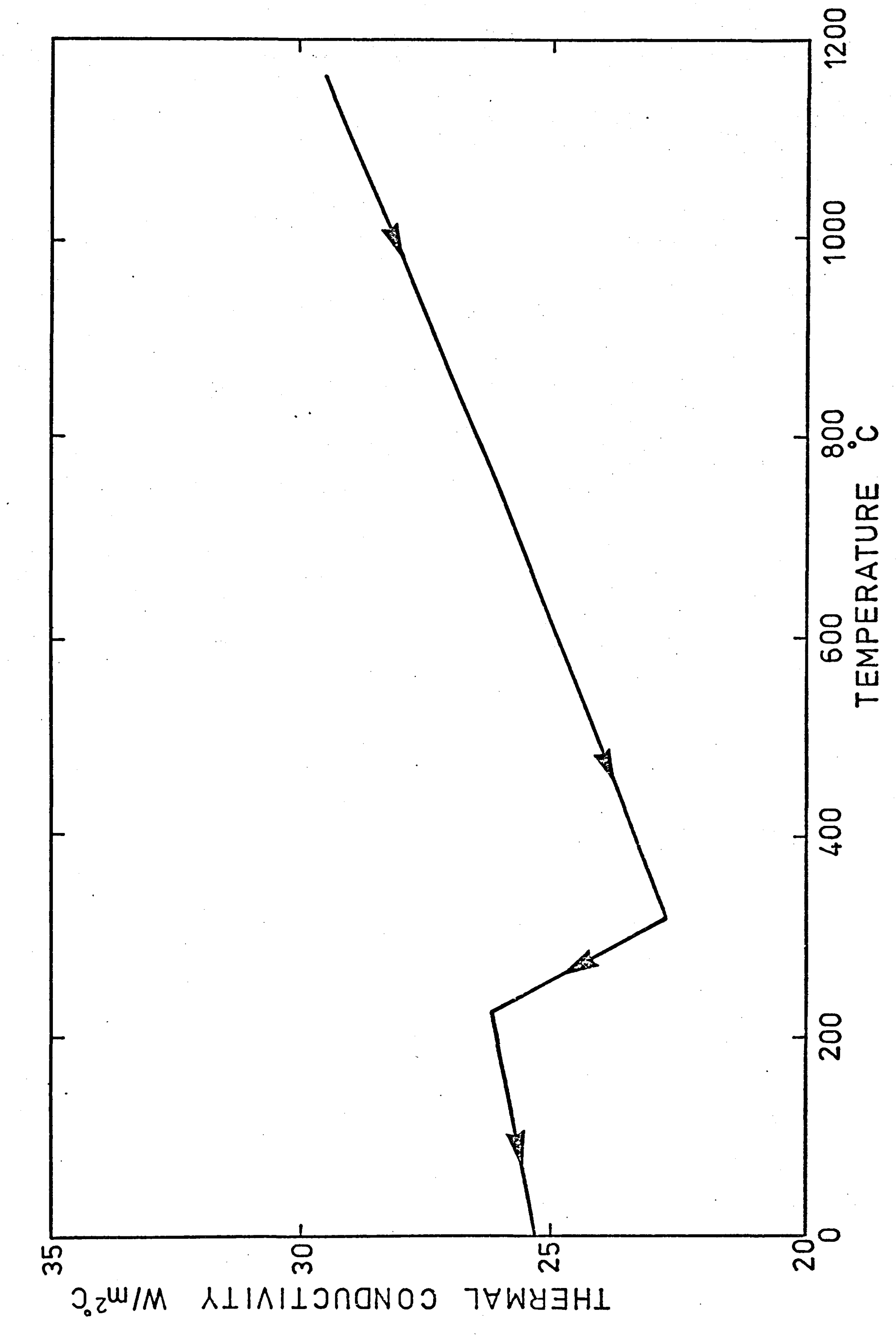
THERMAL CONDUCTIVITY W/m^2°C
35
30
25
20
TEMPERATURE °C
0
200
400
600
800
1000
1200

FIGURE 65: Variation in thermal diffusivity with temperature, used in the calculation of temperature distributions in 835M30 steel during quenching.
(Derived from data given by Atkins et alia[138] for 830A31 steel).

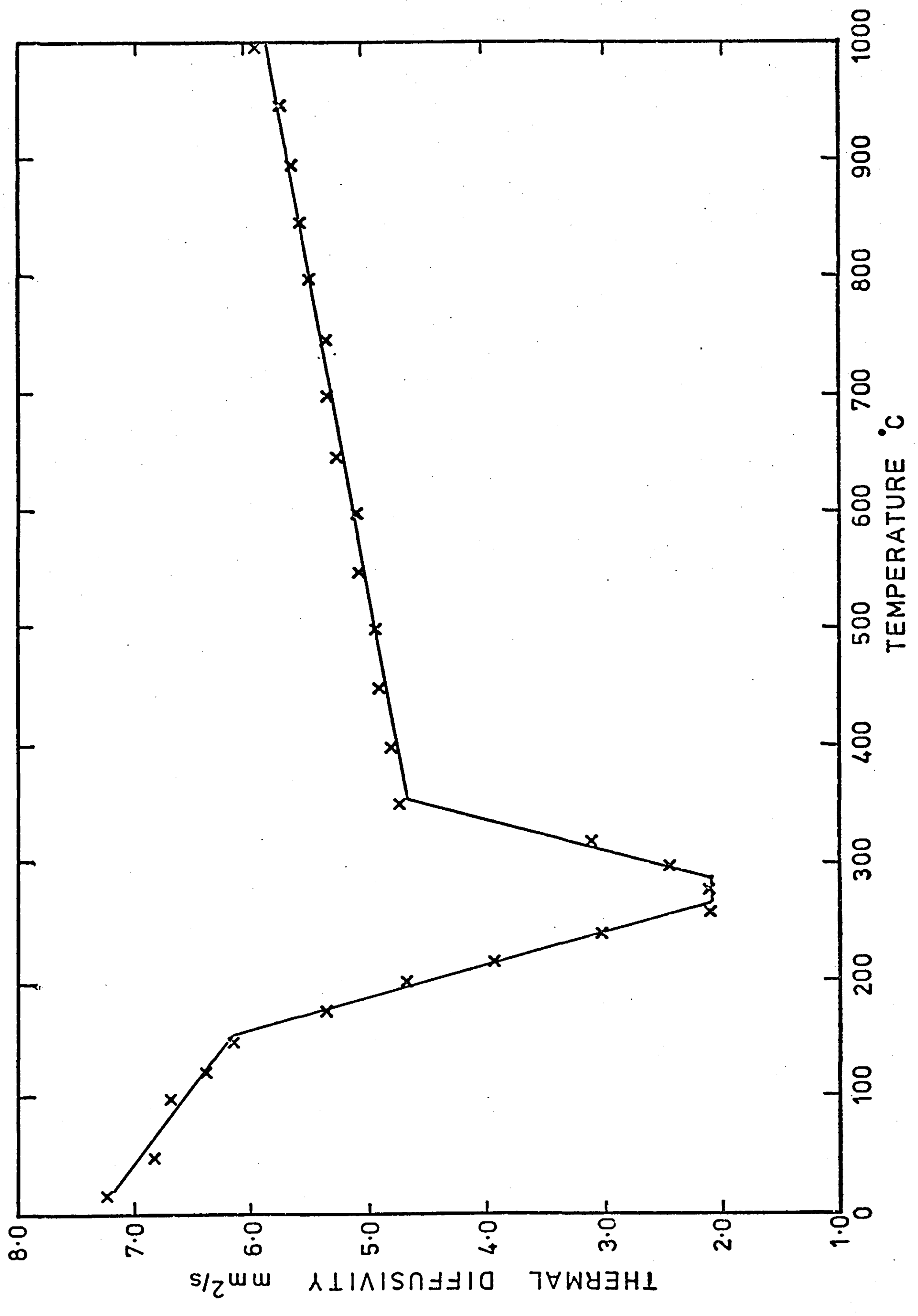

THERMAL DIFFUSIVITY mm²/s
8·0
7·0
6·0
5·0
4·0
3·0
2·0
1·0
TEMPERATURE °C
0
100
200
300
400
500
600
700
800
900
1000

FIGURE 66: Influence of the number of elements used in the calculation of temperature on the temperature at the surface and centre of a plate cooled with a Biot number of 4.0, after 4.7s.

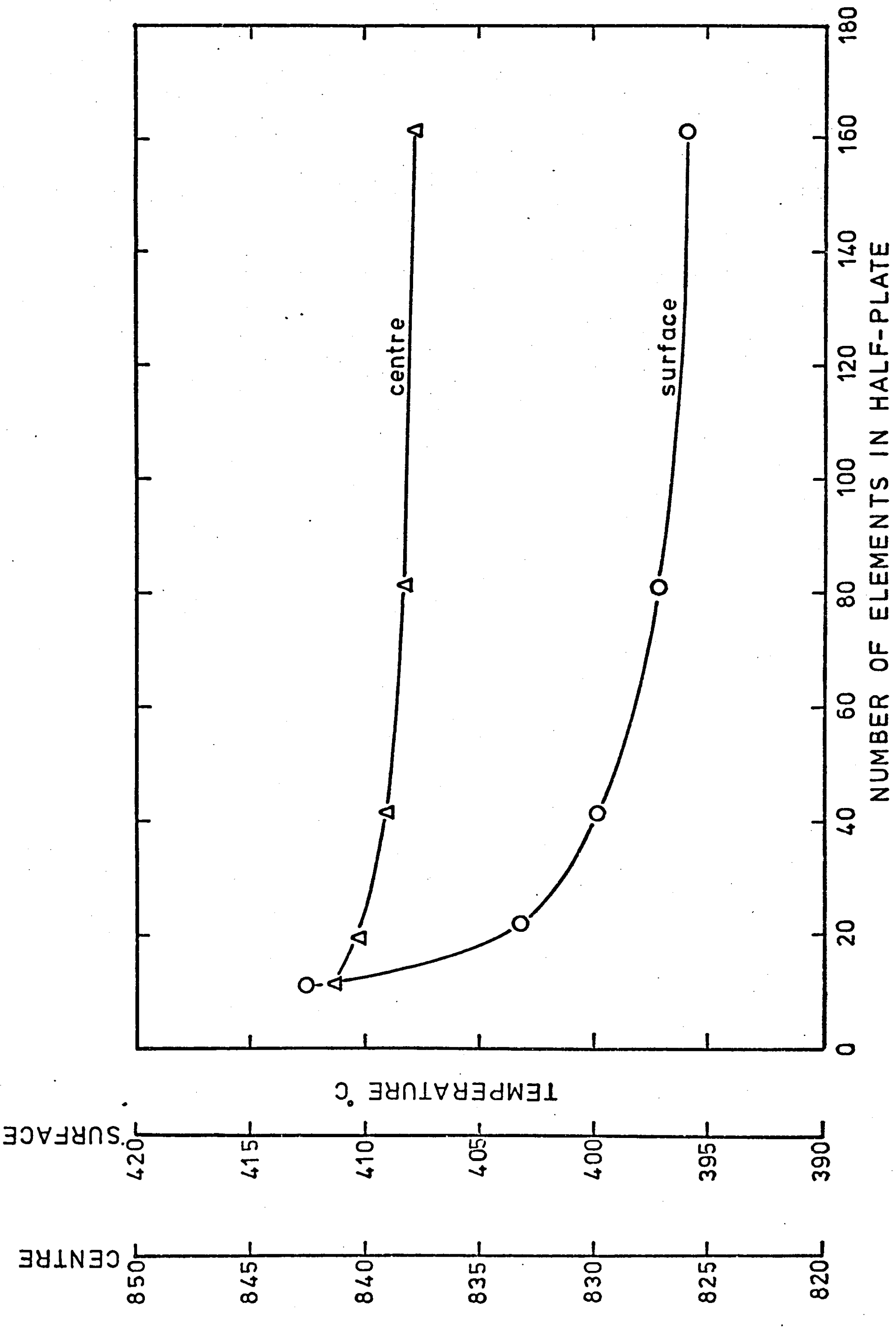
TEMPERATURE °C
SURFACE
420
415
410
405
400
395
390
CENTRE
850
845
840
835
830
825
820
centre
surface
NUMBER OF ELEMENTS IN HALF-PLATE
0
20
40
60
80
100
120
140
160
180

FIGURE 67: Flow chart showing the procedure employed for the calculation of temperature in plates of 835M30 during quenching.

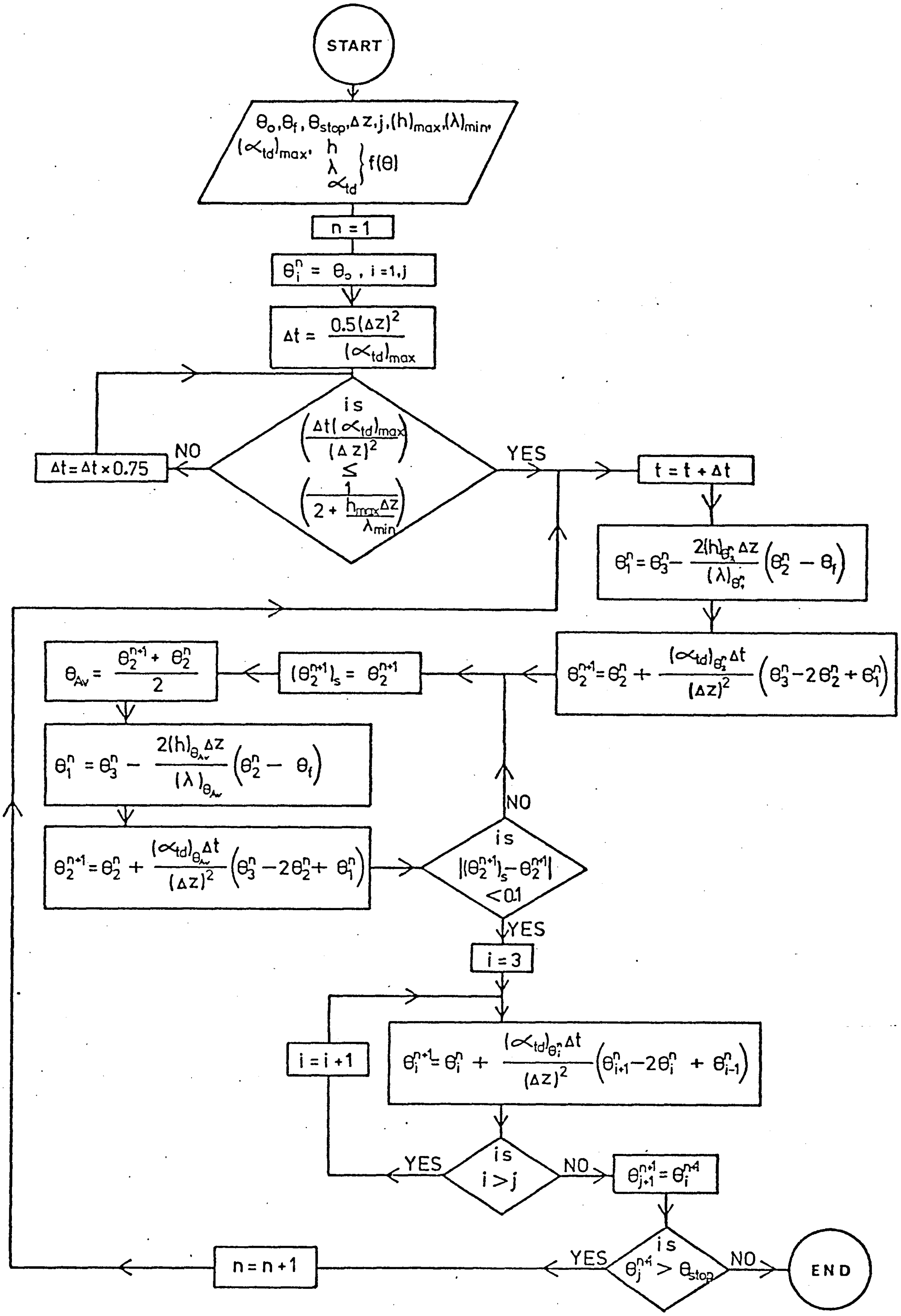
START
$\theta_o, \theta_f, \theta_{stop}, \Delta z, j, (h)_{max}, (\lambda)_{min}, (\alpha_{td})_{max}$, $\left.\begin{matrix} h \\ \lambda \\ \alpha_{td} \end{matrix}\right\} f(\theta)$
n = 1
$\theta_i^n = \theta_o$, i = 1, j
$\Delta t = \frac{0.5(\Delta z)^2}{(\alpha_{td})_{max}}$
is $\left(\frac{\Delta t (\alpha_{td})_{max}}{(\Delta z)^2}\right) \leq \left(\frac{1}{2 + \frac{h_{max}\Delta z}{\lambda_{min}}}\right)$
NO
$\Delta t = \Delta t \times 0.75$
YES
$t = t + \Delta t$
$\theta_1^n = \theta_3^n - \frac{2(h)_{\theta_1^n}\Delta z}{(\lambda)_{\theta_1^n}}(\theta_2^n - \theta_f)$
$\theta_2^{n+1} = \theta_2^n + \frac{(\alpha_{td})_{\theta_2^n}\Delta t}{(\Delta z)^2}(\theta_3^n - 2\theta_2^n + \theta_1^n)$
$(\theta_2^{n+1})_s = \theta_2^{n+1}$
$\theta_{Av} = \frac{\theta_2^{n+1} + \theta_2^n}{2}$
$\theta_1^n = \theta_3^n - \frac{2(h)_{\theta_{Av}}\Delta z}{(\lambda)_{\theta_{Av}}}(\theta_2^n - \theta_f)$
$\theta_2^{n+1} = \theta_2^n + \frac{(\alpha_{td})_{\theta_{Av}}\Delta t}{(\Delta z)^2}(\theta_3^n - 2\theta_2^n + \theta_1^n)$
is $|(\theta_2^{n+1})_s - \theta_2^{n+1}| < 0.1$
NO
YES
i = 3
$\theta_i^{n+1} = \theta_i^n + \frac{(\alpha_{td})_{\theta_i^n}\Delta t}{(\Delta z)^2}(\theta_{i+1}^n - 2\theta_i^n + \theta_{i-1}^n)$
i = i + 1
is i > j
YES
NO
$\theta_{j+1}^{n+1} = \theta_i^{n+1}$
is $\theta_j^{n+1} > \theta_{stop}$
YES
NO
n = n + 1
END

FIGURE 68: Comparison of calculated and experimentally determined cooling curves at the centre of a 40mm plate of 835M30 steel during water quenching.

(a) Calculated using constant values of λ and α_{td}, and the minimum and maximum range of values of h indicated in Figure 54.

(b) Calculated using temperature dependent values of λ and α_{td}, and the minimum and maximum range of values of h indicated in Figure 54.

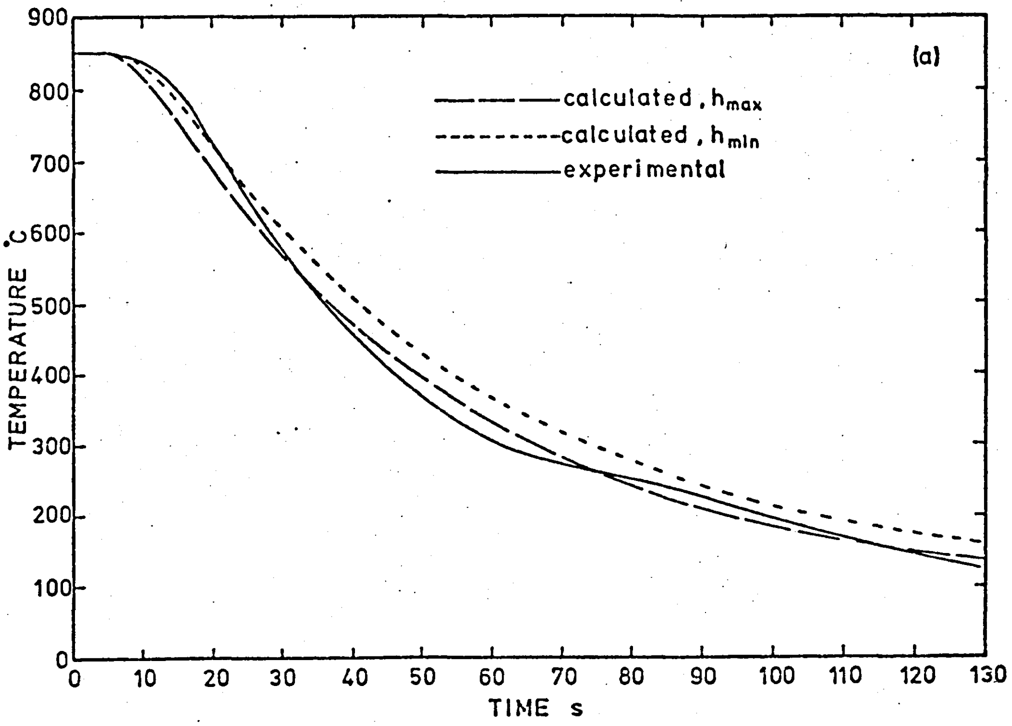
(a)
calculated, h_{max}
calculated, h_{min}
experimental
TEMPERATURE °C
900
800
700
600
500
400
300
200
100
0
TIME s
0
10
20
30
40
50
60
70
80
90
100
110
120
130

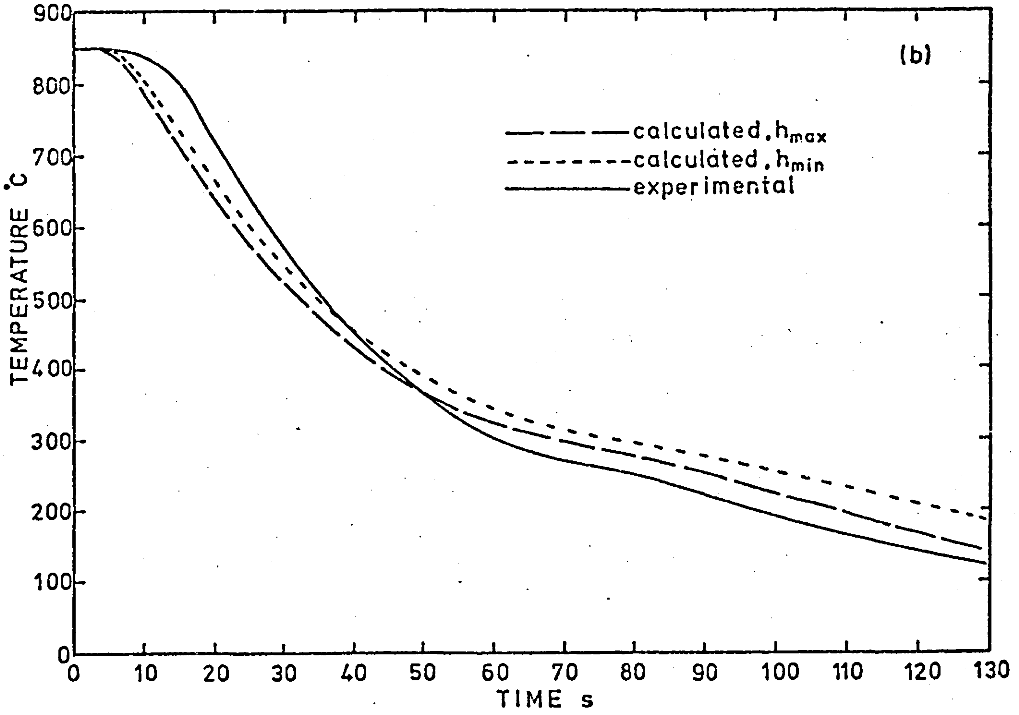
(b)
calculated, h_{max}
calculated, h_{min}
experimental
TEMPERATURE °C
900
800
700
600
500
400
300
200
100
0
TIME s
0
10
20
30
40
50
60
70
80
90
100
110
120
130

FIGURE 69: Comparison between calculated and experimental temperature distributions in a 40mm plate of 835M30 steel during water quenching. (Comparison made on the basis of equal temperatures at the centre of the plate).

— — — calculated using h_{min} values

———— " " h_{av} "

— - — - — " " h_{max} "

(Constant values of λ and α_{td} used in calculations.)

o ----------- o experimental results

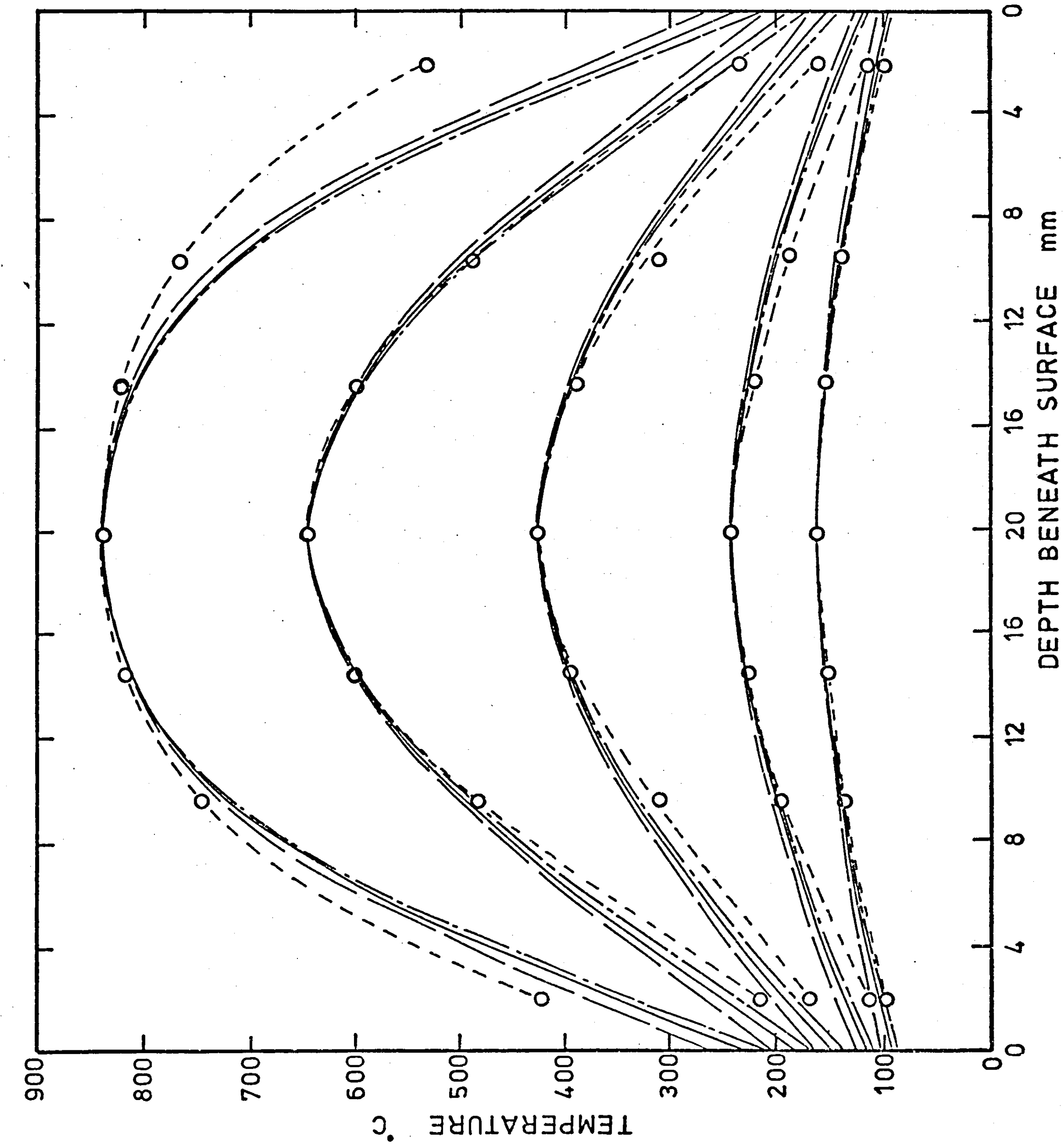
TEMPERATURE °C
0
100
200
300
400
500
600
700
800
900
DEPTH BENEATH SURFACE mm
0
4
8
12
16
20
16
12
8
4
0

FIGURE 70: Comparison between the temperature distribution in a plate of 835M30 during water quenching calculated using constant values for λ and α_{td} (solid lines), and temperature dependent values for λ and α_{td} (broken lines). (h_{av} values used in calculations; comparisons made on the basis of equal temperatures at the centre of the plate).

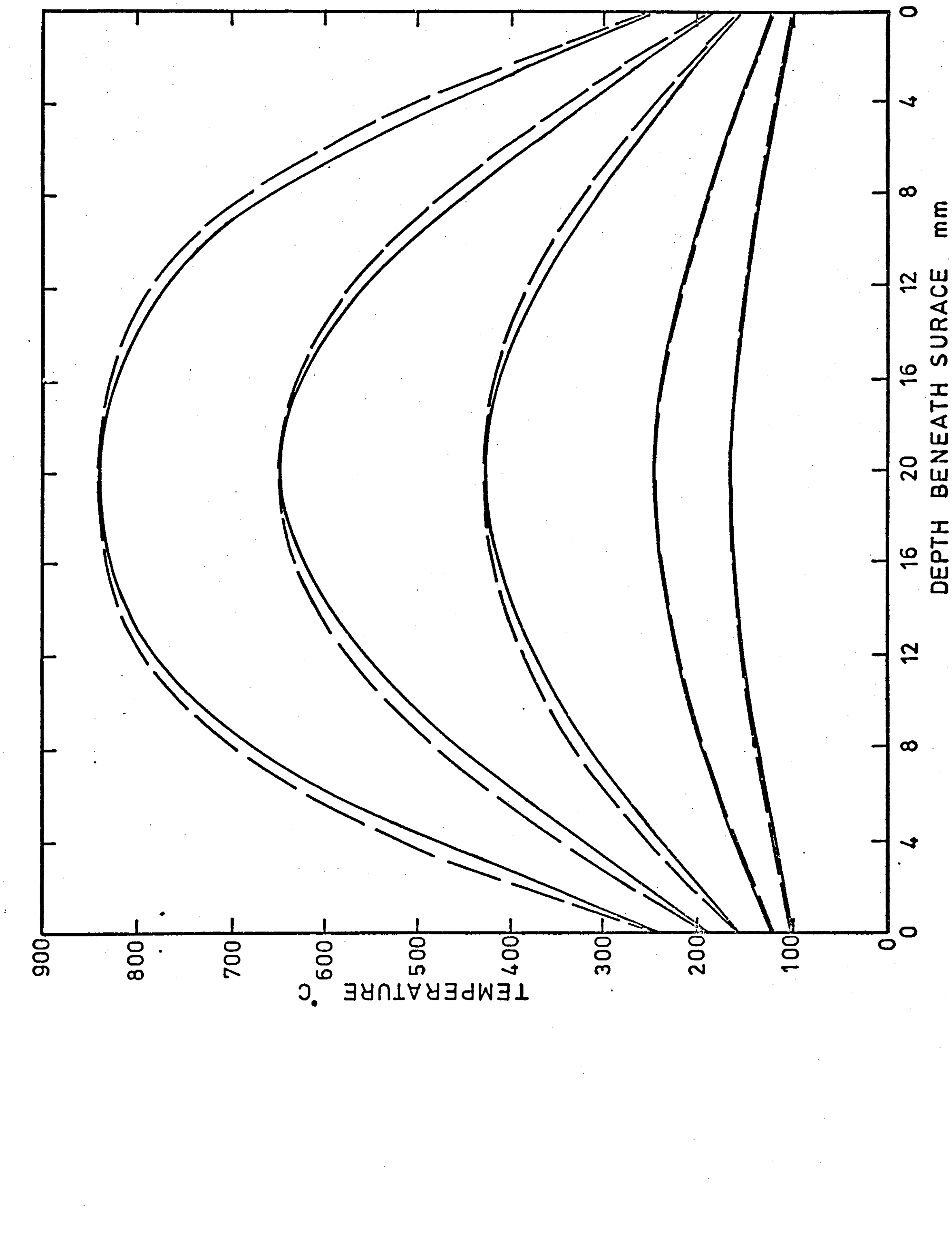
TEMPERATURE °C
900
800
700
600
500
400
300
200
100
0
DEPTH BENEATH SURACE mm
0
4
8
12
16
20
16
12
8
4
0

FIGURE 71: Comparison between calculated and experimental cooling curves at the centre of a 40mm plate of 835M30 steel during oil quenching.

Calculated {
— — — constant λ and α_{td}
----------- temperature dependent λ and α_{td}

———— experimental

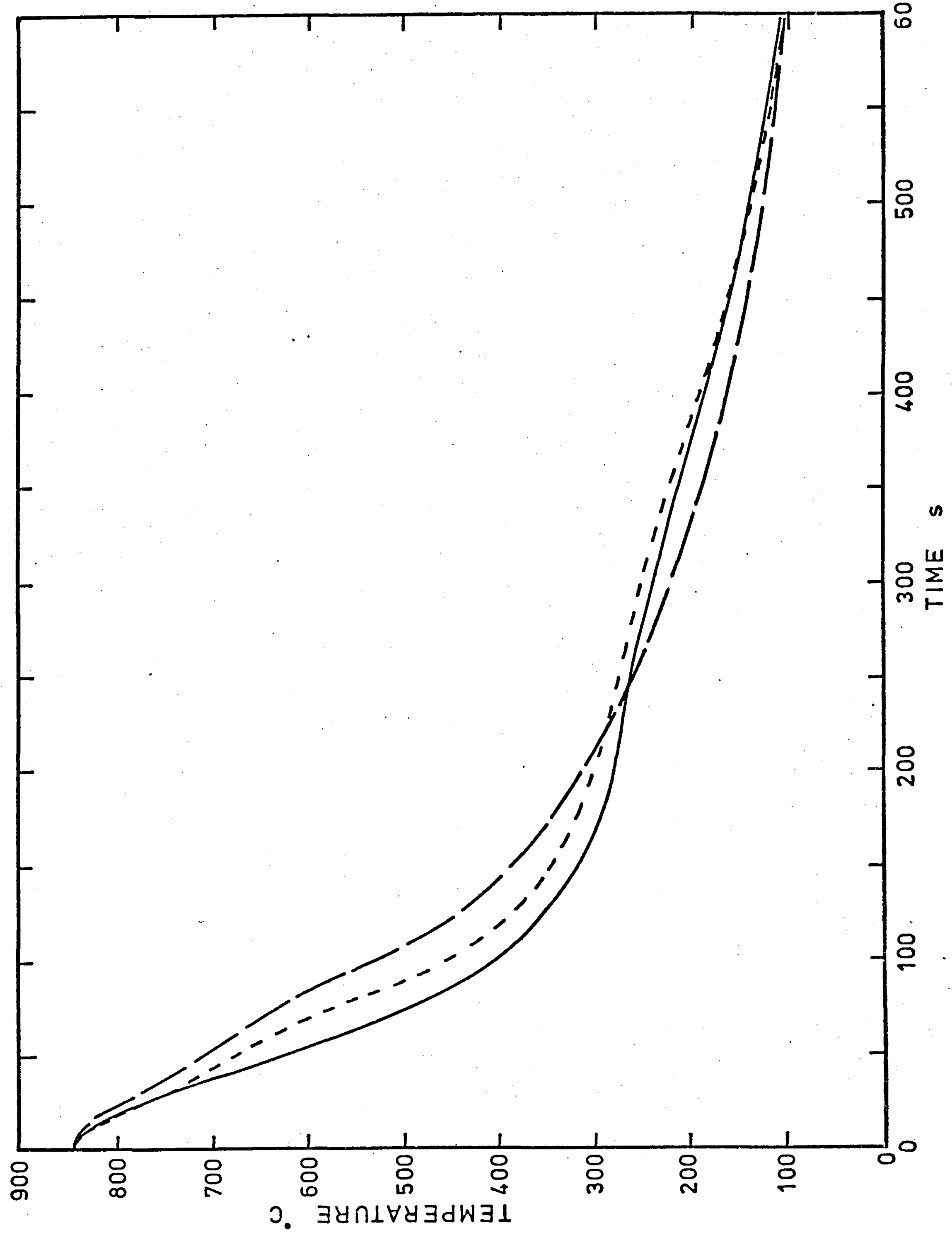
TEMPERATURE °C
900
800
700
600
500
400
300
200
100
0
TIME s
0
100
200
300
400
500
600

FIGURE 72: Comparison between calculated and experimental temperature distributions in a 40mm plate of 835M30 steel during oil quenching. (Calculations carried out using constant values of λ and α_{td}; comparison made on the basis of equal temperatures at the centre of the plate).

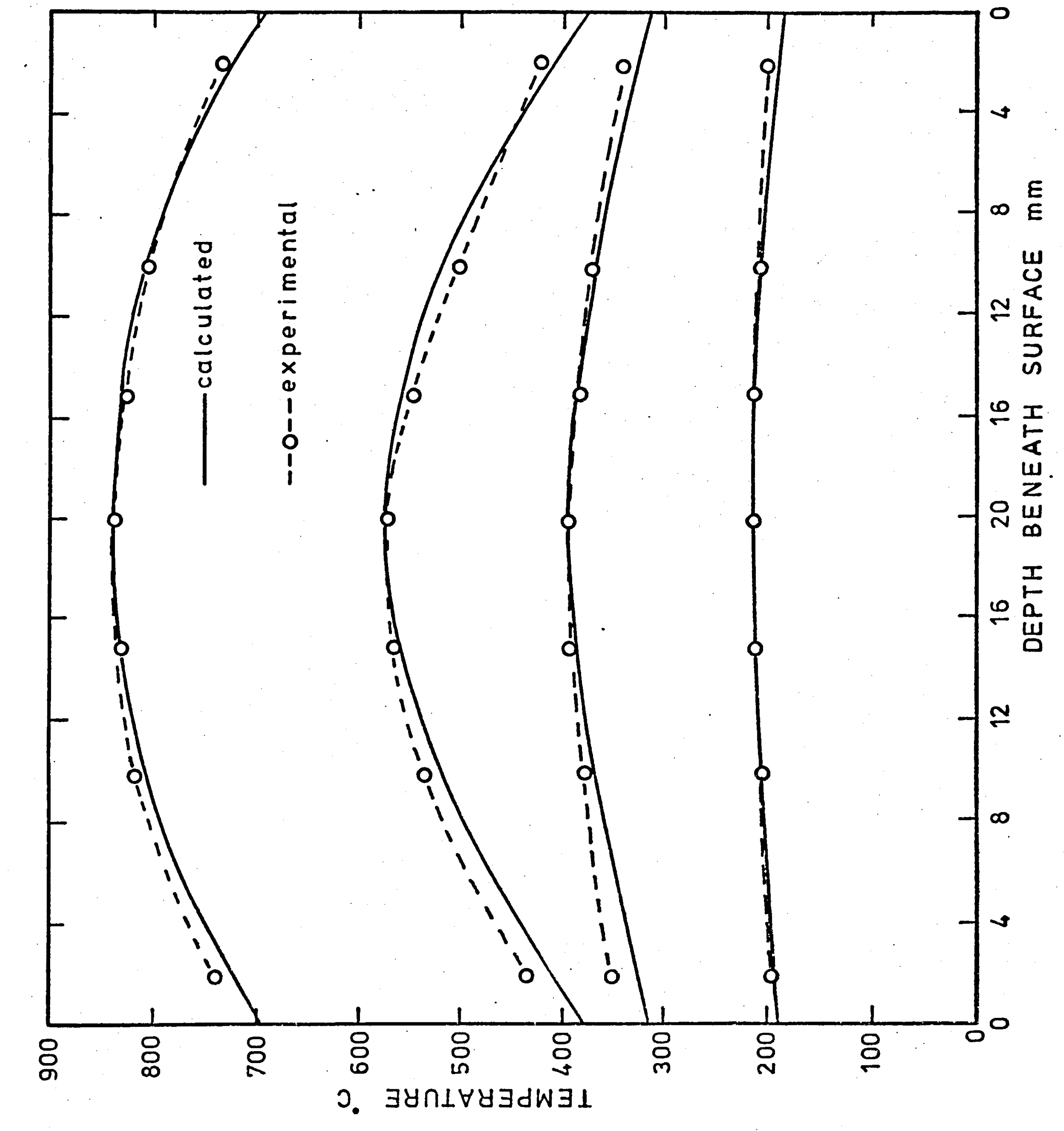
TEMPERATURE °C
0
100
200
300
400
500
600
700
800
900
DEPTH BENEATH SURFACE mm
0
4
8
12
16
20
16
12
8
4
0
calculated
experimental

FIGURE 73: Location of elements used in the calculation of thermal stresses in an infinite plate and the stress system.

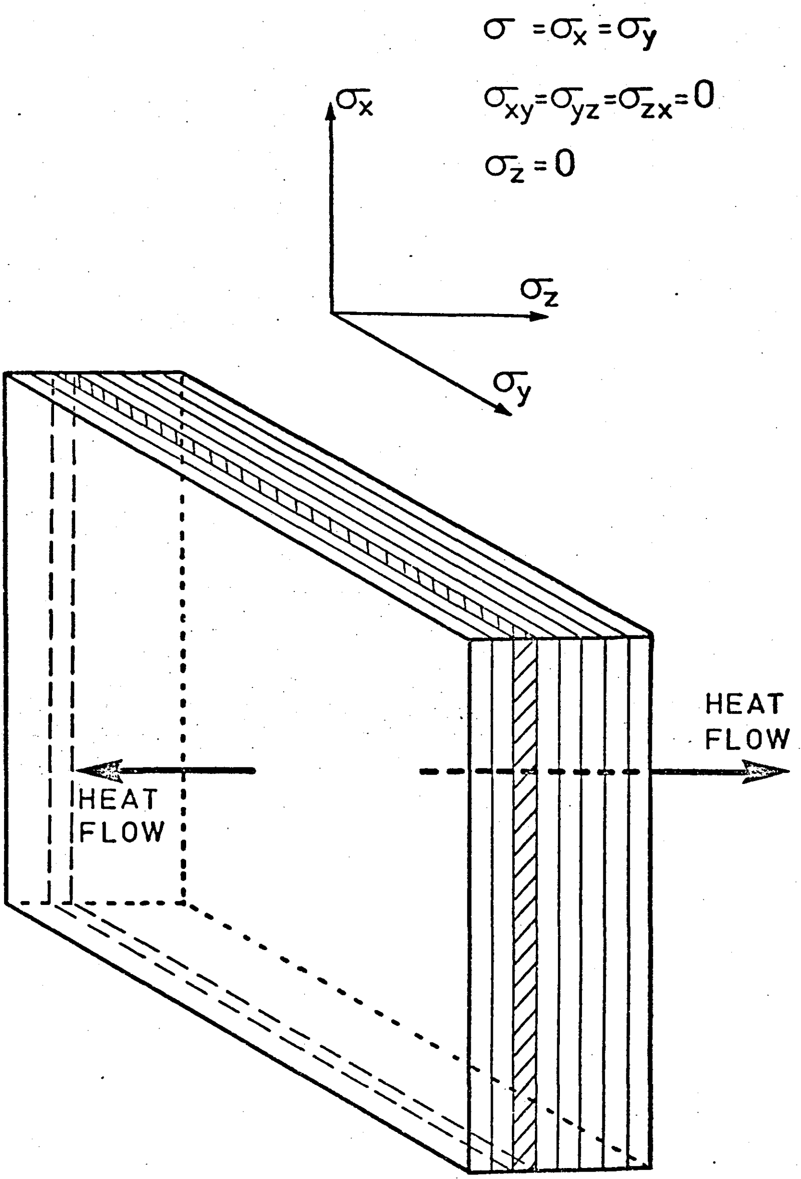
$\sigma = \sigma_x = \sigma_y$
$\sigma_{xy} = \sigma_{yz} = \sigma_{zx} = 0$
$\sigma_z = 0$
σ_x
σ_z
σ_y
HEAT FLOW
HEAT FLOW

FIGURE 74: Variation of $\frac{E}{1-\nu}$ with temperature of 830A31 steel (calculated from data given by Atkins et alia[138]) and relationship used in the calculation of thermal stress in 835M30.

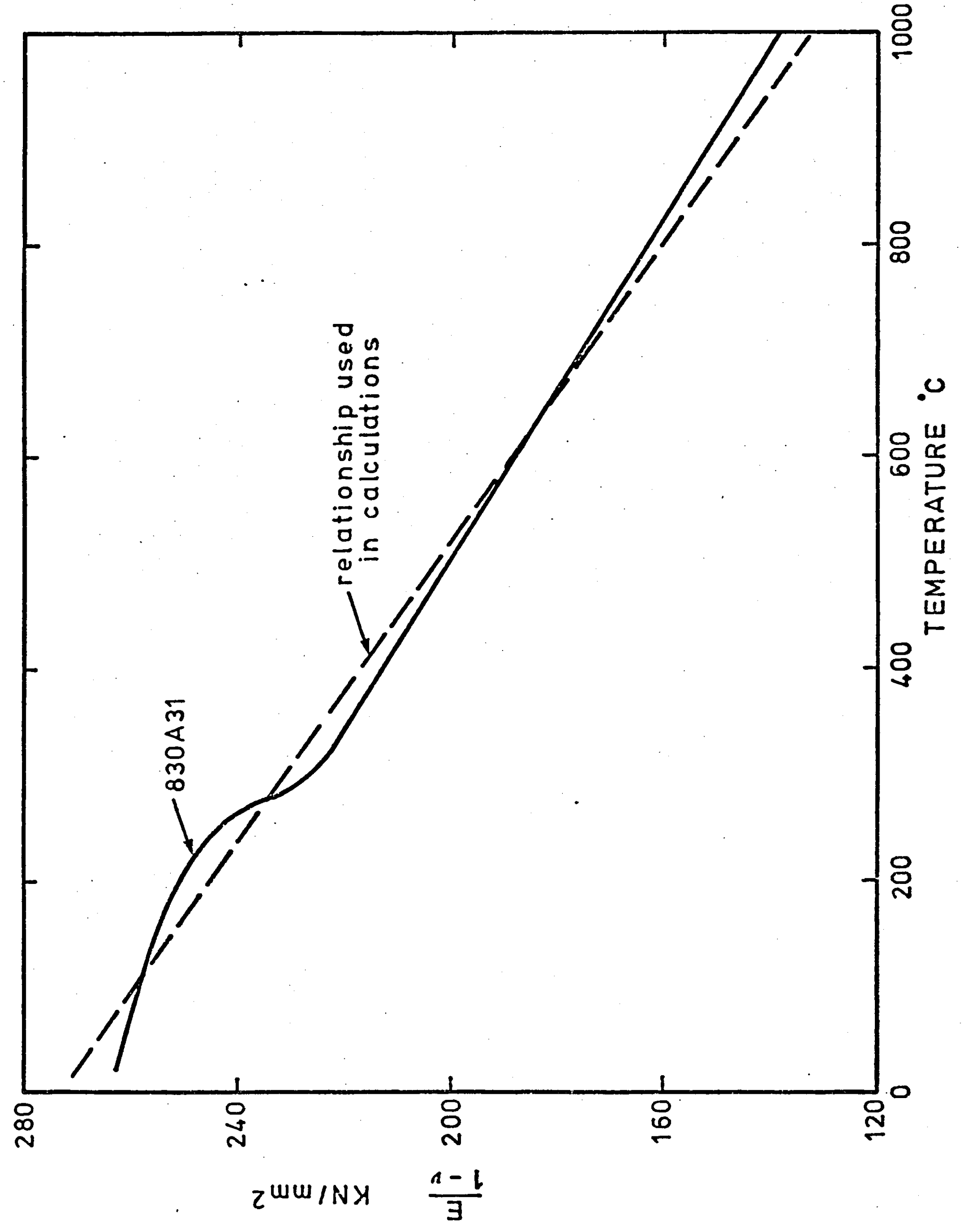

830A31
relationship used in calculations
TEMPERATURE °C
0
200
400
600
800
1000
$\frac{E}{1-\nu}$ KN/mm2
280
240
200
160
120

FIGURE 75: Schematic representation of the application of the yield criterion.

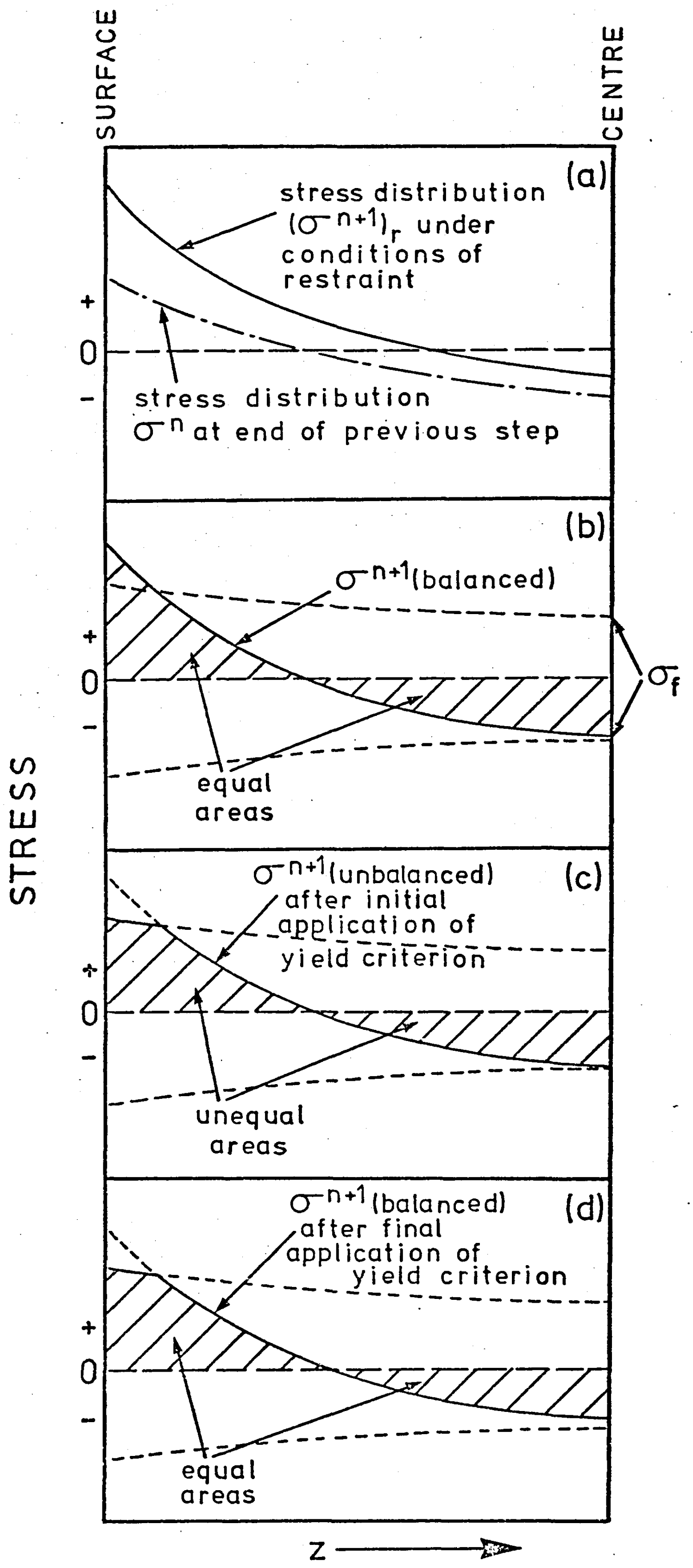
SURFACE
CENTRE
STRESS
(a)
stress distribution $(\sigma^{n+1})_r$ under conditions of restraint
stress distribution σ^n at end of previous step
+
0
-
(b)
σ^{n+1}(balanced)
equal areas
σ_f
(c)
σ^{n+1}(unbalanced) after initial application of yield criterion
unequal areas
(d)
σ^{n+1}(balanced) after final application of yield criterion
equal areas
z

FIGURE 76: Model of uniaxial stress-strain relationship used in the calculation of thermal stress.

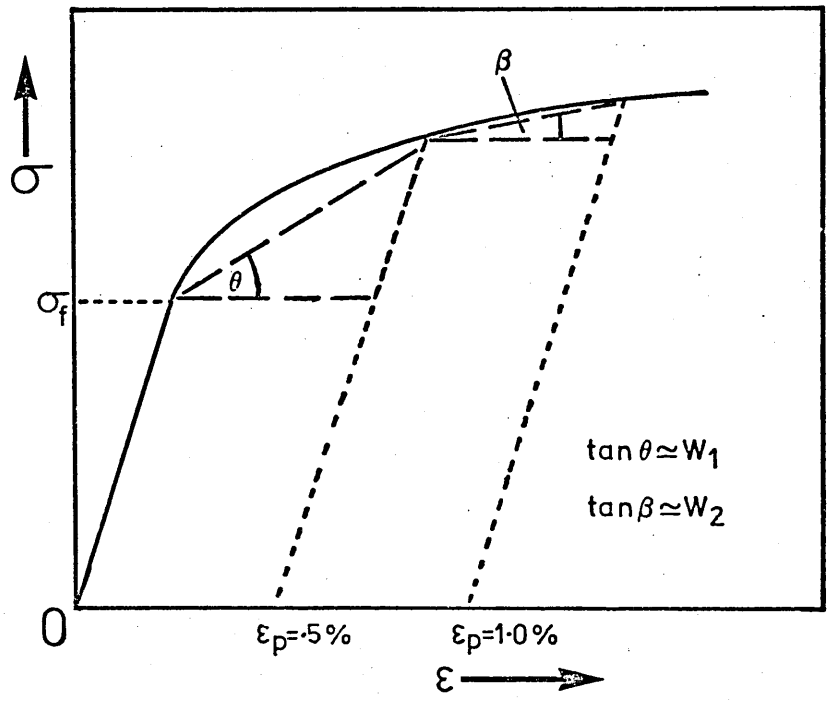
β
σ
σ_f
θ
$\tan\theta \simeq W_1$
$\tan\beta \simeq W_2$
0
$\varepsilon_p = \cdot 5\%$
$\varepsilon_p = 1{\cdot}0\%$
ε

FIGURE 77: Flow chart of the calculation of thermal stress in an infinite plate of 835M30 steel from a given temperature distribution (obtained from the calculation flow chart given in Figure 67).

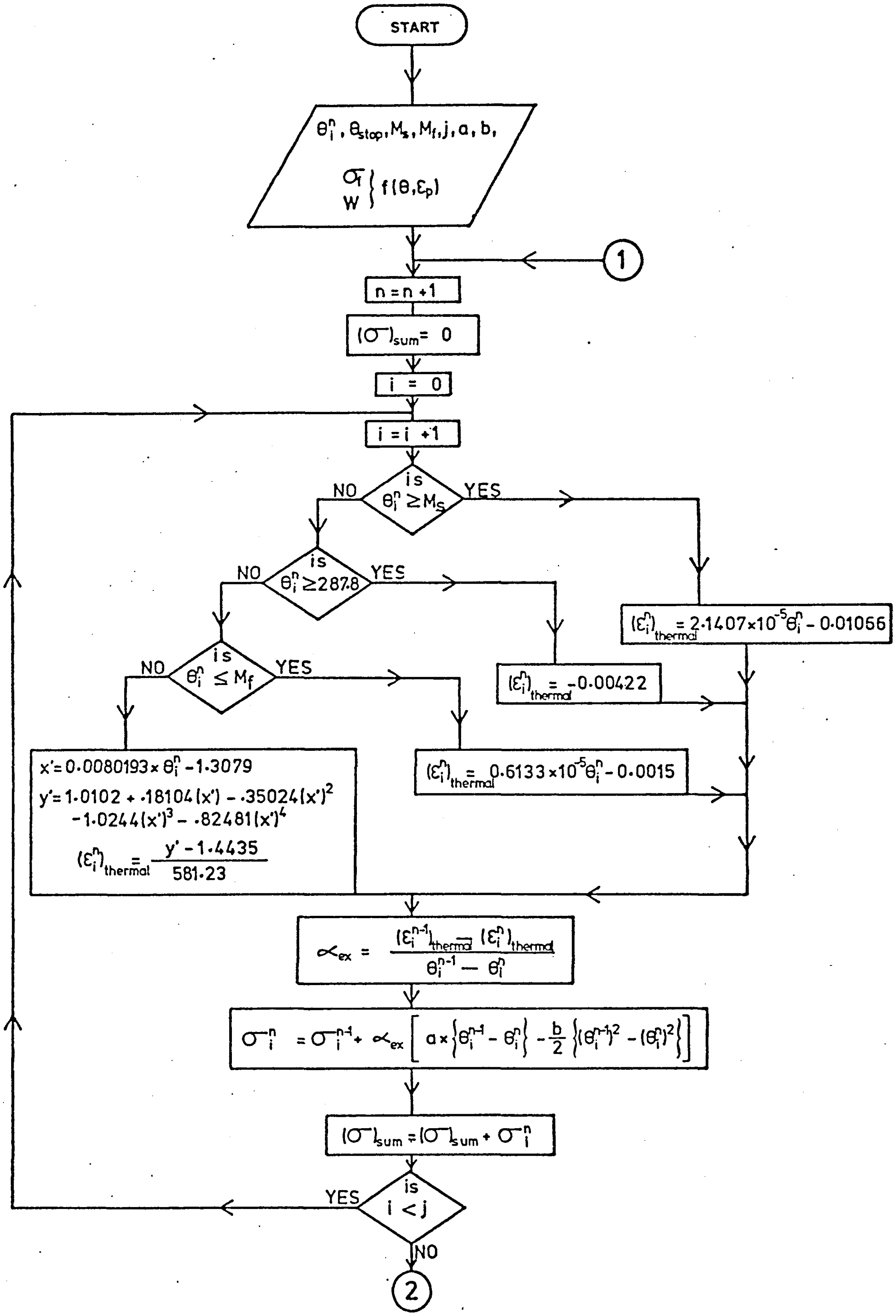
START
θ_i^n, θ_stop, M_s, M_f, j, a, b,
σ_f, W } f(θ, ε_p)
1
n = n + 1
(σ)_sum = 0
i = 0
i = i + 1
is θ_i^n ≥ M_s
NO
YES
is θ_i^n ≥ 287.8
NO
YES
(ε_i^n)_thermal = 2.1407×10^-5 θ_i^n − 0.01066
is θ_i^n ≤ M_f
NO
YES
(ε_i^n)_thermal = −0.00422
x' = 0.0080193 × θ_i^n − 1.3079
y' = 1.0102 + .18104(x') − .35024(x')^2 − 1.0244(x')^3 − .82481(x')^4
(ε_i^n)_thermal = (y' − 1.4435) / 581.23
(ε_i^n)_thermal = 0.6133×10^-5 θ_i^n − 0.0015
α_ex = ((ε_i^(n-1))_thermal − (ε_i^n)_thermal) / (θ_i^(n-1) − θ_i^n)
σ_i^n = σ_i^(n-1) + α_ex [a×{θ_i^(n-1) − θ_i^n} − b/2 {(θ_i^(n-1))^2 − (θ_i^n)^2}]
(σ)_sum = (σ)_sum + σ_i^n
is i < j
YES
NO
2

/cont'd...

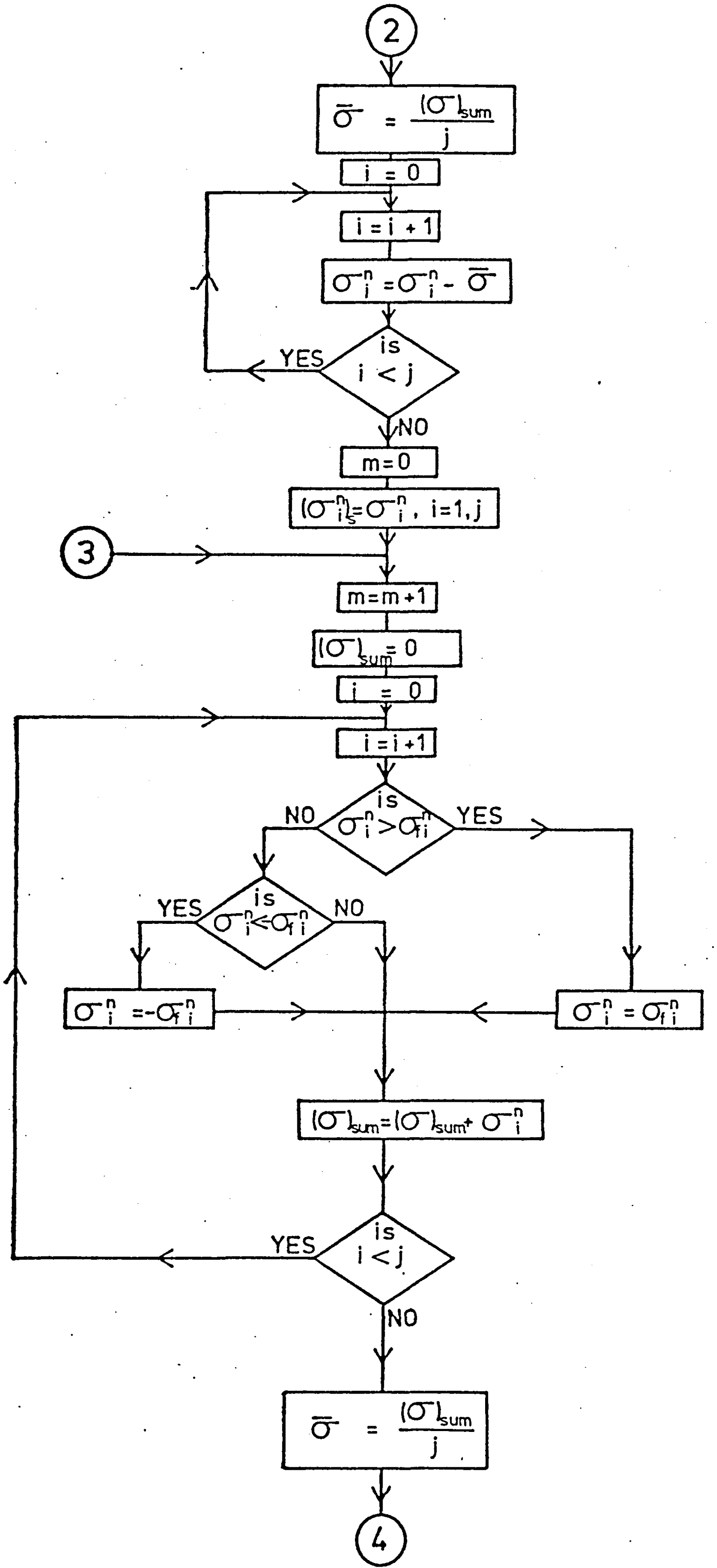
2
$\bar{\sigma} = \frac{(\sigma)_{sum}}{j}$
$i = 0$
$i = i + 1$
$\sigma_i^n = \sigma_i^n - \bar{\sigma}$
is $i < j$
YES
NO
$m = 0$
$(\sigma_i^n)_s = \sigma_i^n$, $i = 1, j$
3
$m = m + 1$
$(\sigma)_{sum} = 0$
$i = 0$
$i = i + 1$
is $\sigma_i^n > \sigma_{fi}^n$
NO
YES
is $\sigma_i^n < \sigma_{fi}^n$
YES
NO
$\sigma_i^n = -\sigma_{fi}^n$
$\sigma_i^n = \sigma_{fi}^n$
$(\sigma)_{sum} = (\sigma)_{sum} + \sigma_i^n$
is $i < j$
YES
NO
$\bar{\sigma} = \frac{(\sigma)_{sum}}{j}$
4

FIGURE 77: Continued...

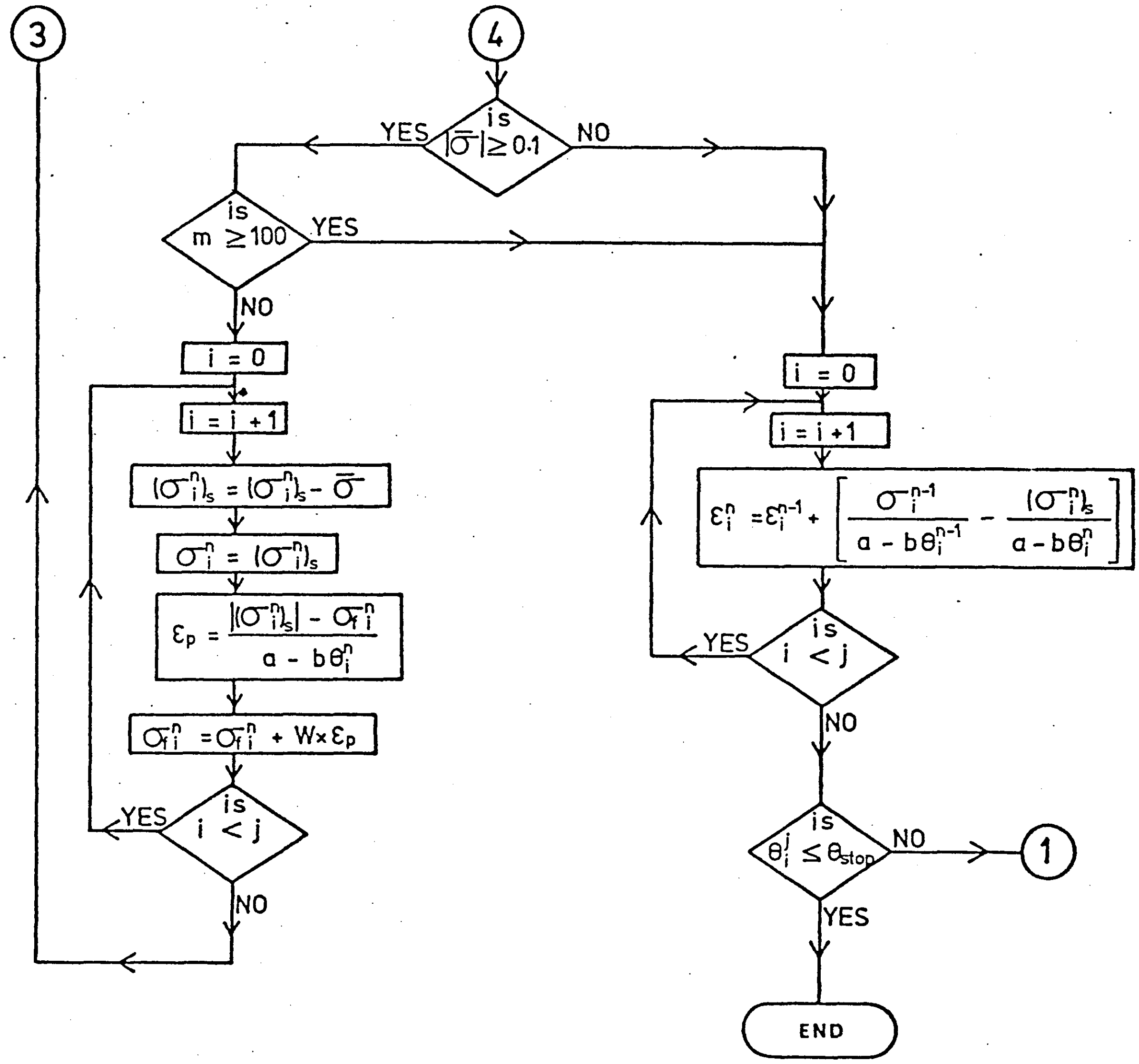

3
4
is $|\bar{\sigma}| \geq 0.1$
YES
NO
is $m \geq 100$
YES
NO
$i = 0$
$i = i + 1$
$(\sigma_i^n)_s = (\sigma_i^n)_s - \bar{\sigma}$
$\sigma_i^n = (\sigma_i^n)_s$
$\varepsilon_p = \frac{|(\sigma_i^n)_s| - \sigma_{f\,i}^n}{a - b\theta_i^n}$
$\sigma_{f\,i}^n = \sigma_{f\,i}^n + W \times \varepsilon_p$
is $i < j$
YES
NO
$i = 0$
$i = i + 1$
$\varepsilon_i^n = \varepsilon_i^{n-1} + \left[\frac{\sigma_i^{n-1}}{a - b\theta_i^{n-1}} - \frac{(\sigma_i^n)_s}{a - b\theta_i^n}\right]$
is $i < j$
YES
NO
is $\theta_i^j \leq \theta_{stop}$
NO
1
YES
END

FIGURE 77: Continued

FIGURE 78: Details of 835M30 specimen location in dilatometer showing heating and cooling arrangements.

FIGURE 79: Isothermal transformation diagram for En30B (835M30).

(After Woolman & Mottran[157])

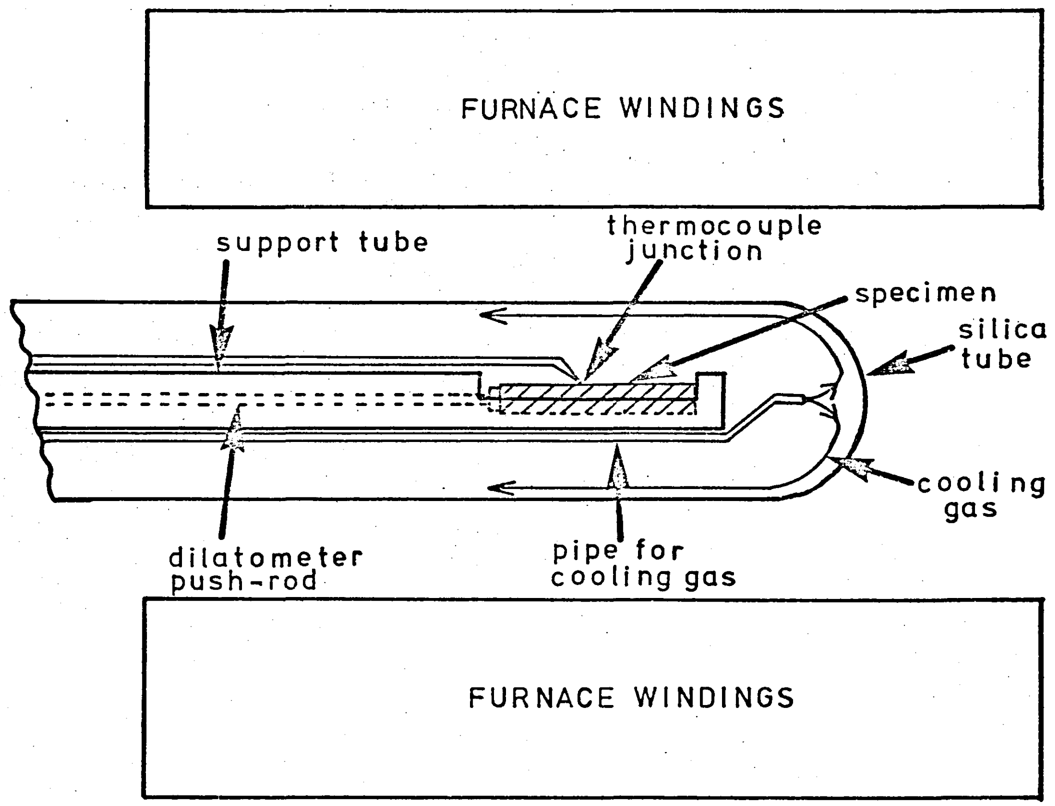
FURNACE WINDINGS
support tube
thermocouple junction
specimen
silica tube
cooling gas
dilatometer push-rod
pipe for cooling gas
FURNACE WINDINGS

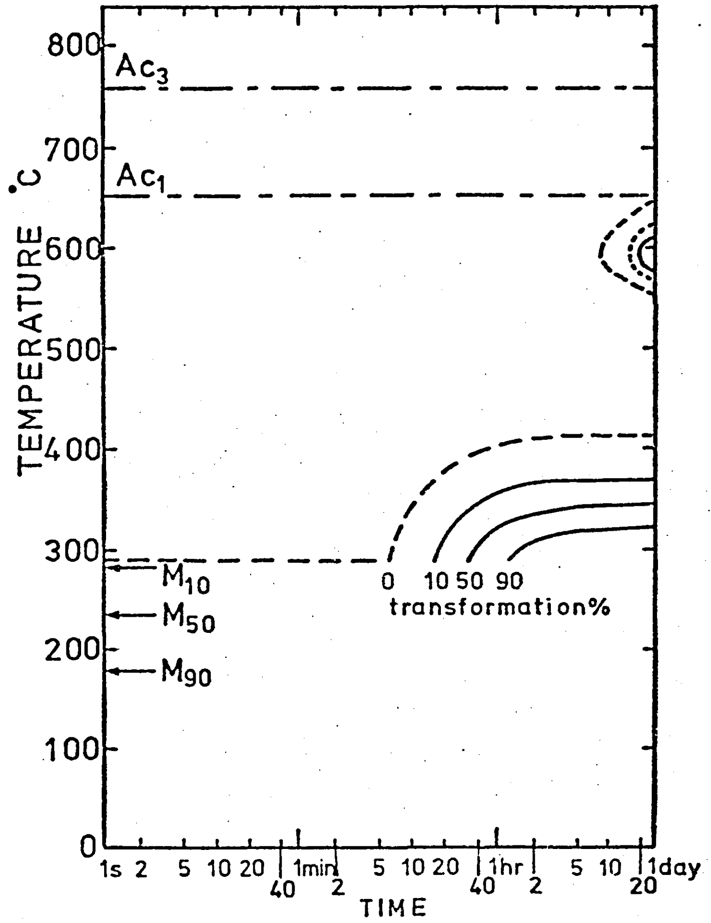
TEMPERATURE °C
800
700
600
500
400
300
200
100
0
Ac3
Ac1
M10
M50
M90
0
10
50
90
transformation%
1s
2
5
10
20
40
1min
2
5
10
20
40
1hr
2
5
10
20
1day
TIME

FIGURE 80: Dilatometer curve for result (e) in Table 7.

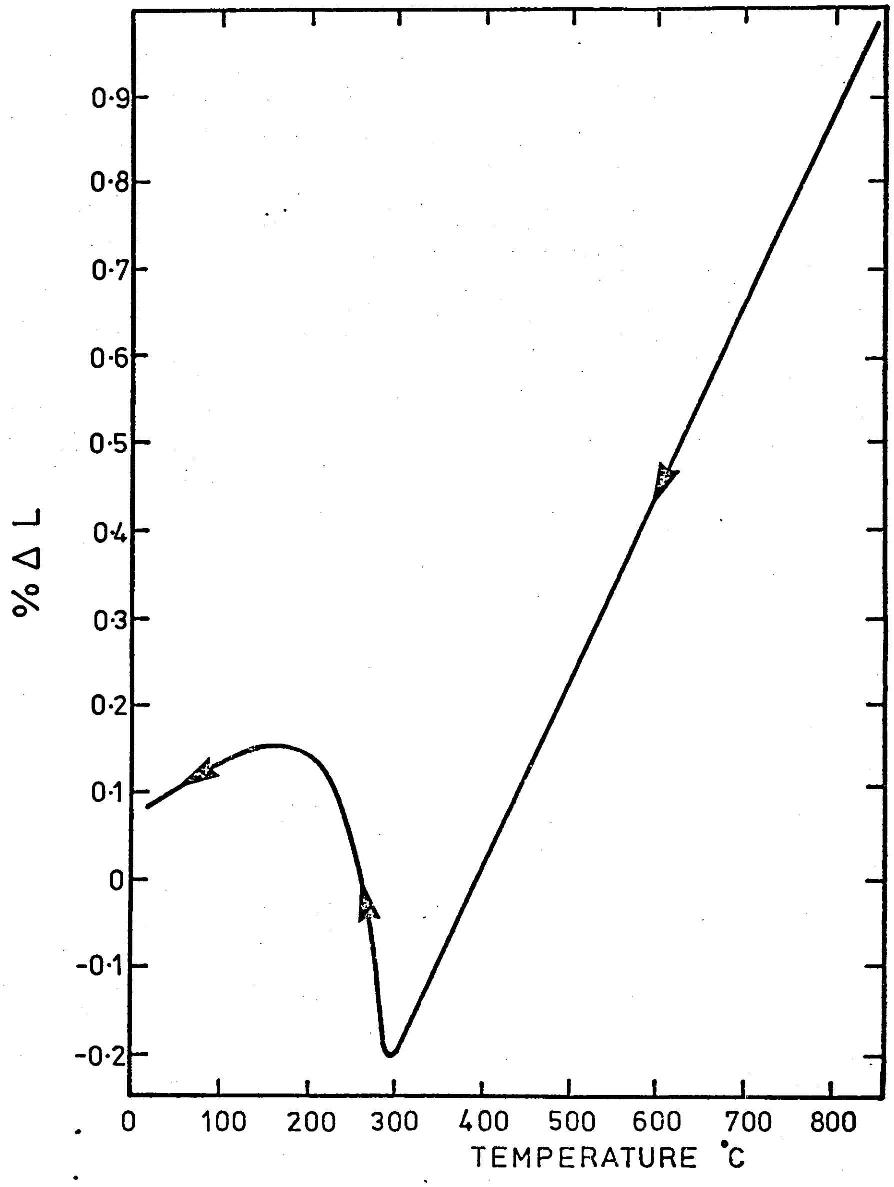
0·9
0·8
0·7
0·6
0·5
0·4
0·3
0·2
0·1
0
-0·1
-0·2
% Δ L
0
100
200
300
400
500
600
700
800
TEMPERATURE °C

FIGURE 81: Apparatus used for the austenitising and quenching of specimens prior to the determination of mechanical properties in the metastable austenitic condition.

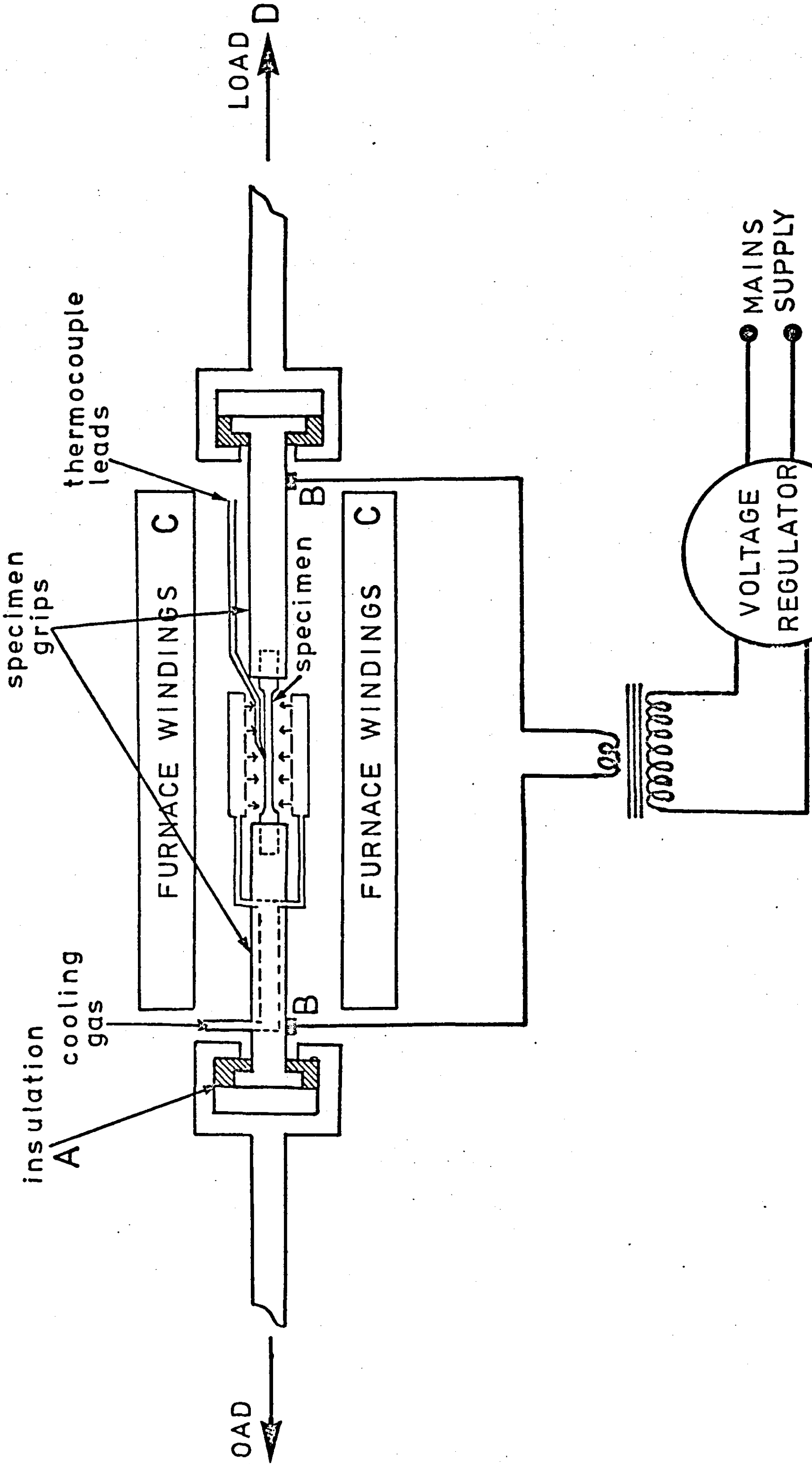
LOAD D
thermocouple leads
specimen grips
specimen
FURNACE WINDINGS C
FURNACE WINDINGS C
B
B
insulation A
cooling gas
LOAD E
VOLTAGE REGULATOR
MAINS SUPPLY

FIGURE 82: Calculated variation in strain with time for a plate cooled with a Biot No. of 4 and using the same mechanical property data as Fletcher[144].

($\dot{\varepsilon}$ = strain rate, s^{-1})

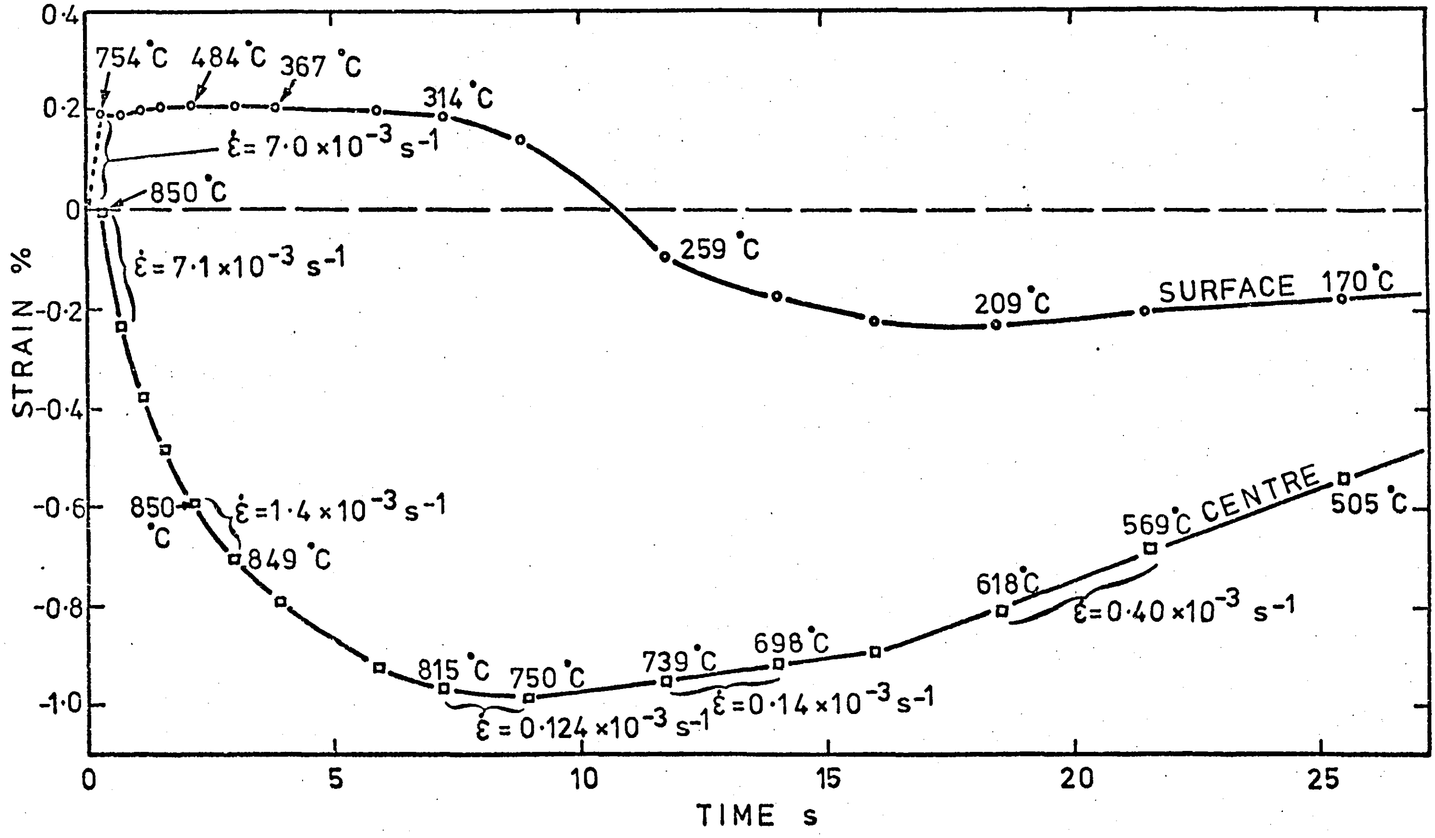

754 °C
484 °C
367 °C
314 °C
$\dot{\varepsilon}= 7{\cdot}0 \times 10^{-3}\ s^{-1}$
850 °C
$\dot{\varepsilon}= 7{\cdot}1 \times 10^{-3}\ s^{-1}$
259 °C
209 °C
SURFACE
170 °C
850 °C
$\dot{\varepsilon}=1{\cdot}4 \times 10^{-3}\ s^{-1}$
849 °C
815 °C
750 °C
$\dot{\varepsilon} = 0{\cdot}124 \times 10^{-3}\ s^{-1}$
739 °C
698 °C
$\dot{\varepsilon}=0{\cdot}14 \times 10^{-3}\ s^{-1}$
618 °C
569 °C
CENTRE
505 °C
$\dot{\varepsilon}=0{\cdot}40 \times 10^{-3}\ s^{-1}$
STRAIN %
0·4
0·2
0
-0·2
-0·4
-0·6
-0·8
-1·0
TIME s
0
5
10
15
20
25

FIGURE 83: Variation of uniaxial flow stress with temperature in 835M30 specimens that had been initially austenitised at 850°C.

Broken lines - experimental results

Solid lines - approximations of austenite flow stress used in subsequent calculations of thermal stress.

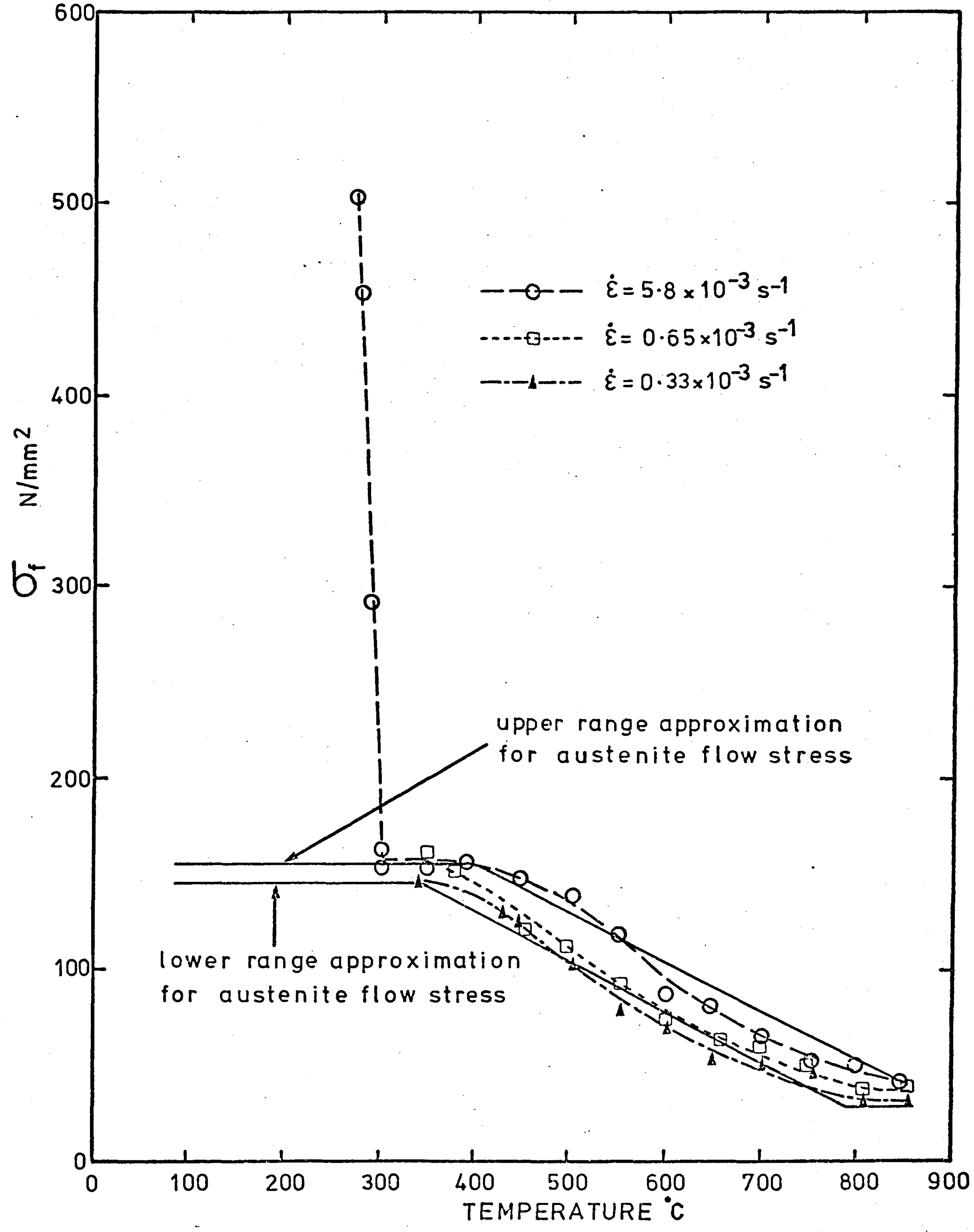

σ_f N/mm^2
600
500
400
300
200
100
0
0
100
200
300
400
500
600
700
800
900
TEMPERATURE °C
$\dot{\varepsilon} = 5{\cdot}8 \times 10^{-3}\ s^{-1}$
$\dot{\varepsilon} = 0{\cdot}65 \times 10^{-3}\ s^{-1}$
$\dot{\varepsilon} = 0{\cdot}33 \times 10^{-3}\ s^{-1}$
upper range approximation for austenite flow stress
lower range approximation for austenite flow stress

FIGURE 84: Method used to determine the volume fractions of austenite and martensite present during the transformation range from the dilatometer curve.

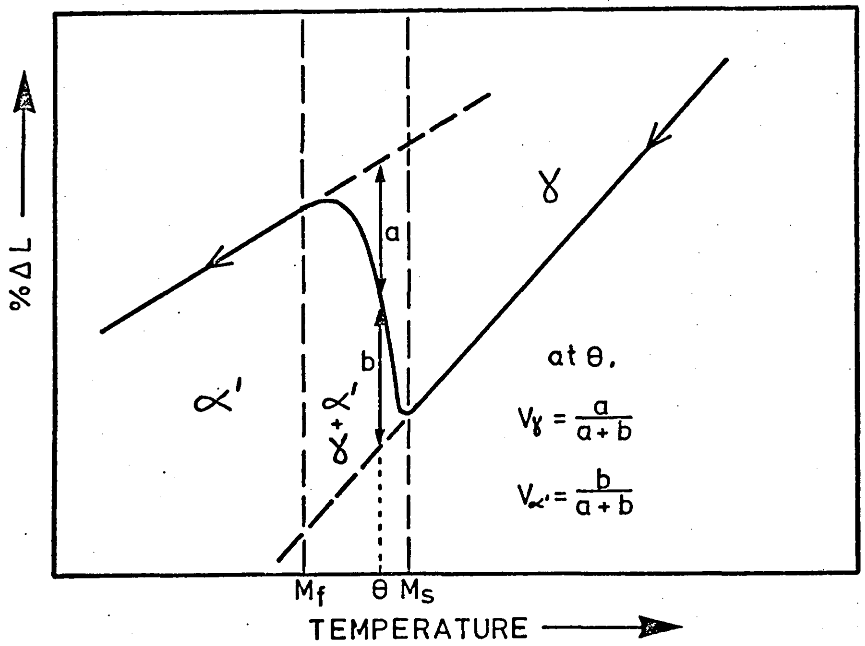
% Δ L
γ
a
b
α'
γ + α'
at θ,
$V_\gamma = \frac{a}{a+b}$
$V_{\alpha'} = \frac{b}{a+b}$
M_f
θ
M_s
TEMPERATURE

FIGURE 85: Variation of strain hardening coefficient with temperature of 835M30 specimens that had initially been austenitised at 850°C.

(a) Strain hardening coefficient W_1 ($0 \rightarrow 0.5\% \ \varepsilon_p$)

(b) Strain hardening coefficient W_2 ($0.5 \rightarrow 1.0\% \ \varepsilon_p$)

The solid lines in (a) and (b) represent the approximations of W_1 and W_2 used in the subsequent calculations of thermal stress.

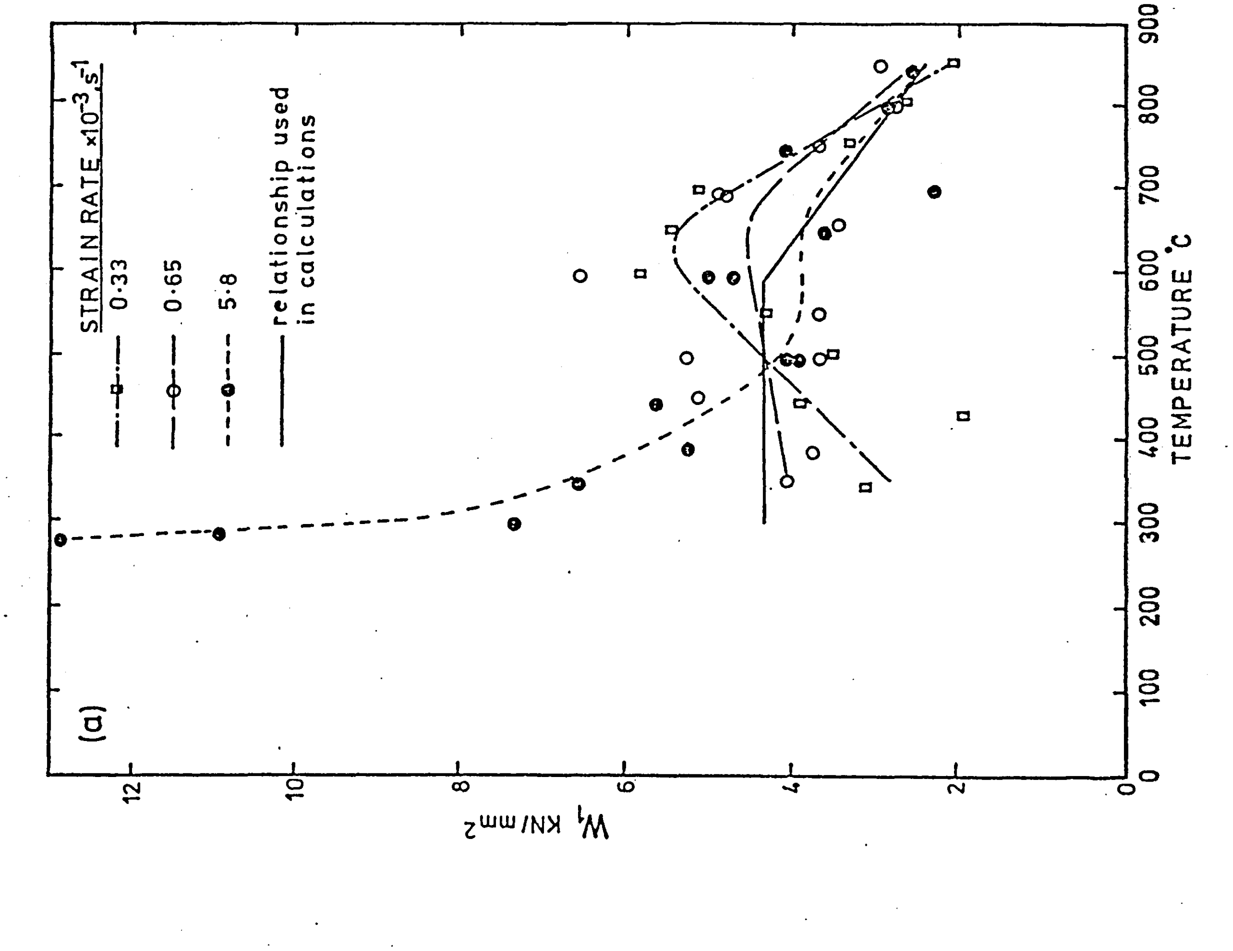
(a)
W₁ KN/mm²
TEMPERATURE °C
STRAIN RATE ×10⁻³.s⁻¹
0·33
0·65
5·8
relationship used in calculations
0
2
4
6
8
10
12
0
100
200
300
400
500
600
700
800
900

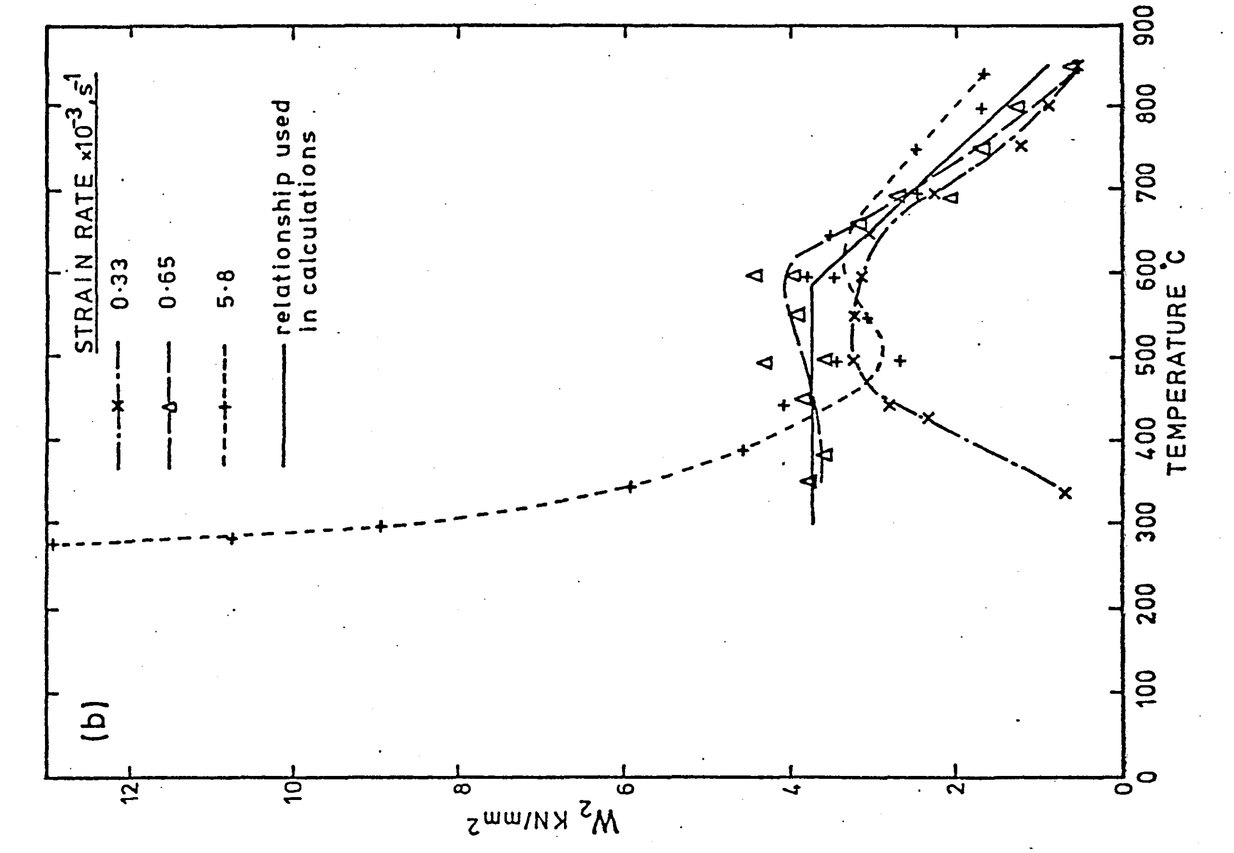
(b)
W₂ KN/mm²
TEMPERATURE °C
STRAIN RATE ×10⁻³.s⁻¹
0·33
0·65
5·8
relationship used in calculations
0
2
4
6
8
10
12
0
100
200
300
400
500
600
700
800
900

FIGURE 86: Relaxation of stress with time in specimens of 835M30 that had been austenitised at 850°C and then strained at the appropriate test temperature to give 1% plastic strain.

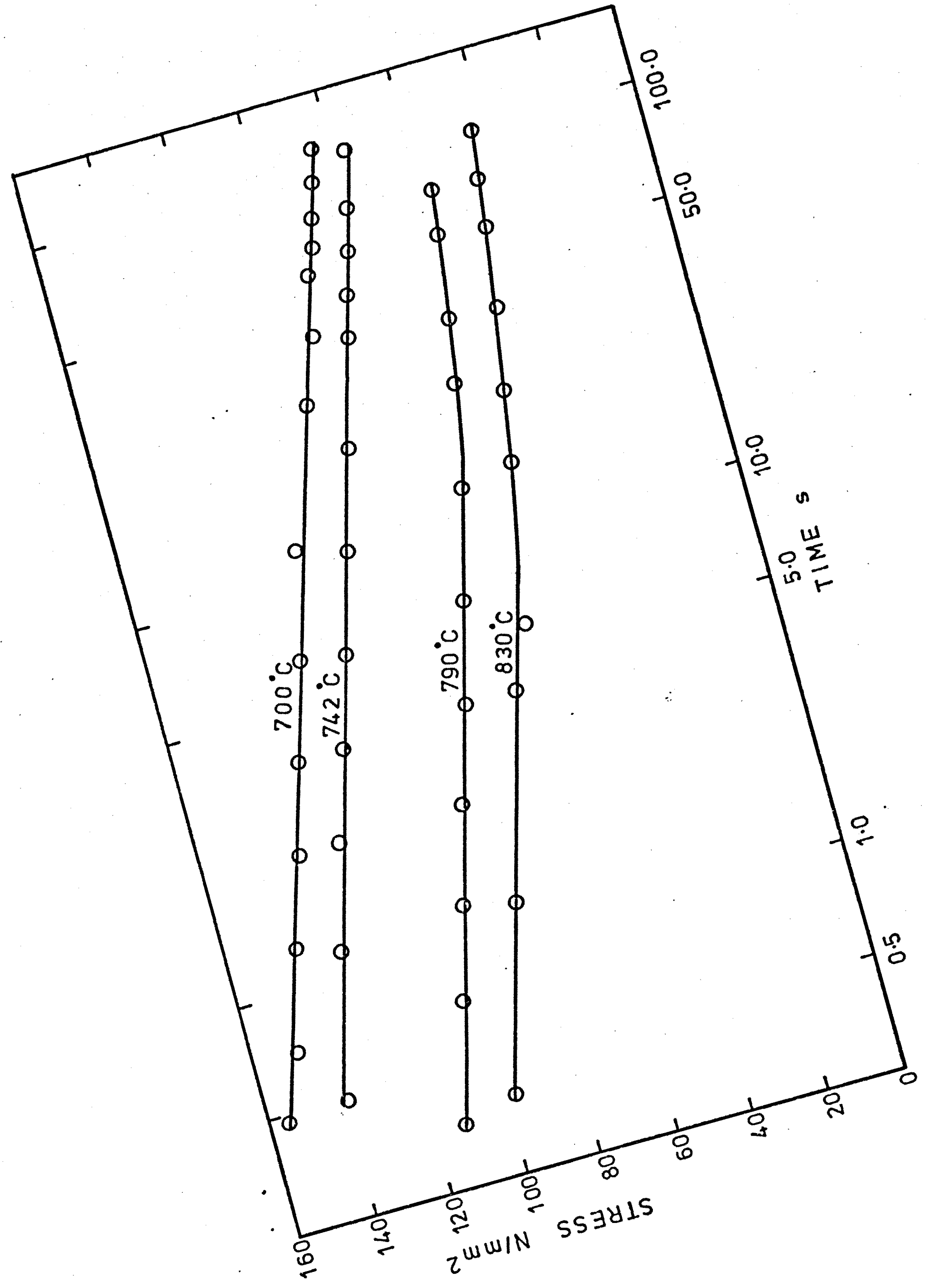

STRESS N/mm2
160
140
120
100
80
60
40
20
0
TIME s
0·5
1·0
5·0
10·0
50·0
100·0
700°C
742°C
790°C
830°C

FIGURE 87: Influence of the number of elements in the half-plate on the thermal stresses and strains calculated in a plate with a Biot No. of 5.03 (see Table 9).

(a) Residual strain distribution

(b) Residual stress distribution

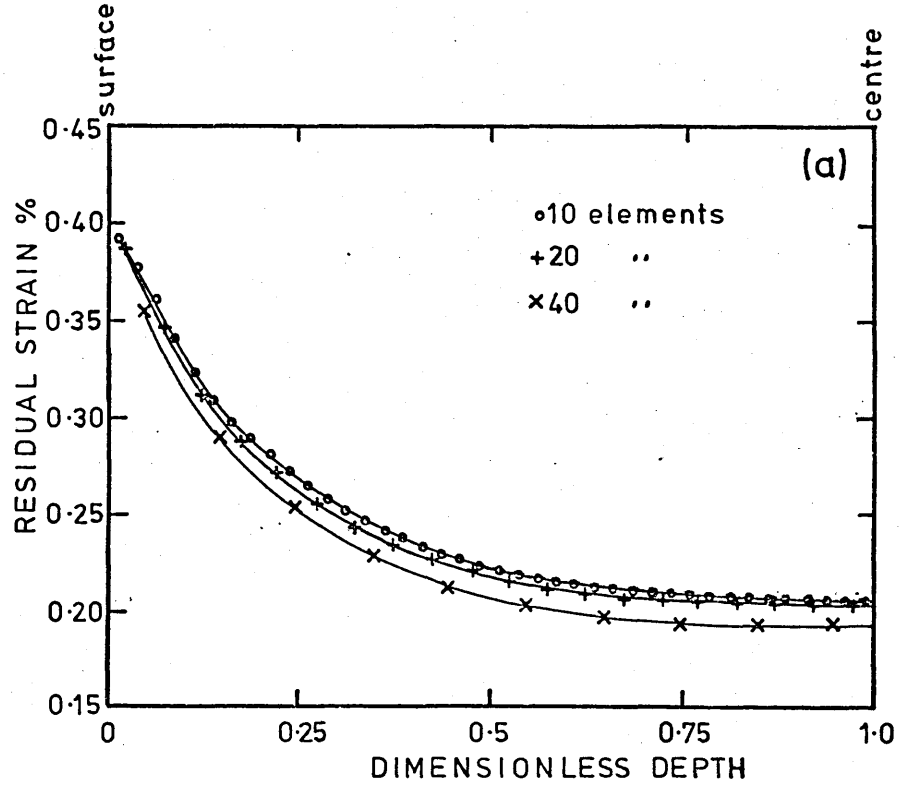
surface
centre
(a)
○10 elements
+20 ,,
×40 ,,
RESIDUAL STRAIN %
0·45
0·40
0·35
0·30
0·25
0·20
0·15
0
0·25
0·5
0·75
1·0
DIMENSIONLESS DEPTH

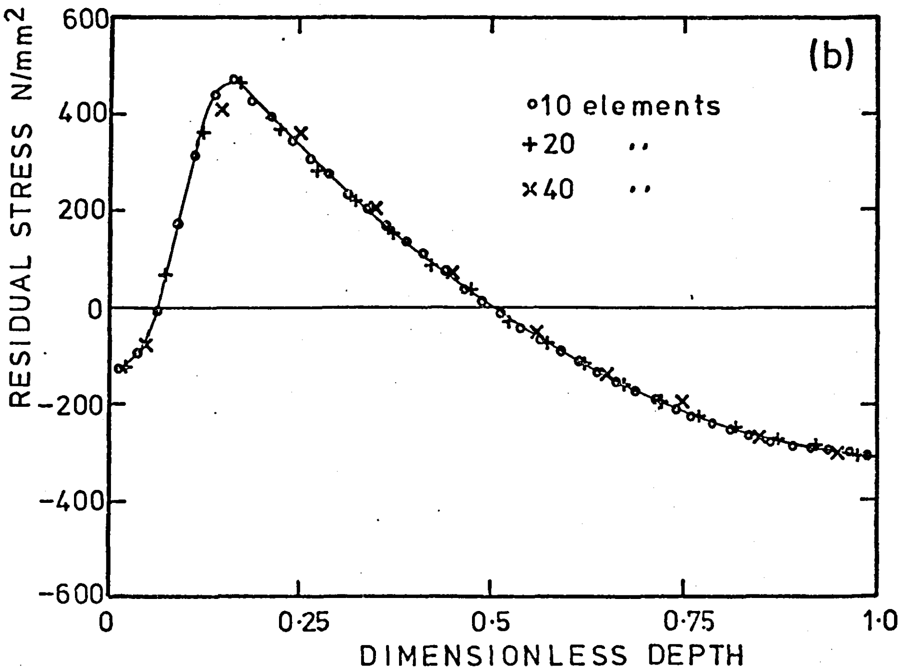
(b)
○10 elements
+20 ,,
×40 ,,
RESIDUAL STRESS N/mm²
600
400
200
0
−200
−400
−600
0
0·25
0·5
0·75
1·0
DIMENSIONLESS DEPTH

FIGURE 88: Influence of the maximum level of unbalanced average stress at the end of the plasticity iterations, on the residual stress and strain at the surface of the plate (see Table 9 for data employed in the calculation).

FIGURE 89: Influence of the total number of time steps on the residual stress and strain at both the surface and centre of the plate (see Table 9 for data employed in the calculation).

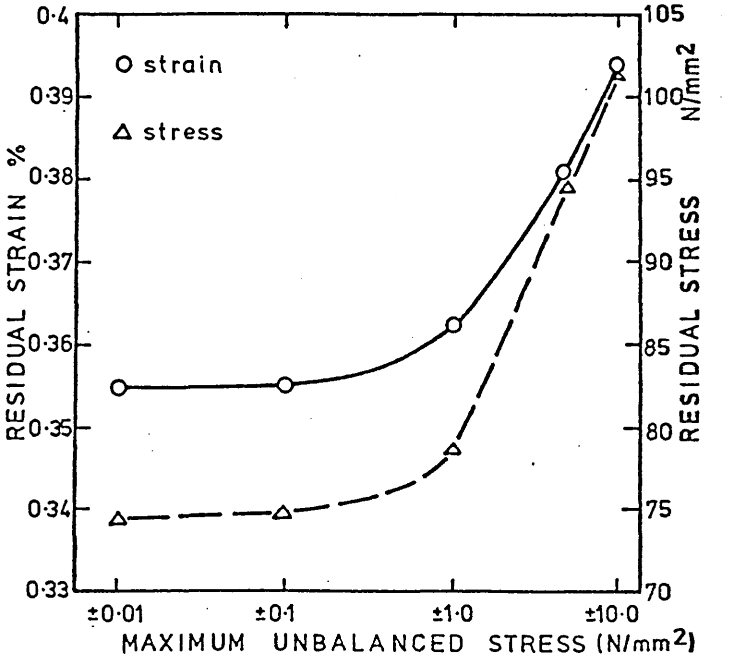
O strain
Δ stress
RESIDUAL STRAIN %
RESIDUAL STRESS N/mm2
0·4
0·39
0·38
0·37
0·36
0·35
0·34
0·33
105
100
95
90
85
80
75
70
±0·01
±0·1
±1·0
±10·0
MAXIMUM UNBALANCED STRESS (N/mm2)

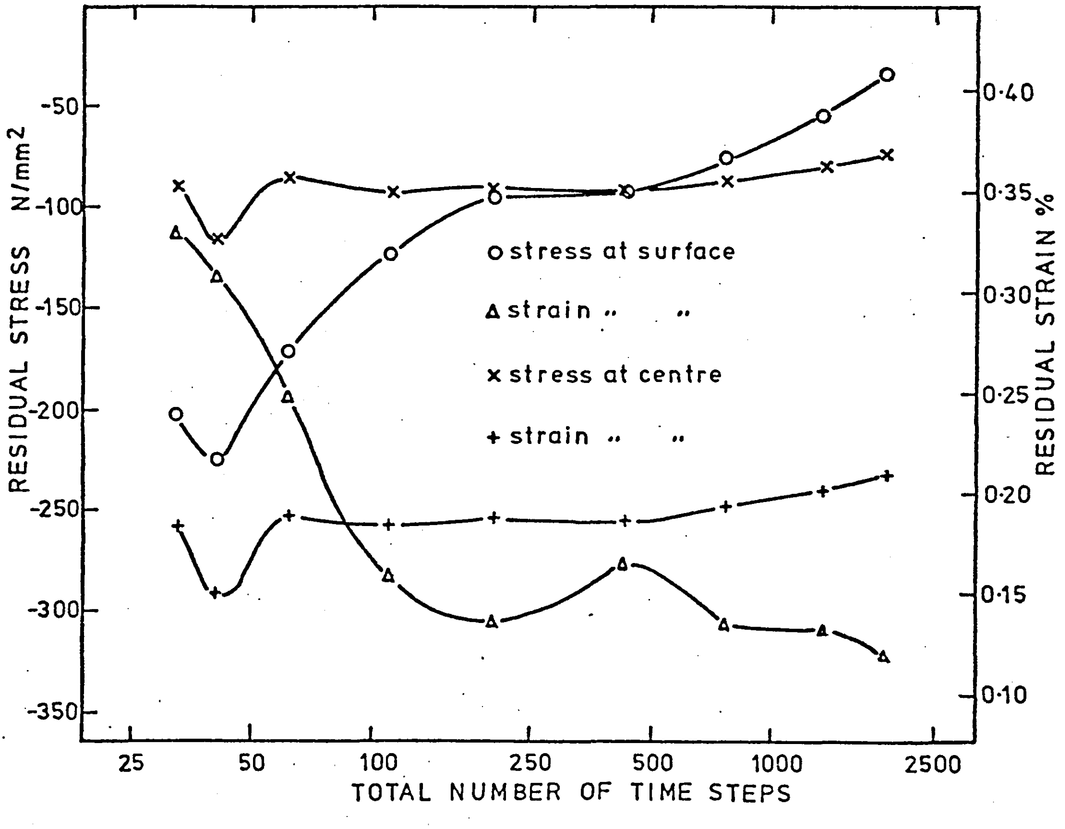
o stress at surface
Δ strain " "
x stress at centre
+ strain " "
RESIDUAL STRESS N/mm2
RESIDUAL STRAIN %
-50
-100
-150
-200
-250
-300
-350
0·40
0·35
0·30
0·25
0·20
0·15
0·10
25
50
100
250
500
1000
2500
TOTAL NUMBER OF TIME STEPS

FIGURE 90: Calculated stress and strain at the centre and surface of a 40mm plate of 835M30 during water quenching. (Computer program run PR1/W40/hAv/UFS - see Table 11).

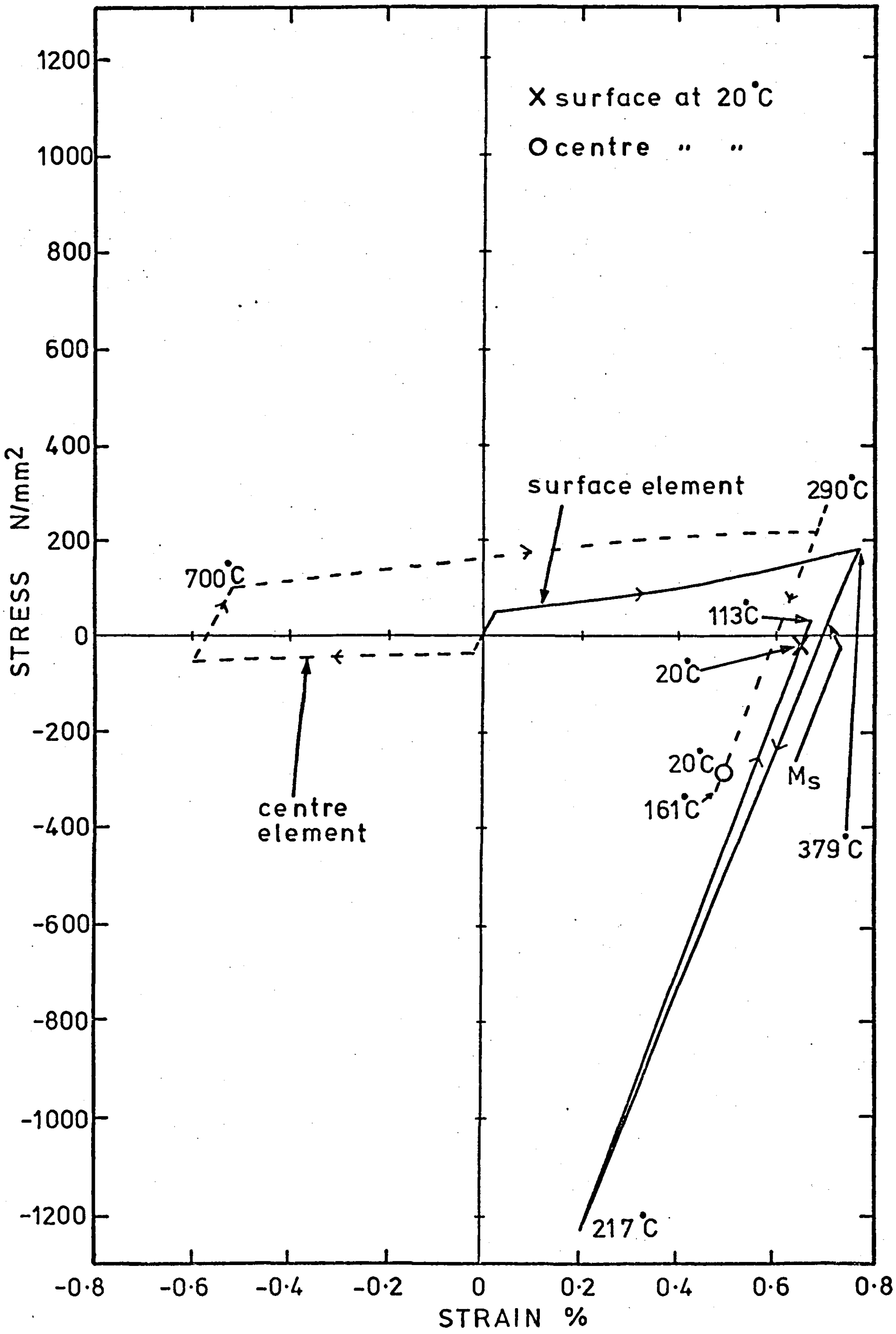
X surface at 20°C
O centre " "
surface element
centre element
700°C
290°C
113°C
20°C
20°C
161°C
Ms
379°C
217°C
STRESS N/mm2
STRAIN %
1200
1000
800
600
400
200
0
-200
-400
-600
-800
-1000
-1200
-0·8
-0·6
-0·4
-0·2
0
0·2
0·4
0·6
0·8

FIGURE 91: Calculated stress distribution in a 40mm plate of 835M30 during water quenching. (Computer program run PR1/W40/hAv/UFS - see Table 11).

(a) t = 3.6s

(b) t = 22.2s

(c) t = 55.7s

(d) t = 67.6s

(e) t = ∞

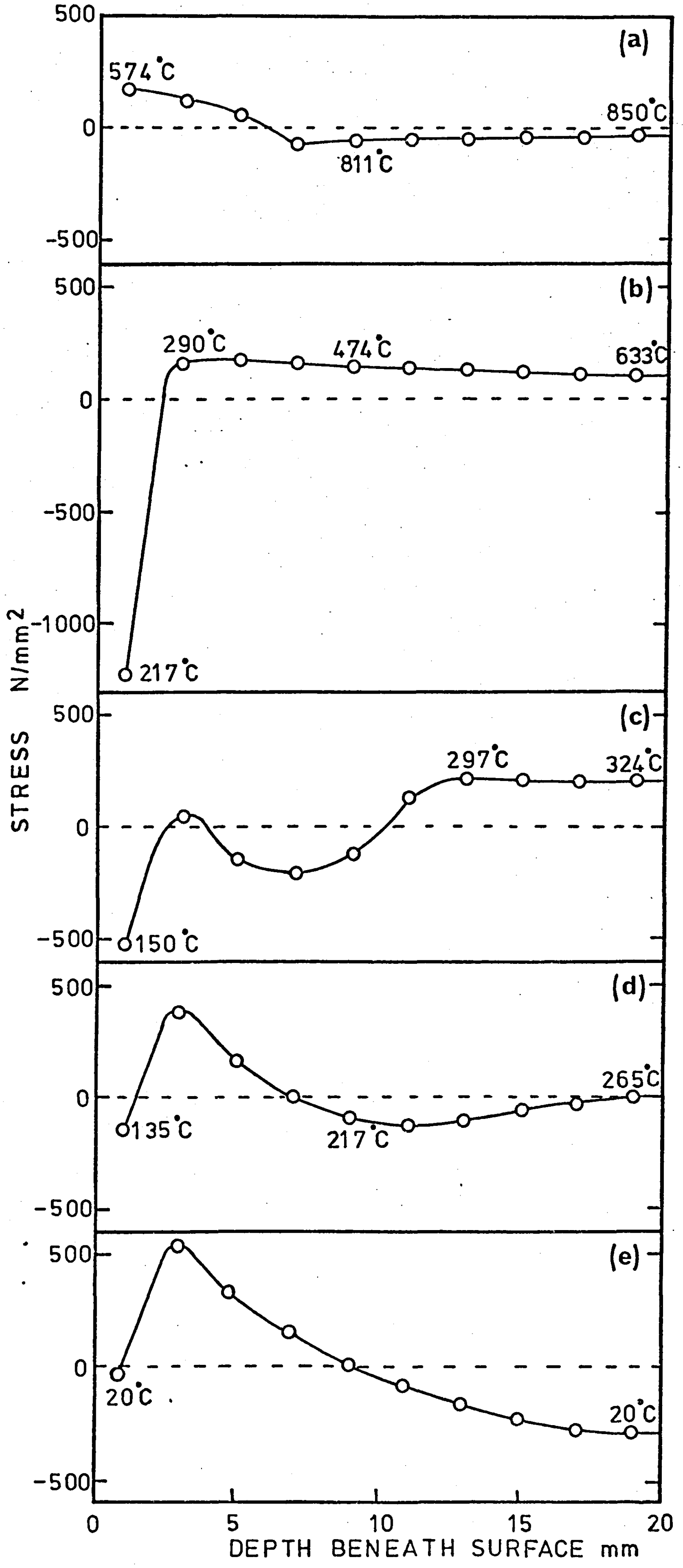
(a)
574°C
850°C
811°C
(b)
290°C
474°C
633°C
217°C
(c)
297°C
324°C
150°C
(d)
265°C
135°C
217°C
(e)
20°C
20°C
STRESS N/mm^2
500
0
-500
-1000
0
5
10
15
20
DEPTH BENEATH SURFACE mm

FIGURE 92: Influence of the austenite flow stress and the surface heat transfer coefficient on the calculated residual stress distribution in a 40mm plate of 835M30 after water quenching.

Computer program runs:

PR3/W40/hMax/UFS)
PR4/W40/hMin/UFS) see Table 11
PR5/W40/hMax/LFS)
PR6/W40/hMin/LFS)

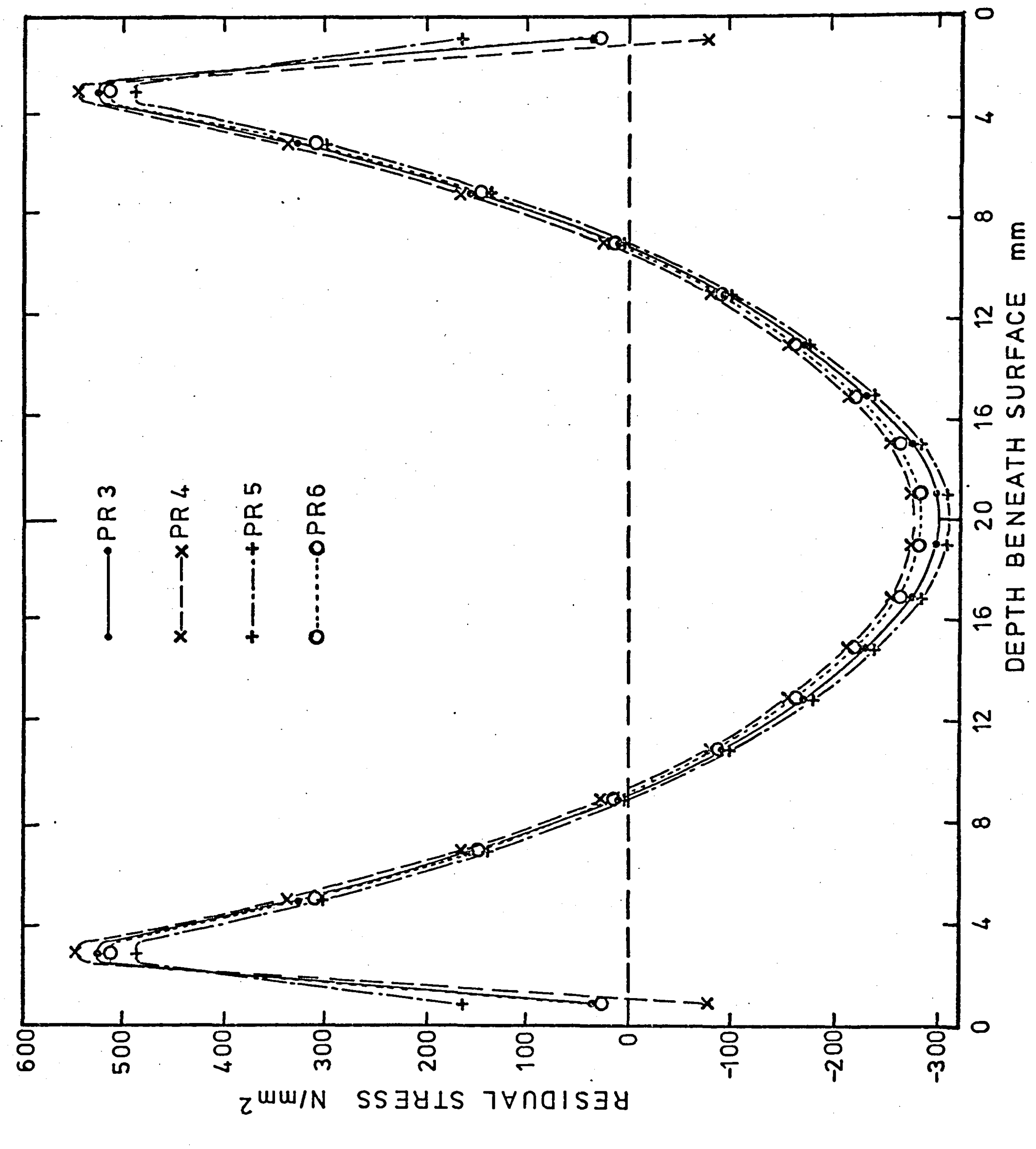
RESIDUAL STRESS N/mm²
600
500
400
300
200
100
0
-100
-200
-300
DEPTH BENEATH SURFACE mm
0
4
8
12
16
20
16
12
8
4
0
PR 3
PR 4
PR 5
PR6

FIGURE 93: Influence of the austenite flow stress and the surface heat transfer coefficient on the residual strain in a 40mm plate of 835M30 after water quenching.

Computer program runs:

PR3/W40/hMax/UFS)
PR4/W40/hMin/UFS) see Table 11
PR5/W40/hMax/LFS)
PR6/W40/hMin/LFS)

(Note the residual strain includes the overall increase in volume accompanying the hardening process).

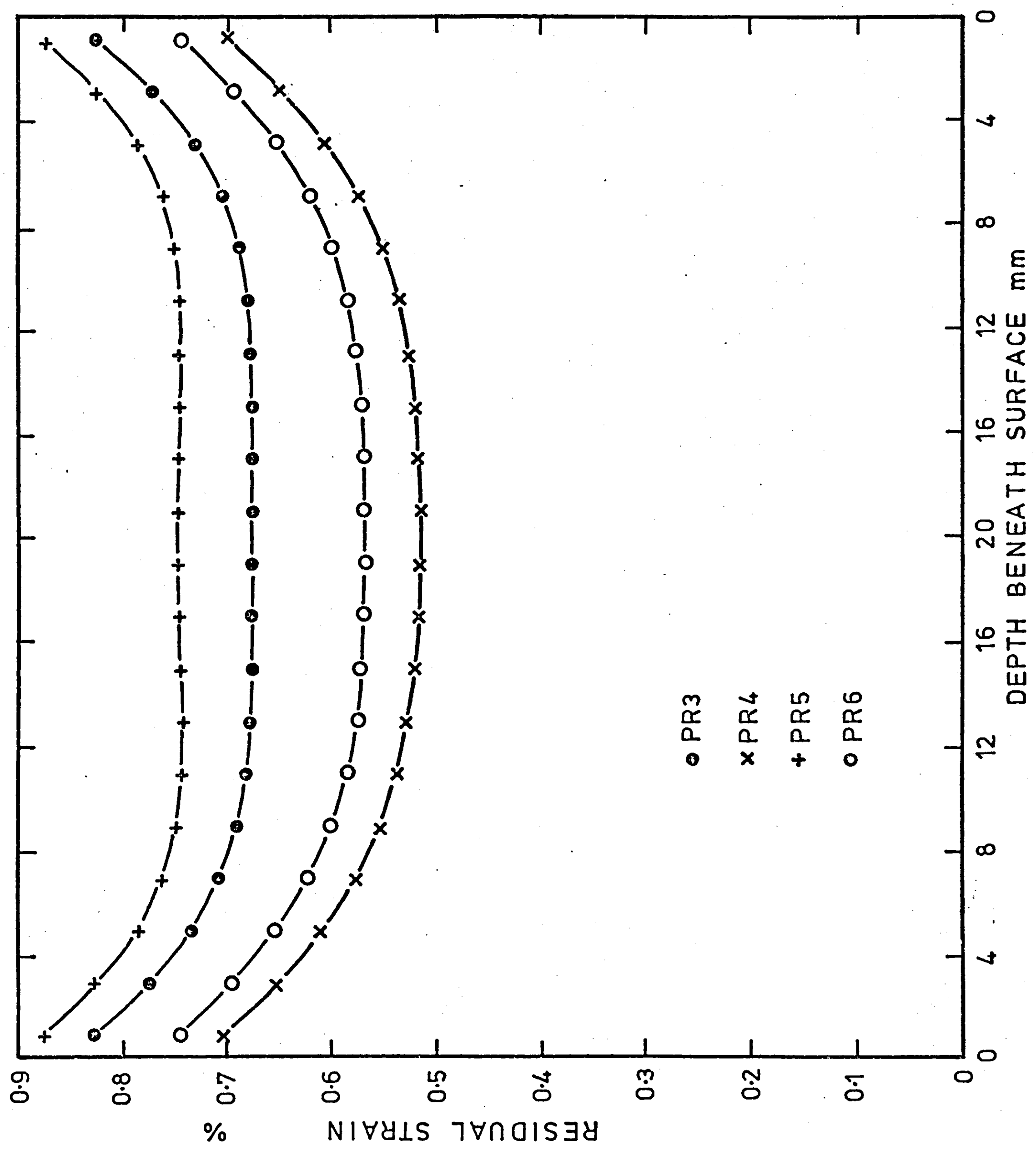
RESIDUAL STRAIN %
0·9
0·8
0·7
0·6
0·5
0·4
0·3
0·2
0·1
0
DEPTH BENEATH SURFACE mm
0
4
8
12
16
20
16
12
8
4
0
PR3
PR4
PR5
PR6

FIGURE 94: Calculated stress and strain at the centre and surface of a 20mm plate of 835M30 during water quenching. (Computer program run PR7/W20/hAv/UFS - see Table 11).

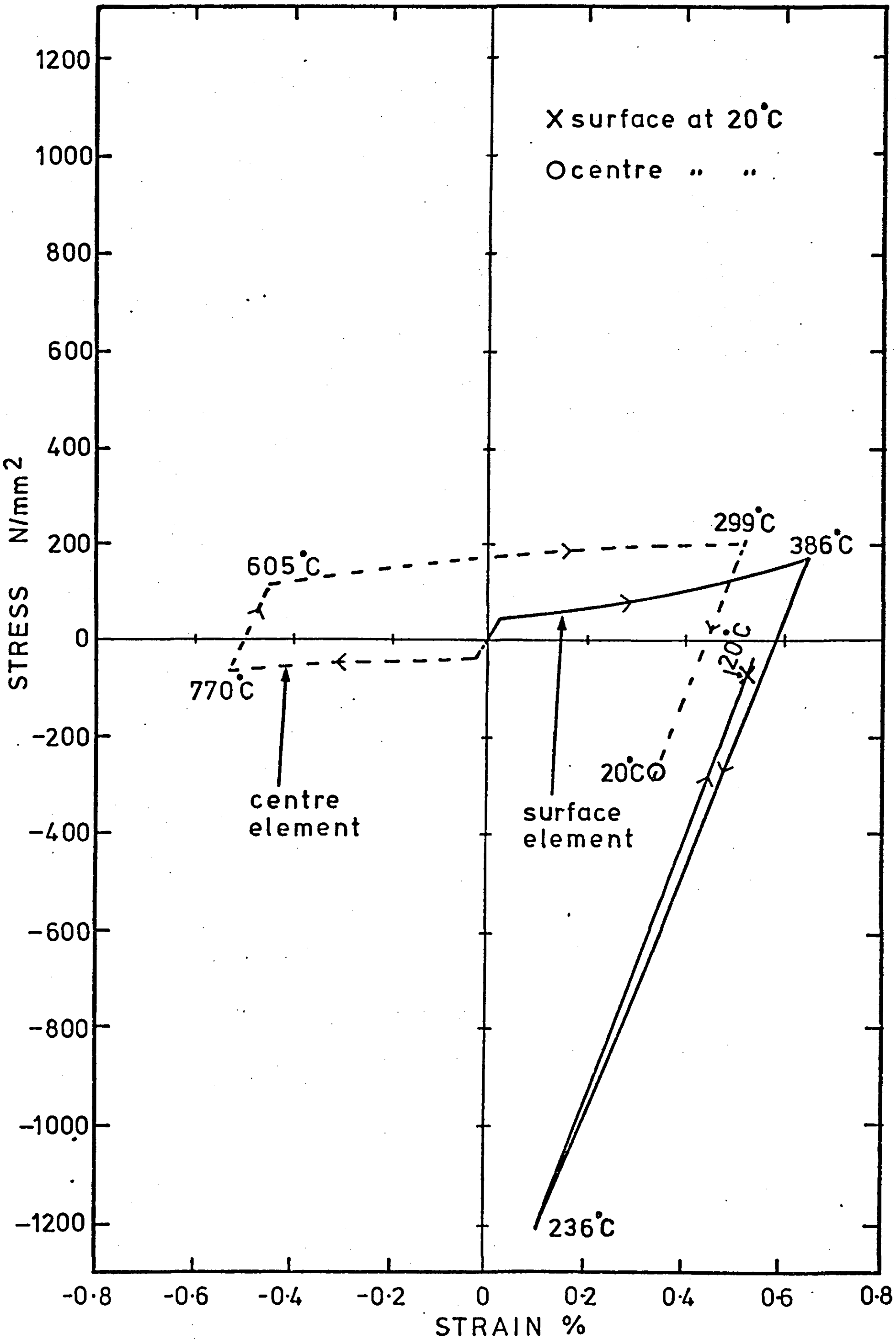
X surface at 20°C
O centre " "
STRESS N/mm2
STRAIN %
1200
1000
800
600
400
200
0
-200
-400
-600
-800
-1000
-1200
-0·8
-0·6
-0·4
-0·2
0
0·2
0·4
0·6
0·8
605°C
770°C
299°C
386°C
120°C
20°C
236°C
centre element
surface element

FIGURE 95: Influence of the austenite flow stress and the surface heat transfer coefficient on the calculated residual stress distribution in a 20mm plate of 835M30 after water quenching.

Computer program runs:

PR9/W20/hMax/UFS)
PR10/W20/hMin/UFS)
PR11/W20/hMax/LFS) see Table 11
PR12/W20/hMin/LFS)

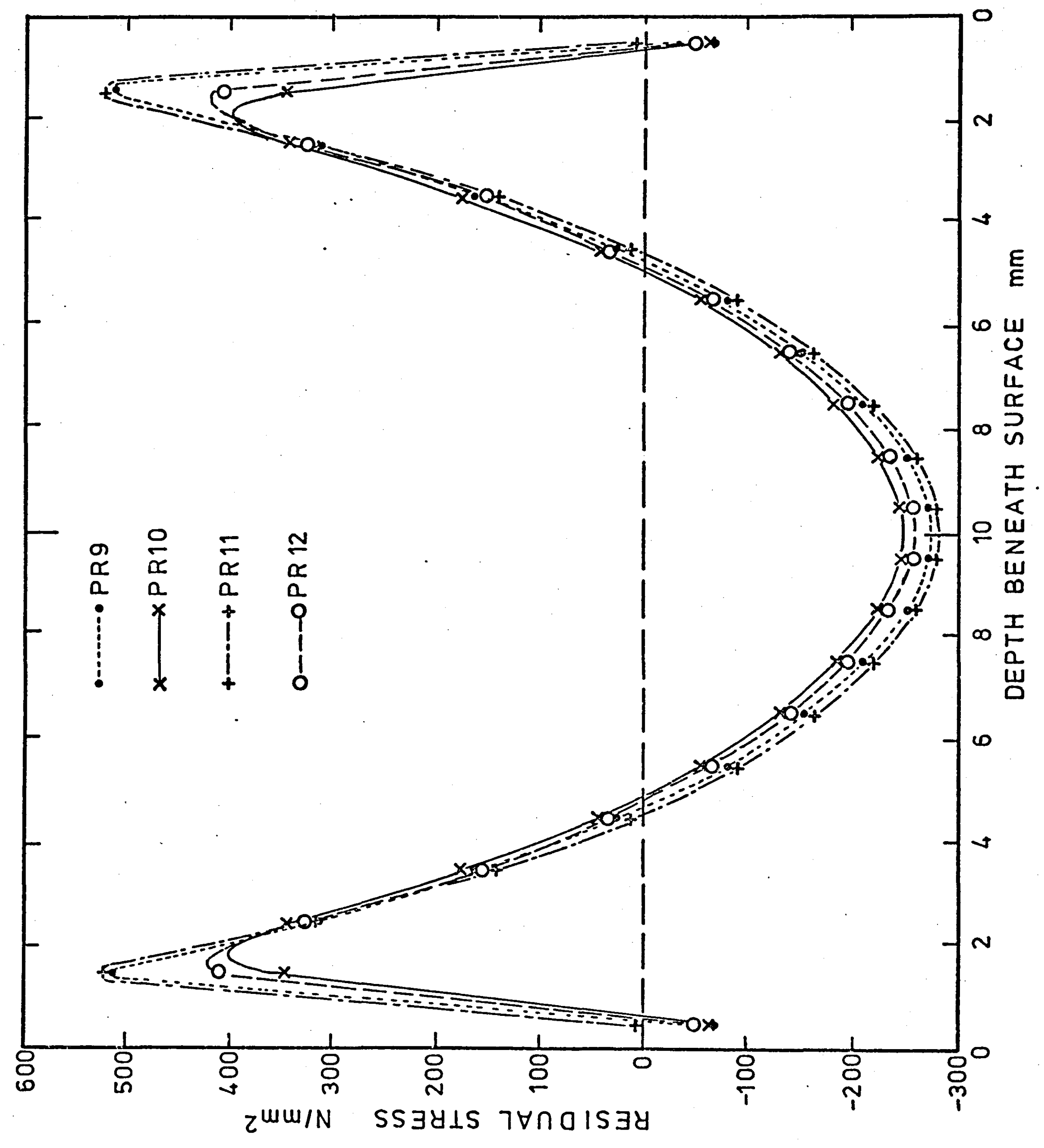
RESIDUAL STRESS N/mm²
600
500
400
300
200
100
0
-100
-200
-300
DEPTH BENEATH SURFACE mm
0
2
4
6
8
10
8
6
4
2
0
PR9
PR10
PR11
PR12

FIGURE 96: Influence of the austenite flow stress and the surface heat transfer coefficient on the residual strain in a 20mm plate of 835M30 after water quenching.

Computer program runs:

PR9/W20/hMax/UFS)
PR10/W20/hMin/UFS) see Table 11
PR11/W20/hMax/LFS)
PR12/W20/hMin/LFS)

(Note the residual strain includes the overall volume increase accompanying the hardening process).

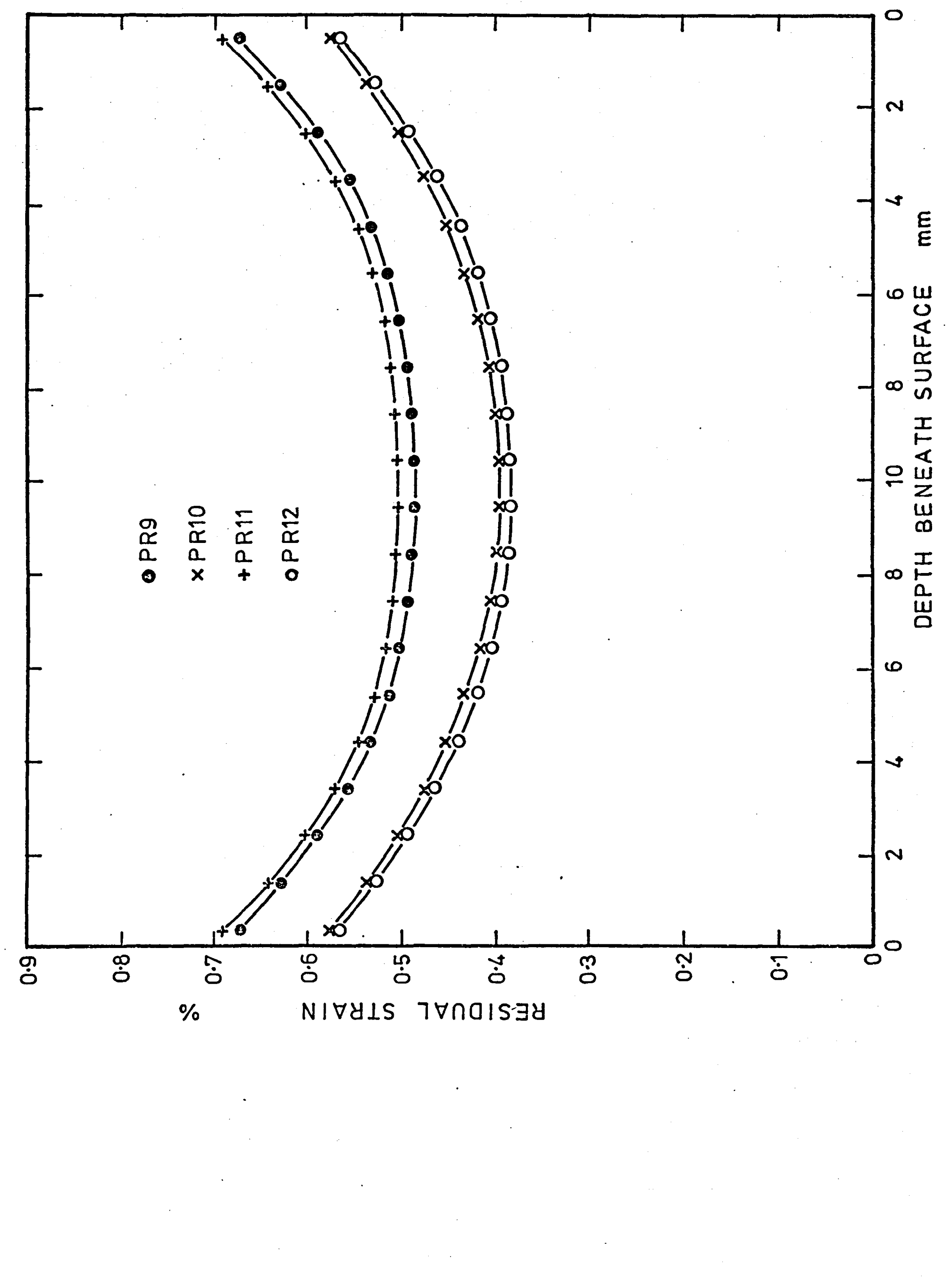

RESIDUAL STRAIN %
0·9
0·8
0·7
0·6
0·5
0·4
0·3
0·2
0·1
0
DEPTH BENEATH SURFACE mm
0
2
4
6
8
10
8
6
4
2
0
● PR9
× PR10
+ PR11
○ PR12

FIGURE 97: Calculated stress and strain at the centre and surface of a 20mm plate of 835M30 during oil quenching.

(Computer program run PR13/OIL20/UFS - see Table 11).

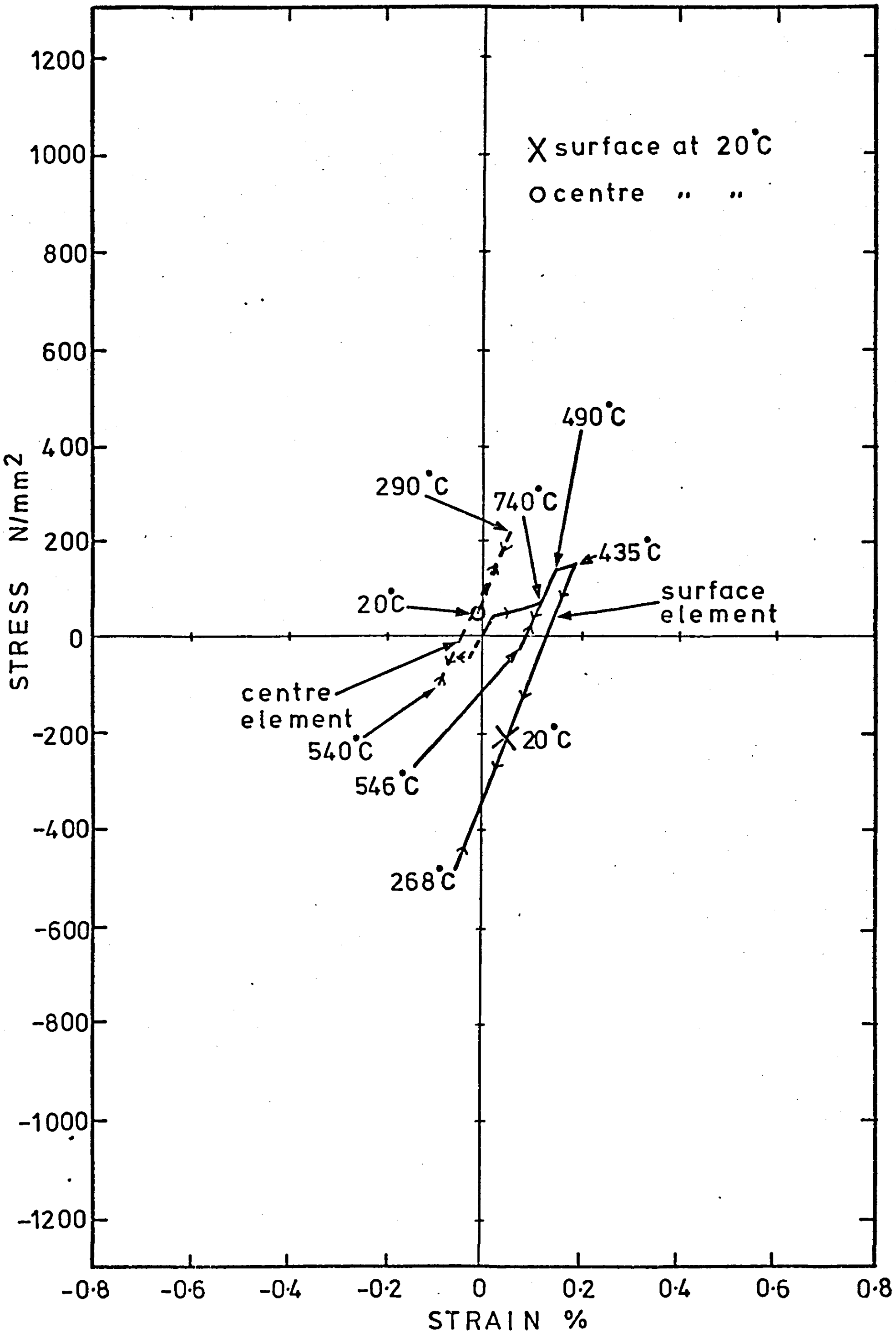
X surface at 20°C
O centre " "
STRESS N/mm²
STRAIN %
1200
1000
800
600
400
200
0
-200
-400
-600
-800
-1000
-1200
-0·8
-0·6
-0·4
-0·2
0
0·2
0·4
0·6
0·8
490°C
290°C
740°C
435°C
20°C
surface element
centre element
540°C
546°C
20°C
268°C

FIGURE 98: Calculated stress distribution in a 20mm plate of 835M30 during oil quenching. (Computer program run PR13/OIL20/UFS - see Table 11).

(a) t = 4.5s

(b) t = 32.8s

(c) t = 37.9s

(d) t = 70.7s

(e) t = 116.7s

(f) t = ∞

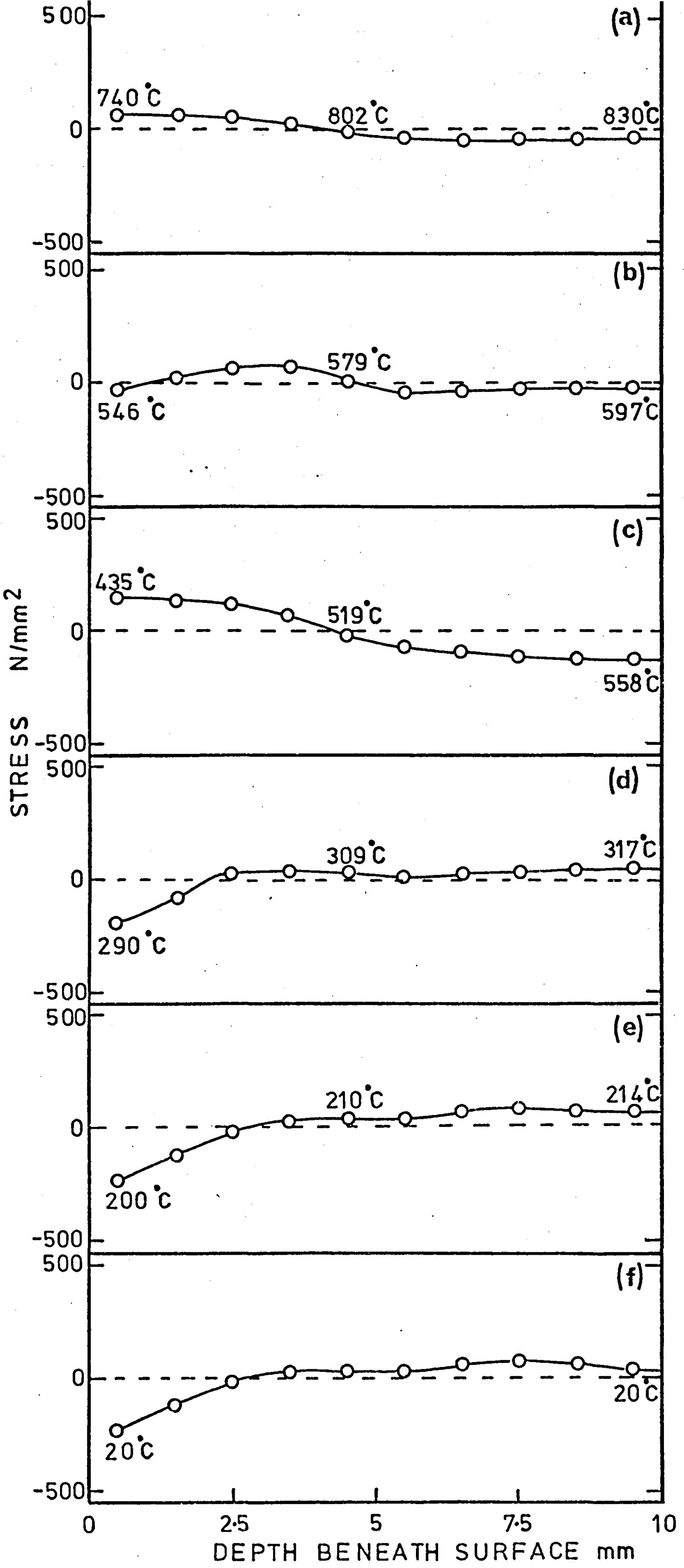

(a)
740°C
802°C
830°C
(b)
579°C
546°C
597°C
(c)
435°C
519°C
558°C
(d)
309°C
317°C
290°C
(e)
210°C
214°C
200°C
(f)
20°C
20°C
500
0
-500
STRESS N/mm^2
0
2·5
5
7·5
10
DEPTH BENEATH SURFACE mm

FIGURE 99: Influence of the austenite flow stress on the calculated residual stress distribution in a 20mm plate of 835M30 after oil quenching.

Computer program runs:

PR13/OIL20/UFS)
PR14/OIL20/LFS) See Table 11

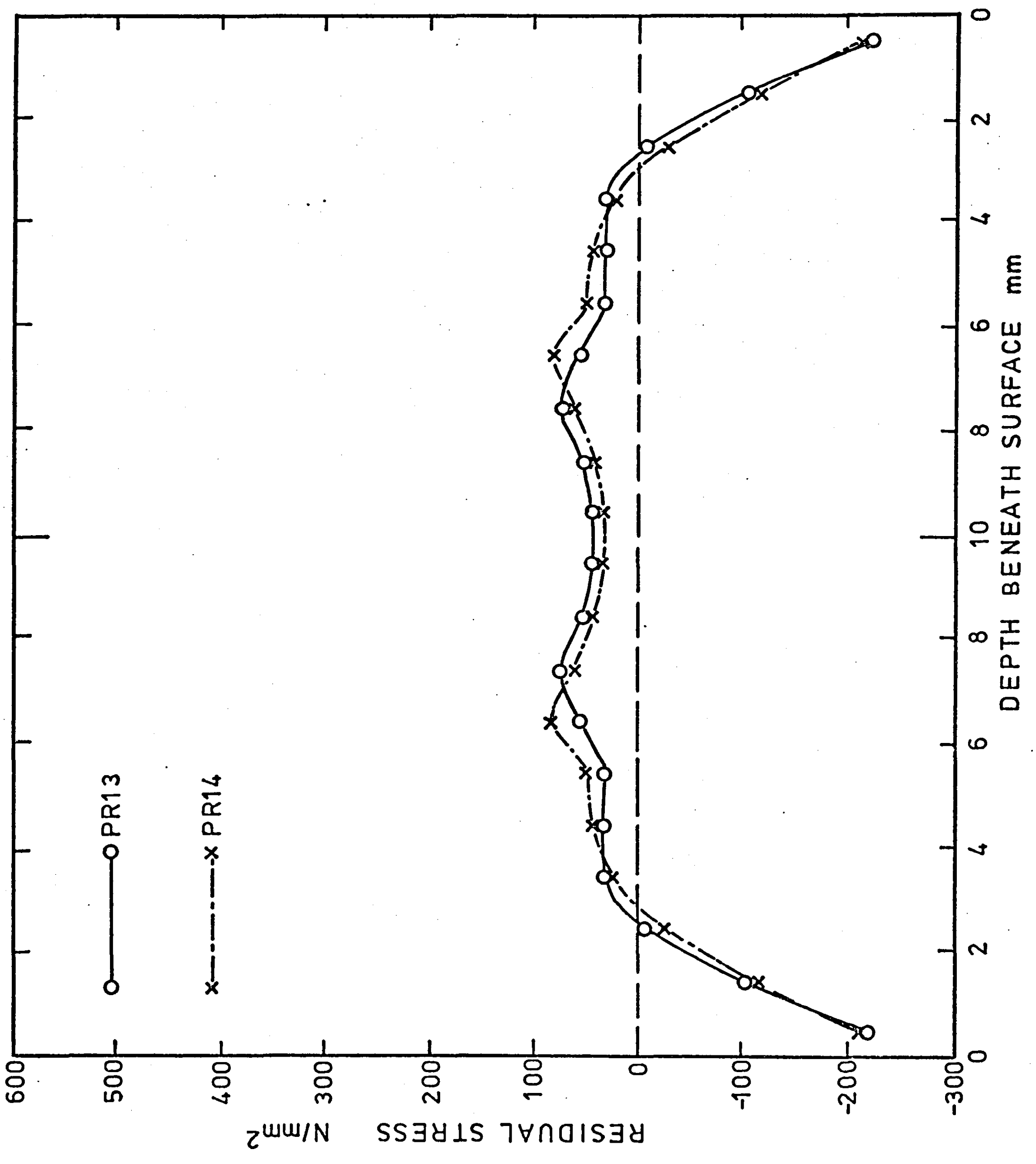
RESIDUAL STRESS N/mm^2
600
500
400
300
200
100
0
-100
-200
-300
DEPTH BENEATH SURFACE mm
0
2
4
6
8
10
8
6
4
2
0
PR13
PR14

FIGURE 100: Influence of the austenite flow stress on the residual strain in a 20mm plate of 835M30 after oil quenching.

Computer program runs:

PR13/OIL20/UFS) PR14/OIL20/LFS)	See Table 11

(Note the residual strain includes the overall volume increase accompanying the hardening process).

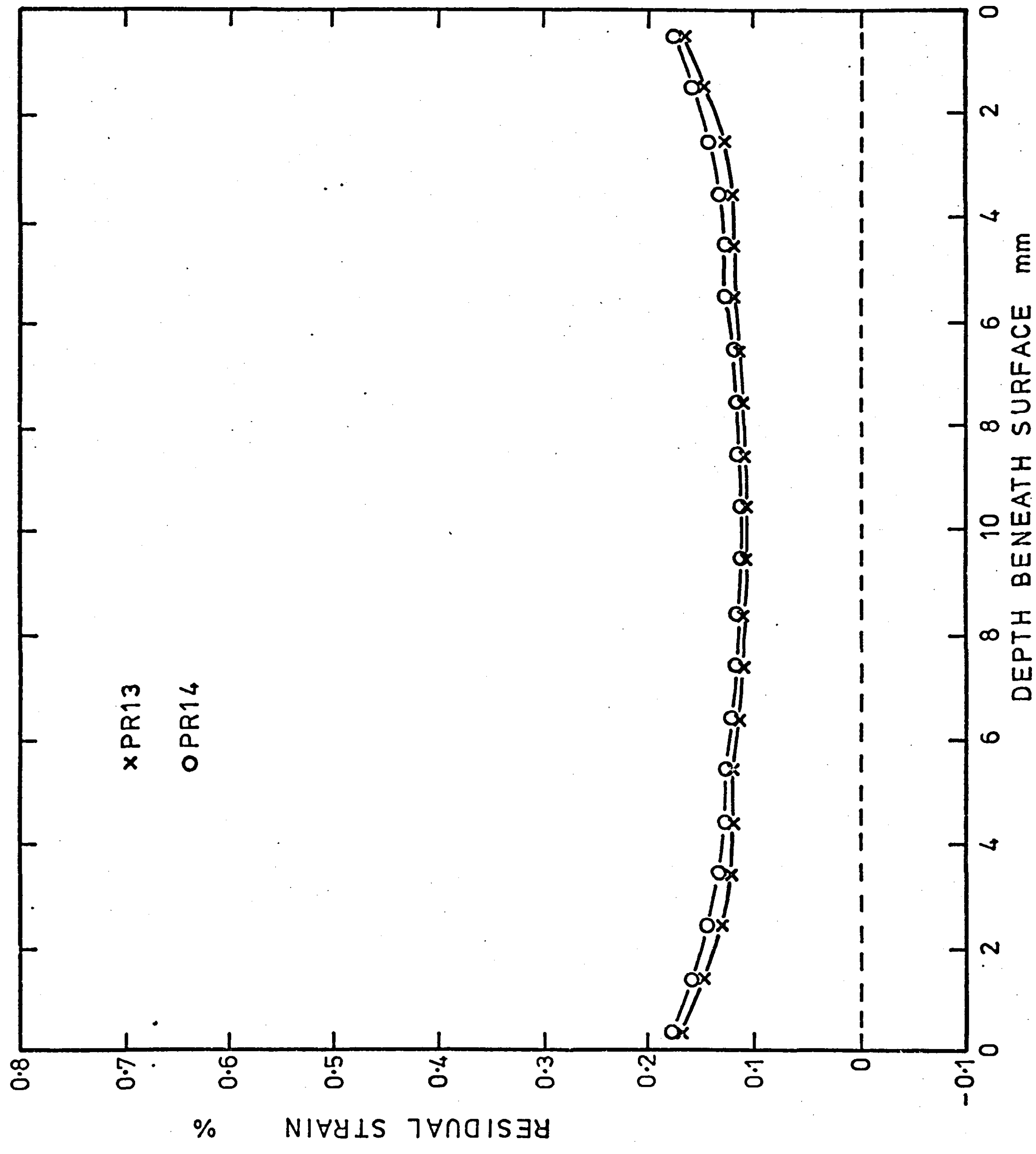
×PR13
○PR14
RESIDUAL STRAIN %
0·8
0·7
0·6
0·5
0·4
0·3
0·2
0·1
0
-0·1
DEPTH BENEATH SURFACE mm
0
2
4
6
8
10
8
6
4
2
0

FIGURE 101: Calculated stress and strain at the centre and surface of a 20mm plate of 835M30 during polymer quenching.

(Computer program run PR15/AQUA20/UFS - see Table 11.)

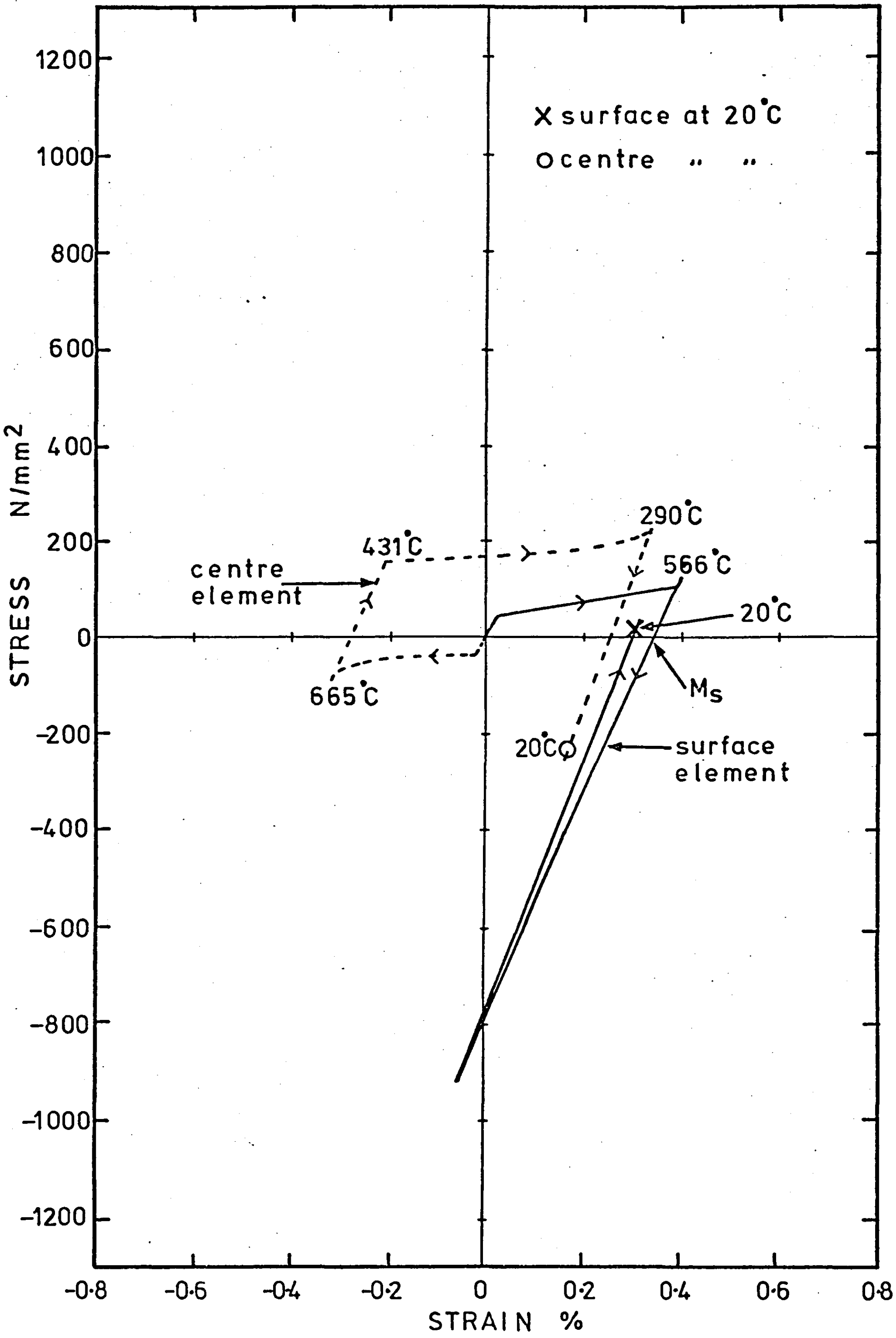

X surface at 20°C
O centre " "
STRESS N/mm^2
STRAIN %
1200
1000
800
600
400
200
0
-200
-400
-600
-800
-1000
-1200
-0·8
-0·6
-0·4
-0·2
0
0·2
0·4
0·6
0·8
431°C
290°C
566°C
20°C
665°C
20°C
M_s
centre element
surface element

FIGURE 102: Calculated stress distribution in a 20mm plate of 835M30 during polymer quenching.

(Computer program run PR15/AQUA20/UFS - see Table 11).

(a) t = 3.2s

(b) t = 12.5s

(c) t = 17.5s

(d) t = 27.8s

(e) t = ∞

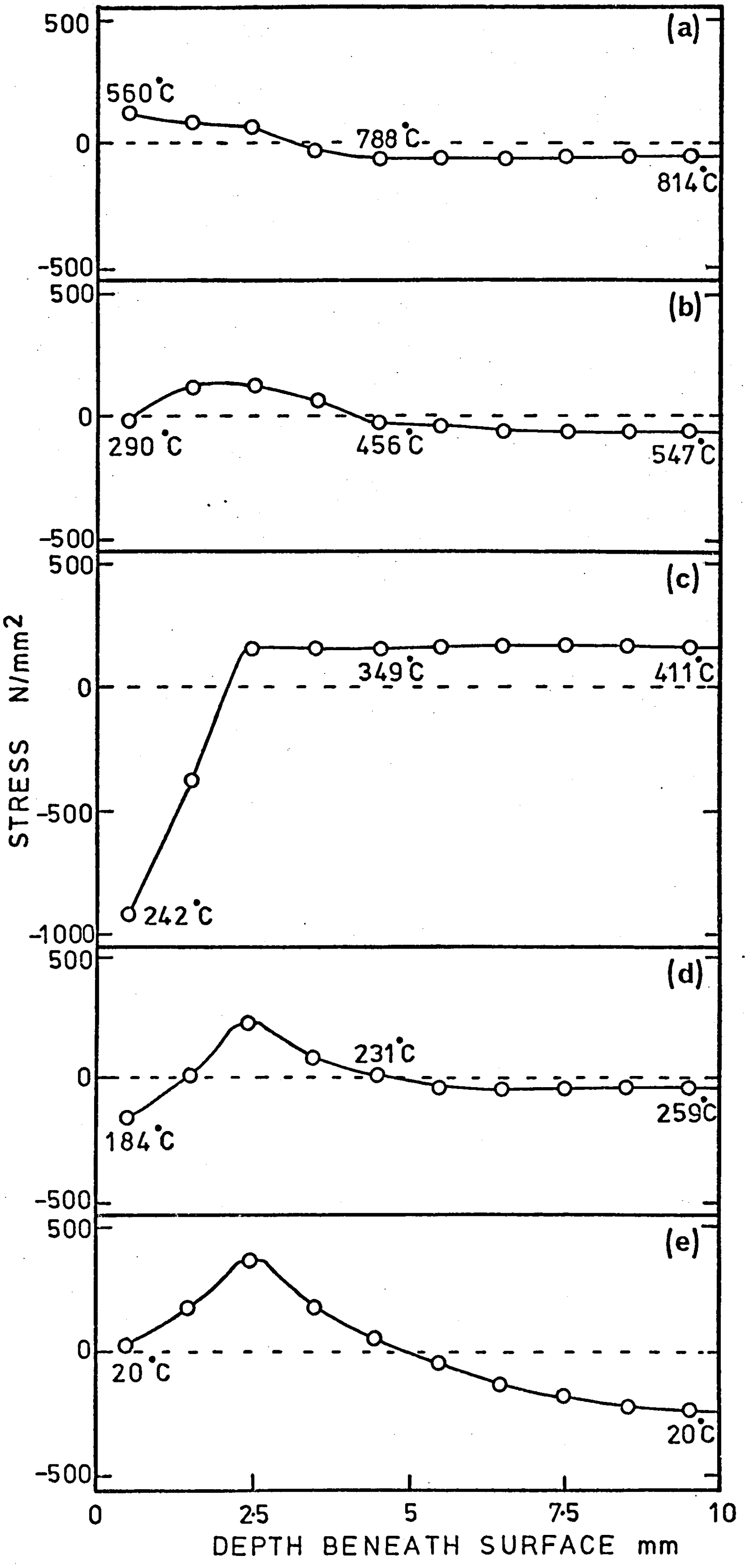
(a)
560°C
788°C
814°C
(b)
290°C
456°C
547°C
(c)
349°C
411°C
242°C
(d)
231°C
184°C
259°C
(e)
20°C
20°C
500
0
-500
-1000
STRESS N/mm2
0
2·5
5
7·5
10
DEPTH BENEATH SURFACE mm

FIGURE 103: Influence of the austenite flow stress on the calculated residual stress distribution in a 20mm plate of 835M30 after polymer quenching.

Computer program runs:

PR15/AQUA20/UFS)
PR16/AQUA20/LFS) See Table 11

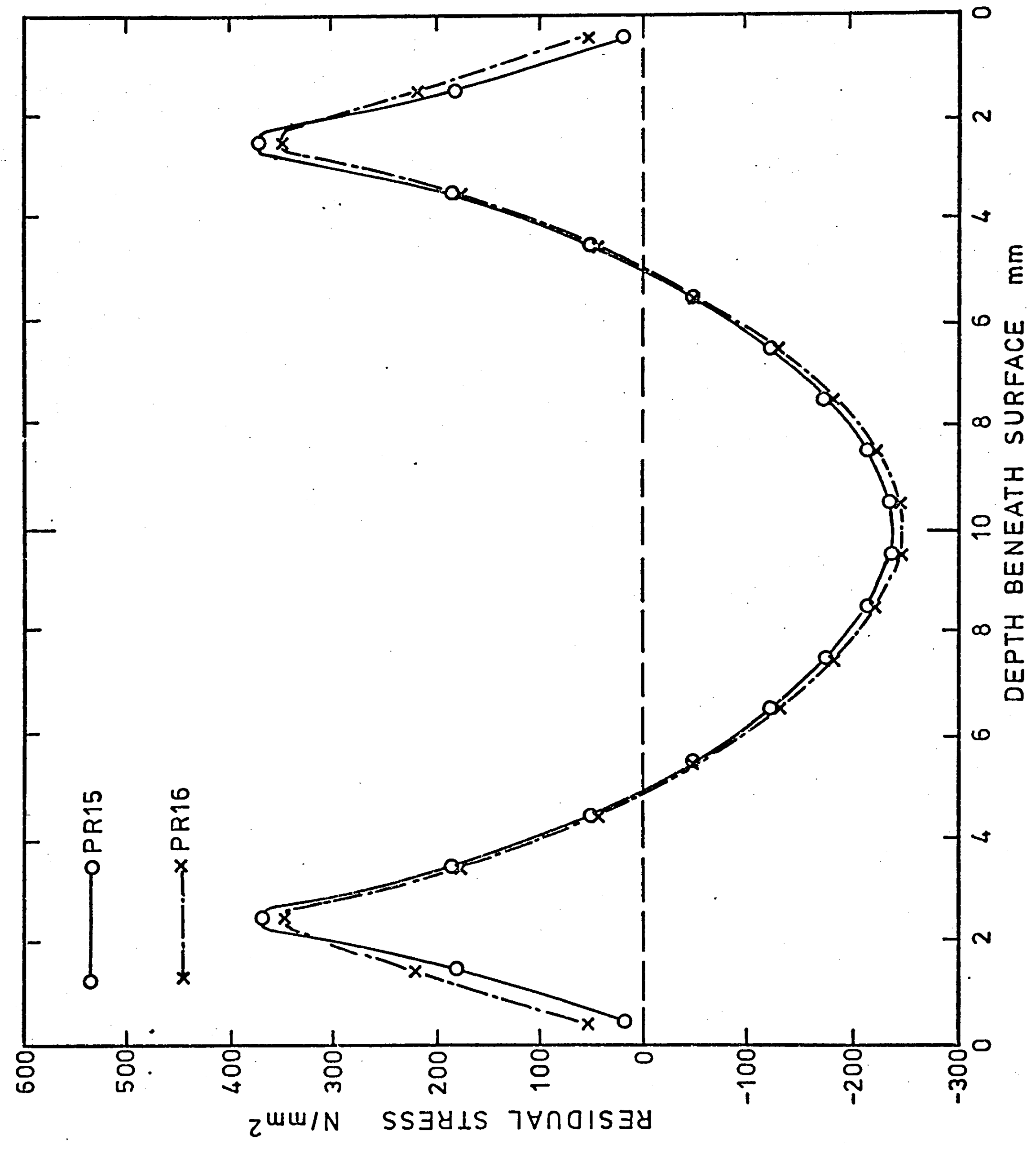
RESIDUAL STRESS N/mm^2
600
500
400
300
200
100
0
-100
-200
-300
DEPTH BENEATH SURFACE mm
0
2
4
6
8
10
8
6
4
2
0
PR15
PR16

FIGURE 104: Influence of the austenite flow stress on the residual strain in a 20mm plate of 835M30 after polymer quenching.

Computer program runs:

PR15/AQUA20/UFS)
PR16/AQUA20/LFS) See Table 11

(Note the residual strain includes the overall volume increase accompanying the hardness process).

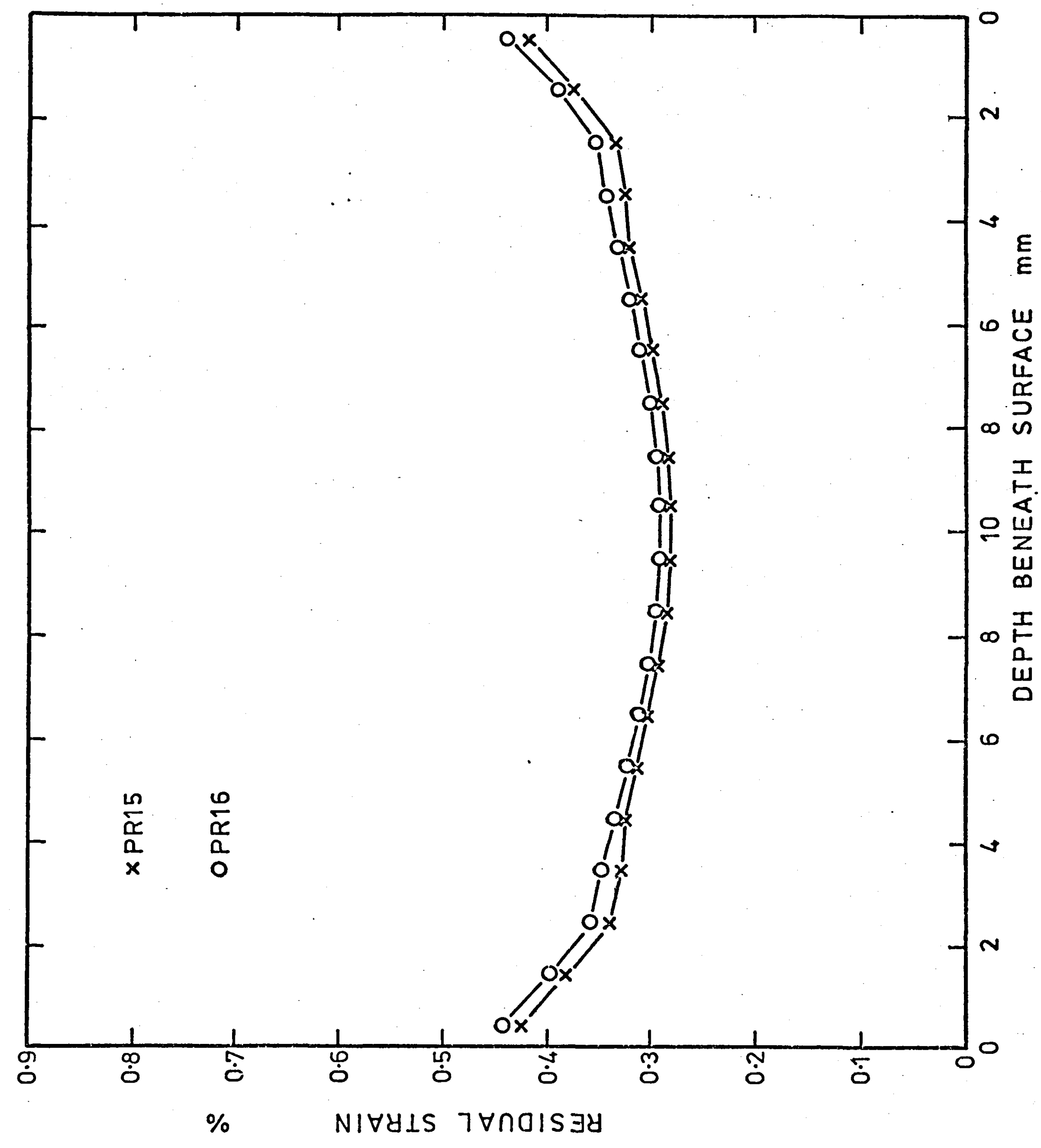
RESIDUAL STRAIN %
0·9
0·8
0·7
0·6
0·5
0·4
0·3
0·2
0·1
0
DEPTH BENEATH SURFACE mm
0
2
4
6
8
10
8
6
4
2
0
× PR15
○ PR16

FIGURE 105: 835M30 specimens used for the experimental determination of residual stress and strain.

Type C - 40mm thick

Type D - 20mm thick

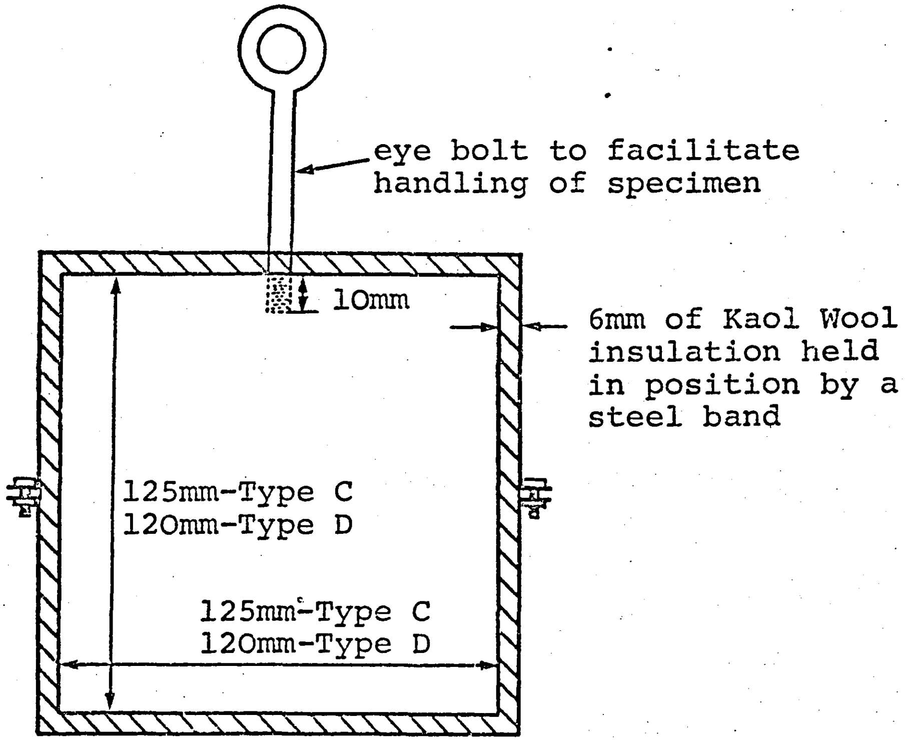
eye bolt to facilitate handling of specimen
10mm
6mm of Kaol Wool insulation held in position by a steel band
125mm-Type C
120mm-Type D
125mm-Type C
120mm-Type D

Material-835M30 steel, all surfaces plated
with 0.05mm of nickel

FIGURE 106: Type C specimen showing the location of the measurements used to determine the distortion between the edges of the plate.

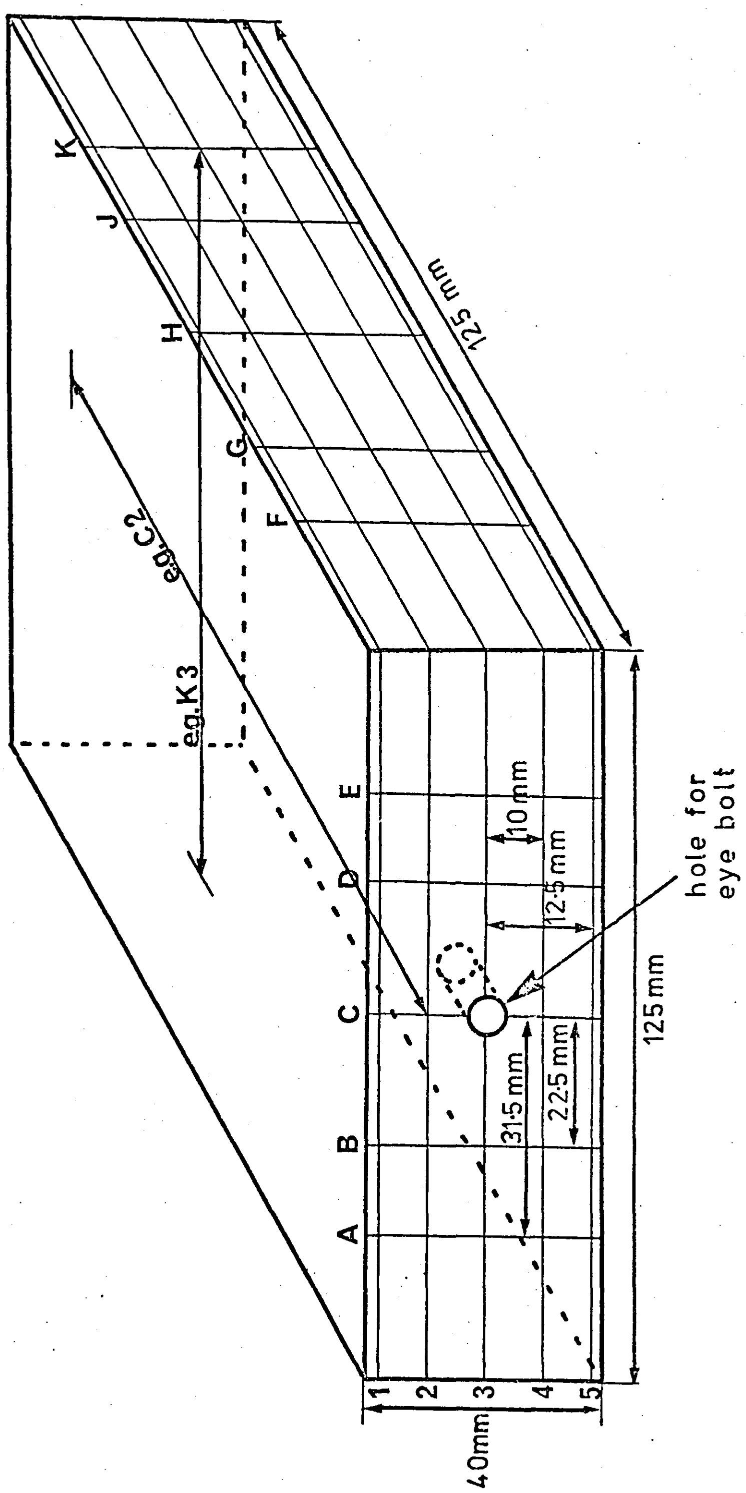
K
J
H
G
F
E
D
C
B
A
e.g. C2
e.g. K3
125 mm
10 mm
12·5 mm
hole for eye bolt
31·5 mm
22·5 mm
125 mm
1
2
3
4
5
40mm

FIGURE 107: Type D specimen showing the location of the measurements used to determine the distortion between the edges of the plate.

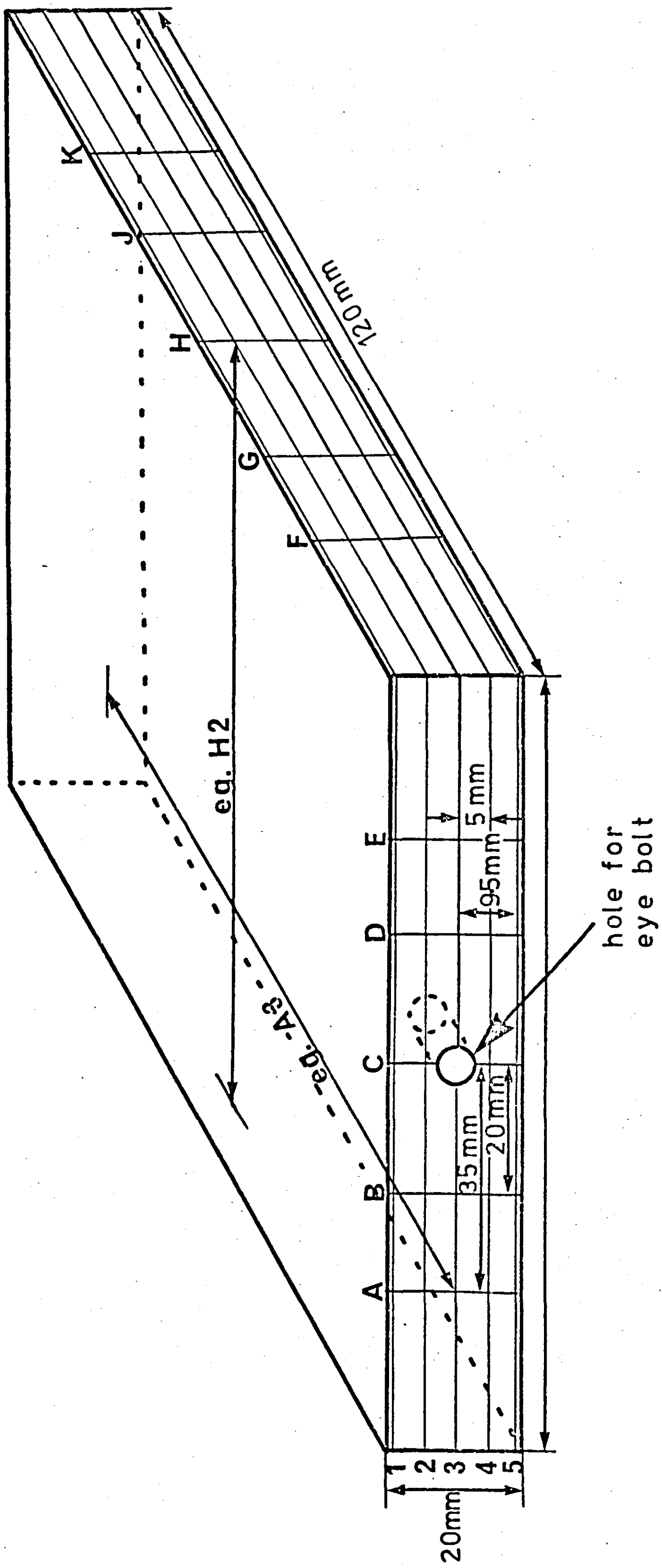
A
B
C
D
E
F
G
H
J
K
1
2
3
4
5
20mm
120mm
eq. H2
eq. A3
5 mm
9·5mm
35mm
20mm
hole for eye bolt

FIGURE 108: Schematic representation of change in shape of a cube at the centre of a plate as a result of quenching.

(a) Softened condition (cross-section)

(b) After quenching (cross-section)

FIGURE 109: Change in thickness at different positions in a 17 x 119 x 119mm plate of 835M30 as a result of water quenching.

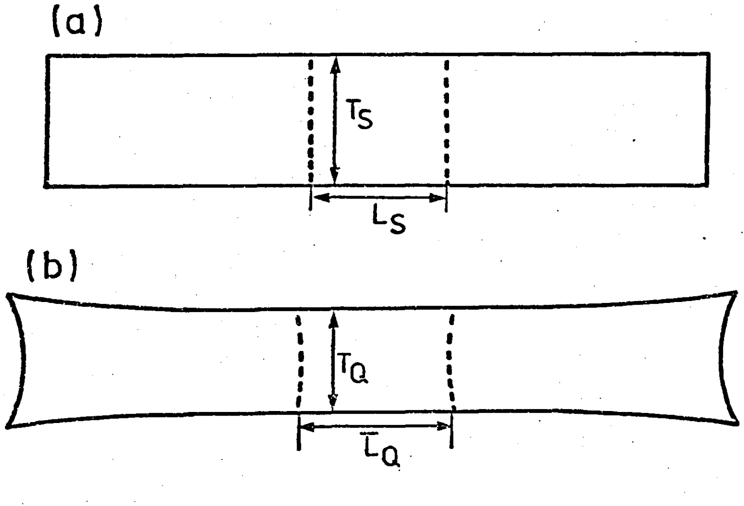
(a)
TS
LS
(b)
TQ
LQ

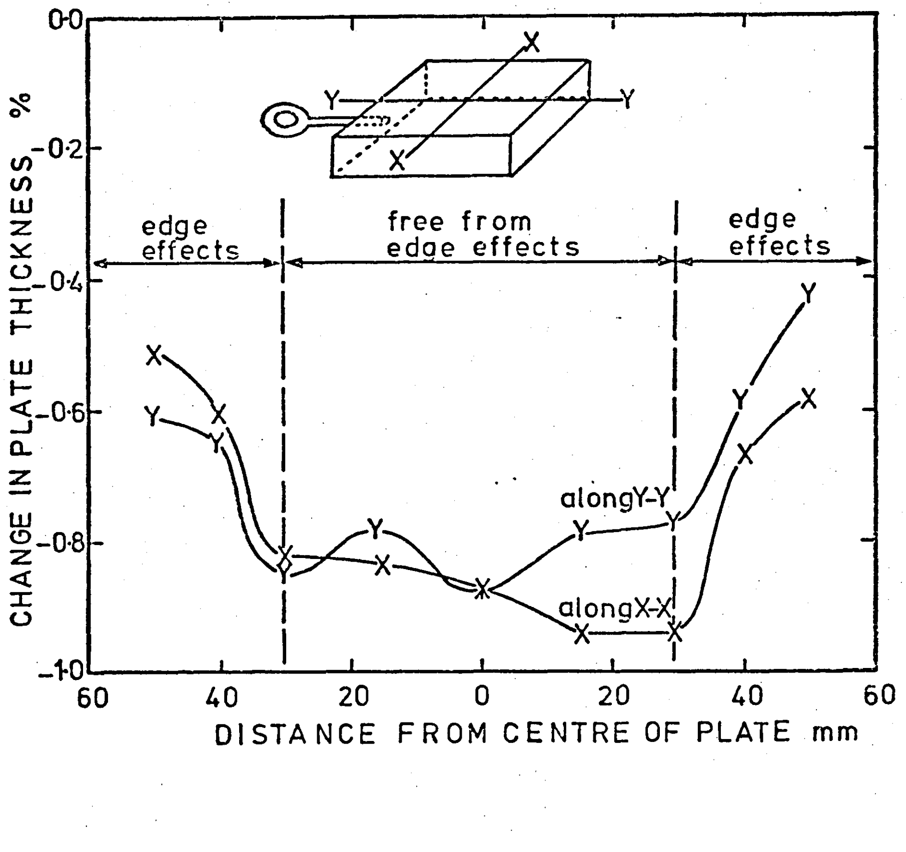
CHANGE IN PLATE THICKNESS %
0·0
-0·2
-0·4
-0·6
-0·8
-1·0
Y
Y
X
X
edge effects
free from edge effects
edge effects
along Y-Y
along X-X
60
40
20
0
20
40
60
DISTANCE FROM CENTRE OF PLATE mm

FIGURE 110: Plan view of underside of plate showing strain gauge installation prior to surface grinding opposite surface of plate for residual stress determination.

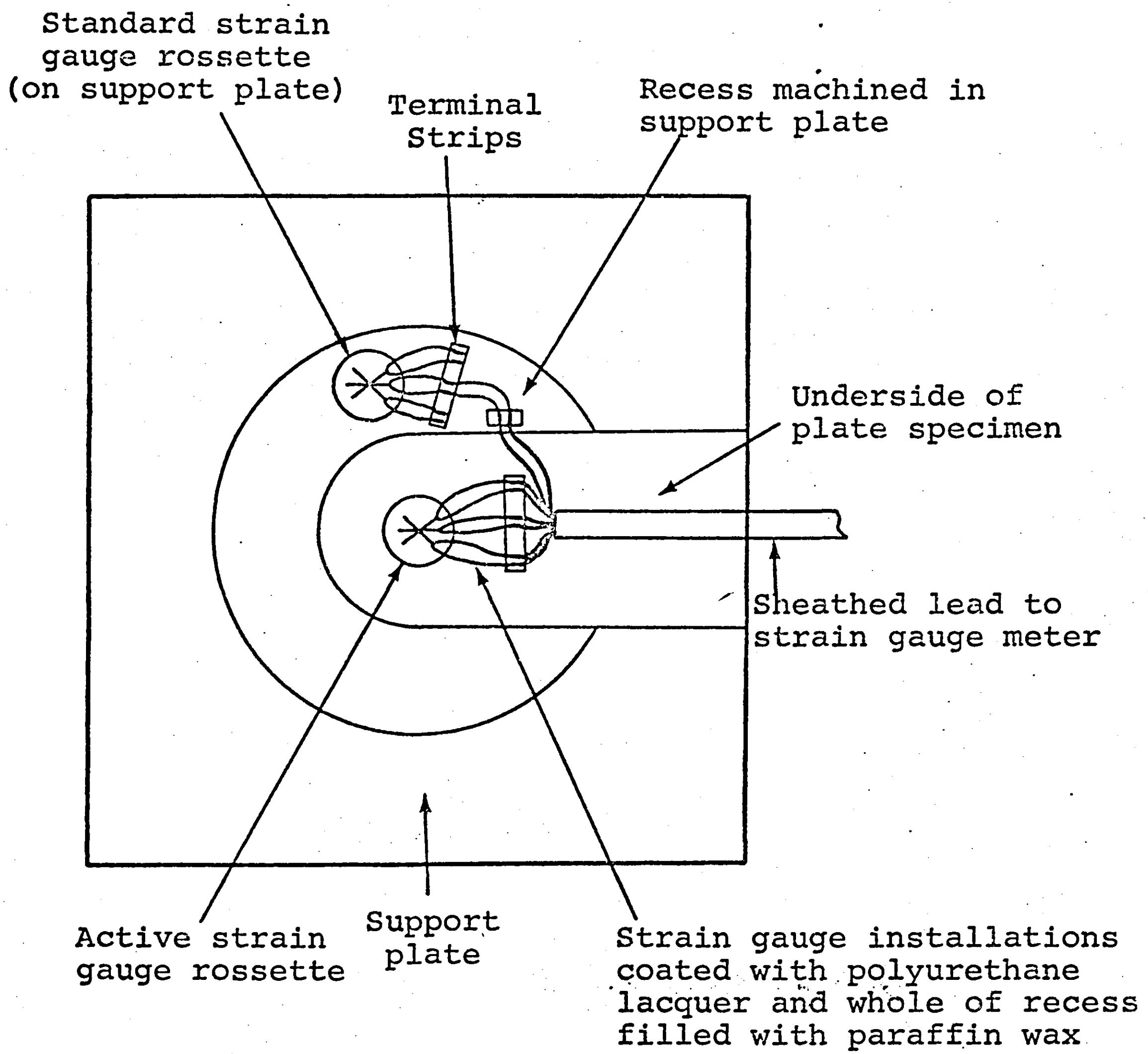
Standard strain gauge rossette (on support plate)
Terminal Strips
Recess machined in support plate
Underside of plate specimen
Sheathed lead to strain gauge meter
Active strain gauge rossette
Support plate
Strain gauge installations coated with polyurethane lacquer and whole of recess filled with paraffin wax

FIGURE 111: Strain gauge installation on underside of plate prior to wax encapsulation.

FIGURE 112: Experimentally determined residual strain in a 40mm plate of 835M30 after water quenching.

o———o measured between edges of plate

—— – —— obtained from the change in thickness at centre of plate (free from edge defects).

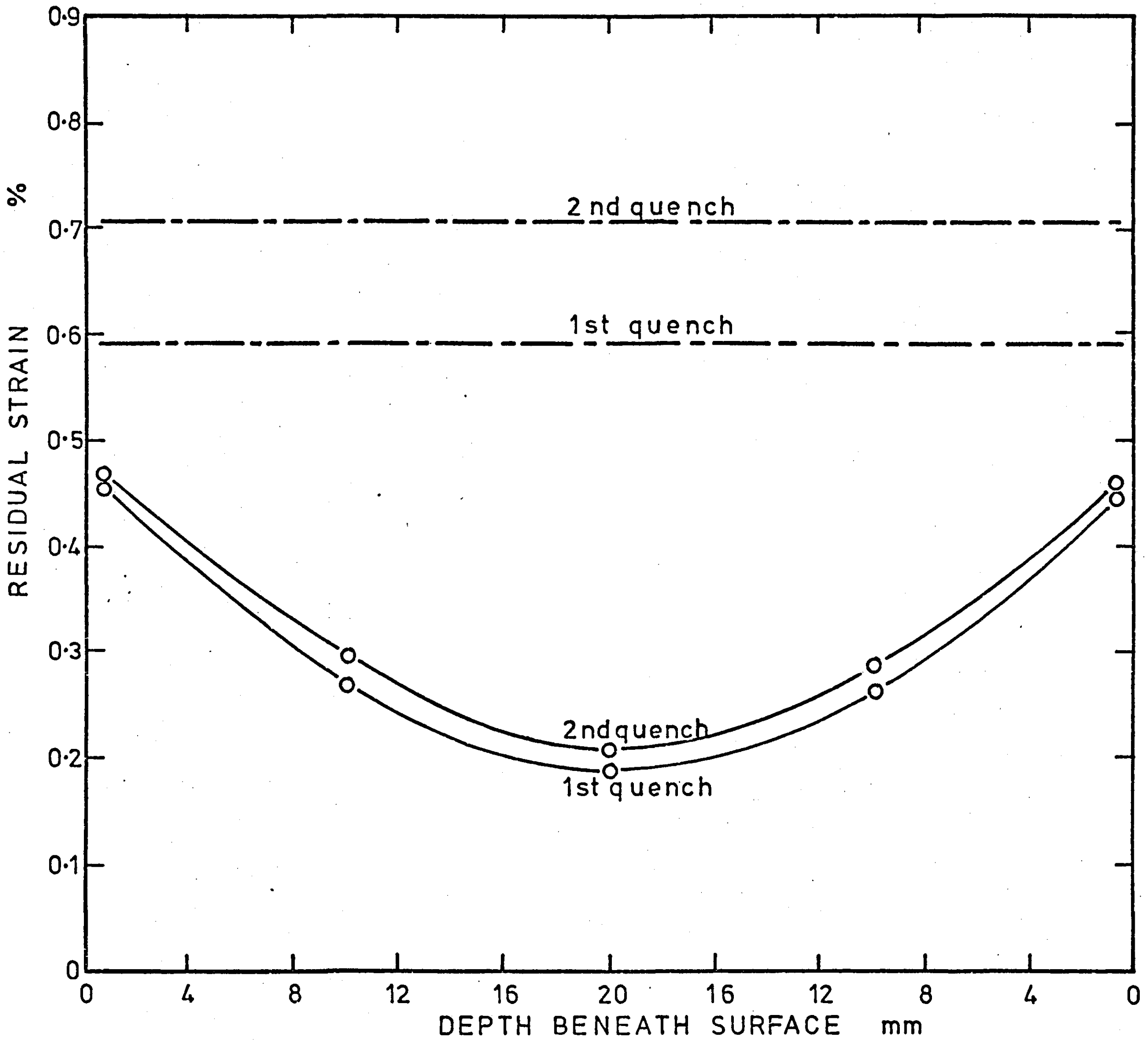
%
RESIDUAL STRAIN
0·9
0·8
0·7
0·6
0·5
0·4
0·3
0·2
0·1
0
2 nd quench
1st quench
2ndquench
1st quench
0
4
8
12
16
20
16
12
8
4
0
DEPTH BENEATH SURFACE mm

FIGURE 113: Experimentally determined residual stress distribution in water quenched 40mm plate of 835M30.

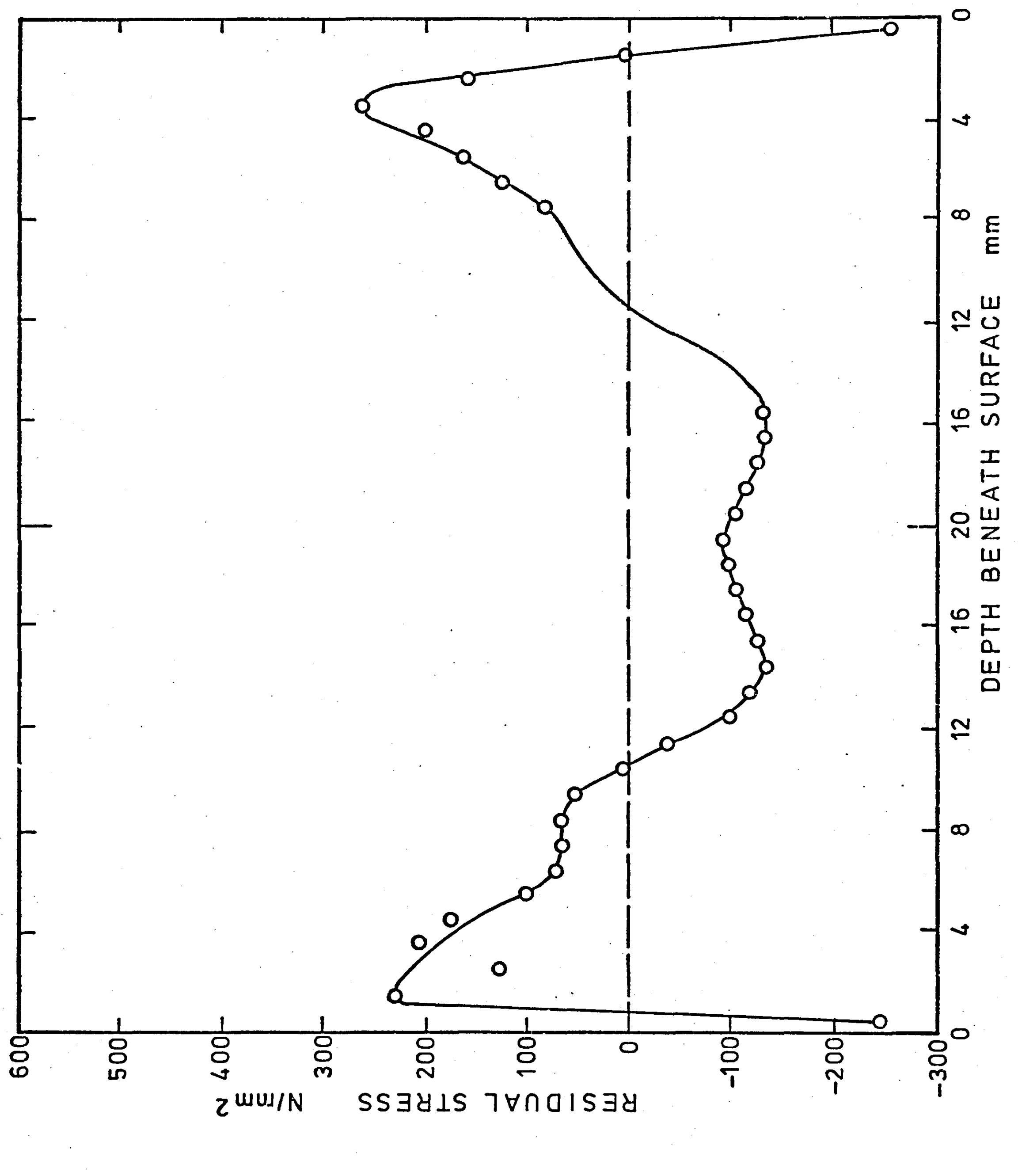
RESIDUAL STRESS N/mm2
600
500
400
300
200
100
0
-100
-200
-300
DEPTH BENEATH SURFACE mm
0
4
8
12
16
20
16
12
8
4
0

FIGURE 114: Experimentally determined residual strain in a 20mm plate of 835M30 after water quenching.

o———o measured between edges of plate

—— – —— obtained from the change in thickness at centre of plate (free from edge effects).

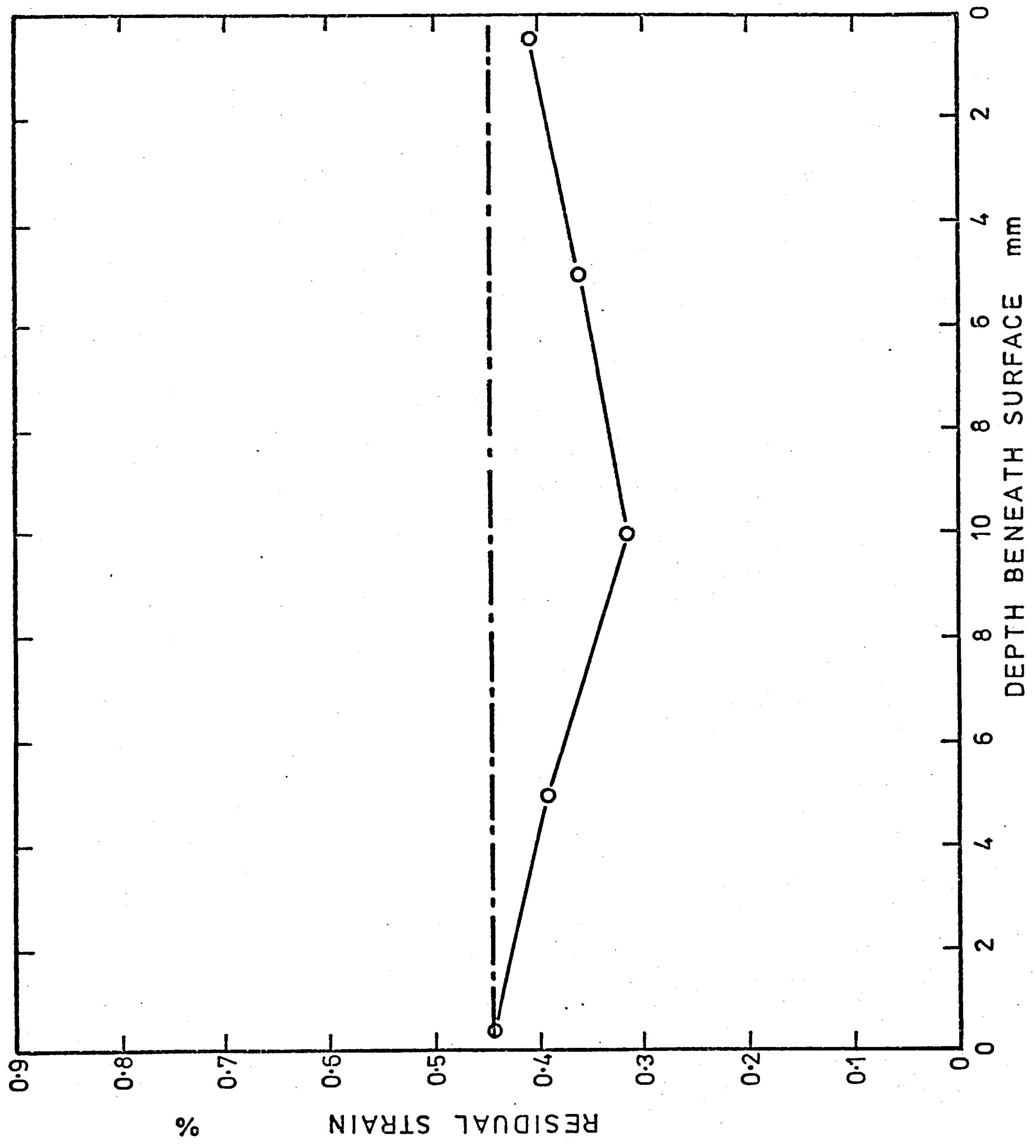
RESIDUAL STRAIN %
0·9
0·8
0·7
0·6
0·5
0·4
0·3
0·2
0·1
0
DEPTH BENEATH SURFACE mm
0
2
4
6
8
10
8
6
4
2
0

FIGURE 115: Experimentally determined residual stress distribution in a water quenched 20mm plate of 835M30.

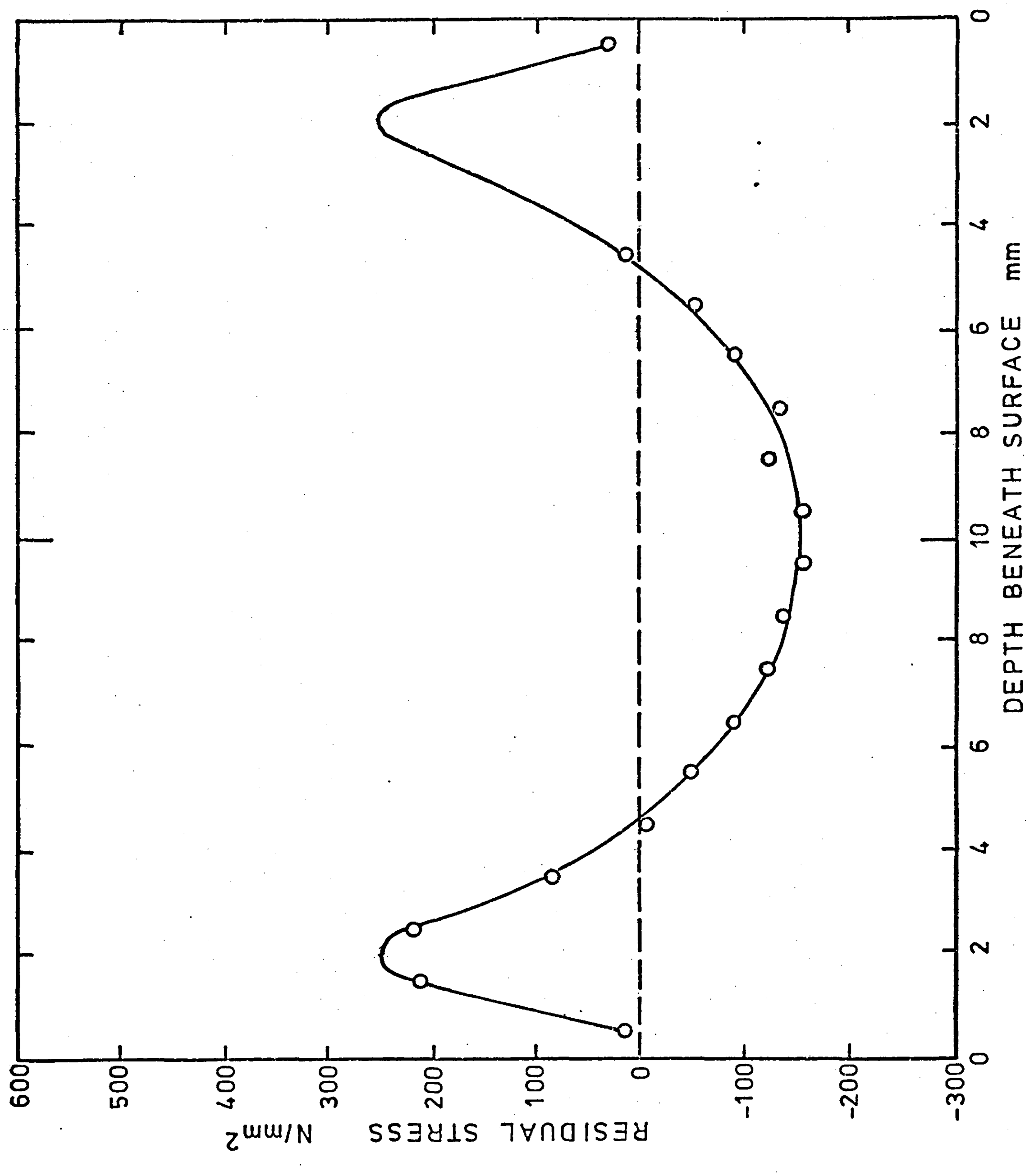

RESIDUAL STRESS N/mm²
600
500
400
300
200
100
0
-100
-200
-300
DEPTH BENEATH SURFACE mm
0
2
4
6
8
10
8
6
4
2
0

FIGURE 116: Experimentally determined residual strain in a 20mm plate of 835M30 after oil quenching.

o———o measured between edges of plate

—— – —— obtained from the change in thickness at centre of plate (free from edge effects).

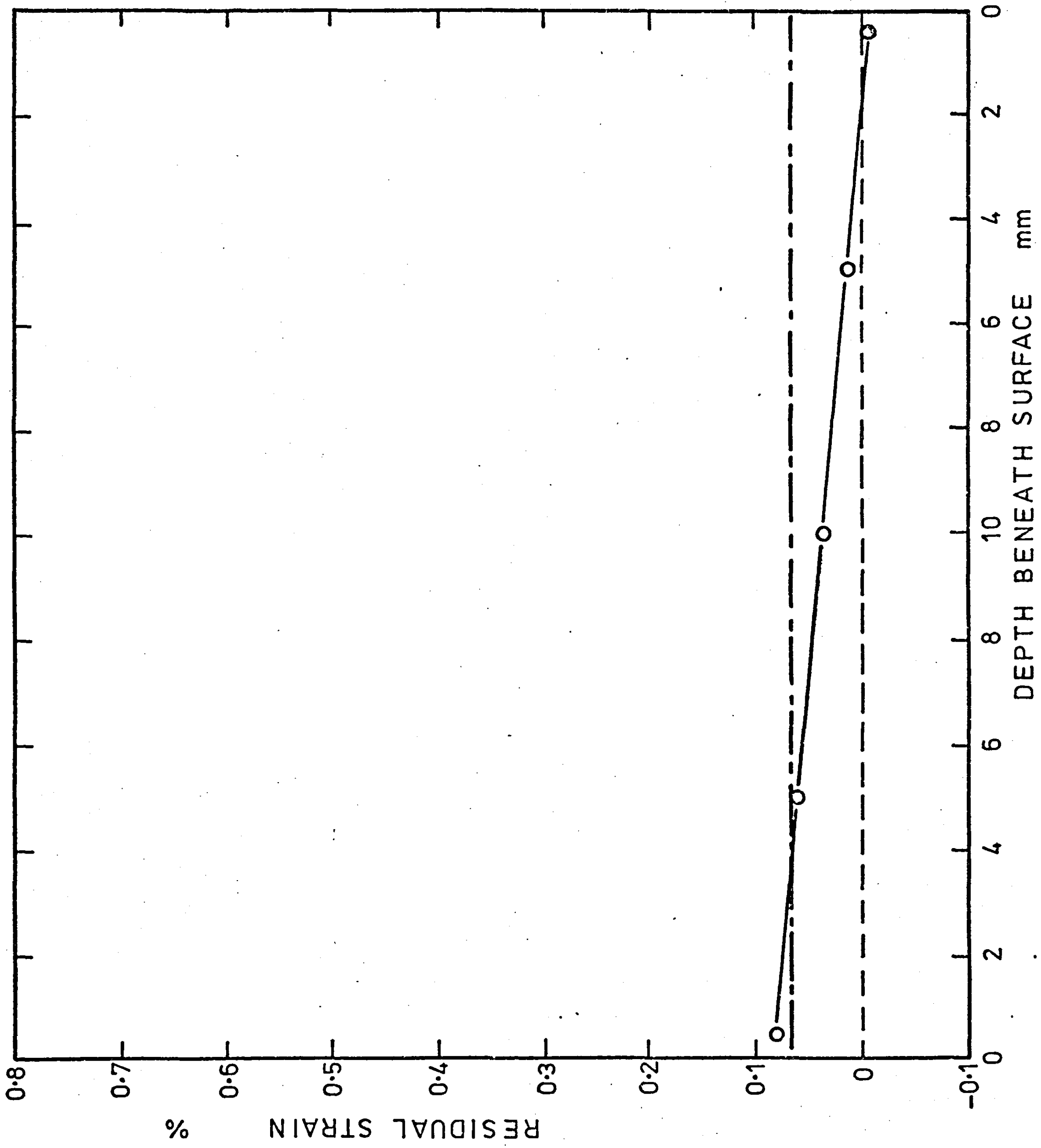
0·8
0·7
0·6
0·5
0·4
0·3
0·2
0·1
0
-0·1
RESIDUAL STRAIN %
0
2
4
6
8
10
8
6
4
2
0
DEPTH BENEATH SURFACE mm

FIGURE 117: Experimentally determined residual stress distribution in an oil quenched 20mm plate of 835M30.

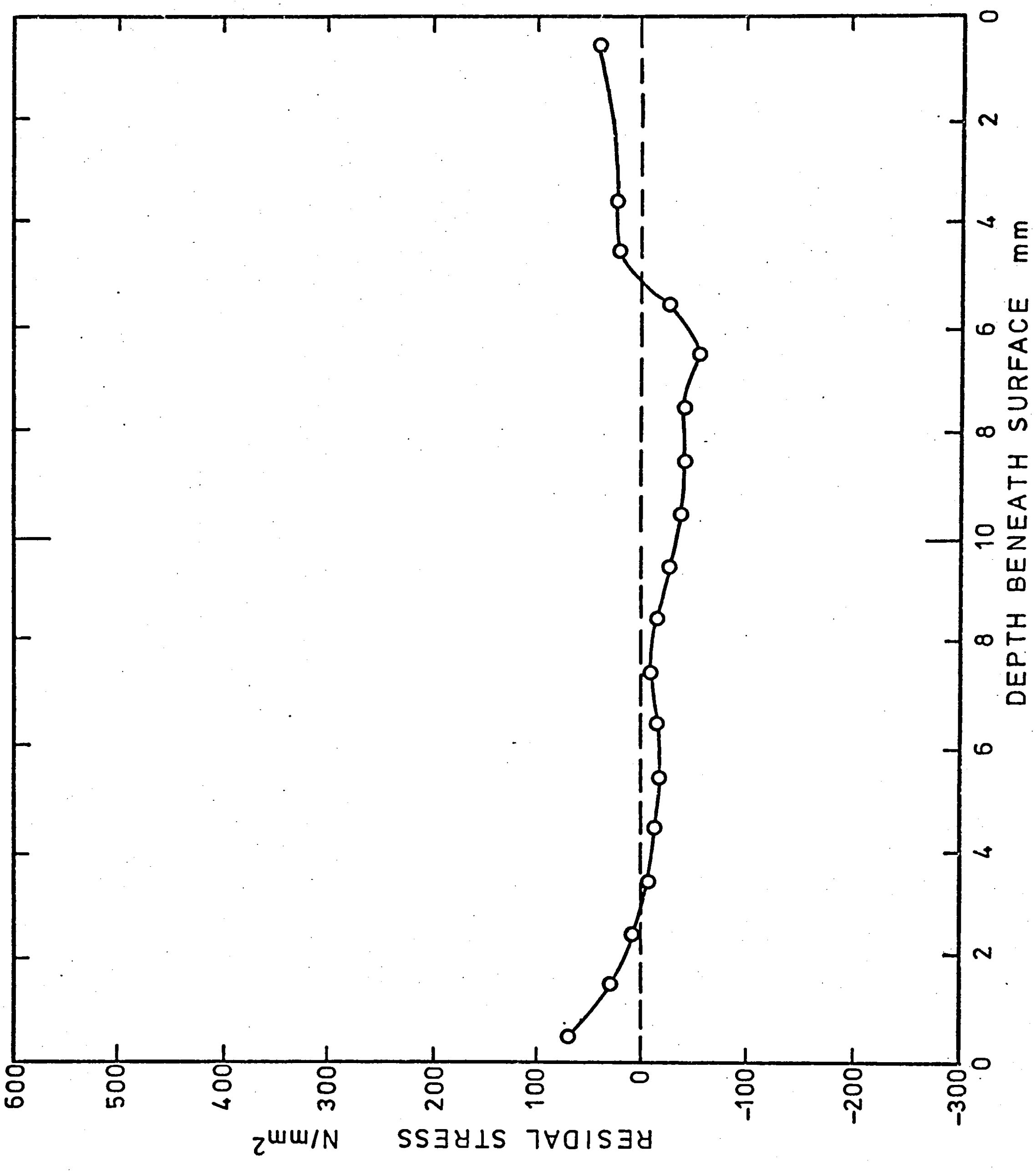
DEPTH BENEATH SURFACE mm
0
2
4
6
8
10
8
6
4
2
0
RESIDAL STRESS N/mm2
600
500
400
300
200
100
0
-100
-200
-300

FIGURE 118: Experimentally determined residual strain in a 20mm plate of 835M30 after polymer quenching.

o————o measured between edges of plate

—— – —— obtained from the change in thickness at centre of plate (free from edge effects).

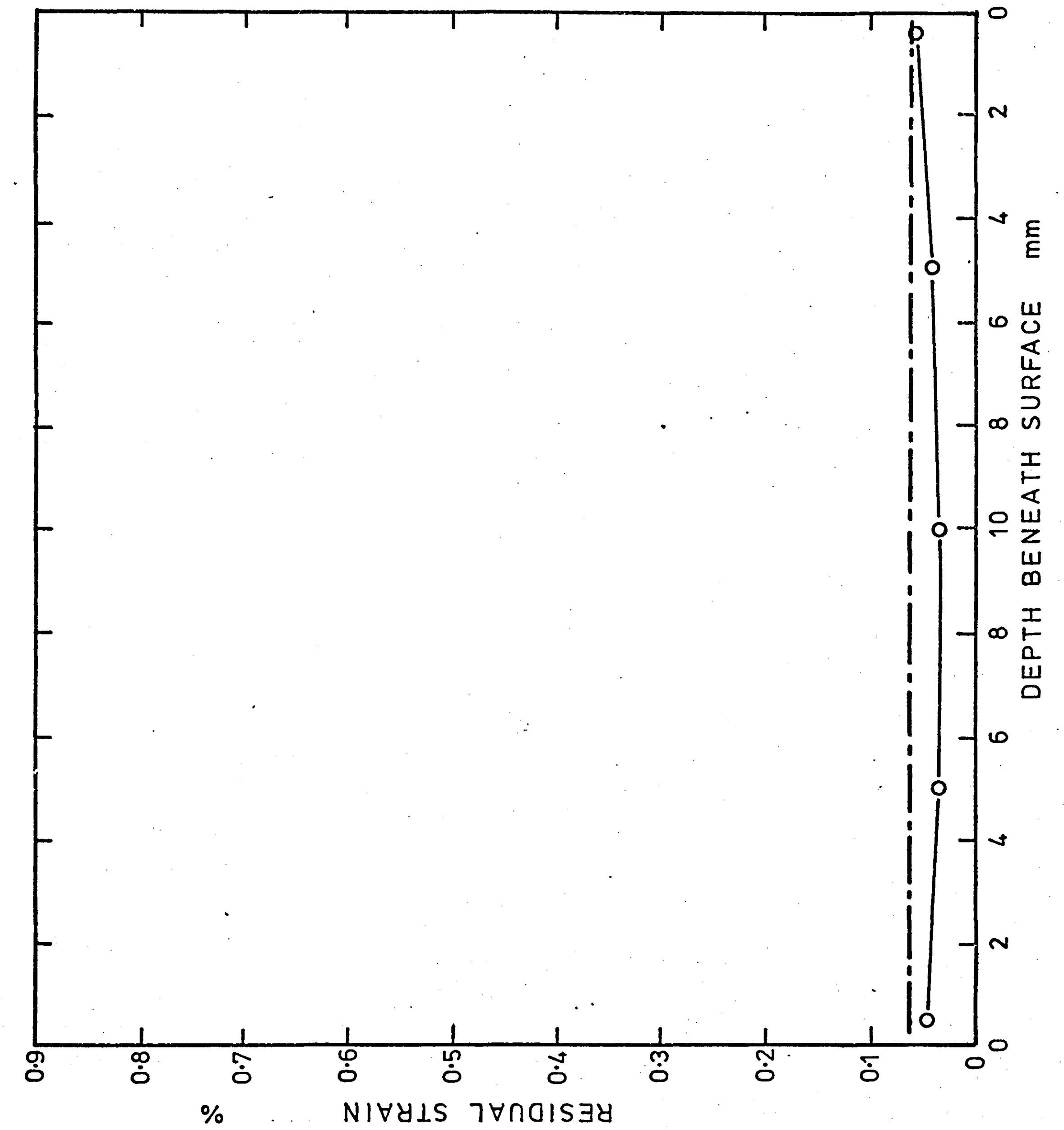
RESIDUAL STRAIN %
0
0·1
0·2
0·3
0·4
0·5
0·6
0·7
0·8
0·9
DEPTH BENEATH SURFACE mm
0
2
4
6
8
10
8
6
4
2
0

FIGURE 119: Experimentally determined residual stress distribution in a polymer quenched 20mm plate of 835M30.

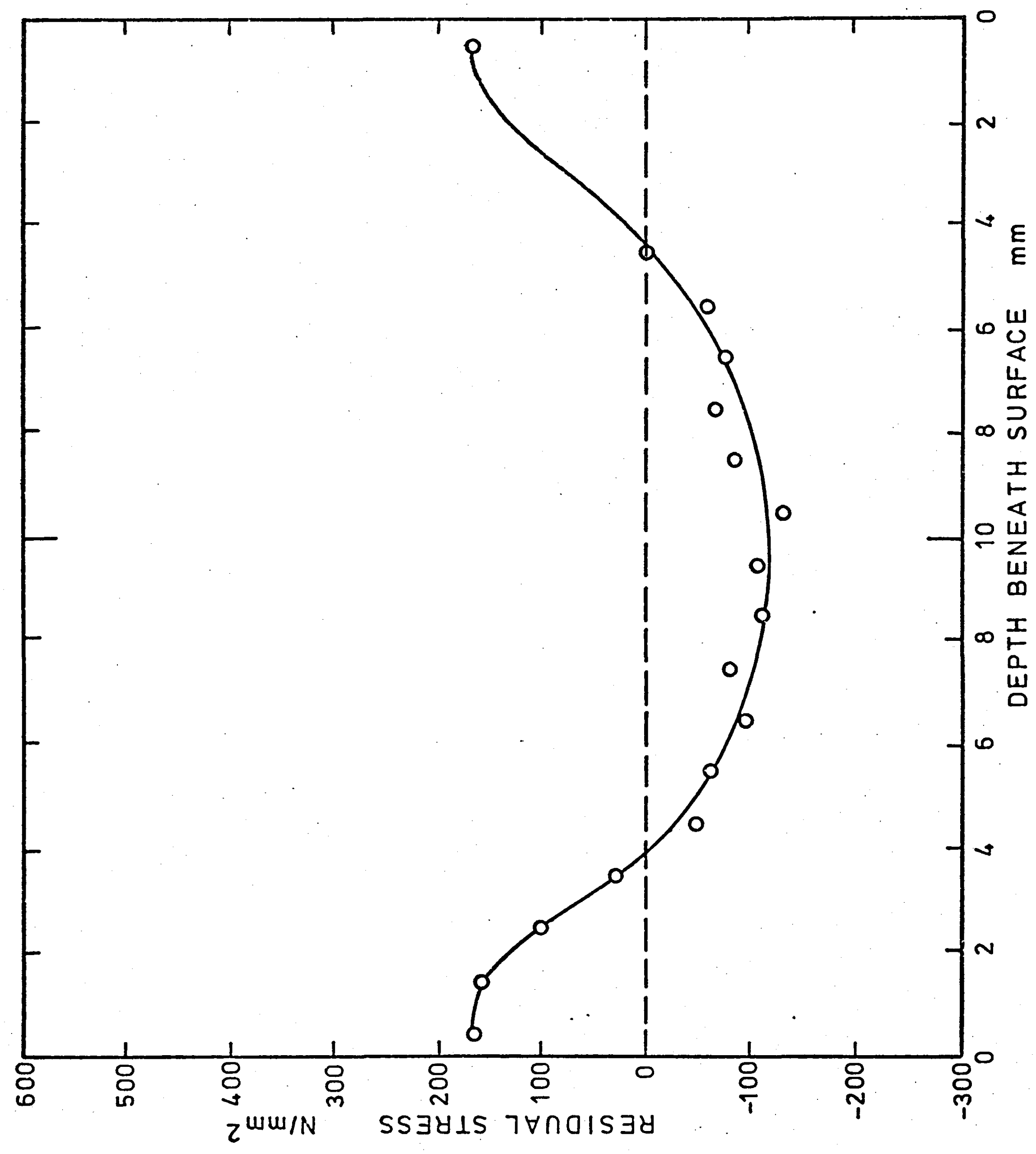

RESIDUAL STRESS N/mm^2
600
500
400
300
200
100
0
-100
-200
-300
DEPTH BENEATH SURFACE mm
0
2
4
6
8
10
8
6
4
2
0

FIGURE 120: Influence of surface temperature on the vapour blanket thickness at the surface of nickel specimens when quenched into water at various temperatures; calculated by Bigot[127].

FIGURE 121: Variation in surface heat transfer coefficient with surface temperature reported by Stolz et alia[94] for water and oil quenches, at 55°C.

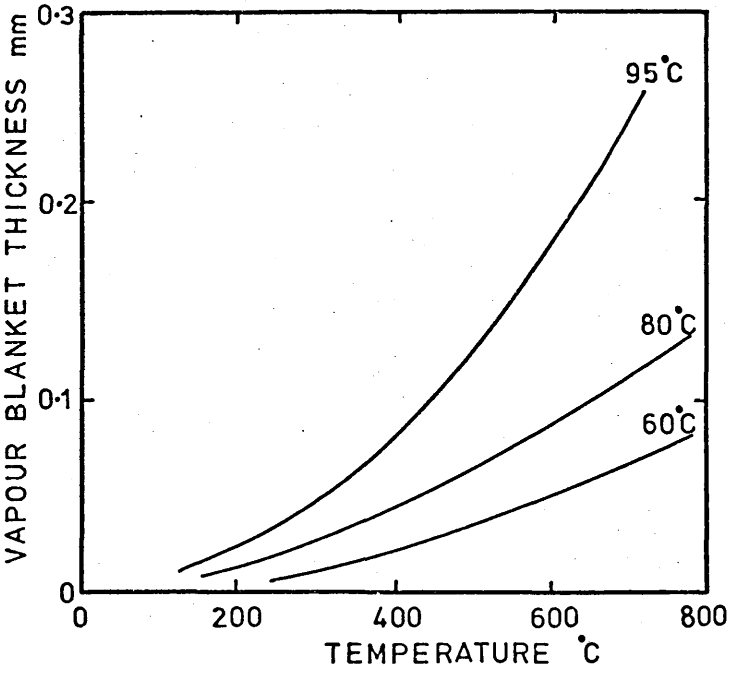

VAPOUR BLANKET THICKNESS mm
0·3
0·2
0·1
0
0
200
400
600
800
TEMPERATURE °C
95°C
80°C
60°C

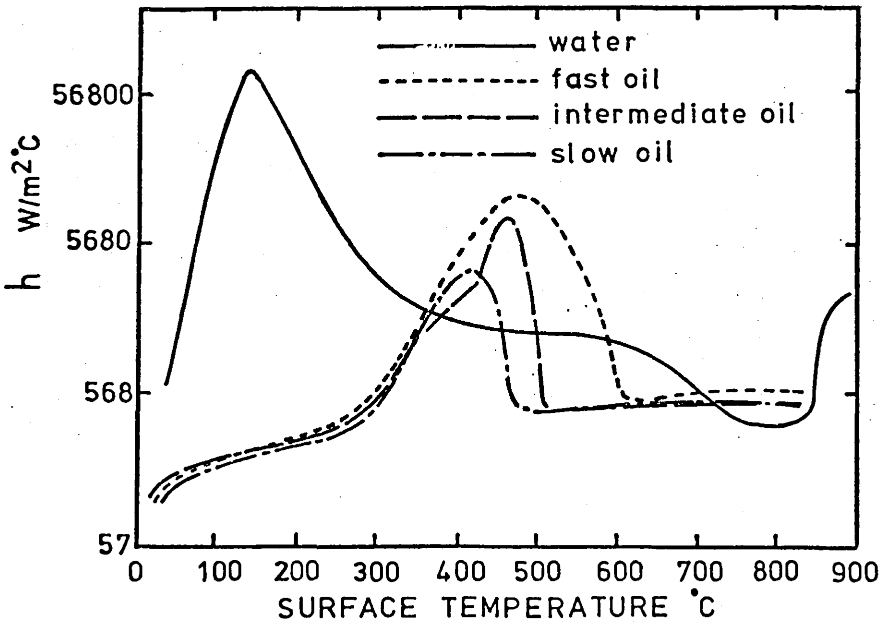

water
fast oil
intermediate oil
slow oil
h W/m²°C
56800
5680
568
57
0
100
200
300
400
500
600
700
800
900
SURFACE TEMPERATURE °C

FIGURE 122: Comparison of the values used for the flow stress of the material whilst in the austenitic condition in the present work with those used by Fujio et alia[150], Toshioka[149] and Fletcher[144].

FIGURE 123: Comparison of the values used for the austenitic strain hardening coefficients, W_1 and W_2, in the present work with the values used by Toshioka[149].

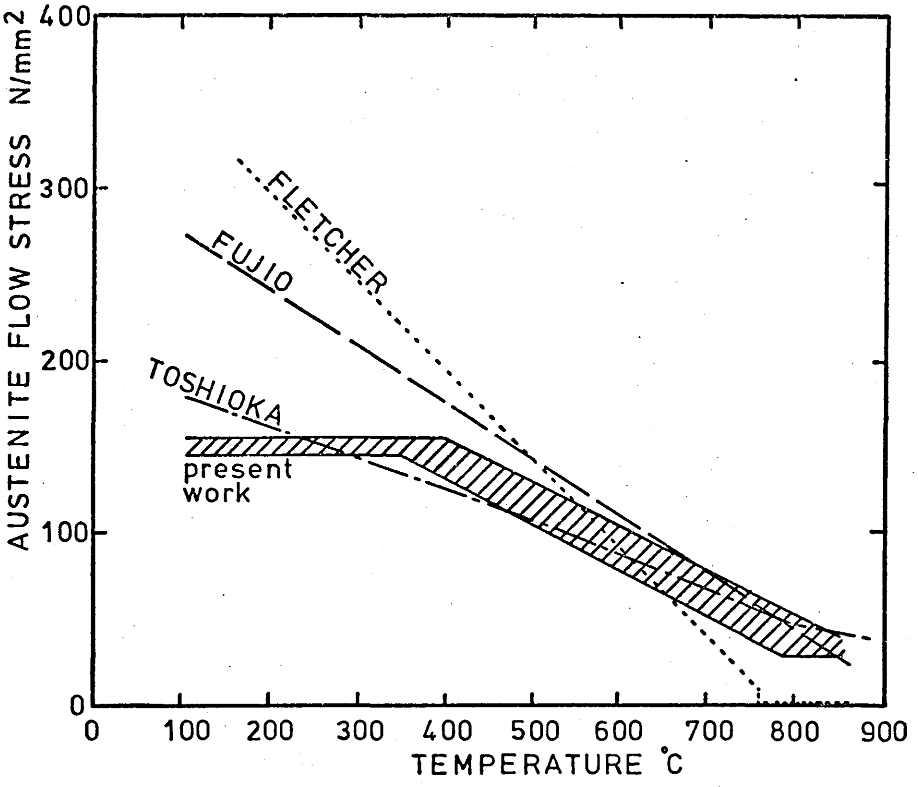

AUSTENITE FLOW STRESS N/mm^2
400
300
200
100
0
FLETCHER
FUJIO
TOSHIOKA
present work
0
100
200
300
400
500
600
700
800
900
TEMPERATURE °C

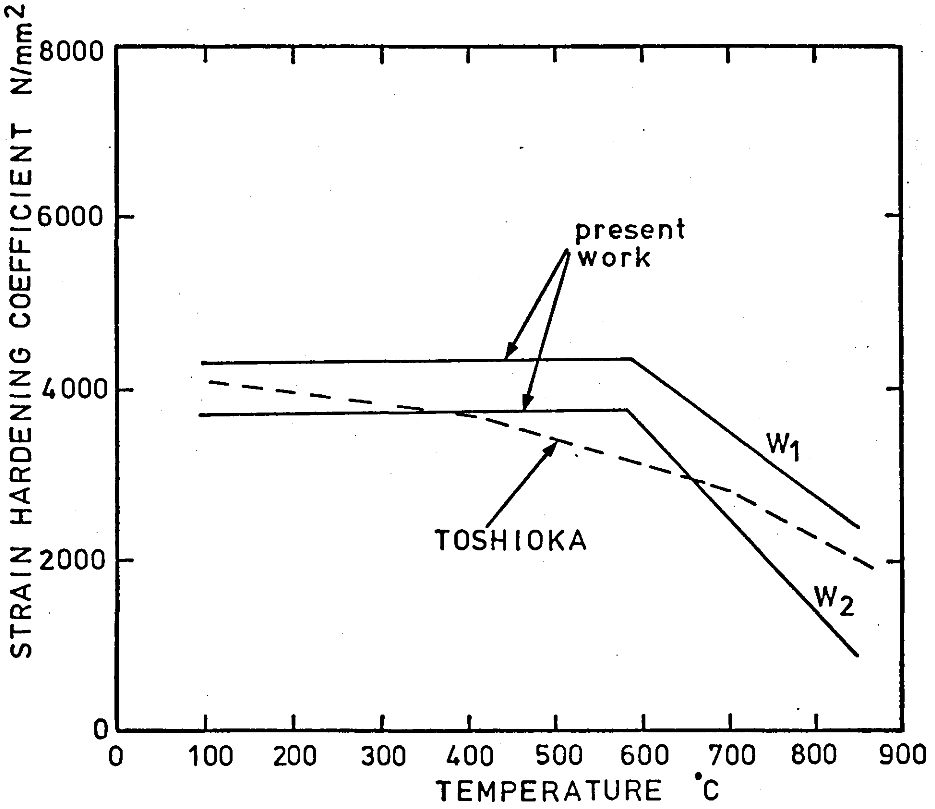

STRAIN HARDENING COEFFICIENT N/mm^2
8000
6000
4000
2000
0
present work
TOSHIOKA
W_1
W_2
0
100
200
300
400
500
600
700
800
900
TEMPERATURE °C

FIGURE 124: Schematic representation of characteristic stages in the stress-strain behaviour of elements at the surface and centre of a plate during quenching.

FIGURE 125: Assumed approximation to the variation in the actual stress in an element, σ_a, across the width of the plate showing influence of edge effects.

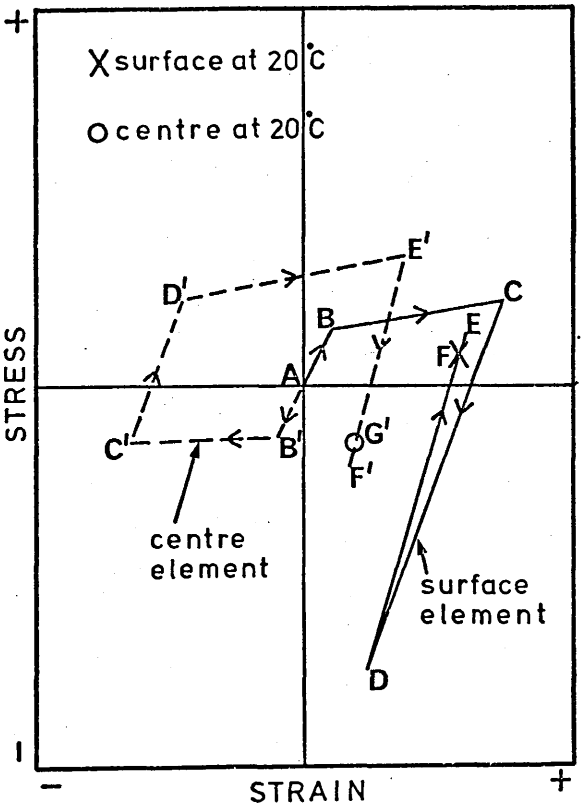
X surface at 20°C
O centre at 20°C
STRESS
STRAIN
+
-
+
A
B
C
D
E
F
B'
C'
D'
E'
F'
G'
centre element
surface element

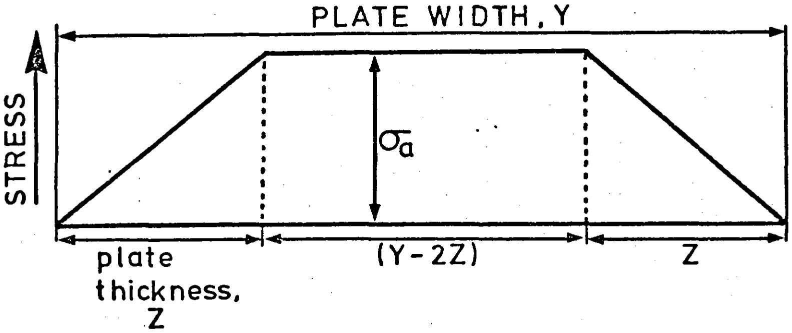
PLATE WIDTH, Y
STRESS
σ_a
plate thickness, Z
(Y-2Z)
Z

FIGURE 126: Calculated residual stress distribution in a 20mm plate of 835M30 after oil quenching assuming:

(i) Martensite flow stress of 600N/mm^2.

(ii) Austenite flow stress reduced such that it was 15N/mm^2 above 790°C and 100N/mm^2 below 350°C.

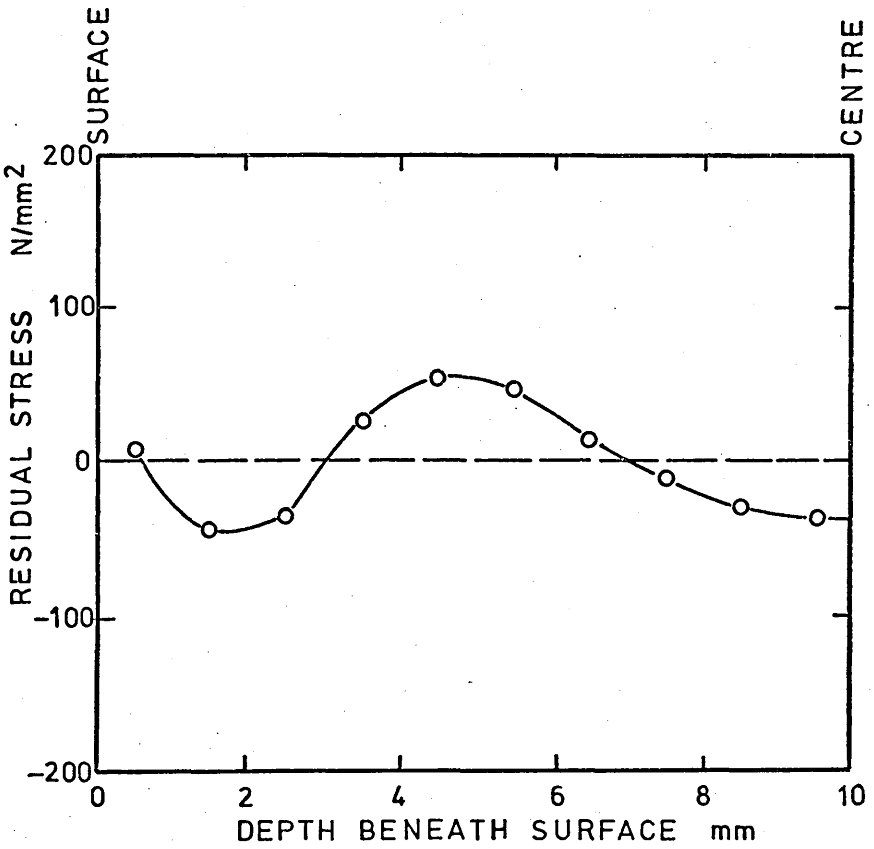
SURFACE
CENTRE
RESIDUAL STRESS N/mm^2
200
100
0
-100
-200
0
2
4
6
8
10
DEPTH BENEATH SURFACE mm

FIGURE 127: Influence of the martensite flow stress on the calculated residual stress distribution in a plate cooled with a Biot number of 2.0.

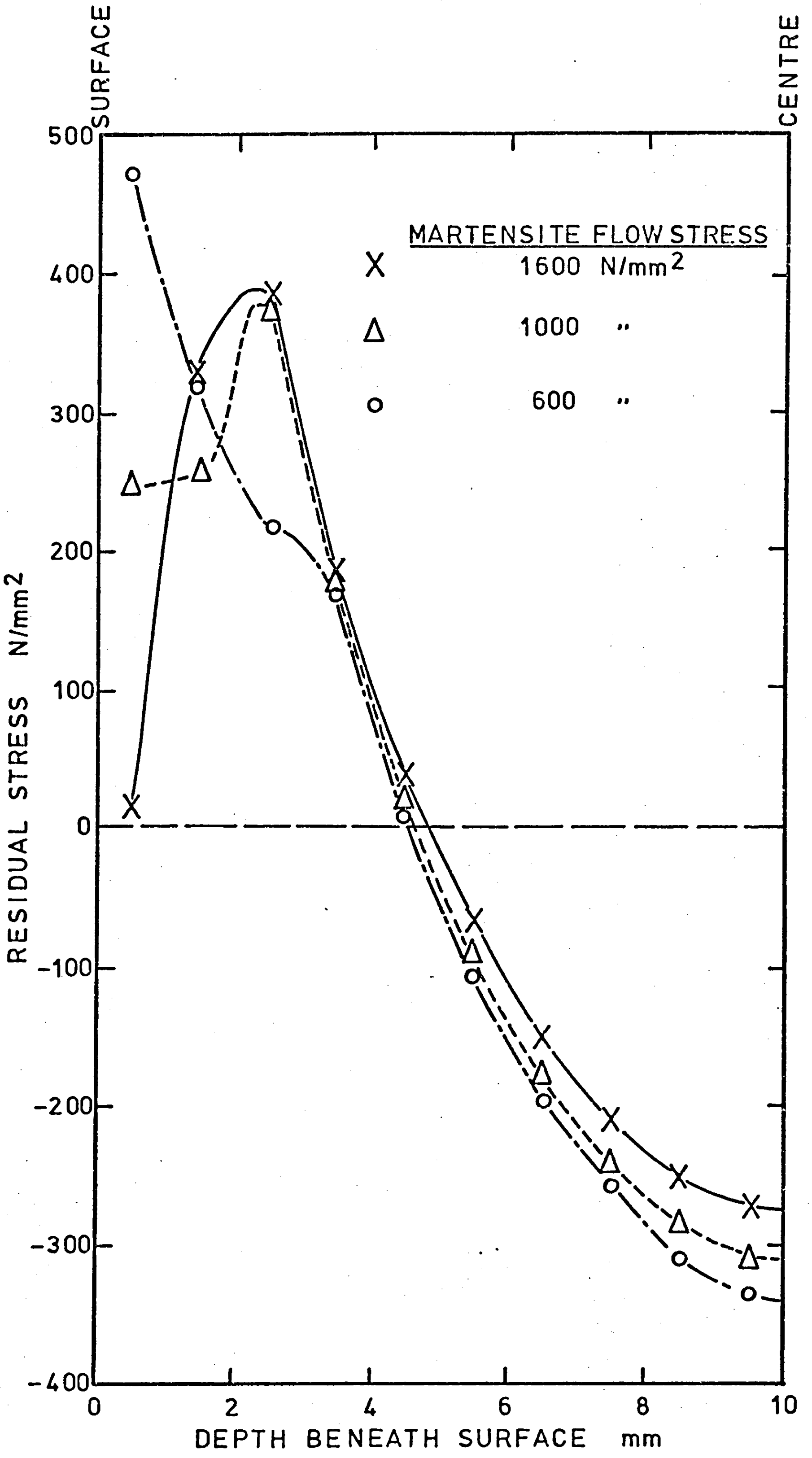
SURFACE
CENTRE
MARTENSITE FLOW STRESS
X 1600 N/mm²
Δ 1000 "
o 600 "
RESIDUAL STRESS N/mm²
500
400
300
200
100
0
-100
-200
-300
-400
0
2
4
6
8
10
DEPTH BENEATH SURFACE mm

Thermal Stress Developed in a Single Planar Element Subjected to Complete Edge Restraint

The change in stress, $d\sigma$, due to a uniform change in temperature of $d\theta$ throughout the element, assuming the element is completely restrained around its edges, is shown from Hooke's law to be:-

$$d\sigma = \frac{E}{1-\nu} \times \alpha_{ex} \times d\theta \qquad \text{(i)}$$

Therefore,
$$\int_{\sigma=\sigma_{t+\Delta t}}^{\sigma=\sigma_t} d\sigma = \alpha_{ex} \int_{\theta=\theta_{t+\Delta t}}^{\theta=\theta_t} \frac{E}{1-\nu} \times d\theta \qquad \text{(ii)}$$

But if $\frac{E}{1-\nu}$ can be expressed as a linear function of θ,

i.e.
$$\frac{E}{1-\nu} = a - b\theta \qquad \text{(iii)}$$

Equation (iii) may be replaced by:-

$$\int_{\sigma=\sigma_{t+\Delta t}}^{\sigma=\sigma_t} d\sigma = \alpha_{ex} \int_{\theta=\theta_{t+\Delta t}}^{\theta=\theta_t} (a - b\theta)\, d\theta \qquad \text{(iv)}$$

Which may be integrated to give:-

$$(\sigma_t - \sigma_{t+\Delta t}) = \alpha_{ex} \left\{ a\,(\theta_t - \theta_{t+\Delta t}) - \frac{b}{2}\,(\theta_t^{\,2} - \theta_{t+\Delta t}^2) \right\} \qquad \text{(v)}$$

or
$$\Delta\sigma = \alpha_{ex} \left\{ a(\theta_t - \theta_{t+\Delta t}) - \frac{b}{2}\,(\theta_t^{\,2} - \theta_{t+\Delta t}^2) \right\} \qquad \text{(vi)}$$

APPENDIX 2

Method for the Calculation of Residual Stresses from the Results of Changes in Strain at the Underside of a Plate

Figure A2.1 shows the changes occurring to a plate after the removal of a layer from the surface of the plate that had contained tensile residual stresses. The stresses that had been present in the layer can be found from a consideration of the forces required to return the plate to its original condition, as shown in Figure A2.2.

Thus from the equilibrium of forces,

$$\sigma_1 \Delta z_1 + \tfrac{1}{2}\sigma_b z_b - \tfrac{1}{2}\sigma_a z_a = 0 \qquad \text{(i)}$$

and from the equilibrium of moments,

$$\sigma_1 \Delta z_1 \left(z_a + \frac{\Delta z_1}{2}\right) = \tfrac{1}{2}\sigma_a z_a \left(\tfrac{2}{3} z_a\right) + \tfrac{1}{2}\sigma_b z_b \left(\tfrac{2}{3} z_b\right) \qquad \text{(ii)}$$

and from the geometry of the system,

$$\frac{\sigma_a}{z_a} = \frac{\sigma_b}{z_b} \qquad \text{(iii)}$$

From (i), (ii) and (iii) it follows that:-

$$z_a = (t - \Delta z_1)(4t - \Delta z_1) \qquad \text{(iv)}$$

where t = original thickness of the plate = $z_a + z_b + \Delta z_1$.
Hence the original stress in the first layer is given by:-

$$\sigma_1 = \frac{\sigma_b (t - \Delta z_1)^2}{(2 + \Delta z_1)\Delta z_1} \qquad \text{(v)}$$

The stress σ_b is required to evaluate equation (v). σ_b may be determined from the change in strain measured experimentally on the underside of the plate:-

$$\sigma_b = \frac{E}{1-\nu^2} (\Delta\varepsilon_x + \nu\Delta\varepsilon_y) \tag{vi}$$

When $\sigma_x = \sigma_y$ (vii)

$$(\text{i.e. } \varepsilon_x = \varepsilon_y) \tag{viii}$$

Equation (vi) reduces to:-

$$\sigma_b = \frac{E}{1-\nu} \Delta\varepsilon_b \tag{ix}$$

Where $\Delta\varepsilon_b$ is the change in strain measured at the underside of the plate after the removal of the first layer.

The removal of the first layer also modifies the stresses present in the underlying layers that are to be removed later. For example, if σ_1 was a tensile stress, the stress at $z = z_a$ will have been reduced by σ_a and the stress at $z = z_b$ will have been increased by σ_b (Figure A2.2). If all the layers to be removed are Δz thick, the removal of the mth layer alters the stress in the nth layer by:-

$$\Delta^m_n = \frac{\sigma_b}{z_b} \left[(z_a) - (n - m)\Delta z + \frac{\Delta z}{2} \right] \tag{x}$$

The total residual stresses originally present in the layers can then be obtained from:-

$$\left.\begin{aligned}
\sigma(1) &= \sigma_1 \\
\sigma(2) &= \sigma_2 - \Delta^2{}_3 \\
\sigma(3) &= \sigma_3 - \Delta^1{}_3 - \Delta^2{}_3 \\
\sigma(4) &= \sigma_4 - \Delta^1{}_4 - \Delta^2{}_4 - \Delta^3{}_4 \\
\sigma(5) &= \sigma_5 - \ldots\ldots\ldots\ldots\ldots
\end{aligned}\right\} \tag{xi}$$

The calculation procedure was computerised such that the only inputs required were the initial plate thickness, the thickness of each layer removed and the change in strain at the underside of the plate after the removal of each layer.

This technique is the same as that described by Andrews[2] with the exception of equations (xi), which he gives as:-

$$\left.\begin{aligned}\sigma(1) &= \sigma_1\\ \sigma(2) &= \sigma_2 + \Delta^1{}_2\\ \sigma(3) &= \sigma_3 + \Delta^1{}_3 + \Delta^2{}_3\\ \sigma(4) &= \sigma_4 + \Delta^1{}_4 + \Delta^2{}_4 + \Delta^3{}_4\\ \sigma(5) &= \sigma_5 + \ldots\ldots\ldots\ldots\ldots\end{aligned}\right\} \qquad \text{(xii)}$$

Figure A2.1(b) clearly shows that the removal of a layer with a positive stress induces a positive stress in the layer immediately below it. Therefore the positive $\Delta^m{}_n$ values shown in (xii) are of incorrect sign, and have been replaced by (xi). Thus the stress measured in the underlying element when it too is removed must be reduced by the subtraction of the $\Delta^m{}_n$ factors in order to determine the true original stress in the element.

FIGURE A2.1: Shape of plate (a) before and (b) after removal of first layer which had contained a tensile residual stress.

(After Andrews[2]).

FIGURE A2.2: Stress distribution induced after an imaginary layer has been replaced on the top of the plate such that the plate is sprung back into its original shape.

(After Andrews[2])

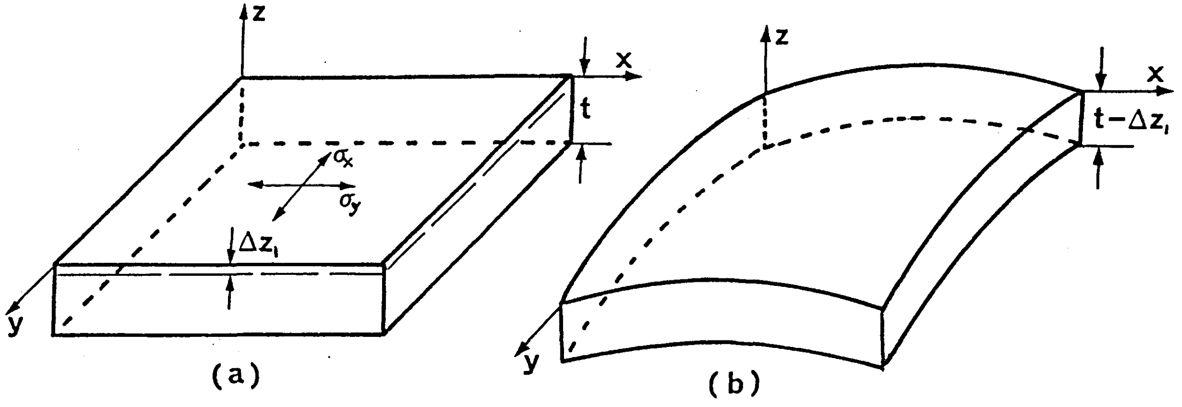
z
x
t
σx
σy
Δz1
y
(a)
z
x
t−Δz1
y
(b)

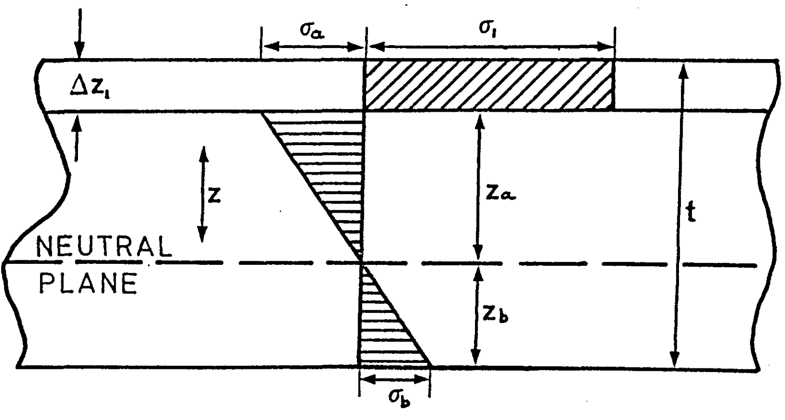
σa
σ1
Δz1
z
za
t
NEUTRAL
PLANE
zb
σb

Case Study: Selection of a Steel that Possess the Minimum Strain After Heat Treatment

16 mm thick discs of a low-alloy steel are required with an as-quenched hardness of at least 450 VPN in all parts of the section. Using the data provided by the En specifications select those alloys that meet this requirement. Hence determine which of these alloys possesses the minimum strain after quenching, making quite clear the assumptions used in the calculation. Is this considered to be the correct commercial choice for an application where residual strain is of great importance?

1. Preliminary Selection of Suitable Steels

The first requirement was the identification of suitable alloys which, under a given set of cooling conditions, will achieve the minimum hardness of 450 VPN in all parts of the 16 mm thick section. In order to identify possible alloys, three cooling conditions were considered, viz quenching in water, oil or air cooling, and those materials with the leanest alloy content were identified that would produce the required hardness after quenching. Consideration of BS 5046:1974 ("Estimation of the Equivalent Diameters in the Heat Treatment of Steel") suggested that a 16 mm thick plate would possess a cooling rate at its centre equivalent to that experienced at the centre of a 28 mm diameter cylinder of the same material. This information, combined with the published hardenability data for the En steels, allowed the following alloy compositions to be identified as possible materials from which the disc could be manufactured:-

Table 1

	Maximum Equivalent Bar Diameter that will produce a hardness of 450 VPN at the centre		
	Water Quench	Oil Quench	Air Cool
En 16	38 mm	23 mm	-
En 17	69 mm	43 mm	4 mm
En 18	38 mm	29 mm	-
En 19	48 mm	23 mm	4 mm
En 24	>254 mm	241 mm	33 mm
En 111	44 mm	29 mm	-

(Source of data: Alloy Steels, Samual Fox & Co Ltd)

Therefore the minimum quenching severities necessary to achieve a hardness of 450 VPN at the centre of a 16 mm thick disc (28 mm equivalent bar diameter) made from these steels were:-

Table 2

En16 (0.3/0.4%C; 1.3/1.8%Mn; 0.2/0.35%Mo) - Water Quench

En17 (0.3/0.4%C; 1.3/1.8%Mn; 0.35/0.55%Mo) - Oil Quench

En18 (0.35/0.45%C; 0.6/0.9%Mn; 0.85/1.15%Cr) - Oil Quench

En19 (0.35/0.45%C; 0.5/0.8%Mn; 0.9/1.5%Cr; 0.2/0.4%Mo) - Water Quench

En24 (0.35/0.45%C; 0.45/0.7%Mn, 1.3/1.8%Ni; 0.9/1.4%Cr; 0.2/0.35%Mo) - Air Cool

En111 (0.3/0.4%C; 0.6/0.9%Mn; 1.0/1.5%Ni; 0.45/0.75%Cr) - Oil Quench

2. Calculation of the Residual Strain Produced as a Result of Quenching Discs made from the Various Possible Steels

The method of calculation used in the determination of the residual strains produced when discs made from each steel were quenched in the appropriate quenchant was that given in Section 4 in the main text of the thesis. The following additional assumptions were made in order to apply the method of calculation to the steels considered in this report:-

(i) The values of Poisson's ratio and Young's modulus of all the steels involved were assumed to be similar to those of 835M30 (En30B) steel.

(ii) The density, specific heat and thermal conductivity of all the steels involved were all assumed to be similar to 835M30 steel.

(iii) The dilatometer curves of the different steels were assumed to be a function of the carbon content, and the M_s and M_f temperatures of the material, as shown in Figure A3.1.

(iv) The flow strength of the different steels during the course of the quenching operation was assumed to vary in a similar manner to that of 835M30 (En30B) steel, except that the increase in strength associated with the formation of martensite was assumed to be dependent on the dilatometer curve and the M_s and M_f temperatures of the steel involved.

(v) Martensite was assumed to be the sole transformation product produced as a result of quenching the discs.

(vi) The variation of the surface heat transfer coefficient with surface temperature during the course of water and oil quenches were assumed to be as shown in Figure A3.2

(vii) The nominal carbon contents, M_s and M_f temperatures and the type of quenchant used in the calculation of residual strains were:-

Table 3

Material	Quenchant	%C	M_s (°C)	M_f (°C)
En16	Water	0.35	335	120
En17	Oil	0.35	330	154
En18	Oil	0.40	354	100
En19	Water	0.40	323	120
En111	Oil	0.35	310	125

Figure A3.3 shows the calculated residual strain between the edges of quenched discs made from the alloys identified in Table 3.

In the case of the air cooled En24 disc, the residual strain was that due to the homogeneous volume change associated with the hardening treatment, since it was assumed that thermal stresses would be negligible in the case of an air cool.

3. Commercial Significance of the Different Levels of Residual Strain

An excessive level of distortion after quenching would necessitate the correction of the dimensions of the discs. This would incur additional grinding costs. However, the selection of the higher hardenability steels that would require a less drastic quench, and thus produce less distortion, would involve additional material costs. Therefore, a costing analysis has been carried out in which the material costs of 70 mm diameter, 16 mm thick discs were considered, together with the grinding costs involved in the correction of various levels of distortion to the diameter of the discs.

(i) Material Costs

Table 4, shown below, shows the cost per tonne of 75 mm diameter annealed black bar of each of the steels under consideration, together with the estimated material costs for 70 mm diameter, 15 mm thick discs, assuming a yield of 1400 discs per tonne of bar.

Table 4

Material	£ per tonne	£ per disc
En16	369	0.2636
En17	386	0.2757
En18	341	0.2438
En19	354	0.2529
En24	468	0.3343
En111	412	0.2946

(ii) Grinding Costs

If it is assumed that unit machining and heat treatment costs are independent of the material from which the disc is made. The sole difference between the machining costs of discs made from the various steels will be that due to post-heat treatment grinding of the outside diameter (which is assumed to be the sole dimension requiring close control). Thus the average increase in the diameter of 70 mm diameter discs was:-

Table 5

Material	Average Increase in Diameter after Hardening
En16 (W.Q.)	0.262 mm
En17 (O.Q.)	0.190 mm
En18 (O.Q.)	0.226 mm
En19 (W.Q.)	0.304 mm
En24 (A.C.)	0.114 mm
En111 (O.Q.)	0.136 mm

In addition to these increases in the diameters, a grinding allowance of 0.125 mm would normally be left on this dimension prior to quenching. Hence the total amount of material to be removed from the diameter was as follows:-

Table 6

Material	Average Material to be Ground Off Diameter
En16 (W.Q.)	0.387 mm
En17 (O.Q.)	0.315 mm
En18 (O.Q.)	0.351 mm
En19 (W.Q.)	0.429 mm
En24 (A.C.)	0.239 mm
En111 (O.Q.)	0.261 mm

The following times and costs have been assumed for the grinding operations:-

Table 7

Setting-up time	5 mins per disc
Grinding rates:	
roughing down to 0.05 mm oversize	0.05 mm/min
finishing of final 0.05 mm	3 mins/disc
Costs of employing one operator	£4000/yr
Operator costs per hour (48 wks/yr, 38 hrs wrk/wk)	£2.19/hr
Standard machine costs	£4.00/hr
(Includes consumables, space, maintenance, power etc)	
Total grinding costs	£6.19/hr

The grinding times and hence grinding costs for discs made from the different steels have been evaluated using the information shown in Tables 6 and 7, and were as follows:-

Table 8

Material	Roughing Time	Set-up + Finishing Time	Total Grinding Time	Grinding Cost per Disc
En16 (W.Q.)	6.8 mins	5 + 3 mins	14.8 mins	£1.527
En17 (O.Q.)	5.3 "	"	13.3 "	£1.372
En18 (O.Q.)	6.0 "	"	14.0 "	£1.444
En19 (W.Q.)	7.6 "	"	15.6 "	£1.609
En24 (A.C.)	3.8 "	"	11.8 "	£1.217
En111 (O.Q.)	4.2 "	"	12.2 "	£1.259

(iii) Material Costs and Grinding Costs

The sum of the material costs and the post-heat treatment grinding costs for discs made from the different steels were thus:-

Table 9

Material	Material Cost	Grinding Cost	Material + Grinding Cost
En16 (W.Q.)	£0.264 per disc	£1.527 per disc	£1.791 per disc
En17 (O.Q.)	£0.276 " "	£1.372 " "	£1.648 " "
En18 (O.Q.)	£0.244 " "	£1.444 " "	£1.688 " "
En19 (W.Q.)	£0.253 " "	£1.609 " "	£1.862 " "
En24 (A.C.)	£0.334 " "	£1.217 " "	£1.551 " "
En111 (O.Q.)	£0.295 " "	£1.259 " "	£1.554 " "

Conclusions

Predictions of the residual strains produced when various En steels were quenched in order to produce the required level of hardness, suggest that the level of distortion was generally reduced as the severity of quench was reduced. Thus water quenching of En19 discs produced the greatest distortion and air cooling of En24 discs the least.

A cost analysis was carried out, in which the initial material costs of discs made from different En steels were considered, in conjunction with the post-heat treatment grinding costs of the discs. This involved the evaluation of the grinding costs, incurred from the correction of the different levels of distortion produced when the discs were were hardened. The results of this analysis showed that discs made from air hardened En24 would be the most economic to produce, though only marginally more economic than discs made from oil quenched En111. An interesting feature of the results was the relatively poor economic performance of materials that required water quenching. This was due to the high levels of distortion produced during quenching and the ensuing high grinding costs, which were greater than the savings in materials costs made by the use of the lower hardenability steels.

Depending upon the production quantities involved, it might be possible to compensate for the expected distortion by initially machining the discs undersize so that less material would need removing after heat treatment. In this case the economics of the process would be influenced by the extent to which consistent distortions could be produced in practice. To a certain extent this can be expected to be a function of the quenching medium employed, air and oil are the most likely to produce high levels of reproducibility.

FIGURE A3.1: Model of dilatometer curve used in the calculation of residual strain.

FIGURE A3.2: Variation of surface heat transfer coefficient used in the calculation of residual strain.

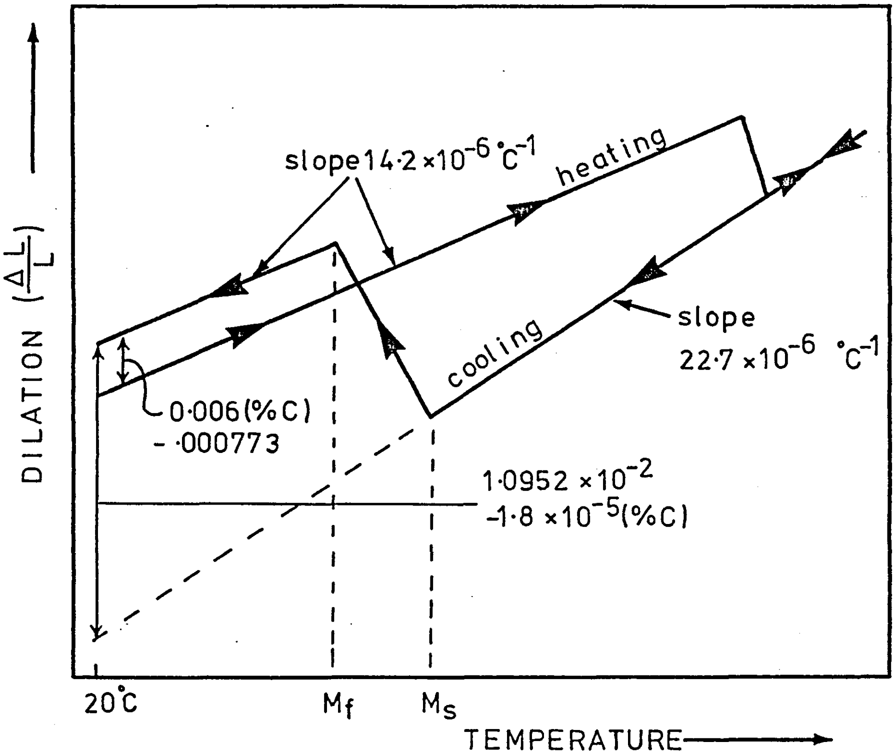
DILATION $\left(\frac{\Delta L}{L}\right)$
slope $14{\cdot}2 \times 10^{-6}$ °C^{-1}
heating
cooling
slope
$22{\cdot}7 \times 10^{-6}$ °C^{-1}
$0{\cdot}006(\%C)$
$-{\cdot}000773$
$1{\cdot}0952 \times 10^{-2}$
$-1{\cdot}8 \times 10^{-5}(\%C)$
20°C
M_f
M_s
TEMPERATURE

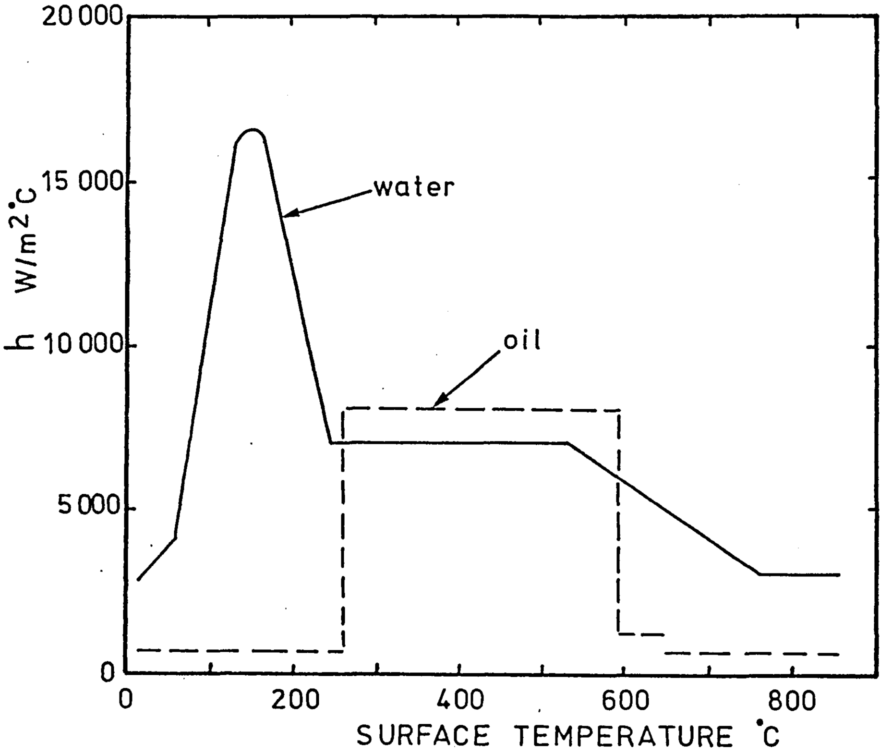
h W/m^2°C
20 000
15 000
10 000
5 000
0
water
oil
0
200
400
600
800
SURFACE TEMPERATURE °C

FIGURE A3.3: Calculated increase in diameter accompanying the hardening of discs made from the different steels.

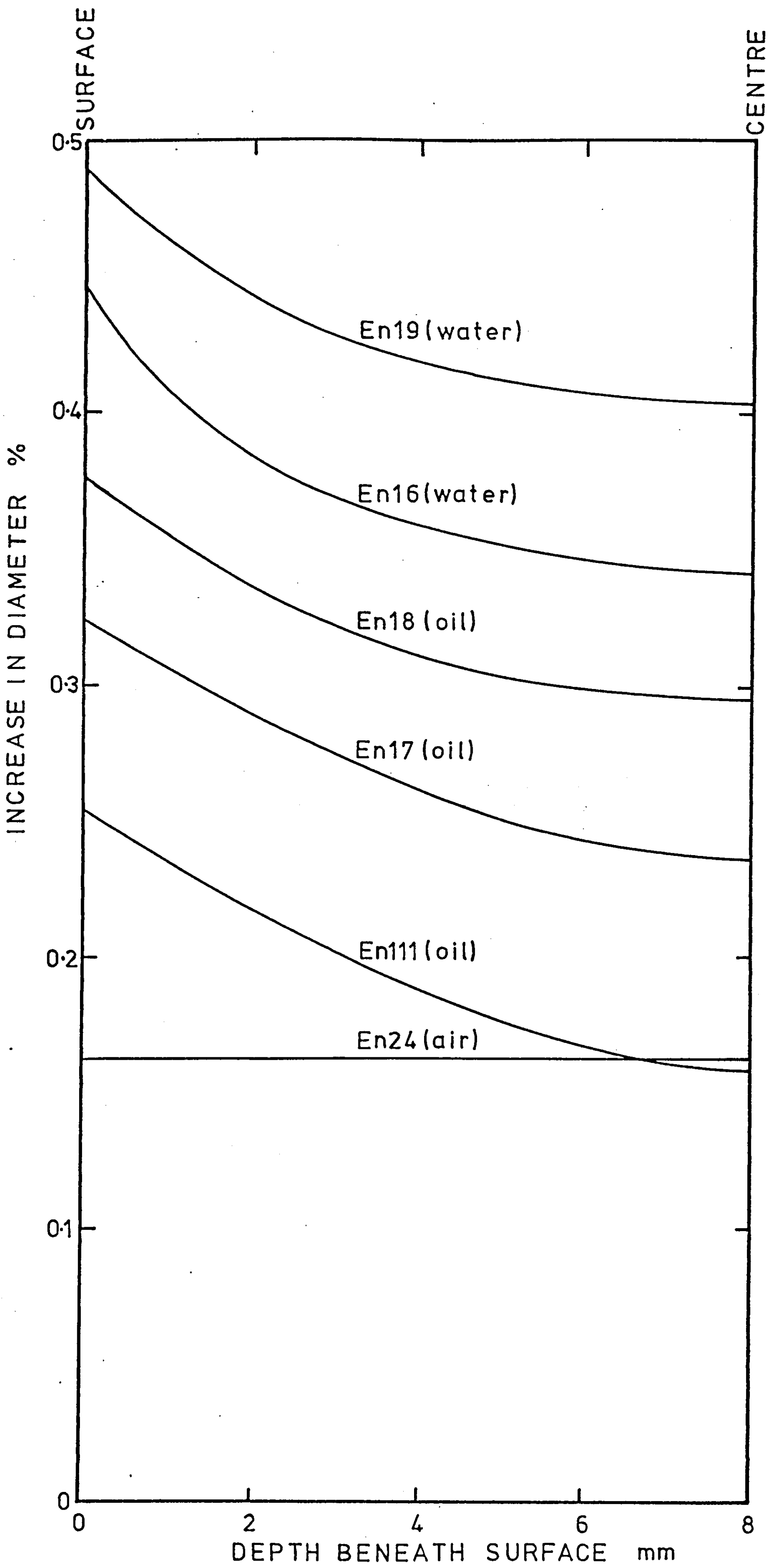
SURFACE
CENTRE
INCREASE IN DIAMETER %
0·5
0·4
0·3
0·2
0·1
0
En19 (water)
En16 (water)
En18 (oil)
En17 (oil)
En111 (oil)
En24 (air)
0
2
4
6
8
DEPTH BENEATH SURFACE mm